The ubiquitination enzymes of *Leishmania mexicana*

Rebecca Jayne Burge

Doctor of Philosophy

University of York

Biology

October 2020

Abstract

Post-translational modifications such as ubiquitination are important for orchestrating the cellular transformations that occur as the *Leishmania* parasite differentiates between its main morphological forms, the promastigote and amastigote. Although 20 deubiquitinating enzymes (DUBs) have been partially characterised in *Leishmania mexicana*, little is known about the role of E1 ubiquitin-activating (E1), E2 ubiquitin-conjugating (E2) and E3 ubiquitin ligase (E3) enzymes in this parasite. Using bioinformatic methods, 2 E1, 13 E2 and 79 E3 genes were identified in the *L. mexicana* genome. Subsequently, bar-seq analysis of 23 E1, E2 and HECT/RBR E3 null mutants generated in promastigotes using CRISPR-Cas9 revealed that the E2s UBC1/CDC34, UBC2 and UEV1 and the HECT E3 ligase HECT2 are required for successful promastigote to amastigote differentiation and UBA1b, UBC9, UBC14, HECT7 and HECT11 are required for normal proliferation during mouse infection. Null mutants could not be generated for the E1 UBA1a or the E2s UBC3, UBC7, UBC12 and UBC13, suggesting these genes are essential in promastigotes. X-ray crystal structure analysis of UBC2 and UEV1, orthologues of human UBE2N and UBE2V1/UBE2V2 respectively, revealed a heterodimer with a highly conserved structure and interface. Furthermore, recombinant *L. mexicana* UBA1a was found to load ubiquitin onto UBC2, allowing UBC2-UEV1 to form K63-linked di-ubiquitin chains *in vitro*. UBC2 was also shown to cooperate with human E3s RNF8 and BIRC2 *in vitro* to form non-K63-linked polyubiquitin chains, but association of UBC2 with UEV1 inhibits this ability. Using affinity purification proteomics, 3 putative UBC2:E3 pairs and potential substrates of UBC2 and UEV1, which include proteins associated with cellular respiration, intracellular transport and pH regulation, were identified. Therefore, the essential requirement for UBC2 and UEV1 in promastigote to amastigote differentiation could be explained by roles for UBC2-UEV1-mediated ubiquitination in regulating the changes in metabolism and protein trafficking that occur during this transition.

Table of contents

List of tables

List of figures

List of accompanying material

Supplemental .csv files containing:

S1: List of oligonucleotides used.

S2: List of plasmids used.

Acknowledgements

First and foremost, I wish to thank my primary supervisor, Jeremy Mottram, for providing invaluable advice and guidance throughout my PhD. I am truly grateful for the opportunities that have been afforded to me during this time, including the scope to learn a wide variety of techniques, exercise my intellectual creativity and attend courses and conferences. I would also like to thank my co-supervisors at UbiQ, Boris Rodenko and Farid El Oualid, for their advice regarding the progression of my project, and Anthony Wilkinson, for helping me to achieve my goals in protein crystallography. Additionally, I extend thanks to the Medical Research Council and The University of York for providing me with the finances and facilities, respectively, to carry out my PhD.

I would like to extend my deepest gratitude to Ubiquigent Ltd, who provided me with a 3-month internship that proved invaluable for the advancement of my PhD project. In particular, I would like to thank Sheelagh Frame for her instruction and guidance, and for helping me to transition smoothly into my temporary home and workplace in Dundee. I would also like to acknowledge Jane Hilton and Jason Brown for their feedback and valuable discussions.

Within the University of York Technology Facility, I am particularly grateful to Adam Dowle, Jared Cartwright and Andrew Leech for their advice and assistance with mass spectrometry, protein production and SEC-MALLS technologies respectively. I would also like to thank Rebecca Preece and Mick Miller for providing technical support and a friendly environment (in which I spent many hours expressing and purifying my proteins) and Karen Hogg for providing technical support. I am grateful to numerous members of the York Structural Biology Laboratory, including Marek Brzozowski for crystal-harvesting and valuable discussions, Juliet Borgia for technical support, Johan Turkenburg for help with data processing and Eleanor Dodson for advice on structure solution and refinement. I also wish to acknowledge Daniel Harris for exchange of materials and protocols and Richard Burchmore and Nia Bryant for valuable discussions.

As part of the Mottram lab, I have been extremely lucky to work with a friendly, inspiring group of colleagues. In particular, I would like to thank Andreas Damianou for countless stimulating discussions and for reminding me to not be stressed, Elaine Brown for her patience in fielding many, many questions and for technical support, Carol Catta-Preta for her help and guidance with carrying out the bar-seq screen, Vincent Geoghegan for

sharing his expertise in mass spectrometry and Nathaniel Jones and Nicola Baker for numerous valuable discussions. In addition to the people mentioned above, I would like to thank the following for their assistance in the lab and for making H block a pleasant place to work: Rachel Neish, Juliana Brambilla Carnielli Trindade, Sergios Antoniou, Charlotte Hughes, Ewan Parry, Jayanthi Anand, Chris Bower-Lepts, Manuel Alejandro Saldivia Concepción, Jaspreet Singh Grewal, Elmarie Myburgh, Ridda Jabbar, Tiago Ferreira and Eliza Ferreira.

Last but not least, I would like to extend my deepest gratitude to my friends and family for supporting me throughout the challenges of the past four years. In particular, I would like to thank Sam, Emma, Nikita, Ewan and Josh for many fun experiences had and Mum, Dad and Angela for their unwavering love and support.

“Greet me with banners and balloons and my hard drive smashed to pieces” -

John K. Samson

Author's declaration

I declare that this thesis is a presentation of original work and I am the sole author. This work has not previously been presented for an award at this, or any other, university. Some of the content has been published (with amendments) in the following paper:

Burge, R. J., Daminaou, A., Wilkinson, A. J., Rodenko, B. and Mottram, J. C. (2020). '*Leishmania* differentiation requires ubiquitin conjugation mediated by a UBC2-UEV1 E2 complex', PLoS Pathog 16(10): e1008784. https://doi.org/10.1371/journal.ppat.1008784

All sources are acknowledged as references.

Rebecca Jayne Burge

1 Introduction

1.1 *Leishmania* and leishmaniasis

1.1.1 Epidemiology

Leishmaniasis is a neglected tropical disease (NTD) caused by protozoan parasites of the genus *Leishmania*. The global disease burden for leishmaniasis is high, with around 0.7-1 million new cases arising per year (World Health Organisation, 2020). Among parasitic diseases, leishmaniasis is the third most common cause of morbidity as measured in disability adjusted life years (DALYs) and the second biggest cause of mortality (after malaria) (Pace, 2014). *Leishmania* parasites, the causative agent of the disease, are transmitted between mammalian hosts by female phlebotomine sand flies of the genera *Phlebotomus* or *Lutzomyia* in the Old and New World respectively. In part due to the geographic distribution of sand fly vectors, leishmaniasis mainly affects poor populations in Africa, Asia and Latin America (Alvar, Yactayo and Bern, 2006; Georgiadou, Makaritsis and Dalekos, 2015).

Problematically, a cycle of mutual reinforcement exists between leishmaniasis and poverty, beginning with an increased risk for developing leishmaniasis amongst those living in poverty. This may be due to, for example, poor housing conditions (increasing exposure to sand flies) and lack of nets and other protective measures. Once infected, morbidity and mortality are potentiated by a number of factors including an inability to afford treatment or weakened immune systems caused by malnutrition or HIV co-infection (Alvar, Yactayo and Bern, 2006). Indeed, the overlap that exists between HIV infections and key leishmaniasis foci in India, Brazil and Eastern Africa is of great concern (Alvar *et al.*, 2008). The financial costs of leishmaniasis treatment, coupled with lasting disfigurement from the disease and associated stigma, result in further impoverishment (Bern, Maguire and Alvar, 2008). Despite clear associations with poverty, however, the prevalence of trade and travel to and from leishmaniasis-endemic areas, in addition to the possible expansion of sand fly ranges in response to climate change, make leishmaniasis a global concern (Sutherst, 2004).

1.1.2 Disease pathology

Clinically, leishmaniasis can be grouped into three main subtypes: cutaneous (CL), mucocutaneous (MCL) and visceral (VL) infection. CL manifests in the form of skin lesions of varying appearance that heal slowly, often with scarring. Such lesions usually

occur in areas exposed to sand flies such as the face and limbs. MCL is caused by dissemination of cutaneous infections into the mucosae of the oral and upper respiratory tract and can result in severe tissue damage and disfigurement (Pace, 2014). Conversely, VL is characterised by infection of the internal organs resulting in, amongst other symptoms, fever, hepatosplenomegaly and death if untreated (Pace, 2014; McCall, Zhang and Matlashewski, 2013). There are around 0.7-1.2 million cases of CL per year with the majority of cases in the Americas, Mediterranean and Western Asia. MCL is less prevalent with around 35,000 cases per year, occurring mainly in Brazil, Bolivia and Peru (Pace, 2014). For VL, around 0.2-0.4 million cases occur per year with most of these in Bangladesh, Brazil, Ethiopia, India and Sudan (Georgiadou, Makaritsis and Dalekos, 2015).

Geographical region	**Predominant clinical form**	**Species**
Old World (subgenus *Leishmania*)	Visceral leishmaniasis	*L. donovani, L. infantum*
	Cutaneous leishmaniasis	*L. tropica, L. major, L. aethiopica*
New World (subgenus *Leishmania*)	Visceral leishmaniasis	*L. infantum*
	Cutaneous leishmaniasis	*L. mexicana, L. amazonensis*
New World (subgenus *Viannia*)	Cutaneous leishmaniasis	*L. peruviana, L. guyanensis, L. panamensis, L. braziliensis*
	Mucocutaneous leishmaniasis	*L. panamensis, L. braziliensis*

Table 1. *Leishmania* species and disease manifestations. Summarised information from Bern et al., 2008 and Pace et al., 2014.

More than 20 species of *Leishmania* are known to infect humans, resulting in the CL, MCL and VL pathologies discussed above. Interestingly, both *Leishmania* species and the host immune response are known to determine the clinical manifestation of the disease (Georgiadou, Makaritsis and Dalekos, 2015). A summary of common *Leishmania* species and the clinical manifestations most commonly associated with them are summarised in Table 1.

1.1.3 Life cycle overview

Leishmania parasites have a complex, digenetic life cycle that alternates between the sand fly vector and mammalian host. Multiple, discrete life cycle stages exist that are associated with different cell morphologies and can be separated into two main forms: the promastigote form, found in the sand fly, and the amastigote form, found in the mammalian host (Figure 1). In terms of morphology, promastigotes have an elongated ovoid cell body and a long, motile flagellum whereas amastigotes have a relatively small, rounded cell body with a short, immotile flagellum (Sunter and Gull, 2017). In the sand fly, the promastigote flagellum is required for movement through the midgut, whereas the amastigote flagellum likely provides sensory functions (Gluenz *et al.*, 2010; Wheeler, Gluenz and Gull, 2015).

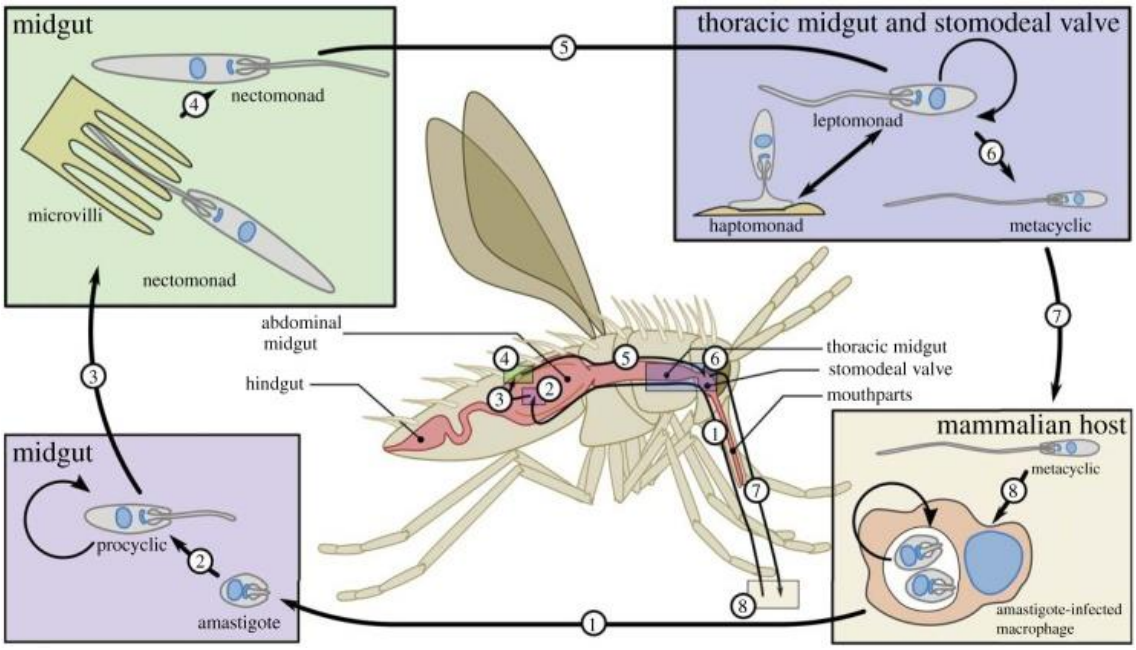

Figure 1. *Schematic depicting the life cycle of Leishmania.* When a sand fly takes a blood meal from an infected mammalian host, amastigotes are ingested. These differentiate into procyclic promastigotes, which proliferate rapidly. Procyclic promastigotes transition into nectomonad promastigotes which can exit the peritrophic matrix and bind to the midgut by inserting their flagella between epithelial microvilli. Nectomonad promastigotes then migrate towards the thoracic (anterior) midgut and stomodeal valve, where they differentiate into the replicative leptomonad form. Leptomonad promastigotes can either differentiate into haptomonad promastigotes, which attach to the stomodeal valve via hemidesmosome-like structures, or metacyclic promastigotes which are transmitted and result in infection when the sand fly bites an uninfected host. Reproduced partial image from Sunter and Gull (2017).

The life cycle proceeds as follows: after a sand fly bites an infected mammalian host, *Leishmania* amastigotes are taken up with the blood meal, encased in the peritrophic matrix (a coating of chitin, proteins and glycoprotein that separates the blood meal from the midgut epithelium) and differentiate into procyclic promastigotes (Dostálová and Volf, 2012; Lehane, 1997). This differentiation process is thought to be triggered partially by a decrease in temperature and increase in pH. The resultant procyclic promastigotes have a short flagellum, are weakly motile and proliferate rapidly (Dostálová and Volf, 2012). Between 48 and 72 hours later, the rate of replication decreases, and the procyclic promastigotes differentiate into non-proliferative nectomonad promastigotes, a more elongated and strongly motile form (Rogers, Chance and Bates, 2002; Dostálová and Volf, 2012). Nectomonad promastigotes can escape the peritrophic matrix and bind to the midgut walls by inserting their flagella between epithelial microvilli, a process that is crucial to prevent them from being excreted during sand fly defecation (Sunter and Gull, 2017).

Following their escape from the peritrophic matrix, nectomonad promastigotes migrate towards the anterior midgut and become shorter, proliferative leptomonad forms (Rogers, Chance and Bates, 2002). Subsequently, leptomonad promastigotes differentiate into either haptomonad or metacyclic promastigotes. Of these, haptomonad promastigotes have an expanded flagellar tip containing hemidesmosomal structures that permits attachment to the sand fly stomodeal valve. Haptomonad promastigote attachment causes damage to the stomodeal valve and contributes to transmission by promoting the reflux of parasites during blood feeding (Volf *et al.*, 2004; Kimblin *et al.*, 2008). Metacyclic promastigotes, on the other hand, are small and highly motile with an elongated flagellum. They are also the predominant form responsible for infection following the transfer of parasites into the mammalian host during blood feeding (Dostálová and Volf, 2012; Sacks and Perkins, 1985). Promastigote secretory gel, a proteophosphoglycan-rich gel secreted mainly by leptomonad promastigotes, surrounds leptomonad and metacyclic forms in the anterior midgut of the sand fly and also contributes to transmission by influencing sand fly feeding behaviour and enhancing infection inside the mammalian host (Rogers *et al.*, 2004; Rogers and Bates, 2007; Rogers, 2012). More recently, it has been shown that following additional blood meals, metacyclic promastigotes remaining inside the sand fly can de-differentiate into a leptomonad-like form. This newly identified form, coined the retroleptomonad promastigote, can proliferate rapidly and differentiate into new haptomonad and metacyclic promastigotes, enhancing parasite transmission upon further blood feedings (Serafim *et al.*, 2018).

Following the transfer of metacyclic promastigotes into the mammalian host, neutrophils infiltrate the bite site (Peters *et al.*, 2008). Next, metacyclic promastigotes can be phagocytosed by neutrophils, macrophages and dendritic cells present at the site of infection (Beattie and Kaye, 2011; Ng *et al.*, 2008). Notably, the Trojan horse hypothesis proposes that the entry of *Leishmania* into host macrophages occurs safely and silently via the ingestion of infected apoptotic neutrophils (Laskay, van Zandbergen and Solbach, 2003; Laskay, van Zandbergen and Solbach, 2008). Inside host cells, metacyclic promastigotes are surrounded by the phagosome membrane. The phagosomes mature into phagolysosomes following their fusion with late endosomes and lysosomes. It is within the phagolysosomes of macrophages that metacyclic promastigotes differentiate into amastigotes (Beattie and Kaye, 2011). This change is thought to be triggered by the increased temperature and decreased pH experienced in the mammalian host environment compared with that of the sand fly digestive tract (Barak *et al.*, 2005). The *in vitro* differentiation of *L. donovani* promastigotes to axenic amastigotes is divided into 4 distinct stages. Between 0-4 hr (phase I), the cells receive signals from their environment without undergoing morphological change. In phase II (5-9 hr), the cells stop moving and aggregate together. In phase III, transformation into cells with amastigote morphology is observed (10-24 hr). By 120 hr (phase IV), the cells have matured completely (Barak *et al.*, 2005; Rosenzweig *et al.*, 2008). Notably, the Old World species of *Leishmania* such as *L. major* have only one amastigote per phagolysososome, whereas New World species such as *L. amazonensis* contain multiple amastigotes per phagolysosome, demonstrating species-specific differences in the infection process (Castro *et al.*, 2006). Inside the macrophage phagolysosomes, amastigotes persist and proliferate. For the infection to be resolved, the host requires an effective adaptive immune response including the generation of antigen-specific CD4+ T cells (Beattie and Kaye, 2011).

1.1.4 Cellular composition

One of the most prominent features of *Leishmania* parasites are the flagella present at the anterior of the cell. As discussed previously, *Leishmania* flagella vary in length between the different life cycle stages, exhibiting the most dramatic change between the metacyclic promastigote and amastigote. In addition, the composition of the flagellum changes from a 9+2 arrangement of the axoneme in promastigotes to a 9+0 arrangement in amastigotes, associated with functions in motility and environmental sensing respectively. Notably, a 9+0 flagellum can be formed following the conversion of an existing 9+2 flagellum or be produced *de novo* (Wheeler, Gluenz and Gull, 2015).

Internally, *Leishmania* cells contain many of the organelles commonly found in other eukaryotic cells including a nucleus, mitochondrion, endoplasmic reticulum, Golgi apparatus and other endocytic pathway components, depicted in Figure 2 (Sunter and Gull, 2017; Besteiro *et al.*, 2007). In addition, they possess a kinetoplast, an organelle that encapsulates the mitochondrial DNA and is unique to the order Kinetoplastida. Within the kinetoplast, mitochondrial DNA is divided up into tens of maxicircles, which encode some of the mitochondrial proteins and ribosomal RNA, and thousands of minicircles, which encode guide RNAs responsible for editing the mRNAs originating from maxicircles, that are topologically linked (Shlomai, 2004). The mitochondrial DNA is connected to the base of the flagellum, known as the basal body. Other notable features include the flagellar pocket, a structure formed by the invagination of the membrane at the base of the flagellum. The flagellar pocket is involved in protein endocytosis and exocytosis and is crucial for cell viability (Field and Carrington, 2009). However, exosomes have also been observed to be secreted from multi-vesicular bodies via plasma membrane fusion, demonstrating that the flagellar pocket is not the sole site for *Leishmania* exocytosis (Atayde *et al.*, 2015). During the differentiation of metacyclic promastigotes into amastigotes, the flagellar pocket neck closes, coinciding with changes in the positioning of flagellar attachment zone (FAZ) proteins. This is proposed to reduce exposure of the amastigote cell surface to the harsh environment of the host phagolysosome (Wheeler, Sunter and Gull, 2016). Another unique feature of the Kinetoplastida is the presence of glycosomes, membrane-bound organelles related to peroxisomes that contain glycolytic and pentosephosphate pathway enzymes and are thought to be important for metabolic adaptability (Hannaert *et al.*, 2003; Michels *et al.*, 2006).

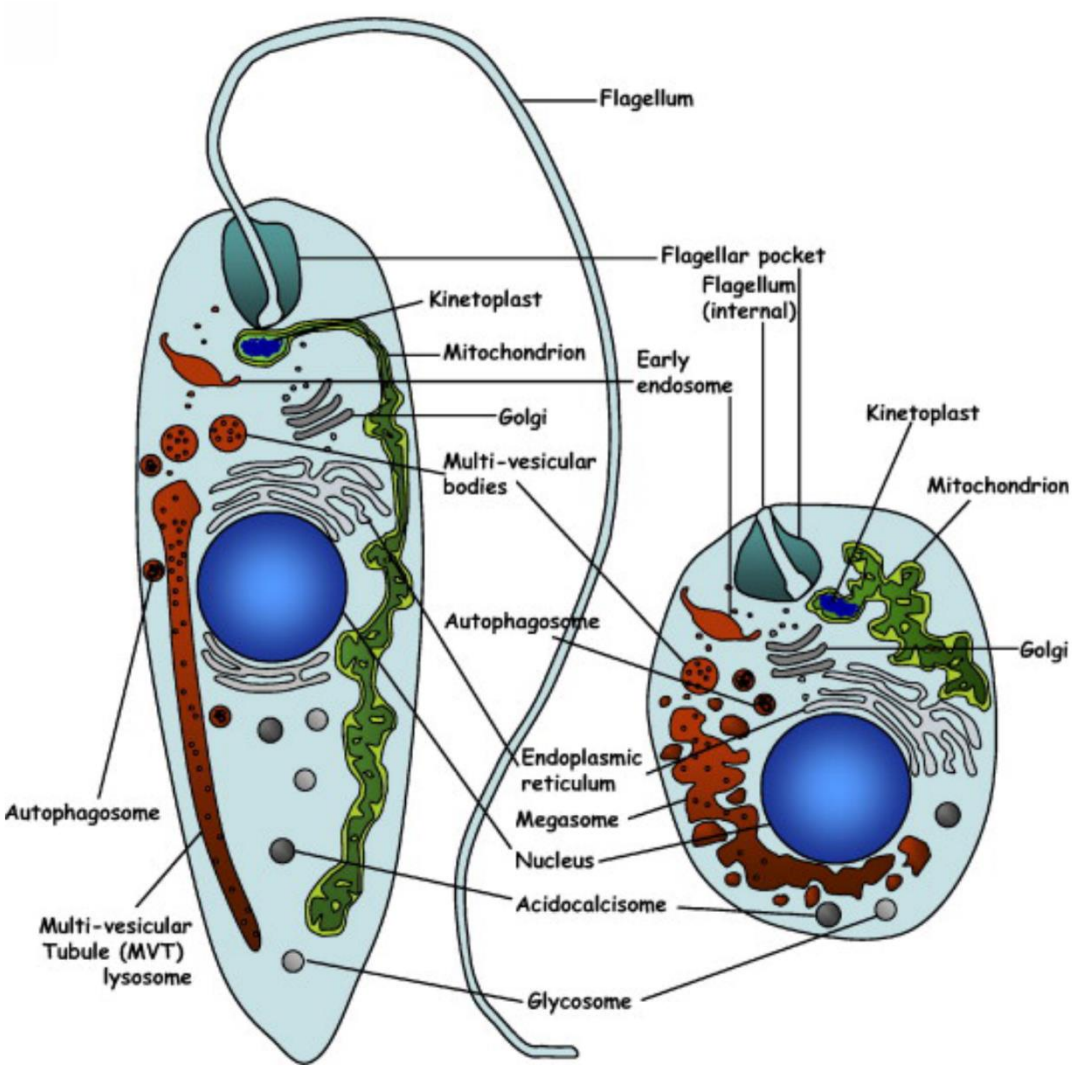

Figure 2. *Organellar composition of Leishmania*. Schematic representation of the organelles in *Leishmania* promastigotes (left) and amastigotes (right). Reproduced partial image from Besteiro *et al.* (2007).

1.1.5 Gene expression

Gene expression in kinetoplastids, including *Leishmania*, differs from that in other eukaryotic species in a number of ways. Firstly, the transcription of protein-coding genes in the nucleus occurs polycistronically, meaning that multiple genes are encoded in each pre-mRNA (Clayton, 2016). Transcription is carried out by RNA polymerase II in a bidirectional manner, starting at divergent strand switch regions (between two polycistronic transcription units facing away from each other), marked by the presence of specific histones and histone modifications, and terminating at convergent strand

switch regions (between two polycistronic transcription units facing towards each other), also marked by epigenetic modifications (Martínez-Calvillo *et al.*, 2003; Siegel *et al.*, 2009; Thomas *et al.*, 2009; Reynolds *et al.*, 2014). Another unique feature is the trans-splicing of a 140 nt spliced leader RNA that occurs in order to add a 39 nt spliced leader cap at the 5' end of the mRNA. This is coupled to cleavage and polyadenylation at the 3' end, generating a mature mRNA transcript (Clayton, 2016). However, due to the polycistronic method of kinetoplastid transcription, individual protein-coding genes cannot be regulated at the level of transcription initiation. As a result, gene regulation in kinetoplastids occurs mainly at the level of RNA and protein and can be achieved through post-transcriptional control of mRNA decay and translation or post-translational control, such as the regulation of protein degradation (De Pablos, Ferreira and Walrad, 2016).

In order for the relevant morphological and metabolic changes associated with the differentiation of *Leishmania* to occur, dramatic changes in gene expression are required. Many studies have reported differential gene expression between the main life cycle stages, with the majority relying on transcriptome analysis. Genes upregulated at the mRNA level in promastigotes versus amastigotes relate to gene ontology (GO) terms involving nucleosomes, glycolysis, sterol biosynthesis, the citric acid (TCA) cycle and flagellar motility, among others (Inbar *et al.*, 2017; Fiebig, Kelly and Gluenz, 2015). Within promastigotes, genes found to be upregulated in procyclic promastigotes versus metacyclic promastigotes relate to cellular processes including nucleosome assembly, DNA replication and glucose metabolism, whereas those upregulated in metacyclic promastigotes versus procyclic promastigotes are associated with fatty acid metabolism, ATP-coupled proton transport and cell signalling (Alcolea *et al.*, 2019; Dillon *et al.*, 2015). Furthermore, it been observed that metacyclic promastigotes have a more amastigote-like profile than procyclic promastigotes, suggesting that metacyclic promastigotes are pre-adapted to survival in the host environment (Inbar *et al.*, 2017). In amastigotes versus promastigotes, enriched genes fall into such categories as membrane transporters, amastins, antioxidant activity, cysteine peptidase activity, DNA repair, vesicular transport and proteasome and ubiquitin machinery-related proteins (Saxena *et al.*, 2007; Fiebig, Kelly and Gluenz, 2015; Inbar *et al.*, 2017; Ruy *et al.*, 2019). Notably, cell cycle-related genes were found to be more up-regulated in procyclic promastigotes and amastigotes than in nectomonad or metacyclic promastigotes, correlating with the replicative status of these developmental stages (Alcolea *et al.*, 2019).

Differential gene expression across the life cycle has also been observed at the post-transcriptional level. For example, whole cell proteome analysis revealed that over 1,100

proteins were differentially expressed in procyclic promastigotes, metacyclic promastigotes or intracellular amastigotes. Furthermore, nearly 300 RNA-binding proteins were shown to be enriched at different life cycle stages, suggesting widespread stage-specific regulation of mRNA transcripts (de Pablos *et al.*, 2019). Protein degradation is also important during the transition from procyclic promastigote to metacyclic promastigote, as shown by the finding that autophagy, the degradation and recycling of unwanted or defective cellular components inside vesicles, is crucial for the differentiation of procyclic promastigotes to metacyclic promastigotes and their subsequent transformation to amastigotes (Besteiro *et al.*, 2006; Williams *et al.*, 2006; Cull *et al.*, 2014). In further support of this, lysosomal cysteine peptidases were found to be upregulated during the differentiation of promastigotes to amastigotes (Brooks *et al.*, 2001; Ueda-Nakamura *et al.*, 2002; Besteiro *et al.*, 2007). Differences in post-translational modification have also been observed, including changes to the phosphorylation and dephosphorylation status of proteins during the promastigote to amastigote transition (Tsigankov *et al.*, 2014; Cayla *et al.*, 2014; Morales *et al.*, 2010). Notably, there appears to be a relationship between differentiation phase and phosphorylation activity, with phases I and III associated with increased phosphorylation and phases II and IV associated with dephosphorylation. In phase I, 4 kinases, asparagine synthetase and heat shock protein DNAJ, are among the proteins shown to exhibit a net increase in phosphorylation (Tsigankov *et al.*, 2014).

1.1.6 Current treatments

Drugs that are currently approved for the clinical treatment of leishmaniasis include amphotericin B, glucantime, miltefosine, paromomycin and pentostam. Despite their clinical use, however, these drugs have a number of drawbacks including prohibitively high cost, long duration of treatment, patient toxicity and emerging drug resistance (Bhattacharya *et al.*, 2020). Notably, the issue of drug resistance is linked to that of patient toxicity, since toxic side effects can lead to treatment discontinuation, contributing more strongly to the development of resistance (de Menezes *et al.*, 2015). Glucantime and pentostam are examples of antimonial compounds, which require the reduction of pentavalent antimony (Sb^{V}) to trivalent antimony (Sb^{III}) for their activity. Following reduction, Sb^{III} can enter *Leishmania* cells through the aquaglyceroporin 1 (AQP1) transporter. Resistance to antimonials has been shown to occur by a variety of mechanisms that may involve a decrease in the reduction of Sb^{V} to Sb^{III}, decreased drug import and increased levels of trypanothione, since trypanothione binds Sb^{III}, leading to its organellar sequestration or efflux (Ponte-Sucre *et al.*, 2017). Amphotericin B, a

naturally-occurring antifungal compound, acts by binding ergosterol-related sterols in the *Leishmania* cell membrane, contributing to cell death by allowing ion exchange through pores in the cell surface and triggering oxidative stress. Historically, resistance to Amphotericin B has been rare but can occur (in cultured *Leishmania* cells) via a mutation in the sterol biosynthesis pathway enzyme sterol 14α-demethylase, which results in the loss of ergosterol from the membrane or through an increase in the ability of *Leishmania* to resist oxidative stress (Mwenechanya *et al.*, 2017; Ponte-Sucre *et al.*, 2017). Miltefosine, the only oral drug available to treat leishmaniasis, enters the cell through the miltefosine transporter and causes cell death by interfering with phospholipid and alkyl-lipid metabolism. Multiple factors are thought to contribute towards miltefosine resistance but can include mutations in the miltefosine transporter, observed in both clinical isolates and cultured *Leishmania* (Ponte-Sucre *et al.*, 2017). Additionally, loss of the miltefosine sensitivity locus (which contains 4 genes) is associated with resistance to miltefosine treatment in clinical isolates from VL patients (Carnielli *et al.*, 2018). Examples of resistance to paromomycin, an inhibitor of protein synthesis, have also been observed in laboratory-derived cells (Singh, Kumar and Singh, 2012). Combined drug treatment is viewed as an attractive option for trying to reduce the development of drug resistance. However, although it less likely to develop, resistance to combination therapies is a possibility, especially when paromomycin is one of the drugs of choice (Ponte-Sucre *et al.*, 2017).

In the past, pharmaceutical companies have shown little interest in developing new drugs for NTDs, including leishmaniasis, since there is less financial incentive to focus on diseases that affect poorer countries and/or populations. For this reason, drug repurposing has often been employed to reduce the overall effort and costs associated with development. Miltefosine, for example, was originally developed as an anticancer drug (Bhattacharya *et al.*, 2020; Ponte-Sucre *et al.*, 2017). In the last two decades, the Drugs for Neglected Diseases initiative (DNDi), a not-for-profit organisation specialising in the development of new treatments for NTDs, has been instrumental in the development of new leishmaniasis treatments, including improved combination therapies (Bhattacharya *et al.*, 2020). Additionally, a number of new, anti-leishmanial compounds were recently identified, including gold-derived complexes that show activity against intracellular amastigotes of *L. infantum* and *L. braziliensis* (Mowbray *et al.*, 2015; Van den Kerkhof *et al.*, 2018; Tunes *et al.*, 2020). A number of potentially targetable proteins have also been identified, including pteridine reductase, carbonic anhydrases, cyclin-dependent kinase 12 and the proteasome (Bhattacharya *et al.*, 2020; Wyllie *et al.*, 2018; Khare *et al.*, 2016; Wyllie *et al.*, 2019). Despite this progress, the current absence of

suitable anti-leishmanial drugs in the clinic underscores the need for a deeper understanding of crucial biological processes in *Leishmania* which could be targeted in the development of new, anti-leishmanial therapies.

1.1.7 Genetic approaches to the study of *Leishmania*

In order to interrogate the role of specific genes in the biology of *Leishmania* and identify new drug targets, a number of genetic approaches can be taken. Historically, the genetic manipulation of *Leishmania* has been challenging, due in part to genomic plasticity and the absence of an RNA interference system in most species (Duncan, Jones and Mottram, 2017). In recent years, however, the development of clustered regularly interspaced short palindromic repeats (CRISPR)-CRISPR-associated gene 9 (Cas9) genome editing technologies have revolutionised the genetic manipulation of many organisms, particularly those that have not been very genetically tractable in the past (Jansen *et al.*, 2002; Wang, La Russa and Qi, 2016). This technique builds on previous gene editing strategies that exploited homologous recombination as a method of inserting DNA into a desired genomic location by providing arms of homology to that region, providing increased efficiency through the generation of double-stranded DNA breaks (Jones *et al.*, 2018).

The CRISPR-Cas system was originally discovered as part of the bacterial immune system and operates as follows: following a viral challenge, bacteria integrate so called “spacer” sequences derived from phage DNA between CRISPR repeat elements (Barrangou *et al.*, 2007; Adli, 2018). Subsequently, short CRISPR RNAs (crRNAs) are transcribed from the spacer sequences and combine with trans-activating crRNAs (tracrRNA) to form a guide for the activity of Cas enzymes, which form breaks in the phage DNA. Interactions between Cas and a protospacer-adjacent motif (PAM) in the target DNA sequence are also important for the system to function (Deveau *et al.*, 2008; Adli, 2018). Later, it was shown that Cas9 enzyme activity could be directed to specific regions of both bacterial and eukaryotic genomes, and that this could be achieved using a fusion of the crRNA and tracRNA known as the single guide RNA (sgRNA) (Jinek *et al.*, 2012; Gasiunas *et al.*, 2012; Adli, 2018). Since then, CRISPR-Cas9 genome editing has been utilised in *Leishmania*, where double-stranded DNA breaks caused by the Cas9 enzyme can be repaired by homologous recombination (when template DNA is provided) or micro-homology mediated end joining (Zhang and Matlashewski, 2015; Sollelis *et al.*, 2015; Duncan, Jones and Mottram, 2017). Notably, Beneke *et al.* (2017; 2019) developed a streamlined method for the tagging and knockout of *Leishmania*

genes using CRISPR-Cas9. In this method, a cell line expressing T7 RNA polymerase (T7RNAP) and Cas9 from the tubulin locus is transfected with gRNAs and repair cassettes produced by PCR. Cells in which the cassette has integrated by homologous recombination are then selected for with antibiotics.

Targeting *Leishmania* genes for deletion with the CRISPR-Cas9 system helps to inform on whether they are essential or non-essential for the parasite. However, since the failure to recover mutants from a transfection may have a technical cause, further genetic manipulations are recommended in order to validate gene essentiality. Possibilities include the generation of a facilitated null mutant, in which an episomal copy of the gene is transfected into the cell line prior to the deletion of chromosomal gene copies. If desired, these cells can then be analysed for their dependence on the episomal gene copy, either by an unforced plasmid shuffle, during which loss or retention of the plasmid is analysed over time (without selective pressure), or by a forced plasmid shuffle, in which negative selective pressure is applied to encourage parasites to lose the episome (Jones *et al.*, 2018). Another genetic manipulation strategy that is of particular use for investigating essential genes is a conditional null mutant. In *Leishmania*, this can be achieved using the DiCre (split Cre recombinase) system, first used to evaluate *CRK3*. In this method, one allele of the gene is replaced with the DiCre sequence and the second with a floxed copy of the gene of interest. When rapamycin is added to the cells, the two halves of the Cre recombinase combine and act to remove the floxed copy of the gene of interest, resulting in gene deletion (Duncan *et al.*, 2016; Duncan, Jones and Mottram, 2017). Genetic evaluation of an essential gene using the DiCre system is considered to represent a 5 (out of 5) star level of drug target validation. Currently, however, this technique cannot be applied to the study of amastigotes, since rapamycin is not very bioavailable and is toxic to amastigotes (Jones *et al.*, 2018). Notably, the advantages of the CRISPR-Cas9 and DiCre systems have recently been combined in order to streamline the conditional analysis of null mutant phenotypes (Yagoubat *et al.*, 2020; Damasceno *et al.*, 2020).

1.2 Ubiquitination in non-trypanosomatids

1.2.1 Introduction to the ubiquitin system

Ubiquitin (Ub) is an 8.5 kDa, highly conserved protein that serves as a post-translational modification in a huge range of biological contexts. In human cells, ubiquitin system components represent around 1.3% of the total cellular protein and, furthermore, tens of

thousands of ubiquitination sites have been identified located on thousands of proteins (Clague, Heride and Urbé, 2015; Swatek and Komander, 2016). Ubiquitin is thought to have evolved from archaeal MoaD and ThiS, sulfur-carrying proteins that are adenylated at their C-terminus during Moco and thiamine synthesis respectively (Hochstrasser, 2009; Grau-Bové, Sebé-Pedrós and Ruiz-Trillo, 2015). Despite the fact that ubiquitin was predicted to be present in the last eukaryotic common ancestor but evolved after the origin of bacteria, a functionally ubiquitin-like protein, Pup, exists in bacteria. However, while ubiquitin and other ubiquitin-like proteins (Ubls) contain a β-grasp fold, Pup does not. Instead, the similarities between ubiquitin and Pup are examples of convergent evolution (Pearce *et al.*, 2008; Grau-Bové, Sebé-Pedrós and Ruiz-Trillo, 2015). To date, most ubiquitin system research has been carried out in humans and *Saccharomyces cerevisiae.*

Addition of ubiquitin to proteins is carried out through the sequential actions of E1, E2 and E3 enzymes (Figure 3). Typically, an E1 activates ubiquitin in an ATP-dependent manner by adenylating its C-terminus, allowing a thioester bond to form between the E1 active site and ubiquitin. Subsequently, ubiquitin is transferred to the active site of an E2 via trans-thioesterification and then onto the substrate with the help of an E3 ligase. Most commonly, ubiquitination occurs between the C-terminal glycine of ubiquitin and the ε-amino group of lysine residues, forming an isopeptide bond. However, modification of cysteine, serine, threonine and the N-termini of proteins are also possible (McClellan, Laugesen and Ellgaard, 2019).

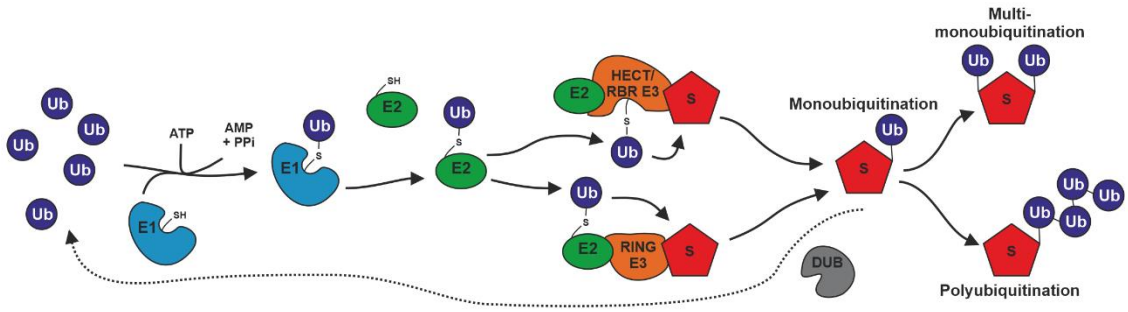

Figure 3. *Schematic of the ubiquitination cascade.* An E1 hydrolyses ATP and adenylates ubiquitin at its C-terminus, allowing ubiquitin to form a thioester bond with the E1 active site cysteine. In this process, free AMP and inorganic pyrophosphate (PP_i) are released. Ubiquitin is then transferred to the E2 active site cysteine via a trans-thioesterification reaction. Cys-dependent E3s such as HECT and RBR E3s form a covalent bond between their active site cysteine and ubiquitin prior to transfer of ubiquitin onto the substrate protein. Cys-independent

E3s such as the RING and U-box E3s form a scaffold to facilitate the direct transfer of ubiquitin from E2 to substrate. Ubiquitin becomes linked to a substrate via an isopeptide bond, usually on a lysine residue. Following monoubiquitination, additional ubiquitins can be conjugated to the substrate, either at separate sites or onto the monoubiquitin, resulting in multi-monoubiquitination or polyubiquitination respectively. DUBs cleave ubiquitin from substrates, replenishing the intracellular pool of free ubiquitin.

E3 ligases can be grouped into two categories based on their mechanism of action. Cys-dependent E3s such as the HECT (Homologous to the E6-AP Carboxyl Terminus) and RBR (Ring-Between-Ring) E3s contain a cysteine residue that forms a covalent linkage with ubiquitin prior to transfer to the substrate (Scheffner, Nuber and Huibregtse, 1995; Spratt, Walden and Shaw, 2014). Conversely, Cys-independent E3s such as the RING (Really Interesting New Gene) and U-box E3s facilitate the direct transfer of ubiquitin between E2 and substrate by providing a scaffold that orients the ubiquitin-charged E2 relative to the substrate (Deshaies and Joazeiro, 2009). In humans, 2 E1s, 40 E2s and over 600 E3s exist, whereas *S. cerevisiae* has 1 E1, 11 E2s and 60-100 E3s (Lorenz *et al.*, 2013; Finley *et al.*, 2012). Ubls such as the small ubiquitin-related modifier (SUMO) and neuronal precursor cell-expressed developmentally downregulated protein 8 (Nedd8) have a similar, but distinct, E1-E2-E3 conjugation pathway to that of ubiquitin and will be discussed later (Taherbhoy, Schulman and Kaiser, 2012). The removal of ubiquitin modifications is carried out by DUBs, of which there are around 100 in humans and 20 in *S. cerevisiae* (Hutchins et al., 2013; Finley et al., 2012).

1.2.2 Diversity and roles of ubiquitin modifications

Ubiquitination begins with the conjugation of a single ubiquitin onto one (monoubiquitination) or more (multi-monoubiquitination) sites on the substrate and the optional extension of these modifications with additional ubiquitins to form chains (polyubiquitination). Beyond this, a huge diversity of ubiquitin modifications exists, due in part to the ability of ubiquitin to be conjugated onto any of the ε-amino groups of its 7 lysine side chains or on the α-amino group of its N-terminus. This allows for the formation of polyubiquitin chains with a large range of conformations. These can be described as homogeneous (ubiquitins connected by the same linkage type), heterogenous (ubiquitins connected by different linkage types), linear and/or branched in nature. An additional layer of complexity is added by the ability of ubiquitin to be acetylated at 6 different sites, phosphorylated on at least 9 sites and modified with other Ubls, including SUMO and Nedd8 (Swatek and Komander, 2016; Komander and Rape, 2012). This huge array of

potential modifications allows ubiquitin to play roles in diverse processes including cell cycle control, intracellular trafficking, epigenetic regulation, mitophagy and proteasomal degradation (Swatek and Komander, 2016). For example, Lys48-linked chains, the most common ubiquitin chain type, target proteins for proteasomal degradation. In contrast, Lys63-linked chains typically provide a non-degradative signal, for example to promote recruitment of proteins to sites of DNA damage or regulate the NF-κB signalling pathway (Komander and Rape, 2012; Chen and Sun, 2009). Of the less common linkage types, Met1 has been linked to NF-κB pathway activation (Rahighi *et al.*, 2009), Lys6 to UV genotoxic stress and mitochondrial homeostasis (Elia *et al.*, 2015; Durcan *et al.*, 2014), Lys11 to proteasomal degradation tied to cell cycle regulation and the DNA damage response (Wickliffe *et al.*, 2011; Paul and Wang, 2017), Lys27 to triggering protein recruitment (Swatek and Komander, 2016), Lys29 to epigenetic regulation and the innate immune response (Swatek and Komander, 2016; Yu *et al.*, 2016) and Lys33 to numerous processes including intracellular trafficking (Yuan *et al.*, 2014). Branched chains can also have distinct functions. For example, Lys63-linked polyubiquitination of the tumour suppressor TXNIP by the human E3 ligase ITCH seeds assembly of Lys48/Lys63 branched chains that target TXNIP for proteasomal degradation (Ohtake *et al.*, 2018).

Specificity exists within the ubiquitin system both at the level of interactions between different ubiquitination enzymes (E1-E2 and E2-E3 interactions) and between E2 and E3 enzymes and the types of ubiquitin chain that they form. A few examples of such specificity in the human ubiquitin system will be described here. Some enzymes, such as the RBR E3 ligase HOIP, exclusively produce one kind of chain linkage, in this case Met1-linked chains (Kirisako *et al.*, 2006). Alternatively, E2 and E3 enzymes can have broader specificity, allowing them to form different chain linkages. For example, the HECT E3 ligase AREL1 mainly assembles Lys33, Lys11 and Lys48 linkages (Michel *et al.*, 2015). In some contexts, chain specificity can be provided at the level of E2s, as for the Lys11-specific UBE2S, which is utilised by the anaphase-promoting complex or cyclosome (APC/C), a multiprotein E3 ubiquitin ligase complex critical for cell cycle regulation (Wickliffe *et al.*, 2011). The APC/C is also interesting in that its predominant ubiquitination activity involves the formation of branched Lys48/Lys11 chains, which act as signals for proteasomal degradation (Swatek and Komander, 2016). Like E2s and E3s, most DUBs show specificity towards one or more types of ubiquitin chain linkage. As examples, OTULIN exhibits total specificity for Met1-linked polyubiquitin chains and USP30 preferentially cleaves Lys6 linkages (Keusekotten *et al.*, 2013; Rivkin *et al.*, 2013; Cunningham *et al.*, 2015; Gersch *et al.*, 2017).

While ubiquitin exerts many of its biological roles through its conjugation to substrate proteins, unanchored ubiquitin chains and even single ubiquitin molecules can perform additional, second-messenger-like functions (Swatek and Komander, 2016; Xia *et al.*, 2009; Banerjee *et al.*, 2014). For example, Xia *et al.* (2009) showed that unanchored Lys63 polyubiquitin chains could activate both TAK1 and IKK, protein kinases in the human NF-κB signalling pathway. In the case of TAK1, this seems to occur via binding of Lys63 chains to TAK1-binding proteins TAB2 or TAB3, resulting in the dimerisation, auto-phosphorylation and subsequent activation of TAK1 (Sato *et al.*, 2009; Xia *et al.*, 2009). In another report, unanchored ubiquitin chains were shown to be carried by the influenza A virus in order for it to hijack the host aggresome pathway and allow viral uncoating (Banerjee *et al.*, 2014). Other possible roles for acetylation or phosphorylation of ubiquitin include control of chain architecture, since such modification of the relevant amino acid residues would simultaneously preclude ubiquitination at these sites (Swatek and Komander, 2016). Phosphorylation on Ser65, for example, affects the ability of ubiquitin to be assembled into chains (Wauer *et al.*, 2015; Swaney, Rodríguez-Mias and Villén, 2015). Additionally Ser65-phosphoUb acts as an "activator ubiquitin" that contributes allosterically to the activation of the human RBR E3 ligase Parkin (Swatek and Komander, 2016).

1.2.3 E1 ubiquitin-activating enzymes

During the first step of ubiquitination, an E1 enzyme binds $ATPMg^{2+}$ and ubiquitin to allow it to catalyse adenylation of the ubiquitin C-terminus. Subsequently, the catalytic cysteine residue of the E1 attacks the ubiquitin-adenylate intermediate, forming an E1~Ub thioester-linked complex (Schulman and Harper, 2009). As per common convention, a tilde (~) is used here to indicate a thioester covalent bond, whereas a dash (-) indicates a non-thioester covalent linkage. Subsequently, a second ubiquitin is adenylated by the E1 and triggers transfer of ubiquitin to an E2 enzyme via trans-thioesterification (Pickart *et al.*, 1994; Huang *et al.*, 2007; Schulman and Harper, 2009). E1s are thought to have evolved from the bacterial enzymes molybdopterin biosynthetic enzyme B (MoeB) and ThiF (ThiS adenylyltransferase), which catalyse the adenylation of MoaD and ThiS during Moco and thiamine synthesis respectively (Taylor *et al.*, 1998; Leimkühler, Wuebbens and Rajagopalan, 2001). Indeed, sequence homology can be observed between MoeB and ThiF and the Ubl recognition/adenylation domains of all eukaryotic E1s. Other structural features include the catalytic cysteine domain and a C-terminal ubiquitin-fold domain that binds to the N-terminus of E2s (Schulman and Harper, 2009; Stewart *et al.*, 2016).

In humans, there are two E1s for ubiquitin, UBA1 and UBA6, which share only 40% amino acid identity with one another (Jin *et al.*, 2007; Pelzer *et al.*, 2007; Chiu, Sun and Chen, 2007). Notably, UBA6 has a more restricted E2 specificity than UBA1, including utilisation of a UBA6-specific E2, UBE2Z (Jin *et al.*, 2007). However, UBA6 has also been shown to conjugate the Ubl FAT10 (Chiu, Sun and Chen, 2007). Notably, UBA1 appears to be regulated by phosphorylation (Stephen *et al.*, 1997; Schulman and Harper, 2009). UBA1 and UBA6 are examples of canonical E1s, since only one of their two MoeB/ThiF-homologous repeats are involved in ATPMg^{2+} and Ubl binding. Non-canonical E1s, in contrast, contain two functional adenylation domains (Schulman and Harper, 2009). In *S. cerevisiae*, which has only one E1, deletion of the UBA1 gene is lethal (McGrath, Jentsch and Varshavsky, 1991).

Since ubiquitination regulates such a wide range of biological processes, dysregulation of the system can lead to numerous diseases including cancer and neurodegeneration (Zhang, Linder and Bazzaro, 2020; Graham and Liu, 2016). As a result, components of the ubiquitination system have attracted substantial attention for their potential as drug targets. The targeting of E1 enzymes, which have a well-defined catalytic pocket, is one such area of exploration. Existing UBA1 inhibitors include PYR-41, the first cell permeable UBA1 inhibitor to be identified, and PYZD-4409, both of which preferentially induce cell death in malignant cells (Yang *et al.*, 2007; Xu *et al.*, 2010). However, there are no inhibitors of ubiquitin E1 enzymes in clinical trials, and, since E1s exert effects on a huge number of proteins by virtue of their position at the start of the ubiquitination cascade, inhibition of E1s is likely to cause toxicity. Consequently, targeting of more downstream ubiquitination system components, such as E2s and E3s, may provide a better therapeutic strategy (Huang and Dixit, 2016).

1.2.4 E2 ubiquitin-conjugating enzymes

After ubiquitin is transferred from E1 to E2 enzyme, E2s facilitate the transfer of ubiquitin to substrate protein. In most cases, this involves interactions between E2s and E3 ligases. The core catalytic, or UBC, domain of E2s consists of around 150 amino acids (including the conserved catalytic cysteine residue) that form 4 α-helices and a 4-stranded β-sheet. Additionally, some E2s, like UBE2O, possess N- and/or C-terminal extensions. In addition to the catalytic cysteine residue, a conserved HPN loop is typically found in catalytically competent members of the E2 family, usually 10 amino acids N-terminal to the catalytic cysteine (Wenzel, Stoll and Klevit, 2011). In the past, this asparagine has been proposed to stabilise the oxyanion intermediate formed during the

nucleophilic attack of lysine on E2-Ub (Wu *et al.*, 2003; Jones *et al.*, 2019). However, structural studies suggest that the main role of N79 is to stabilise an active site loop required for catalytic activity (Berndsen *et al.*, 2013).

As discussed previously, E2s, of which there are 40 in humans, often show specificity for the formation of different ubiquitin linkage types (Stewart *et al.*, 2016). Similarly, E2s can possess ubiquitin chain priming activity (addition of monoubiquitin to substrates) and/or extension activity (extension of chains on monoubiquitinated substrates) (Christensen, Brzovic and Klevit, 2007; Windheim, Peggie and Cohen, 2008). The building of ubiquitin chains on E2s prior to *en bloc* transfer of the whole ubiquitin chain to substrate is also possible, as has been observed during ubiquitination of human proliferating cell nuclear antigen (PCNA) (Masuda *et al.*, 2012). An additional role for E2s in regulating protein activity is seen in the ability of some E2s to regulate DUB or kinase activity by binding to them (Wiener *et al.*, 2013; Pruneda *et al.*, 2014).

Notably, E2 activity can be regulated by the non-covalent binding of proteins opposite the E2 active site, also known as “backside binding” (Stewart *et al.*, 2016). The first example of this to be described was the non-covalent binding of ubiquitin to the backside of human UBE2D3, which promotes its ubiquitin chain building activity (Brzovic *et al.*, 2006). Backside binding has also been shown to restrict the ubiquitination activity of some E2s, as is seen in the restriction of human UBE2E3 activity to monoubiquitination (versus polyubiquitination) by backside binding with ubiquitin (Nguyen *et al.*, 2014). SUMOylation, phosphorylation, alkylation and disulphide bond formation also regulate the activity of E2s. In the case of ubiquitination, this can be achieved through targeting of the E2 for proteasomal degradation or through alternative mechanisms, such as allosteric regulation (Stewart *et al.*, 2016). For example, UBE2T, a human E2 involved in the Fanconi Anaemia DNA repair pathway, exhibits decreased ubiquitin transfer activity following its multi-monoubiquitination (Machida *et al.*, 2006). E2 activity can also be regulated by N-terminus phosphorylation, since such modifications can inhibit E1 and E3 interactions (Lv *et al.*, 2017).

Due to their greater numbers, E2s offer more substrate specificity than E1s. This makes them more attractive as potential drug targets. Although E2 enzymes have yet to be targeted therapeutically, the identification of CC0651, a specific allosteric inhibitor for the human E2 CDC34, shows that targeting of these enzymes is possible in principle (Ceccarelli *et al.*, 2011). Despite this promising discovery, difficulties in optimisation have prevented the further development of CC0651 (Huang and Dixit, 2016). Inhibitors of

human UBE2N, an E2 that functions as a heterodimer with catalytically inactive ubiquitin E2 variant (UEV) family proteins (namely UBE2V1 and UBE2V2) have also been described (Hodge, Spyracopoulos and Glover, 2016). In particular, investigation into the interaction between UBE2N and covalent inhibitors NSC697923 (UBE2N-specific (Pulvino *et al.*, 2012)) and BAY 11-7082 (broad E2 inhibitor) revealed that the groove occupied by the NSC697923 derivative in UBE2N is occluded in other E2s, suggesting that UBE2N-specific inhibitors could be developed (Hodge *et al.*, 2015). Furthermore, successful development of an assay to screen for inhibitors of the UBE2N/RNF8 interaction highlights the range of strategies that could be utilised to target UBE2N and could be applied to the targeting of other E2 enzymes (Weber *et al.*, 2017).

1.2.5 E3 ubiquitin ligases

E3 ligases assist or directly catalyse the transfer of ubiquitin from an E2 to the substrate protein. There are two functional categories of E3, the Cys-dependent E3s (HECT and RBR E3s) and Cys-independent E3s (RING and U-box E3s) (Metzger, Hristova and Weissman, 2012; Spratt, Walden and Shaw, 2014; Deshaies and Joazeiro, 2009). Structurally, HECT E3s contain a C-terminal, conserved HECT domain of around 350 amino acids that is divided into 3 parts. The N-terminal N-lobe interacts with the E2 and the C-terminal C-lobe contains an active site cysteine that reacts with ubiquitin to form a thioester linkage. These are connected by the third and final part, a flexible linker region that allows the N- and C-lobes to move such that the E2 and E3 active sites are brought closer together, facilitating ubiquitin transfer between the E2 and E3 (Sluimer and Distel, 2018; Huang *et al.*, 1999). Notably, the ubiquitin chain linkage specificity of HECT E3s appears to originate from the last 60 amino acids of the HECT domain C-lobe (Kim and Huibregtse, 2009). In contrast to the C-terminus, the N-terminus of HECT E3s is more diverse and functions in substrate interaction, often harbouring protein or lipid interaction domains (Metzger, Hristova and Weissman, 2012; Rotin and Kumar, 2009). In humans, 28 HECT family E3s exist and function in diverse processes including protein trafficking, cell signalling and the immune response (Scheffner and Kumar, 2014; Rotin and Kumar, 2009). These are subdivided into 3 families based on the structure of their N-termini. Nedd4 family members, of which there are 9 in humans, contain an N-terminal C2 (phospholipid-binding) domain and 2-4 WW (protein-binding) domains. HERC family members, of which there are 6, have regulator of chromosome condensation 1 (RCC1)-like domains. The third group is formed of HECT E3s that do not fit into either of the other two families and have diverse N-terminal domains (Rotin and Kumar, 2009). In contrast, *S. cerevisiae* has 5 HECT E3s (Finley *et al.*, 2012). Interestingly, two bacterial effector

proteins, *Salmonella* SopA and *Escherichia coli* NleL, resemble HECT E3s, suggesting that these pathogens interact with the host ubiquitination system during infection (Diao *et al.*, 2008; Lin *et al.*, 2011; Lin, Diao and Chen, 2012).

RBR family E3s utilise a hybrid catalytic mechanism that incorporates aspects of both HECT and RING E3 behaviour, first reported for the human RBR E3 HHARI (Wenzel *et al.*, 2011). Structurally, they contain a RING1 domain which is involved in E2 interactions, an R_{cat} (required-for-catalysis) domain containing a catalytic cysteine residue to which ubiquitin is transferred and a BR_{cat} (benign-catalytic) domain (also known as an in-between-ring or IBR domain), which is structurally similar to the R_{cat} domain but lacks the catalytic cysteine residue. These are arranged in the following order: RING1-BR_{cat}-R_{cat} (Spratt, Walden and Shaw, 2014). The activity of most RBR E3 ligases is regulated by auto-inhibition, with conformational changes required to trigger their activation (Dove and Klevit, 2017). For example, the RBR E3 Parkin, which has been implicated in the neurodegenerative disorder Parkinson's disease, is auto-inhibited by its ubiquitin-like domain and can be activated through substrate binding (Chaugule *et al.*, 2011; Smit and Sixma, 2014). Similarly, the ubiquitin-associated (UBA) domain of the RBR E3 HOIP is involved in its auto-inhibition. When another RBR E3 ligase, HOIL-1L, sequesters this UBA domain, HOIP activation occurs (Lechtenberg *et al.*, 2016). Additional inhibitory domains include Ariadne domains (found in multiple RBR E3s) and the RING0 domain of Parkin (Spratt, Walden and Shaw, 2014). Around 15 RBR E3 ligases exist in humans whereas *S. cerevisiae* has 2 RBR E3s (Eisenhaber *et al.*, 2007; Finley *et al.*, 2012). RBR E3s are thought to be regulated by alternative splicing and phosphorylation (Eisenhaber *et al.*, 2007; Spratt, Walden and Shaw, 2014). Like other E3s, RBR E3s are involved in a wide range of cellular processes including endoplasmic reticulum-associated degradation (ERAD), cell cycle regulation and regulation of translation (Eisenhaber *et al.*, 2007).

RING family E3s represent the largest class of E3 ligases, with more than 300 putative RING E3 genes present in the human genome and around 50 in *S. cerevisiae* (Li *et al.*, 2008; Finley *et al.*, 2012). As Cys-independent E3s, RING E3s contain a RING domain, which binds to the E2 enzyme, and substrate-interaction domains. These features allow them to facilitate the direct transfer of ubiquitin from E2 to substrate. More specifically, RING domains contain conserved cysteine and histidine residues that bind two zinc atoms and are found in a "cross-brace" arrangement as follows: Cys-X_2-Cys-$X_{(9-39)}$-Cys-$X_{(1-3)}$-His-$X_{(2-3)}$-Cys-X_2-Cys-$X_{(4-48)}$-Cys-X_2-Cys (where X is any amino acid). Unlike the catalytic cysteines of HECT and RBR E3 enzymes, however, RING domain cysteines do

not form covalent linkages with ubiquitin (Deshaies and Joazeiro, 2009). Notably, binding of E2s to RING domains has been shown to result in allosteric activation of the E2 (locking of the E2~Ub conjugate into a closed conformation), stimulating ubiquitin release (Ozkan, Yu and Deisenhofer, 2005; Plechanovová *et al.*, 2012; Branigan, Carlos Penedo and Hay, 2020). Contributing to their diversity, RING E3s can be found in monomeric, homo- or hetero-dimeric forms or as components of multi-subunit complexes, such as in the case of the cullin RING ligase (CRL) family (Metzger, Hristova and Weissman, 2012; Petroski and Deshaies, 2005). Typically, CRLs contain a catalytic core consisting of a RING E3 ligase and a cullin family member, substrate receptors and adaptor proteins which form a bridge between the catalytic core and substrate receptor (Petroski and Deshaies, 2005). Structurally, the U-box domain of U-box E3 ligases is similar to the RING domain but is stabilised by hydrogen bonds and salt bridges rather than by two zinc atoms (Metzger, Hristova and Weissman, 2012). There are 9 U-box family members in humans and 2 in *S. cerevisiae* (Li *et al.*, 2008; Finley *et al.*, 2012). Other variations on the RING domain include the RING-CH-type domain, found in the MARCH subfamily of RING E3 ligases that function in immune regulation. In humans, 11 RING-CH-type E3s have been reported, whereas only one has been identified in *S. cerevisiae* (Lin, Li and Shu, 2019).

Altogether, around 600 E3s are predicted to exist in the human genome (Li *et al.*, 2008). Due to their abundance and diversity (including in the catalytic mechanism utilised), it is thought that E3s can provide a better source of new drug targets than E1s and E2s, since compounds with higher specificity and lower toxicity can more easily be developed (Huang and Dixit, 2016). For example, the F-box substrate receptor component of the Skp Cullin F-box (SCF) RING E3 ligase SCF^{SKP2}, SKP2, has been shown to be overexpressed in numerous human cancers and inversely correlates with the expression of $p27^{KIP1}$, a cell cycle regulator and SCF^{SKP2} substrate. Multiple inhibitors that act by inhibiting protein-protein interactions with SKP2 have been shown to impair the ability of SCF^{SKP2} to ubiquitinate $p27^{KIP1}$ and promote its degradation (Wu *et al.*, 2012; Chan *et al.*, 2013). Similarly, the overexpression of MDM2, an E3 ligase that regulates the degradation of the tumour suppressor p53, has been reported in many cancers. Numerous inhibitors of MDM2 have been developed, including the Nutlin class of compounds, which has entered clinical trials (Huang and Dixit, 2016; Vassilev *et al.*, 2004). Inhibitors targeting inhibitor of apoptosis proteins (IAPs), which are also implicated in human cancers, have additionally entered clinical trials. Although the field of E3 ligase drug development is still in its early stages, the development of SKP2-, MDM2- and IAP-targeted drugs, which inhibit these enzymes by interfering with their protein-protein

interactions, shows that it is possible to target Cys-independent E3 enzymes, despite them having previously been labelled as “undruggable” (Huang and Dixit, 2016).

Another area of ubiquitin system research attracting substantial interest is proteolysis-targeting chimeric molecules, also known as PROTACs. PROTACs are heterobifunctional molecules consisting of a ligand that binds an E3 ligase connected via a linker region to a second ligand that binds a protein of interest. With this arrangement, PROTACs can bring E3 ligases into close proximity with a desired substrate, permitting the selective ubiquitination and subsequent degradation of these proteins (Huang and Dixit, 2016). Since PROTAC approaches result in the complete destruction of proteins of interest and do not rely on small-molecule-based inhibition of well-defined active sites, they offer the advantages of being able to target a wider range of proteins and of being able to remove all potential protein functions (Nalawansha and Crews, 2020). Indeed, PROTACs have been used to target a variety of substrates including epigenetic readers, kinases and transmembrane receptors (Zhou *et al.*, 2020). In the early days of PROTAC research, PROTACs were peptides. In recent years, however, the synthesis of smaller, more drug-like molecules has been possible (Huang and Dixit, 2016). Currently, two orally bioavailable PROTACs are in phase I clinical trials. The first, ARV-110, targets the androgen receptor and is being tested for its application in the context of prostate cancer. The second, ARV-471, acts on the oestrogen receptor and is being tested for its effectiveness in breast cancer treatment (Mullard, 2019).

Additional players in the formation of ubiquitin chains include E4 enzymes, which catalyse the extension of existing ubiquitin chains to control their size and/or shape (Neutzner and Neutzner, 2012). The first E4 ligase to be described was the U-box-type E4 UFD2 in *S. cerevisiae* but, since then, numerous other E4s have been identified (Koegl *et al.*, 1999). These include the U-box type E4 named carboxyl terminus of HSC70-interacting protein (CHIP) in humans and the non-U-box E4s p300 in humans and BUL1-BUL2 in *S. cerevisiae* (Hoppe, 2005). As an example of E4 function, the E4 activity of the human HECT E3/E4 ligase UBE3A is responsible for enhancing and sustaining Lys48- and Lys63-linked ubiquitin chains at double-stranded DNA breaks. These modifications are required for the recruitment of proteins involved in DNA repair (Baranes-Bachar *et al.*, 2018).

1.2.6 Deubiquitinating enzymes

DUBs are responsible for ubiquitin chain removal and editing, which can function to maintain the pool of free ubiquitin in the cell, protect proteins from proteasomal degradation and/or change the overall signal provided by ubiquitin modifications (Komander and Rape, 2012). Over 100 DUB genes have been identified in the human genome and can be divided into 7 structural classes: ubiquitin C-terminal hydrolases (UCHs), ubiquitin-specific proteases (USPs), ovarian tumour proteases (OTUs), Josephins, motif interacting with Ub-containing novel DUB family (MINDY), zinc finger with UFM1-specific peptidase domain protein (ZUFSP) and JAB1/MPN/MOV34 metalloenzymes (JAMM/MPN+) (Ndubaku and Tsui, 2015; Abdul Rehman *et al.*, 2016; Hermanns *et al.*, 2018). Of these classes, the JAMM/MPN+ family are metalloenzymes, whereas the other 6 classes contain cysteine proteases (Ndubaku and Tsui, 2015). As has previously been discussed, DUBs often demonstrate specificity for the cleavage of certain ubiquitin linkage types (Neutzner and Neutzner, 2012). The balance of cellular ubiquitination and de-ubiquitination activity determines the functional outcome of ubiquitination on protein substrates. Despite this, both E3 ligase and DUB activities have been observed in a single protein, with these activities observed to cooperate in a non-antagonistic manner. In this case, the DUB portion of the human dual E3 ligase/DUB A20 removes Lys63-linked ubiquitin chains from the target protein receptor interacting protein (RIP), which is subsequently polyubiquitinated by the E3 portion to form Lys48-linked chains, targeting RIP for degradation (Wertz *et al.*, 2004).

Similar to E1, E2 and E3 enzymes, DUBs have attracted interest as potential drug targets due to their dysregulation in various human diseases, including cancer. Inhibition of DUBs can be used to increase the degradation of specific target proteins that are stabilised in disease contexts or may suppress other DUB functions. For example, multiple selective inhibitors of USP7, which has a critical role in p53 regulation, have been developed and include P5091, which induces apoptosis of both cultured and patient multiple myeloma cells, and FT671, which inhibits tumour growth in mice (Huang and Dixit, 2016; Chauhan *et al.*, 2012; Turnbull *et al.*, 2017). Although drugs targeting DUBs have yet to enter clinical trials, this strategy offers substantial promise for future drug development (Huang and Dixit, 2016; Yuan *et al.*, 2018).

1.2.7 The proteasome

Many types of ubiquitin modification, including Lys48- and Lys11-linked chains, target proteins for proteasomal degradation. Indeed, regulation of protein turnover is one of the most predominant and well-characterised functions of the ubiquitination system. Proteasomes, which are large protein complexes, degrade proteins in both the nucleus and the cytosol of eukaryotic cells (Muñoz *et al.*, 2015). In various eukaryotes including mammals and *S. cerevisiae*, they consist of two subcomplexes: the 20S proteasome, which is the highly conserved, core catalytic particle, and one or two 19S regulatory particles which bind at either end of the 20S proteasome to activate it. When combined, these subcomplexes are referred to as the 26S proteasome. The 20S subunit is barrel-shaped and made up of 4 rings, each of which contains either 7 α or 7 β subunits (Tanaka, 2009). These rings are stacked so as to have two outer α-rings and two inner β-rings (Muñoz *et al.*, 2015). The β1, β2 and β5 subunits have threonine protease activity that is peptidyl-glutamyl peptide-hydrolysing, trypsin-like and chymotrypsin-like respectively, allowing them to cleave the peptide bonds associated with acidic, basic and hydrophobic amino acids. This activity generates oligopeptides of 3-15 amino acids long that can be further processed in the cytosol into free amino acids. The 19S particle consists of around 20 subunits and is responsible for the recognition of proteins marked for degradation by polyubiquitin, removal of ubiquitin chains, protein unfolding and the transfer of substrates to the interior of the 20S particle (Tanaka, 2009).

Currently, 3 proteasome inhibitors are approved by the Food and Drug Administration (FDA) of the United States of America, mainly for the treatment of multiple myeloma: bortezomib, carfilzomib and ixazomib (Huang and Dixit, 2016; Park *et al.*, 2018). Bortezomib predominantly acts by reversibly forming tetrahedral adducts with the threonine residues of β5 proteasomal subunits, inhibiting their chymotrypsin-like activity and leading to a number of potentially beneficial effects. In contrast, carfilzomib binds irreversibly to the threonine residues of β5 subunits, preventing substrate proteins from accessing its catalytic residues. Due to its irreversible mechanism of inhibition, carfilzomib is more potent than bortezomib (Huang and Dixit, 2016). A major disadvantage of both bortezomib and carfilzomib is that they must be systemically administered. Ixazomib, the most recent proteasome inhibitor to become FDA-approved, offers the advantage of being orally bioavailable, while still acting to inhibit the β5 (and to a lesser extent the β1 and β2) proteolytic subunits (Hungria *et al.*, 2019). Other proteasome inhibitors are currently being evaluated in clinical trials for improved efficacy, pharmacokinetics and pharmacodynamics (Park *et al.*, 2018).

1.2.8 Ubiquitin-like modifiers

Ubls represent a group of proteins that are related to ubiquitin in three-dimensional structure but may have divergent secondary sequences. In humans, these include SUMO, Nedd8, autophagy-related protein 8 (Atg8), autophagy-related protein 12 (Atg12), interferon-stimulated gene 15 (ISG15), HLA-F adjacent transcript 10 (FAT10), ubiquitin-fold modifier 1 (Ufm1) and ubiquitin-related modifier 1 (Urm1) (van der Veen and Ploegh, 2012). SUMO, which has a large number of nuclear substrates, has roles in transcription, chromatin organisation, nuclear transport and DNA repair (Gill, 2004). It has also been reported to regulate the ubiquitination system. For example, association of one SUMO family member, SUMO-1, with the RBR E3 Parkin is known to modulate its activity and cellular localisation (Um and Chung, 2006). Additionally, neddylation plays a substantial role in regulating ubiquitination through targeting cullin RING E3 ligases, which are neddylated on a conserved lysine residue in the cullin-homology domain, resulting in enhanced ubiquitination activity (Osaka *et al.*, 2000; Petroski and Deshaies, 2005). In most cases, Ubls have their own dedicated E1, E2, E3 and Ubl-specific protease enzymes. For SUMO, the SAE1/SAE2 heterodimer, also known as AOS1/Uba2, and Ubc9 are the dedicated E1 and E2 enzymes respectively. For Nedd8, the dedicated E1 and E2 enzymes are NAE1/Uba3 and Ubc12 respectively. In the heterodimeric E1s SAE1/SAE2 and NAE1/Uba3, SAE2 and Uba3 contain the conserved catalytic cysteine residues, whereas SAE1 and NAE1 are non-catalytic subunits (van der Veen and Ploegh, 2012). While SAE1/SAE2, NAE1/Uba3 and UBA7 (ISG15 E1) are canonical E1 enzymes, the E1 enzymes for Ufm1, Urm1 and Atg8/Atg12 are non-canonical in structure (Schulman and Harper, 2009).

1.3 Ubiquitination in trypanosomatids

1.3.1 Discovery of the trypanosomatid ubiquitin system

Ubiquitin is found in all eukaryotic organisms, including trypanosomatids. Initial studies performed in the 1980s and 1990s identified and partially characterised ubiquitin genes belonging to members of the *Trypanosoma* and *Leishmania* genera. Tandemly repeating ubiquitin sequences, consisting of multiple repeats of the 76 amino acid ubiquitin sequence, were found to be present in these species, similar to what had been observed for other eukaryotic organisms such as *S. cerevisiae*. These sequences encode polyubiquitins that can be proteolytically processed into functional, monomeric ubiquitins (Jonnalagadda *et al.*, 1987; Kirchhoff *et al.*, 1988). The amino acid sequence of ubiquitin is highly conserved in trypanosomatids, with only 2 amino acids differing between *L.*

major and human ubiquitin, 4 differing between *T. brucei* and human and 3 between *T. cruzi* and human (Graeff *et al.*, 1993; Wong and Campbell, 1989; Télles *et al.*, 1999). However, trypanosomatids are distinct in having high numbers of ubiquitin repeats, with ≥44 found to be present in a single gene in *L. donovani*, ≥30 in *T. brucei* and ≥17 in *T. cruzi* (Kirchhoff *et al.*, 1988). Prior to this, the highest number of ubiquitin repeats within a single gene reported was 12, observed in *Xenopus laevis* (Dworkin-Rastl, Shrutkowski and Dworkin, 1984). Contrastingly, only 5 ubiquitin repeats are found in the *S. cerevisiae* polyubiquitin gene (Ozkaynak *et al.*, 1987). Polymorphism in the number of ubiquitin repeats were also observed between alternative gene alleles and different strains of *T. brucei*, suggesting that heterogeneity is common both between and within species (Wong *et al.*, 1992). Considerable heterogeneity was also observed at the transcript level for both the number and sizes of ubiquitin coding RNAs present in the trypanosomatid species (including *T. brucei*, *T. cruzi*, *L. mexicana* and *L. donovani*) profiled (Kirchhoff *et al.*, 1988).

Typically, ubiquitin is encoded either as polyubiquitin (multimers of ubiquitin coding regions) or as fusion proteins consisting of the ubiquitin sequence followed by a different protein at the C-terminus (Callis, 2014). Accordingly, *T. cruzi* contains 5 copies of a ubiquitin fusion (*FUS*) gene consisting of a single copy of ubiquitin fused to a 52 amino acid-long sequence at the C-terminus (Kirchhoff *et al.*, 1988; Swindle *et al.*, 1988). Also present are 5 polyubiquitin gene (*PUB*) copies, consisting of multiple tandem repeats of the ubiquitin sequence terminating in a fusion protein coding sequence (Swindle *et al.*, 1988). Both of these types of gene are clustered closely in the genome. Similar to the *T. cruzi FUS* gene, *L. major* and *T. brucei* contain a ubiquitin fusion gene consisting of a single ubiquitin sequence fused to a 52 amino acid-long sequence (Graeff *et al.*, 1993). In *T. cruzi*, *L. major* and *T. brucei*, this additional 52 amino acid-long protein contains a putative zinc finger domain and is annotated as ribosomal protein S27a in TriTrypDB (Graeff *et al.*, 1993; Swindle *et al.*, 1988; Finley, Bartel and Varshavsky, 1989; TriTrypDB, 2020). *L. tarantolae* was also shown to contain both polyubiquitin-encoding (*ubiC*) and ubiquitin fusion protein genes (*ubiA* and *ubiB*), all of which are expressed (Fleischmann and Campbell, 1994). Unlike the *T. cruzi* FUS genes, *T. brucei* polyubiquitin genes appear to terminate with a single amino acid extension (Wong and Campbell, 1989).

In addition to the inter- and intra-species differences observed in ubiquitin repeat number between trypanosomatids, differences in transcript size were also seen between different life cycle stages, specifically between procyclic (PCF) and bloodstream form (BSF) *T.*

brucei rhodesiense (Kirchhoff *et al.*, 1988). Differences in ubiquitin gene expression were also observed between logarithmic and stationary phase *T. cruzi* (Swindle *et al.*, 1988). In this case, expression of *PUB* genes was increased in procyclic stationary phase cultures whereas *FUS* gene expression was reduced, indicating that ubiquitin transcripts are regulated in response to stress (Swindle *et al.*, 1988; Manning-Cela, Jaishankar and Swindle, 2006). This is similar to the upregulation of polyubiquitin observed during the *S. cerevisiae* stress response (Ozkaynak *et al.*, 1987). Differences in expression between *FUS* and *PUB* genes in *T. cruzi* trypomastigotes, epimastigotes and amastigotes were also observed, although the functional relevance of these changes are not known (Manning-Cela, Jaishankar and Swindle, 2006).

Despite the high conservation between *T. cruzi* and human ubiquitin, the two proteins are immunologically distinct, as demonstrated by the ability of antibody sera from *T. cruzi* patients to react with *T. cruzi*, but not human, ubiquitin. This is thought to be due to differences at amino acid residues 19 and 57, which lie on the surface of ubiquitin. Interestingly, *Leishmania* ubiquitin, which has different amino acids relative to *T. cruzi* at both of these residues, does not react with chagasic sera, suggesting that *T. cruzi* ubiquitin could work well as a specific diagnostic marker for Chagas disease (Télles *et al.*, 1999). *T. brucei* ubiquitin also appears to be immunologically distinct from that of human ubiquitin (Steverding, 2006).

1.3.2 Ubiquitination in the life cycle of trypanosomatids

Following the identification of ubiquitin genes in trypanosomatids, evidence of ubiquitin conjugation was obtained by Lowrie *et al.* (1993), who demonstrated incorporation of ^{125}I-labelled ubiquitin into proteins in the cytosol of *T. brucei brucei* cells. Additionally, differences in the rate of ubiquitination activity were observed between the short stumpy and long slender and intermediate BSFs, suggesting stage-specific regulation of the ubiquitination system. Complementing this, *T. cruzi* trypomastigote to amastigote differentiation has been associated with a strong increase in the cellular content of ubiquitinated proteins (de Diego *et al.*, 2001). Indeed, multiple roles for the ubiquitin-conjugating system in the life cycle of trypanosomatids have now been assigned. For example, *T. brucei* CDC27 and APC1, components of the APC/C, are required for normal cell growth in both PCFs and BSFs. In other eukaryotes, the APC/C spurs chromosome segregation and mitotic exit by ubiquitinating cell cycle regulators, triggering their degradation (Zhou *et al.*, 2016). Curiously, depletion of either CDC27 or APC1 leads to metaphase arrest in PCFs and anaphase arrest in BSFs, suggesting stage-specific

regulation of mitosis by the *T. brucei* APC/C (Kumar and Wang, 2005). Knockdown of another APC/C component, AP2, results in mitotic arrest of PCFs and stabilisation of a potential substrate, the mitotic cyclin CycB2/cyc6 (Bessat *et al.*, 2013). This demonstrates that, despite the high divergence observed between the *T. brucei* and *S. cerevisiae* APC/C components, its function in mitotic exit is conserved. Interestingly, deletion of only 3 out of the 10 identified APC/C components produces a phenotype, showing that the *T. brucei* APC/C has a smaller group of core components than the *S. cerevisiae* one (Bessat *et al.*, 2013; Kumar and Wang, 2005).

A similar, component-by-component investigation into a putative *T. brucei* SKP1-CULLIN1-F-box complex (SCFC), another multi-subunit E3 complex important for cell cycle progression, revealed a conserved role for SKP1 in the G1/S transition, a possible role for RBX1 in kinetoplast DNA (kDNA) replication and a role for the E2 ubiquitin-conjugating enzyme CDC34 in cytokinesis. Presumably due to the rapid growth arrest observed in cells in which CDC34 is depleted, CDC34 is essential for infection progression in mice. Furthermore, no phenotype was observed following depletion of CULLIN1, suggesting that redundancy in function with other *T. brucei* cullins may exist (Rojas *et al.*, 2017).

In *Leishmania*, numerous cysteine protease DUBs are required for successful promastigote-amastigote differentiation, namely DUBs 4, 7 and 13. Furthermore, DUBs 3, 5, 6, 8, 10, 11 and 14 are required for normal amastigote proliferation in mice and, in promastigotes, DUBs 1, 2, 12 and 16 are essential, demonstrating stage-specific requirements for different DUBs in the *Leishmania* life cycle. Additionally, DUB2, which has broad linkage specificity and is related to human USP5 and USP13, was validated as an essential gene in *L. mexicana*, further demonstrating that components of the ubiquitin system, including *T. brucei* CDC34 and *L. mexicana* DUB2, could provide new targets for future anti-trypanosomal therapies (Damianou *et al.*, 2020). In *T. cruzi*, differentiation of trypomastigotes to amastigotes involves the ubiquitination and consequent targeting of cytoskeletal flagellar proteins to the proteasome for degradation, demonstrating a role for the ubiquitin system in regulating morphological changes during trypanosomatid differentiation (de Diego *et al.*, 2001). Whether DUBs 4, 7 and 13 are associated with similar morphological changes during *Leishmania* differentiation is an interesting area for future investigation.

1.3.3 Roles for ubiquitin in trypanosomatid endocytosis

In numerous eukaryotic organisms, ubiquitination plays an important role in controlling receptor endocytosis and the sorting of proteins through the endosomal system (Haglund and Dikic, 2012). In *T. brucei*, the glycosomal matrix receptor PEX5 is ubiquitinated in a manner that is conserved throughout eukaryotic evolution, specifically by the E2 ubiquitin-conjugating enzyme PEX4, which also localises to the glycosome. This function of PEX4 appears to be at least partially redundant, however, since PEX5 remains ubiquitinated in a Δ*pex4* background (Gualdrón-López *et al.*, 2013). An interactome of *L. mexicana* DUB2, an essential gene, revealed association between VPS4 and a dynamin-1 like protein and DUB2, suggesting involvement of this DUB in endosomal trafficking (Besteiro *et al.*, 2006; Damianou *et al.*, 2020). Furthermore, two UBA domains in *Leishmania* myosin XXI are required for normal endocytic trafficking (and cell division), although the exact mechanism underlying this requirement is not known (Bajaj, Ambaru and Gupta, 2020). These studies demonstrate a role for ubiquitination in endocytic processes in trypanosomatids.

Following a high-throughput RNA interference (RNAi) screen to investigate genes involved in the susceptibility of *T. brucei* to suramin, Alsford *et al.* (2012) identified two genes encoding DUBs, Usp7 (UbH1) and Vdu1, that were linked to suramin action. Subsequently, Usp7 was shown to regulate expression of another hit from the screen, the invariant surface glycoprotein (ISG) ISG75, suggesting that the expression level of ISG75, which may be regulated by its ubiquitination status, was important in suramin resistance. Indeed, ensuing studies showed that the cytoplasmic domains of both ISG65 and ISG75 can be modified by ubiquitination, leading to their internalisation and degradation, probably at the lysosome (Chung *et al.*, 2008; Leung *et al.*, 2011). Cycloheximide chase experiments showed that, under normal conditions, Usp7 can destabilise ISG75 and Vdu1 destabilises both ISG65 and ISG75. Since knockdown of both Usp7 and Vdu1 results in blocked endocytosis, it is clear that the destabilisation of ISG65 and ISG75 by Usp7 and/or Vdu1 depends on the ability of these DUBs to facilitate ISG65/ISG75 endocytosis (Zoltner *et al.*, 2015). The ubiquitination of surface proteins to trigger their degradation is likely to be a common mechanism in *T. brucei*. As another example of this, BSFs contain a plasma membrane ectophosphatase that exists in mono-, di- and tri-ubiquitinated forms and localises to the flagellar pocket, suggesting its ubiquitination may serve as a signal for endocytosis (Steverding, 2006).

1.3.4 Ubiquitination and the infection process

In addition to the internal roles described for the ubiquitination system, many trypanosomatids secrete ubiquitination system components and/or manipulate the host ubiquitination system in order to achieve successful infection. For example, in *T. cruzi*-infected human cells the interaction between $cFLIP_L$, an inhibitor of death receptor-mediated host cell apoptosis, and Itch, an E3 ubiquitin ligase, is inhibited. This is thought to contribute to an observed reduction in ubiquitination and proteasomal degradation of $cFLIP_L$, thereby inhibiting apoptosis of *T. cruzi*-infected cells (Murata, Hashimoto and Aoki, 2008). Furthermore, during the acute phase of *T. cruzi* human infection, the E3 ubiquitin ligase GRAIL, a negative regulator of CD4 T cell responsiveness, was found to be upregulated in CD4 T cells. GRAIL upregulation is thought to be achieved through disruption of the Akt-mTOR pathway, resulting in the downregulation of Otubain-1, a human DUB that negatively regulates GRAIL function (Whiting *et al.*, 2011; Stempin *et al.*, 2017). During later stages of infection, GRAIL expression is downregulated as Otubain-1 expression is upregulated (Stempin *et al.*, 2017). An example in *L. infantum* involves OtuLi, a DUB with preference for K48-linked over K63-linked polyubiquitin chains and which is capable of stimulating lipid droplet biogenesis and the release of IL-6 and TNF-α from peritoneal macrophages. Although the ability of OtuLi to be secreted into host cells has yet to be confirmed, this hints at a role for this DUB in the pro-inflammatory response of macrophages during *L. infantum* infection (Azevedo *et al.*, 2017). Ubiquitin system components, including two RING E3 ligases, an E2-conjugating enzyme and two DUBs, have also been implicated in determining resistance of *T. brucei brucei* to apolipoprotein-L1 (apo-L1), a component of two trypanolytic complexes (TLF1 and TLF2) found in human serum. RNAi knockdown of one of the E3 ligases (Tb927.10.12940) in particular resulted in a dramatic increase in parasite sensitivity to apo-L1. This may help to explain the differences observed in the ability of different African trypanosome species to be lysed by human serum (Currier *et al.*, 2018).

One way in which trypanosomatids can manipulate the host ubiquitination system is by secreting their own ubiquitination system components. For example, the SPRING (secretory protein with a RING finger domain) E3 ligase of *T. cruzi* amastigotes is secreted into host cells where it becomes localised to the nucleus. Subsequently, SPRING, which is not found in *T. brucei* or *L. major*, can utilise the human E2-conjugating enzymes UBE2D1 and UBE2N. A potential substrate of SPRING is breast cancer-associated protein 3, with which it interacts and ubiquitinates *in vitro* (Hashimoto, Murata and Aoki, 2010). Manipulation of the ubiquitin system of non-mammalian hosts is also

possible. For example, during infection of the salivary glands of *Glossina morsitans* by *T. brucei*, several ubiquitin system components were found to be upregulated in the host, including a ubiquitin C-terminal hydrolase, an E1 ubiquitin-activating enzyme and an E3 ubiquitin ligase. SUMO and the proteasome subunit beta type 4 were also significantly upregulated (Kariithi *et al.*, 2016). Therefore, manipulation of both insect vector and mammalian host ubiquitination (and Ubl) systems appears to occur during the complex life cycles of trypanosomatids.

1.3.5 Trypanosomatid ubiquitin system inhibitors

Two E1 ubiquitin-activating enzymes exist in *T. brucei*, TbUBA1a (Tb927.8.2640) and TbUBA1b (Tb927.9.12650), which are both more closely related to human UBA1 than to UBA6 (Boer and Bijlmakers, 2019). Knockdown of either TbUBA1a or TbUBA1b leads to a growth defect which is made even more severe by combined knockdown of these proteins (Chung *et al.*, 2008; Alsford *et al.*, 2011). TAK-243, an ATP mimetic that inhibits human UBA1 by binding its adenylation site, showed reduced ability to bind both TbUBA1a and TbUBA1b, although the effect was more pronounced for UBA1a (Hyer *et al.*, 2018; Boer and Bijlmakers, 2019). This differential inhibition of human and trypanosome enzymes occurs due to mutations in the enzyme adenylation sites, specifically Q534 and S560 in TbUBA1a and T657 in TbUBA1b. Interestingly, the *L. major* orthologue of TbUBA1a, LmUBA1a, also shows resistance to TAK-243. These findings suggest that specific targeting of trypanosomal E1 enzymes is feasible and could provide a route for the development of new, anti-trypanosomal therapies (Boer and Bijlmakers, 2019).

In the last couple of decades, much research has been conducted into the tractability of trypanosomatid proteasomes as drug targets for treating leishmaniasis, African trypanosomiasis and Chagas disease, with promising results. Like mammals and *S. cerevisiae*, *Leishmania*, *T. brucei* and *T. cruzi* contain both 20S and 26S proteasomes (Muñoz *et al.*, 2015; Li *et al.*, 2002; de Diego *et al.*, 2001). In *L. chagasi*, the proteasome is required for cell growth and amastigote survival inside macrophages (Silva-Jardim, Horta and Ramalho-Pinto, 2004). Similarly, inhibition of the *T. brucei* proteasome using lactacystin inhibits proliferation (but not differentiation) of cells during transformation from BSF to PCF (Mutomba and Wang, 1998). Conversely, the *T. cruzi* proteasome is required for both cell growth and differentiation of parasites between trypomastigote and amastigote life cycle stages (González *et al.*, 1996; de Diego *et al.*, 2001). Selective inhibition of the trypanosomatid proteasome appears possible, as exemplified by the

ability of GNF6702, a non-competitive inhibitor, to reduce parasite burden in animal models of (cutaneous and visceral) leishmaniasis, African trypanosomiasis and Chagas disease with little toxicity to the mammalian host (Khare *et al.*, 2016). Another parasite-selective proteasome inhibitor, GSK3494245, was also shown to reduce parasite burden in a VL mouse model (Wyllie *et al.*, 2019). Therefore GNF6702, GSK3494245 or analogues thereof, have the potential to lead to new, anti-leishmanial or trypanosomal therapies. In addition, multiple HIV protease inhibitors, which include indinavir and saquinavir, have been shown to have activity against *Leishmania* or *T. cruzi in vitro* and are of particular interest in the context of HIV co-infection (Savoia, Allice and Tovo, 2005; van Griensven *et al.*, 2013; Sangenito *et al.*, 2016).

The trypanosomatid proteasome has also been utilised for vaccine development, specifically in the use of *L. donovani* LePa (related to the human 20S proteasome a-type subunit) DNA, which, when used to vaccinate Balb/c mice, reduced lesion size upon challenge with *L. major* parasites up until 7 weeks post-infection. Beyond week 7, however, lesions sizes were comparable between the vaccinated and control groups, suggesting additional vaccine components may be required to obtain a maximally protective response (Christensen *et al.*, 2000). In addition to the 20S and 26S proteasomes, *Leishmania* and *Trypanosoma* contain a bacterial-like protease, HslVU, that is found in many eukaryotes but is absent in animals (Ruiz-González and Marín, 2006). Of the 3 HslVU subunits, all are mitochondrially localised and two, HslV and HslU1, are essential for the growth of PCF and BSF *T. brucei,* adding HslVU to the list of promising drug targets for treating African trypanosomiasis (Mbang-Benet *et al.*, 2014).

1.3.6 Ubls in trypanosomatids

In *Leishmania*, the best characterised Ubls are Atg8 and Atg12, which play a role in parasite autophagy (Williams *et al.*, 2009; Williams *et al.*, 2012). In *L. major*, four *ATG8*-like genes exist, *ATG8*, *ATG8A*, *ATG8B* and *ATG8C*, 3 of which can complement ATG8 deficiency in *S. cerevisiae*. The ATG8, ATG8A, ATG8B and ATG8C proteins are differentially targeted by the cysteine peptidases ATG4.1 and ATG4.2 and, while ATG8A has been shown to play a role in starvation-induced autophagy, ATGB and ATGC do not appear to have an autophagic role (Williams *et al.*, 2009; Williams, Mottram and Coombs, 2013). A functional ATG8 conjugation system has also been found in *T. brucei* and *T. cruzi*, although differences exist in these systems relative to the *Leishmania* one (Alvarez *et al.*, 2008; Proto *et al.*, 2014). The ATG12-ATG5 conjugation system has also been

described in *Leishmania* and involves the conjugation of ATG12 to ATG5 by the E1-like enzyme ATG7 and the E2-like enzyme ATG10. ATG12-ATG5 is required for phagophore development, including the attachment of ATG8-phosphatidylethanolamine to autophagic membranes (Williams *et al.*, 2012).

Although it has yet to be properly characterised in *Leishmania*, a SUMO-conjugation system exists in *T. brucei*. TbAos1/TbUba2 (heterodimeric SUMO E1), TbUbc9 (SUMO E2) and TbSIZ1 (SUMO E3 ligase) all play a role in TbSUMO conjugation. A SUMO-specific protease, SENP, has also been described (Ye *et al.*, 2015; Klein, Droll and Clayton, 2013; López-Farfán *et al.*, 2014). TbSUMO, which has a nuclear localisation, is required for cell cycle regulation, expression of variant surface glycoprotein (VSG) genes and chromatin organisation (Liao *et al.*, 2010; López-Farfán *et al.*, 2014; Iribarren *et al.*, 2018). Additionally, the RNA pol I complex, which is responsible for VSG transcription, is SUMOylated in BSF by TbSIZ1, demonstrating one way in which SUMOylation could contribute towards VSG expression (López-Farfán *et al.*, 2014). SUMOylation of TbCentrin, which plays an important role in cell motility, has also been observed *in vitro* (Wei *et al.*, 2014; Ye *et al.*, 2015). These studies point towards roles for SUMO in both nuclear and non-nuclear functions.

Another Ubl that has been partially characterised in *T. brucei* but not in *Leishmania* is Nedd8. TbNedd8, like its putative E2-conjugating enzyme, TbUbc12, is found throughout the cell but with particular enrichment in the nucleus and flagellum. Upon depletion of TbNedd8, reduced levels of ubiquitination, DNA re-replication, impaired spindle assembly and defective FAZ filament assembly, resulting in an increase in the number of cells with detached flagella, were observed. Additionally, six cullins, namely TbCUL1-TbCUL6, were identified as substrates of TbNedd8 (Liao *et al.*, 2017). As mentioned previously, neddylation is known to positively regulate the activity of CRLs (Deshaies and Joazeiro, 2009). Based on bioinformatic evidence, a homologue of Urm1 was also predicted to exist in both *Leishmania* and *Trypanosoma* (Ponder and Bogyo, 2007). Subsequently, the structures of TbUrm1, which shares only 11% sequence identity with human ubiquitin, and TbUfm1 were determined using NMR spectroscopy (Zhang *et al.*, 2009; Diwu *et al.*, 2020). In *L. donovani,* Ufm1 conjugation involves the action of LdUba5, a Ufm1 E1 enzyme, and LdUfc1, a Ufm1 E2 enzyme. LdUfm1, LdUba5 and LdUfc1 localise to the mitochondrion and Ufmylation is important for β-oxidation and amastigote growth in macrophages (Gannavaram *et al.*, 2011; Gannavaram *et al.*, 2012). *L. donovani* Urm1, which is associated with early endosome proteins, and its E1, LdUba4, have also been identified (Sharma *et al.*, 2016). Furthermore, a novel ubiquitin-like

protein, TbUb11, which, despite possessing a conserved tertiary structure, shares less than 20% sequence identity with ubiquitin and lacks a di-glycine motif at the C-terminus, has been reported in *T. brucei* (Mi *et al.*, 2018).

1.4 Aims

Initially, the work presented in this thesis aimed to provide a broad overview of the E1, E2 and E3 ligase enzymes of *L. mexicana.* This would be achieved through the identification of related genes in the *L. mexicana* genome followed by the generation of endogenous tagging and null mutant libraries that could be used to assess the localisation and essentiality of E1, E2 and E3 proteins respectively, in addition to providing a resource for further studies. Following this, more detailed analysis would be carried out on one or more proteins deemed to be “interesting” either by virtue of their contributions to key cell biological processes or their potential as drug targets. Completion of these aims would provide valuable insight into the role of ubiquitination in *Leishmania* biology and/or facilitate the identification of new drug targets. In this thesis, the bioinformatic identification of E1, E2 and E3 genes, followed by the generation and analysis of endogenous tagging and null mutant libraries, is described first. Second, a detailed biochemical and structural analysis of an “interesting” E2-conjugating heterodimer is provided. Finally, the cellular functions of the E2-conjugating heterodimer are explored in more detail.

2 Materials and methods

2.1 Bioinformatics

2.1.1 Protein domain searches

Interpro and PFAM domain searches were performed by searching for protein motif patterns in the *Leishmania mexicana* genome using TriTrypDB (https://tritrypdb.org/tritrypdb/) versions 29 and 46. To search for E1 genes, IPR018075 (Ubiquitin-activating enzyme E1), PF10585 (Ubiquitin-activating enzyme active site [PICTLKNFP motif]), IPR019572 (Ubiquitin-activating enzyme, catalytic cysteine domain [PICTLKNFP motif]) and IPR028077 (Ubiquitin/SUMO-activating enzyme ubiquitin-like domain) were used. To look for E2 genes, IPR000608 (Ubiquitin-conjugating enzyme E2) was used. For E3 ligase genes, IPR000569 (HECT domain), PF00632 (HECT-domain [ubiquitin-transferase]), IPR002867 (IBR domain), PF01485 (IBR domain, a half RING-finger domain), IPR001841 (Zinc finger, RING-type), IPR011016 (Zinc finger, RING-CH-type), IPR003613 (U-box domain) and PF04564 (U-box) were used. UniProt (https://www.uniprot.org/) was also used to look for genes in the *L. mexicana* genome annotated with the terms “HECT” or “RBR”.

2.1.2 Other searches

Protein Basic Local Alignment Search Tool (BLAST) searches were performed in the blastp suite using the blastp algorithm. Alignments of human and *L. mexicana* E1, E2 and HECT E3 genes were performed using T-Coffee (Notredame, Higgins and Heringa, 2000) to identify the presence or absence of conserved catalytic residues. Interpro was used to identify the HECT domains used in the HECT E3 alignment. Structural annotations were performed using ESPript 3.0 (Robert and Gouet, 2014). Signal peptide prediction was performed using SignalP 5.0. Data on gene product molecular weight and orthology between *L. mexicana* and *T. brucei* genes was obtained by searching for the relevant gene identification (ID) in TriTrypDB. Gene ontology enrichment was performed in TriTrypDB by adding genes of interest to a basket and searching for gene ontology terms linked to biological processes. For this purpose, a p value cut-off of 0.05 was used.

2.2 Molecular biology

2.2.1 Polymerase chain reaction (PCR)

Primers for PCR were designed using Primer-BLAST online software (https://www.ncbi.nlm.nih.gov/tools/primer-blast/) or manually and synthesised by Eurofins or Sigma-Aldrich. Unless otherwise stated, PCRs were performed using either Q5® High-Fidelity DNA Polymerase (NEB) or LongAmp® Taq DNA Polymerase (NEB) with the manufacturer's protocols. For Q5 polymerase, the reaction setup was as follows: 1 x Q5 Reaction Buffer (NEB), 1 x Q5 High GC Enhancer (NEB), 0.2 mM deoxynucleotide triphosphates (dNTPs), 0.5 µM forward primer, 0.5 µM reverse primer, <1,000 ng template DNA, 0.02 $UµL^{-1}$ Q5 polymerase and nuclease-free water up to 25 or 50 µL. A typical PCR was run with an initial denaturation step of 98°C for 30 sec, 25-35 cycles of 98°C for 10 sec, 50-72°C (depending on primer melting temperature) for 30 sec and 72°C for the required extension time (around 30 seconds per kb of the intended target). A final extension of 72°C for 2 min was also included.

For LongAmp Taq, the reaction setup was as follows: 1 x LongAmp Taq Reaction Buffer (NEB), 0.3 mM dNTPs, 0.4 µM forward primer, 0.4 µM reverse primer, <1 µg template DNA, 0.1 $UµL^{-1}$ LongAmp Taq polymerase and nuclease-free water up to 25 µL. The PCR was run with an initial denaturation step of 94°C for 30 sec, 30 cycles of 94°C for 30 sec, 45-65°C (depending on primer melting temperature) for 30 sec and 65°C for the required extension time (around 50 sec per kb of the intended target). A final extension of 65°C for 10 min was also included.

2.2.2 Agarose gel electrophoresis

Gels were prepared using 1% or 2% (for sgDNAs) w/v agarose in 0.5 x TBE (20 mM Tris, 20 mM boric acid and 0.5 mM EDTA, pH 7.2) or 1 x TAE (40 mM Tris, 20 mM acetic acid and 1 mM EDTA, pH 8) buffer, heating in the microwave and allowing to set in plastic gel moulds with combs to produce the wells. 1 x SYBR Safe DNA Gel Stain (Invitrogen) was added to the gel mixture to allow DNA visualisation. 1 x Purple Gel Loading Dye (NEB) was added to DNA samples prior to gel loading and a few microliters of 1 kb Plus DNA Ladder (NEB) or PCRBIO Ladder I (PCR Biosystems) added alongside samples to allow estimations of fragment size. Samples were run at 100 V for 30-45 minutes, followed by visualisation (by UV illumination) and image capture on a Chemidoc (Bio-Rad).

2.2.3 Transformations

Except where otherwise indicated, transformations were performed into NEB® 5-alpha Competent *E. coli* (NEB) or NEB® Stable Competent *E. coli* (NEB) as per the manufacturer's protocols. For both cell lines, this involved thawing the cells on ice, adding 1 µL of 1-100 ng plasmid DNA to the cells and gently mixing them prior to incubation on ice for 30 min. The cells were then heat shocked at 42°C for 30 sec, placed on ice for 5 min and SOC media (NEB) or NEB 10-beta/Stable Outgrowth Medium (NEB) added as required. Incubation at 37°C and shaking at 250 rpm for 60 min was then followed by plating onto Luria Broth (LB) agar with either 100 μgmL^{-1} ampicillin or 50 μgmL^{-1} kanamycin for overnight selection at 37°C as appropriate.

2.2.4 Bacterial culture and storage

Bacterial cultures for DNA extraction or long-term storage were prepared by picking colonies from LB agar plates and growing in LB broth with either 100 μgmL^{-1} ampicillin or 50 μgmL^{-1} kanamycin as appropriate at 37°C overnight with shaking. Cultures were prepared for long-term storage by putting 600 µL of overnight culture and 400 µL of 50% v/v glycerol (final concentration 20%) into a cryovial and storing at -80°C.

2.2.5 DNA extraction from *E. coli*

Preparation of DNA from *E. coli* strains was performed using 5-10 mL of overnight culture as described in section 2.2.4 and using the QIAprep Spin Miniprep Kit (Qiagen) with the manufacturer's protocol. DNA concentration and purity were determined using a NanoDrop™ 1000 Spectrophotometer (Thermo Fisher Scientific).

2.2.6 Restriction digestion

Restriction digestion was performed using enzymes obtained from NEB and carried out as described by the NEBcloner® Single/Double Digestion planner (https://nebcloner.neb.com/#!/redigest). Typically, 1-10 µg of plasmid DNA was digested in a total volume of 50 µL containing 1 x CutSmart Buffer (NEB), 10-20 U of each restriction enzyme and nuclease-free water up to 50 µL at 37°C for at least 15 min (maximum incubation was overnight).

2.2.7 DNA sequencing

DNA sequencing was carried out by Eurofins Genomics using cycle sequencing technology (dideoxy chain termination/cycle sequencing) on ABI 3730XL sequencing machines and using primers obtained from Eurofins or Sigma-Aldrich.

2.3 *Leishmania* cell culture

2.3.1 Promastigote cell culture

L. mexicana (MNYC/BZ/62/M379) promastigotes were grown in HOMEM (Gibco) supplemented with 10% v/v heat-inactivated Fetal Bovine Serum (FBS) (Gibco) and 1% v/v Penicillin/Streptomycin (Sigma-Aldrich) at 25°C. Typically, cells were split around twice a week. Selection drugs were added to the medium as appropriate: 10 µg mL^{-1} blasticidin (InvivoGen), 40 µg mL^{-1} puromycin (InvivoGen), 10-15 µg mL^{-1} G418 (InvivoGen), 50 µg mL^{-1} hygromycin (InvivoGen) and 50 µg mL^{-1} nourseothricin (Jena Bioscience).

To generate stabilates for long-term storage, 1 mL of mid-log phase cultures (around 5 x 10^6 cells mL^{-1}) were prepared with 20% v/v FBS and 5% v/v DMSO, mixed gently and stored at -80°C or in liquid nitrogen. To recover stabilates, cells were warmed at 37°C and then placed into HOMEM supplemented with 20% v/v FBS and 1% v/v Penicillin/Streptomycin. Antibiotics were added after overnight recovery.

2.3.2 Promastigote to amastigote differentiation

L. mexicana promastigote cultures were grown to stationary phase by seeding at 1 x 10^5 cells per mL (or up to 4 x higher if growth defects had previously been observed) and growing for at least 3 days. Next, cells were centrifuged at 1,000 x g for 10 min and resuspended in amastigote medium (Schneider's Drosophila medium [Gibco], 20% FBS [Gibco] and 15 µg mL-1 HEMIN [Sigma], adjusted to pH 5.5) at 33°C with 5% CO_2, similar to conditions described for the cultivation of lesion-derived amastigotes (Bates *et al.*, 1992). For growth of amastigotes in 6-well plates, cells were seeded at 2 x 10^6 cells per well. For culture in flasks, amastigotes were kept at or below 1 x 10^7 cells per mL. In order to count amastigote cells, 500 µL of culture was taken and passed 10 x through a needle to separate cell clusters. Cells were then counted using the Beckman Coulter Z1 Particle Counter as described in section 2.3.3.

2.3.3 Cell counting

Cell density was determined for both promastigote and amastigote stage parasites either by manually counting with a haemocytometer or placing 100 µL of mid-log phase/amastigote culture or 50 µL of late-log/stationary phase culture (>1 x 10^7 mL^{-1}) into 10 mL of Beckman Coulter™ ISOTON™ II Diluent and counting using the Beckman Coulter Z1 Particle Counter (set to count particles above 3 µm in diameter).

2.3.4 Axenic amastigote viability assay

L. mexicana promastigote cultures were grown to stationary phase as described in section 2.3.2 and resuspended at 1 x 10^6 cells per mL in amastigote medium (Schneider's Drosophila medium [Gibco], 20% FBS [Gibco] and 15 µg mL-1 HEMIN [Sigma], adjusted to pH 5.5). 200 µL cell samples were prepared in sextuplicate in 96-well plates and included the parental cell line as a positive control. Also included were media-only, negative control samples. At 0 h, 48 h and 120 h, 20 µL of 125 µg mL^{-1} resazurin (in 1 x Phosphate Buffered Saline [PBS]) was added to sample wells and the plate incubated at 37°C for 8 h. The fluorescence at 590 nm (to detect the relative level of conversion of resazurin to resorufin) was then read using the POLARstar Omega Plate Reader (BMG Labtech).

2.3.5 Transfection and selection

Transfections were performed using whole PCR reactions as described in sections 2.3.6 and 2.3.8 or around 2.5 µg of DNA purified from PCR reactions using the QIAquick PCR Purification Kit (Qiagen). Either 1 x 10^6 or 8 x 10^6 log phase cells were prepared by centrifugation (1,000 x g for 10 min), washing with 1 x PBS and resuspending in 1 x Cytomix (66.7 mM Na_2HPO_4, 23.3 mM NaH_2PO_4, 5 mM KCl, 50 mM HEPES and 150 µM $CaCl_2$, pH 7.3) or P3 solution from the P3 Primary Cell 4D-NucleofectorTM X Kit (Lonza). When 1 x 10^6 cells were used, cells were resuspended in 20 µL of P3 solution and transfected using the 16-well transfection strips from the P3 Primary Cell 4D-NucleofectorTM X Kit S (Lonza) and the FI-115 programme. When 8 x 10^6 cells were used, cells were resuspended either in 200 µL 1 x Cytomix or 100 µL P3 solution and transfected using the NucleofectorTM 2b Device (Lonza) and two pulses with the X-001 programme or using the Amaxa™ 4D-Nucleofector™ (Lonza) and the FI-115 programme respectively. As a negative control, the parental cell line was transfected with water in place of DNA. Following transfection, cells were placed in 5-10 mL of HOMEM

(Gibco) supplemented with 20% v/v heat-inactivated FBS (Gibco) and 1% v/v Penicillin/Streptomycin (Sigma-Aldrich) and allowed to recover at 25°C.

Following overnight recovery (minimum time 6 h) of the cells, appropriate antibiotics were added as detailed in section 2.3.1 in order to select for transfectants. Selection was performed either on a population level (on 10 mL containing the total transfected population) or along with cloning into 96-well plates at 1:6, 1:66 and 1:726 dilutions. Dilutions were carried out in HOMEM supplemented with 20% v/v FBS and 1% v/v Penicillin/Streptomycin.

2.3.6 CRISPR-Cas9-based endogenous tagging

N-terminal endogenous tagging was performed using a CRISPR-Cas9-based approach (Beneke *et al.*, 2017) and an *L. mexicana* cell line expressing Cas9 and T7RNAP. Primer sequences to allow amplification of the single guide DNAs (sgDNAs) and repair cassettes for tagging were designed using a web tool (http://www.leishgedit.net/Home.html). Guide primers contained sequences corresponding to the T7RNAP promoter, 20 nt of complementarity to the DNA target and a 20 nt Cas9 scaffold. The forward and reverse primers for cassette amplification had an extra 30 nt of homology with the regions upstream and downstream of the planned double-stranded break respectively to facilitate homologous recombination.

PCR reactions for cassette amplification contained 30 ng of plasmid (pPLOTv1 blast-mNeonGreen-blast, pPLOTv1 puro-mNeonGreen-puro (Beneke and Gluenz, 2019), pGL2822, pGL2835, pGL2823 or pGL2836), 0.2 mM dNTPs, 2 µM each of forward and reverse primer, 1U Q5® DNA Polymerase (NEB), 1x Q5 reaction buffer (NEB) and distilled water to make the volume up to 40 µL. The reverse primer used for generating all guides was OL6137. The PCR was run with the following settings: 94°C for 5 min, 45 cycles of 94°C for 30 s, 65°C for 30 sec and 72°C for 2 min 15s and 72°C for 7 min. For the sgRNAs, PCR reactions were set up in a similar manner but with a total volume of 20 µL. The PCR program used was: 98°C for 30 s, 35 cycles of 98°C for 10 s, 60°C for 30 sec and 72°C for 15s and 72°C for 10 min. Transfections were performed as described in section 2.3.5 and cell lines selected at the population level.

2.3.7 Live cell imaging

1-4 x 10^6 cells were centrifuged (1,000 x g for 10 min), resuspended in 1 x PBS containing 10-20 µg mL-1 Hoechst 33342 (Thermo Fisher Scientific) and incubated at room temperature for 10 min. Cells were then washed in 1 x PBS and resuspended in 50 µL of chilled CyGEL™ (Biostatus). CyGEL™ mixture was placed onto slides, a coverslip added and the mixture allowed to solidify at room temperature. The slides were then imaged with 488 and 405 nm lasers using a Zeiss LSM880 confocal microscope or with 488 and 385 nm lasers using a Zeiss Axio Observer. DIC images were also obtained to document the whole cell appearance. To ensure cell viability, imaging was only performed up to 3 hours following slide preparation.

2.3.8 CRISPR-Cas9-based null mutant generation

Primer design and PCR reactions were carried out using the same online tool and protocols as for the endogenous tagging strategy (section 2.3.6) respectively. Additionally, a tag, a 10 nt linker and a 12 nt unique barcode were inserted into the 5' end of the upstream forward primer in the following order: 5'-TAATACGACTCACTATAAAACTGGAAGXXXXXXXXXXX-3', where X represents the barcoded region. The knockout strategy also differs from the tagging strategy in that two sgDNAs (for targeting the Cas9 enzyme to both the 5'- and 3'-UTR of the gene of interest), rather than one, are used. Plasmids used for amplification of the cassettes were pTBlast_v1, pTPuro_v1 or pTNeo_v1 (sequences available at leishgedit.net). Transfections were performed as described in section 2.3.5.

2.3.9 Genomic DNA extraction

To harvest genomic DNA from *Leishmania* cells, 500 µL-5 mL of mid-log phase promastigotes were centrifuged (1,000 x g for 10 min), washed once in 1 x PBS and then resuspended in 200 µL 1 x PBS. DNA extraction was then carried out using the Qiagen DNeasy Blood and Tissue Kit and the manufacturer's protocol.

2.3.10 Pooled bar-seq screen

Null mutant promastigote cell lines were grown to mid-log phase, centrifuged at 1,000 x g for 10 min and pooled in equal proportions in 250 mL Grace's medium (Grace's insect media [Sigma-Aldrich] with 4.2 mM $NaHCO_3$, 10% FCS [Gibco], 1 x

Penicillin/Streptomycin [Gibco] and 1 x BME Vitamins [Sigma-Aldrich] and adjusted to pH 5.25) up to a total concentration of 2 x 10^6 cells mL^{-1}. Cultures were prepared in sextuplicate to provide biological replication. Next, the pooled cells were grown at 25°C for 7 days to allow for the enrichment of metacyclic promastigote cells.

To prepare axenic amastigotes from the enriched metacyclic promastigote population, cells were centrifuged and plated in 6-well plates as described in section 2.3.2. Cells were then cultured at 35°C with 5% CO_2. To obtain DNA from procyclic promastigote, metacyclic promastigote or axenic amastigote populations, 2-5 mL of culture was centrifuged and processed using the Qiagen DNeasy Blood and Tissue Kit.

In order to infect mouse bone marrow macrophages (from female BALB/C mouse femur), cells were equilibrated in warm L-glutamine (GE Life Sciences), centrifuged at 200 x g for 10 min, resuspended in macrophage medium (DMEM [Invitrogen] plus 10% FCS and 2 mM L-glutamine) in order to have 2.5 x 10^6 cells per well and incubated at 37°C overnight. The next day, enriched metacyclic cells were purified using a Ficoll 400 (Sigma-Aldrich) gradient (40%, 10% and 5% Ficoll) and centrifugation at 1,300 x g for 10 min. Following washing with Grace's medium, metacyclic promastigotes were added to the macrophages in a 1:1 ratio and left to interact for 4 h at 35°C with 5 % CO_2. Excess *Leishmania* cells were then removed by washing with DMEM and the cells left in macrophage medium. To obtain DNA from macrophages, macrophages were scraped from the bottom of a well and processed using the Qiagen DNeasy Blood and Tissue Kit.

To perform the mouse infections, 10^6 purified metacyclic cells were injected into the left footpad of BALB/c mice. Mice were culled at 3 and 6 weeks post-inoculation and DNA extracted from footpad lesions using the Qiagen DNeasy Blood and Tissue Kit.

DNA samples were prepared for next-generation sequencing by first amplifying unique barcodes using OL8684 and OL8685 by PCR. This was carried out using Q5 polymerase as described in section 2.2.1 but with the following changes to the reaction setup: just 0.5 x of Q5 Reaction Buffer (NEB) and 0.5 x Q5 High GC Enhancer (NEB) were used. Additionally, the cycling conditions were modified to an initial denaturation step of 98°C for 5 min and 20-25 cycles of 98°C for 30 sec, 60°C for 30 sec and 72°C for 10 sec. OL8684 and OL8685 bind to the tag and linker region and 5' PGKβ of the repair cassette respectively and contain universal adaptors for Illumina sequencing. Following purification of the PCR reactions using the Qiagen MinElute PCR Purification Kit, a

second PCR was performed using primers that bind to the universal adaptors and contain barcodes permitting sample identification. The samples were then sequenced using an Illumina HiSeq 3000. Library preparation and processing of sequencing data were carried out by Katherine Newling (Technology Facility, University of York) as described in Damianou *et al.* (2020).

Relative fitness of null mutants at each life cycle stage was calculated from the sequencing data by taking the number of unique barcode reads for each null mutant line and dividing it by the total number of expected barcode reads. Significant increases or decreases in null mutant line fitness between adjacent samples in the experimental workflow were analysed using unpaired t-tests and the Holm-Šídák method in GraphPad Prism 7. This experiment was performed in collaboration with Carolina Catta-Preta, Andreas Damianou and Jaspreet Grewal.

2.4 Biochemical techniques

2.4.1 Activity-based protein profiling

3 x 10^7 promastigote cells were grown to mid or late log-phase and centrifuged at 1,000 x g for 10 min at 4°C. Cells were washed twice with 1 mL of ice-cold wash buffer (44 mM NaCl, 5 mM KCl, 3 mM NaH_2PO_4, 118 mM sucrose, 10 mM glucose, pH 7.4), centrifuged again and resuspended in 40 µL of ice-cold lysis buffer (50 mM Tris-HCl [pH 7.4], 120 mM NaCl, 1% w/v NP40 [Sigma-Aldrich], 1 µg mL^{-1} pepstatin [Sigma-Aldrich], 1 x protease inhibitor cocktail [Roche], 1 mM DTT, 1 mM PMSF [Sigma-Aldrich] and 0.01 mM E64 [Sigma-Aldrich]) containing 40 µg mL^{-1} of Cy5-Ub-Dha probe (UbiQ) and rotated for 15 min at 4°C. Next, lysates were centrifuged at 16,000 x g for 15 min at 4°C to remove debris. Samples for protein profiling were then prepared with around 1 mg mL^{-1} lysate, 20 µg mL^{-1} of Cy5-Ub-Dha, 7.5 mM ATP, 10 mM $MgCl_2$, and labelling buffer (50 mM Tris-HCl, 120 mM NaCl, pH 7.4) to make the volume up to 25 µL. Samples were subsequently incubated at 37°C for 1 h. At 20 min intervals, 1 mM ATP and $MgCl_2$ were added to the reactions to replenish depleted reagents. The reaction was terminated by addition of 3 x SDS-PAGE buffer (1 x NuPAGE® LDS Sample Buffer [Thermo Scientific], 7.5% β-mercaptoethanol) and heating of samples at 90°C for 10 min. Samples were then run on a NuPAGE® Bis-Tris Protein Gel (Thermo Scientific) with MOPS SDS Running Buffer (Thermo Scientific) and visualised using fluorescence scanning (Typhoon™ imager, Amersham Pharmacia Biotech) and InstantBlue™ stain (Sigma-Aldrich).

2.4.2 Generation of *E. coli* expression plasmids

Genes were codon-optimised for bacterial expression and synthesised by DC Biosciences. Cloning into expression vectors (pETFPP_1-4, obtained from the Technology Facility, University of York) in frame with N-terminal His, His-MBP (maltose binding protein), His-GST (glutathione S-transferase) or His-Im9 (*E. coli* immunity protein of colicin E9) tags (Shevket *et al.*, 2018) was performed by first using KOD Hot Start DNA Polymerase (Millipore) or Q5® polymerase (NEB) to obtain the insert and vector fragments by PCR. PCRs were performed using the manufacturer's protocol or as described in section 2.2.1 respectively. The vector was optionally digested with DpnI (NEB) to remove any remaining template and PCR cleanup performed on all fragments using a QIAquick PCR purification kit (Qiagen). Vector was provided pre-prepared by the University of York Technology Facility.

Next, insert and vector fragments were combined using the In-Fusion HD Cloning Kit (Takara) using the manufacturer's protocol and transformed into NEB® 5-alpha cells (described in section 2.2.3). Following miniprep using a QIAprep Spin Miniprep Kit (Qiagen), plasmid identity was confirmed using restriction digests (*Eco*RV for UBA1, *Xba*I and *Pst*I for UBC2 and *Nco*I and *Bam*HI for UEV1 [all enzymes obtained from NEB]) and sequencing. All expression plasmids were transformed into BL21-Gold (DE3) (Agilent Technologies) cells using the manufacturer's protocol and glycerol stocks made.

2.4.3 Bacterial expression

For expression, 5 mL of overnight culture was added to 500 mL of LB or auto-induction medium (1 mM $MgSO_4$, 1x metals [50 µM $FeCl_3 \cdot 6H_2O$, 20 µM $CaCl_2$, 10 µM $MnCl_2 \cdot 4H_2O$, 10 µM $ZnSO_4 \cdot 7H_2O$, 2 µM $CoCl_2 \cdot 6H_2O$, 2 µM $CuCl_2 \cdot 2H_2O$, 2 µM $NiCl_2 \cdot 6H_2O$, 2 µM $Na_2MoO_4 \cdot 5H_2O$, 2 µM $Na_2SeO_3 \cdot 5H_2O$, 2 µM H_2BO_3], 1x 5052 [5 $mgmL^{-1}$ glycerol, 0.5 $mgmL^{-1}$ glucose, 2 $mgmL^{-1}$ α-lactose], 1x NPS [3.3 $mgmL^{-1}$ $(NH_4)_2SO_4$, 6.8 $mgmL^{-1}$ KH_2PO_4, 7.1 $mgmL^{-1}$ Na_2HPO_4, pH 6.75], 10 gL^{-1} N-Z-amine AS and 5 gL^{-1} yeast extract) supplemented with 25 μgmL^{-1} kanamycin (Thermo Fisher Scientific) and incubated at 37°C with shaking. For growth in LB, when an optical density of around 0.5 at 600 nm was reached, cultures were equilibrated to 20°C and 1 mM of isopropyl 1-thio-β-D-galactopyranoside (IPTG) added to induce protein expression. Cultures were then grown for a further 24 h at 20°C. Protein induction was demonstrated by running whole cell lysates collected before and 24 h after induction on an SDS-PAGE gel (see section 2.4.10) and staining using InstantBlue™ (Expedeon).

2.4.4 Bacterial cell lysis

500 mL bacterial pellets were resuspended in 25 mL HisA buffer (20 mM $NaH_2PO_4 \cdot 2H_2O$, 20 mM $Na_2HPO_4 \cdot 12H_2O$, 0.3 M NaCl, 5 mM β-mercaptoethanol and 30 mM imidazole, pH 7.4), 400 U DNAse (Sigma-Aldrich) or around 1,250 U of Basemuncher (Expedeon) added and bacteria homogenised using a cell disruptor (Constant Systems Ltd).

2.4.5 Nickel affinity purification

Following centrifugation at 35,000 x g for 10 min at 4°C, the supernatant was filtered using a 0.8 µm filter and purified by nickel affinity purification. For this purpose, a 5 mL HisTrap™ Fast Flow Crude column (GE Healthcare) and an ÄKTA pure chromatography system (GE Healthcare) were used. The protocol included washes with HisA buffer and gradient elution with HisB buffer (20 mM $NaH_2PO_4 \cdot 2H_2O$, 20 mM $Na_2HPO_4 \cdot 12H_2O$, 0.3 M NaCl, 5 mM β-mercaptoethanol and 0.5 M imidazole, pH 7.4).

2.4.6 Tag cleavage and removal

His-Im9 tags were cleaved using between 1:5 and 1:10 H3C protease (Protein Production Facility, University of York) relative to newly expressed protein during overnight dialysis at 4°C in HisC buffer (20 mM $NaH_2PO_4 \cdot 2H_2O$, 20 mM $Na_2HPO_4 \cdot 12H_2O$, 0.3 M NaCl and 5 mM β-mercaptoethanol, pH 7.4). For this purpose, SnakeSkin™ dialysis tubing (Thermo Fisher Scientific) with an appropriate molecular weight cut-off was used. Alternatively, cleavage was carried out for 2 hr at 4°C prior to running on a desalt column to remove imidazole. The next day, the sample was reapplied to the HisTrap™ column with isocratic application of HisA and HisB buffers to remove the tag from the solution.

2.4.7 Size-exclusion chromatography

Size-exclusion chromatography (SEC) was carried out following concentration of samples in Amicon® spin columns (with appropriate molecular weight cut-offs) using the ÄKTA pure and HiLoad™ 16/600 Superdex™ 200 Superdex prep grade (pg) or 75 pg columns (both GE Healthcare) for UBA1 and UBC2/UEV1 respectively. Buffer used contained 50 mM HEPES and 150 mM NaCl with either 2 mM DTT or 1 mM tris(2-carboxyethyl)phosphine (TCEP).

2.4.8 Assessment of protein purity and storage

After each purification step, protein fractions were run on an SDS-PAGE gel and analysed by InstantBlue™ (Expedeon) staining to determine the location and purity of the desired protein. Fully purified protein was pooled, concentrated and the concentration determined by measuring the absorbance at 280 nm and dividing by the extinction coefficient estimated by ProtParam (https://web.expasy.org/protparam/). Samples in their final purification buffers were snap frozen in liquid nitrogen and stored at -80°C.

2.4.9 Size Exclusion Chromatography-Multi-Angle Laser Light Scattering (SEC-MALLS)

For the UBC2 and UEV1 used for SEC-MALLS, purification was carried out as described in sections 2.4.3-2.4.8 but with the following minor changes: buffers A-C did not contain β-mercaptoethanol, UBC2 was not purified by SEC and the buffer used for SEC of UEV1 was 25 mM Tris-HCl, 150 mM NaCl, pH 8. Storage was in the final purification buffers plus 1 mM DTT.

SEC-MALLS was performed using a Superdex 200 HR10/300 gel filtration column (Sigma-Aldrich) and buffer containing 25 mM Tris-HCl, 150 mM NaCl and 1 mM DTT, pH 8 and filtered with a 0.2 µm filter. The system included a HPLC system (Shimadzu) and HELEOS-II light scattering and Optilab rEx refractive index detectors (Wyatt). Concentrations of samples loaded were between 1.2 and 2 mg mL^{-1}.

2.4.10 SDS-PAGE

SDS-PAGE was typically carried out on samples in 3 x NuPAGE™ LDS Sample Buffer with 1 M β-mercaptoethanol added as a reducing agent. Spectra™ Multicolor Broad Range Protein Ladder (Thermo Fisher Scientific) or SeeBlue™ Plus2 Pre-stained Protein Standard (Invitrogen) were run alongside samples to permit molecular weight estimation. Samples were loaded into NuPAGE™ 4-12% Bis-Tris Protein Gels (Invitrogen) and run at 200 V in 1 x NuPAGE™ MOPS SDS Running Buffer (Invitrogen) or 1 x NuPAGE™ MES SDS Running Buffer (Invitrogen). Gel staining, when performed, was carried out using InstantBlue™ (Expedeon) and incubation at room temperature with shaking for between 15 min and 1 h.

2.4.11 Western blotting

Western blotting was carried out by first incubating SDS-PAGE gels for 10 min in 20% ethanol with gentle shaking and then blotting using nitrocellulose or PVDF iBlot™ 2 Transfer Stacks (Invitrogen) and the iBlot™ 2 (Thermo Fisher Scientific). The program used was: 20 V for 1 min, 23 V for 4 min and 25 V for 7 min. Blocking was performed in either 5% BSA (Sigma-Aldrich) or 5% milk in 0.05% Tween 20 (Sigma-Aldrich) in Tris-Buffered Saline (TBSt, TBS from Thermo Fisher Scientific) for 1 h at room temperature with shaking. Primary antibodies were incubated in the dilutions indicated in 1% or 5% BSA or 5% milk in TBSt and incubated either at room temperature for 1 h or at 4°C overnight with shaking. Following incubation with primary antibody, blots were washed 3 x in 10 min TBSt and secondary antibody added in 5% milk at the dilutions indicated. The blot was then incubated for 1 h at room temperature with shaking and washed three times in TBSt. For HRP-conjugated secondary antibodies, Clarity™ or Clarity™ Max Western ECL Substrate (both Bio-Rad) was added to the blot and incubated for 5 min. Imaging in the colourimetric, fluorescent and chemiluminescent channels was performed using a ChemiDoc system (Bio-Rad).

2.4.12 Thioester assay

Except where otherwise indicated, reactions were set up to contain 300 nM E1 (*L. mexicana* UBA1a or UBA1b or human UBA1), 2.5 µM E2 (*L. mexicana* UBC2 or UEV1 or human UBE2W) and 20 µM human or bovine ubiquitin (obtained from Boston Biochem or Ubiquigent respectively) in reaction buffer (50 mM HEPES, pH 7.5, 100 mM NaCl, 10 mM $MgCl_2$, 2 mM DTT and 5 mM ATP) to a total volume of 40 µL as required and incubated as indicated at room temperature. 1 x of LDS sample buffer (Invitrogen) with or without 7.5% β-mercaptoethanol or NuPAGE™ Sample Reducing Agent (Invitrogen) was then added and the samples containing reducing agent heated at 90°C for 5 min. SDS-PAGE was performed as described in section 2.4.10. For the thioester assay with UBA1b (provided by Daniel Harris, University of Glasgow), the protocol differed slightly in that 300 nM E1, 2.5 µM E2, 100 µM human ubiquitin and 10 mM ATP were used and the reactions were incubated at 30°C.

2.4.13 Diubiquitin formation assay

Reactions were prepared with the indicated combinations of 100 nM UBA1, 2.5 µM of UBC2 and/or UEV1, 100 µM of human ubiquitin (Boston Biochem for wild-type, 2B

Scientific for K63R) and 5 mM ATP (Sigma-Aldrich) in 40 µL of reaction buffer containing 50 mM HEPES, pH 7.5, 100 mM NaCl, 10 mM $MgCl_2$ and 2 mM DTT. Samples were incubated at 37°C for the length of time indicated. For the inhibitor assay, up to 50 µM of NSC697923 (Abcam) was pre-incubated with UBC2 and UEV1 in reaction buffer for 15 min at room temperature prior to addition of UBA1 and ATP. The reaction was then incubated at 37°C for 90 min. The final DMSO concentration in these reactions was 0.5%. Following sample incubation, NuPAGE™ LDS Sample Buffer and NuPAGE™ Sample Reducing Agent (both Invitrogen) were added to 1 x and the samples heated at 90°C for 5 min.

Following denaturation, samples were loaded onto NuPAGE™ 4-12% Bis-Tris Protein Gels (Invitrogen) and run at 200 V in 1 x MES SDS Running Buffer (Invitrogen) with 1 x NuPAGE™ Antioxidant (Invitrogen). 100 ng K63 diubiquitin positive control (Ubiquigent) was loaded where indicated.

Western blotting was performed using nitrocellulose iBlot™ 2 Transfer Stacks (Invitrogen) as described in section 2.4.11. Blocking was performed in either 5% BSA (Sigma-Aldrich) or 5% milk in TBSt as appropriate. Primary antibodies used were: 1:1,000 FK2 ubiquitin conjugate (Ubiquigent) or 1:250 K63 linkage-specific (Thermo Fisher Scientific) primary mouse antibodies in 1% BSA or 5% milk respectively. HRP-conjugated anti-mouse secondary antibody (GE Healthcare or Promega) at 1:10,000 dilution was used. Imaging in the colourimetric and chemiluminescent channels was performed using a ChemiDoc system (Bio-Rad).

2.4.14 E3 cooperation assay

Reactions were prepared with 100 nM UBA1a, 2.5 µM E2 (UBC2 or UEV1), 1 µM human E3 (BIRC2, RNF8 or HUWE1, all from Ubiquigent), 100 µM ubiquitin (Boston Biochem) and 5 mM ATP (Sigma-Aldrich) in reaction buffer containing 50 mM HEPES, pH 7.5, 100 mM NaCl, 10 mM $MgCl_2$ and 2 mM DTT in 40 µL total reaction volume. Samples were then incubated at 30°C for 1 h prior to SDS-PAGE and Western blotting as described in section 2.4.13. To look for E3 ubiquitination, GST rabbit antibody (Abcam) was used at 1:1,000 dilution in 5% milk in TBSt followed by 1:10,000 HRP-conjugated anti-rabbit secondary antibody (GE Healthcare).

2.4.15 CHIP chain priming/extension assay

Reactions were prepared with the indicated combinations of 0.1 µM *L. mexicana* UBA1a, 2.5 µM human UBE2W (Ubiquigent), 1 µM CHIP (Ubiquigent), 0.1 mM human ubiquitin (Boston Biochem) and 2 mM ATP (Sigma-Aldrich) in 50 mM HEPES, pH 7.5, 100 mM NaCl, 10 mM $MgCl_2$ and 2 mM DTT. Samples were incubated at 30°C for 1 h prior to SDS-PAGE and Western blotting as described in section 2.4.13. Antibodies used for blotting were FK2 antibody (Ubiquigent), used as described in section 2.4.13, and CHIP antibody (Calbiochem), which was used 1:1,000 in 5% milk in TBSt, followed by 1:10,000 HRP-conjugated anti-rabbit secondary antibody (GE Healthcare).

2.4.16 X-ray crystallography

UBC2 and UEV1 (in buffer containing 50 mM HEPES, 150 mM NaCl and 2 mM DTT) were mixed in a 1:1 molar ratio to a final concentration of 6.6 mg mL^{-1} and incubated on ice for 30 min. 96-well PACT premier™ (Molecular Diagnostics), Crystal Screen HT™ (Hampton) and INDEX™ (Hampton) sitting drop screens were set up using a Mosquito (TTP Labtech) in order to have drops containing 150 nL of protein and 150 nL of reservoir solution above 100 µL of reservoir solution. Crystals grown in 0.1 M Bis-Tris propane, pH 7.5, 0.2 M sodium formate and 20% PEG (PACT premier™ screen) or in a 24-well plate hanging drop format (1 µL of protein and 1 µL of reservoir solution in the drop above 1 mL reservoir solution) with the same buffer plus 0.05% dimethylformamide appeared after 2 days at 25°C. Crystals were captured in a fine, rayon loop, cryo-cooled in liquid N_2 and sent to the Diamond Light Source (beamlines I03 and I04 respectively) for data collection. The best diffraction dataset, which extended to a resolution of 1.7 Å, was selected for further processing and processed using the 3dii pipeline in *xia2* (Winter, Lobley and Prince, 2013). The crystals belonged to space group $P2_1$ with two UBC2-UEV1 heterodimers in the asymmetric unit.

To solve the UBC2-UEV1 structure, molecular replacement using data from the human UBE2N-UBE2V2 complex (PDB ID: 1J7D) was performed in MOLREP using the CCP4i2 interface (Vagin and Teplyakov, 1997; Potterton *et al.*, 2018). Model rebuilding and refinement were carried out using iterations of the programs Buccaneer (Cowtan, 2006), Refmac5 (Murshudov, Vagin and Dodson, 1997; Murshudov *et al.*, 2011) and Coot (Emsley *et al.*, 2010) in CCP4i2 (version 1.0.2 (Potterton *et al.*, 2018)). The coordinates and structure factors for the *L. mexicana* UBC2-UEV1 complex are available in the Protein Data Bank (PDB ID: 6ZM3).

Superposition of structures and RMSD determination were performed using “superpose structures” in CCP4mg (McNicholas *et al.*, 2011). UBC2-UEV1 interface analysis was performed using PISA (version 1.52) (Krissinel and Henrick, 2007).

2.5 Mass spectrometry

2.5.1 Immunoprecipitation of myc-tagged proteins

Cells were centrifuged at 1,000 x g for 10 min and washed twice in 1 x PBS. For amastigote cells, 1 x PBS containing 1 x cOmplete™, Mini, EDTA-free Protease Inhibitor Cocktail (Roche), 20 µM E64 (Sigma-Aldrich) and 10 µM E64d (Santa Cruz Biotechnology) was used for washes. For Western blotting, around 1.6 x 10^8 promastigote parasites were used per immunoprecipitation whereas for mass spectrometry 8 x 10^8 (promastigote or amastigote) cells were used. Parasites were then resuspended in 1 x PBS containing 10 mM DSP (dithiobis(succinimidyl propionate), Thermo Fisher Scientific) and incubated for 10 min at 25°C. 20 mM Tris, pH 7.5 was then added to quench the reaction. Parasites were centrifuged at 1,000 x g for 3 min and then transferred to Protein LoBind tubes (Eppendorf). Cell lysis was carried out on ice by first resuspending parasites in 400 µL of lysis buffer (50 mM Tris, pH 7.5, 250 mM NaCl, 1 mM EDTA and 1% NP40 [Sigma-Aldrich]) supplemented with protease inhibitors. For the promastigote interactome experiment, inhibitors included around 3.3 x cOmplete™, Mini, EDTA-free Protease Inhibitor Cocktail (Roche), 1 x PhosSTOP™ (Roche), 1.5 mM Pepstatin A (Sigma-Aldrich), 1 mM PMSF (Sigma-Aldrich), 10 µM E64, 0.4 µM 1-10 phenanthroline (Sigma-Aldrich) and 2 x Proteoloc™ Protease Inhibitor Cocktail (Expedeon). For the amastigote interactome experiment, 3 times the concentration of Pepstatin A, PMSF, E64 and 1-10 phenanthroline were used and Proteoloc™ Protease Inhibitor Cocktail excluded. Sonication was then carried out for 3 x 10 sec at amplitude 25 using a Vibra-Cell™ Ultrasonic Processor (Sonics).

Prior to application onto beads, cell lysate was centrifuged at 10,000 x g for 10 min at 4°C and 30 µL of Pierce™ Anti-c-Myc Magnetic Beads (Thermo Fisher Scientific) per sample washed twice with PBS wash/bind buffer (50 mM NaH_2PO_4, 150 mM NaCl and 0.025% Tween® 20, pH 7.5), first with 175 µL and then with 1 mL. Cell lysate supernatants were then added to the beads and rotated for 2.5 h at 4°C.

Following incubation, Anti-c-Myc beads were washed 4 x in 300 µL lysis buffer, leaving them on ice for 5 min between each wash. Beads were then resuspended in 300 µL 1 x PBS in a clean Protein LoBind tube and washed twice in 300 µL 1 x PBS. Myc-tagged protein was eluted from the beads by adding 25 µL of 0.1 M glycine, pH 2 and shaking at 700 rpm using a Vortex IR (Starlab) for 15 min at room temperature. 1/10 volume Tri-HCl, pH 8.5 was then added to neutralise the acid and the elution step repeated twice more.

2.5.2 Sample preparation

Following elution from Anti-c-Myc beads, 4 volumes of methanol and 1 volume of chloroform were added to the protein samples and the samples vortexed for 0.5-1 min. Samples were then centrifuged at 17,000 x g for 1 h at 4°C. Supernatant was removed and the pellet washed with 3 volumes of methanol. Next, the sample was centrifuged at 17,000 x g for 10 min at room temperature, supernatant removed and the pellet allowed to dry. Resuspension of the protein pellet in 150 µL 50 mM triethylammonium bicarbonate (TEAB), pH 8.5 containing 0.1% PPS silent surfactant (Expedeon) was followed by shaking at 800 rpm using a Vortex IR (Starlab) for 1 h at room temperature. Next, 10 mM TCEP was added to reduce proteins and 10 mM iodoacetamide (VWR Life Science) added to cause alkylation and the mixture incubated for 30 min at room temperature in the dark. To digest proteins, 200 ng of Trypsin/Lys-C Mix (Promega) and 1 mM $CaCl_2$ were added and the samples incubated at 37°C overnight with shaking.

To desalt peptides, the PPS silent surfactant was first cleaved with 0.5% trifluoroacetic acid (TFA) for 1 h at room temperature and the samples centrifuged for 17,000 x g for 10 min. C18 resin (3M™ Empore™) was then placed into a 200 µL pipette tip and wet with 100 µL acetonitrile by centrifuging liquid through the column at 2,000 x g. The column was then washed with 100 µL 80% acetonitrile, 0.1% TFA and then 100 µL 0.1% TFA. Next, the sample was applied to the resin three times. Following washing of the C18 resin with 2 x 100 µL 0.1% TFA, peptides were eluted using 2 x 30 µL applications of 80% acetonitrile, 0.1% TFA. Peptides were then dried for an hour at 40°C and stored at -20°C prior to use.

2.5.3 Liquid chromatography with tandem mass spectrometry (LC-MS/MS)

Samples were taken up in aqueous 0.1% TFA and loaded onto a PepMap, C18 EasyNano nanocapillary column (Thermo Fisher Scientific) using an mClass nano-UPLC

(Waters). Peptides were eluted into an Orbitrap Fusion™ Tribrid™ Mass Spectrometer (Thermo Fisher Scientific) over a 1 h acquisition. Data were acquired in data dependent acquisition mode with MS^1 measurement in the Orbitrap and a 1 sec cycle and MS^2 in the linear ion trap.

2.5.4 Data analysis

Peak lists were imported into PEAKS StudioX+ (Bioinformatics Solutions Inc.) to allow peak picking and database searching against the *L. mexicana* proteome in the TriTrypDB database. Variable modifications considered included: phosphorylation and ubiquitination. Peptide identifications were filtered to achieve a peptide spectrum match false discovery rate of <1% as assessed against a reversed database. Accepted peptide identifications were then used for label-free protein quantification. Differences in abundance between sample groupings were tested using ANOVA, requiring a minimum of two peptides per protein. The steps described in sections 2.5.3 and 2.5.4 were performed by Adam Dowle (Technology Facility, University of York). Interactors were additionally scored by the author using SAINTq (Teo *et al.*, 2016), using a false discovery rate threshold of <5% to select for high confidence interactors.

3 A global view of *Leishmania* ubiquitination

3.1 Introduction

3.1.1 Ubiquitin and Ubl systems in *Leishmania*

The amino acid sequence of ubiquitin is highly conserved between *Leishmania* and humans (Graeff *et al.*, 1993). Two E1 ubiquitin-activating enzymes, named UBA1a and UBA1b, have also been described in *Leishmania major* and are 55% and 59% identical to *Trypanosoma brucei* UBA1a and UBA1b respectively. Interestingly, *T. brucei* UBA1a was shown to be resistant to inhibition by the human E1 inhibitor TAK-243, which targets human UBA1 by acting as an ATP mimetic and binding to its adenylation site, probably due to the presence of a serine residue (alanine in human UBA1) at the gatekeeper position (Misra *et al.*, 2017; Hyer *et al.*, 2018; Boer and Bijlmakers, 2019). These findings suggest that there are important structural differences between E1 enzymes in humans and *Leishmania* and that these differences could potentially be exploited for the development of parasite-selective E1 inhibitors (Boer and Bijlmakers, 2019).

Many types of ubiquitin modification, including K48-linked polyubiquitin chains, can target proteins for degradation at the proteasome (Komander and Rape, 2012). That the *L. mexicana* and *L. major* proteasomes are essential for normal parasite growth *in vitro* and *in vivo* respectively highlights the importance of ubiquitination for normal *Leishmania* proliferation, including in the context of mammalian infection (Robertson, 1999; Khare *et al.*, 2016; Wyllie *et al.*, 2019). Furthermore, 4 out of 20 *L. mexicana* cysteine peptidase DUBs (DUBs 1, 2, 12 and 16), which may rescue proteins from proteasomal degradation or other ubiquitin-dependent effects by virtue of their deubiquitinating activity, were shown to be essential in promastigotes. Additionally, DUBs 4, 7, and 13 are required for the successful transformation from metacyclic promastigotes to amastigotes and DUBs 3, 5, 6, 10, 11 and 14 are required for normal amastigote proliferation in mice (Damianou *et al.*, 2020). Accordingly, ubiquitination may play a role in the morphological changes that occur during *Leishmania* differentiation, as was observed for the differentiation of the closely related parasite *T. cruzi* (de Diego *et al.*, 2001). Together, these findings indicate that the ubiquitin-proteasome system plays a crucial role in the differentiation processes and life cycle progression of *Leishmania* parasites.

Currently, the Ubls known to exist in *Leishmania* include Atg8, Atg12, SUMO, Ufm1 and Urm1 (Williams *et al.*, 2009; Williams *et al.*, 2012; Williams, Mottram and Coombs, 2013;

Ponder and Bogyo, 2007; Gannavaram *et al.*, 2011; Sharma *et al.*, 2016). An orthologue of Nedd8 is also likely to exist based on its identification in *T. brucei* (Liao *et al.*, 2017). However, little is currently known about the role that ubiquitin E1, E2 and E3 enzymes play in *Leishmania* biology. To address this deficiency, this chapter describes the bioinformatic identification and characterisation of E1, E2 and E3 enzyme genes in *L. mexicana*, followed by the generation and subsequent analysis of E1, E2 and HECT/RBR E3 endogenous tagging and null mutant libraries. Phenotypic characterisation of the null mutant library was carried out using both activity-based probes (ABPs) and bar-seq approaches, which will be described shortly.

3.1.2 Activity-based probes for ubiquitination enzymes

ABPs are designed to specifically target the active form of proteins. In this way, ABPs provide a clear picture of the influence that a specific enzyme has within the cell. This is in contrast to more indirect methods that measure, for example, mRNA transcript or protein abundance (Taylor and McGouran, 2019). Of the ABPs described to specifically target ubiquitination (E1, E2 and E3) enzymes, probes for E1, E2, HECT/RBR E3 and RING E3 enzymes have been reported. For capturing E1s, a ubiquitin (residues 1-71)-based probe that mimics the adenylate intermediate formed in the E1 active site and can be captured by virtue of a vinyl sulphonamide electrophilic trap at its C-terminus has been described (Lu *et al.*, 2010). An alternative approach involved the construction of a ubiquitin (residues 1-75)-AMP probe containing dehydroalanine as the electrophilic trap. Although both of these probes show specificity to ubiquitin E1s, the latter probe has limited use in cell lysates due to its ability to be cleaved by the DUB IsoT (An and Statsyuk, 2016). While the two probes described so far can be used to measure ubiquitin binding to E1 active sites, trans-thiolation activity between E1s and E2s (human UBA1 and UBE2N) can also be monitored using E2-based probes (Stanley *et al.*, 2015).

Numerous ABPs also exist for the identification of the Cys-dependent E3s, HECT and RBR E3 ligases (Love *et al.*, 2009; Pao *et al.*, 2016; Mulder *et al.*, 2016; Pao *et al.*, 2018; Xu *et al.*, 2019). Of particular interest is a cascading activity-based probe, Ub-Dha, which can be passed from E1s to E2s to Cys-dependent E3s (triple-E) through sequential trans-thioesterification reactions (Figure 4). At each step in the cascade, Ub-Dha can react irreversibly with the active site cysteine of the enzyme to permit its detection. This reaction happens with less than 100% efficiency, allowing the ABP to cycle through ubiquitination cascades and label multiple classes of enzyme (Mulder *et al.*, 2016). More recently, specific labelling of RING E3 ligases using photocrosslinking ABPs, made from

modified E2s, has been demonstrated (Mathur *et al.*, 2020). Since RING E3s are the most abundant E3 ligase family, of which many are important in human disease processes, this is an significant advancement for the future study of these enzymes (Metzger, Hristova and Weissman, 2012). Uses of ABPs for ubiquitination enzymes include but are not limited to the discovery of new ubiquitination enzymes, the study of enzyme regulation, stabilising proteins for structural analyses, inhibitor screening and inhibitor selectivity profiling (Mathur *et al.*, 2020). To date, activity-based probes targeting ubiquitin E1, E2 and E3 enzymes have not been used in *Leishmania*, although activity-based probes targeting DUB enzymes have been used successfully (Damianou *et al.*, 2020).

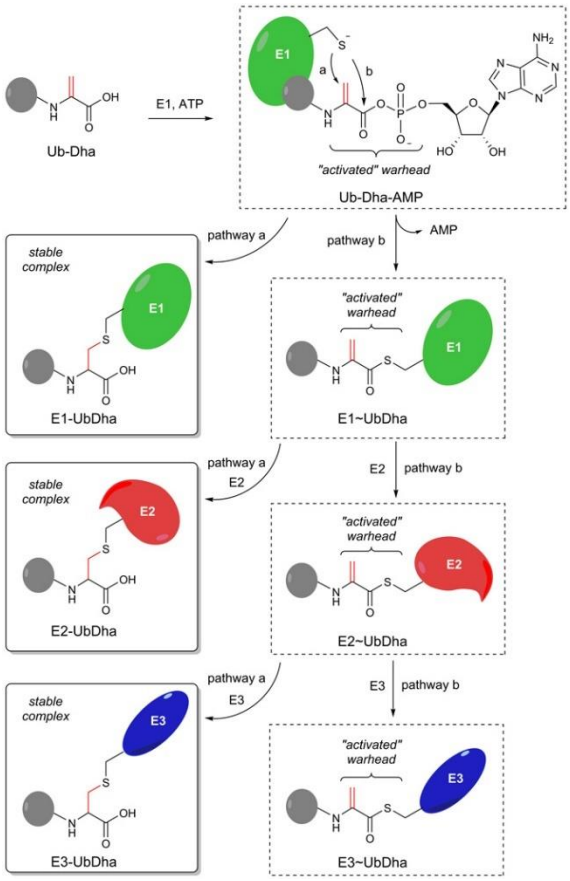

Figure 4. *Mechanism of the cascading activity-base probe described by Mulder et al., 2016.* The UbDha probe can be passed between E1, E2 and Cys-dependent E3 enzymes in a native manner (pathway b), forming thioester intermediates (E~UbDha) or can become covalently trapped by any of these enzymes (pathway a), forming a thioether-linked adduct (E-UbDha). Grey circle represents ubiquitin. Image reproduced with permission from Mulder *et al.*, 2016.

3.1.3 Bar-seq approaches

Over the past 10 years, bar-seq (barcode analysis by sequencing) approaches, which involve the parallel phenotyping of pools of mutant cell lines using sequencing, have been gaining popularity. This is due in part to their scalability and cost-effectiveness, since many more cell lines/conditions can be profiled in a pooled context than could be assessed individually, as well as the fact that they capitalise on recent advances in high-throughput, next-generation sequencing (Smith *et al.*, 2010; Robinson *et al.*, 2014). Bar-seq methods have been used to identify fitness phenotypes in multiple contexts and species, including bacteria (Wetmore *et al.*, 2015), budding yeast (Smith *et al.*, 2009; Smith *et al.*, 2010), fission yeast (Han *et al.*, 2010), *T. brucei* (Alsford *et al.*, 2011), *Plasmodium berghei* (Gomes *et al.*, 2015; Bushell *et al.*, 2017) and *Toxoplasma gondii* (Sidik *et al.*, 2016). To conduct a bar-seq screen, numerous strategies can be employed. For example, RNAi libraries can be generated using RNAi vector inserts that provide both the gene knockdown tool and the barcode for sequencing. Alternatively, CRISPR-based knockout can be carried out using a library of sgRNAs in vectors used for both gene knockout and as a barcode for sequencing. Another approach involves the generation of knockout libraries using barcoded repair cassettes, either as a pool or as individual cell lines which can be pooled later (Beneke and Gluenz, 2020).

3.1.4 Aims

This chapter aims to provide a broad overview of Leishmania E1, E2 and E3 ligase enzymes, including their identification, localisation and essentiality throughout the L. mexicana life cycle. In particular, use of the triple-E ABP (Mulder et al., 2016) for the profiling of L. mexicana promastigote cell lysates will be discussed. Furthermore, the generation and imaging of an mNeonGreen endogenous tagging E1, E2 and HECT/RBR E3 library is detailed. Additionally, the individual generation of barcoded L. mexicana E1, E2 and HECT/RBR E3 null mutant lines followed by pooled life cycle phenotyping using bar-seq will be described.

3.2 Results

3.2.1 Identification of E1, E2 and E3 genes

To identify the E1 ubiquitin-activating, E2 ubiquitin-conjugating and E3 ubiquitin ligase genes present in the *L. mexicana* genome, a domain search strategy was used. More

specifically, the *L. mexicana* genome was scanned for selected Interpro and PFAM domains in the kinetoplastid genomics resource TriTrypDB. To search for E1s, IPR018075 (Ubiquitin-activating enzyme E1), PF10585 (Ubiquitin-activating enzyme active site), IPR019572 (Ubiquitin-activating enzyme, catalytic cysteine domain) and IPR028077 (Ubiquitin/SUMO-activating enzyme ubiquitin-like domain) domains were used. The descriptions of IPR018075, PF10585 and IPR019572 report inclusion of the PICTLKNFP motif, a collection of amino acid residues that specify the conserved E1 active site (Tokumoto, Nagahama and Tokumoto, 2000). Conversely, IPR028077 represents the C-terminal domain of human SUMO-activating enzyme 2, which has a direct role in SUMO transfer between SUMO E1-activating enzyme and SUMO E2-conjugating enzyme. A search for this domain was included to allow SUMO E1 genes to be distinguished from those of other E1s (Lois and Lima, 2005). To look for E2 genes, IPR000608 (Ubiquitin-conjugating enzyme E2), which includes the E2 active site in its signature, was used.

In order to identify all known categories (HECT, RBR, RING and U-box) of E3 ligase genes, several types of domain search were performed. For HECT E3 ligases, IPR000569 (HECT domain) and PF00632 (HECT-domain [ubiquitin-transferase]), representing the HECT domain (of which the C-lobe contains the catalytic domain) were used (Huibregtse *et al.*, 1995). Similarly, to look for RBR E3 ligase genes, IPR002867 (IBR domain) and PF01485 (IBR domain, a half RING-finger domain), which represent the IBR domain (equivalent to the BR_{cat} domain) were used. IPR001841 (Zinc finger, RING-type), which broadly describes RING-type zinc finger domains, and IPR011016 (Zinc finger, RING-CH-type), representing the RING-CH-type zinc finger found mainly in membrane-bound E3s (Lin, Li and Shu, 2019), were used to identify RING (and confirm RBR) E3 ligase genes. U-box family E3s were searched for using IPR003613 (U-box domain) and PF04564 (U-box), signatures which represent the U-box domain, related to RING finger domains but lacking the zinc atoms (Aravind and Koonin, 2000). Additionally, UniProt (https://www.uniprot.org/) was used to look for genes in the *L. mexicana* genome annotated with the terms “HECT” or “RBR”.

By performing the analyses described above, 4 E1 ubiquitin-activating (UBA1-4), 15 E2 ubiquitin-conjugating (UBC1-15) and 81 E3 ubiquitin ligase (HECT, RBR or RING) genes (Table 2) were initially identified. The putative E3s included 14 HECT, 1 RBR, 57 RING, 4 RING-CH-type and 5 U-box E3s. Upon more detailed analysis using the OrthoMCL orthologue data in Tritrypdb (Li, Stoeckert and Roos, 2003), however, LmxM.08.0220 and LmxM.02.0390 were found to be orthologues of *T. brucei* Uba2 and Ubc9, an E1

catalytic subunit and E2 enzyme for the ubiquitin-like modifier SUMO respectively. Based on this orthology, they were named UBA2 and UBC9 (Ye *et al.*, 2015). Similarly, LmxM.01.0710 (UBA3) was found to share more similarity with HsUBA3 (68% query cover, 35.8% identity, E value: $8e^{-64}$), a Nedd8-activating enzyme catalytic subunit, than the ubiquitin E1 HsUBA1 (46% query cover, 31.7% identity, E value: $3e^{-25}$) and LmxM.24.1710 (UBC12) appears to be an orthologue of *T.* brucei Ubc12, a Nedd8 E2 (Liao *et al.*, 2017). For two of the HECT domain-containing proteins, HECT13 and HECT14, only partial HECT domains of 69 and 60 amino acids were identified respectively. Following the removal of Ubl E1 and E2s and possible pseudo-HECTs from the list of identified ubiquitination genes, 2 ubiquitin E1s, 13 ubiquitin E2s and 79 E3 ligase genes were proposed to be present in the *L. mexicana* genome. Of these, UBC1, a ubiquitin E2, is related to *T. brucei* CDC34 (99% query cover, 55.2% identity, E value: $2e^{-105}$) that is required for cytokinesis and infection progression of the BSF in mice (Rojas *et al.*, 2017). UBC4, also a ubiquitin E2, is related to *T. brucei* PEX4 (100% query cover, 58.6% identity, E value: $5e^{-72}$), implicated in the ubiquitination of TbPEX5, a cytosolic receptor involved in peroxisome biogenesis (Gualdrón-López *et al.*, 2013).

Gene name	**Type**	***L. mexicana* gene ID**	**Size (kDa)**	***T. brucei* orthologue**
UBA1a	Ubiquitin E1	LmxM.23.0550	115.1	Tb927.8.2640
UBA1b	Ubiquitin E1	LmxM.34.3060	126.7	Tb11.v5.0675, Tb927.9.12650
UBA2	SUMO E1	LmxM.08.0220	109.7	Tb927.5.3430
UBA3	Nedd8 E1	LmxM.01.0710	56.1	Tb927.9.4620
UBC1/CDC34	Ubiquitin E2	LmxM.31.0960	30	Tb11.01.5790
UBC2	Ubiquitin E2	LmxM.04.0680	17.1	Tb927.9.8000
UBC3	Ubiquitin E2	LmxM.05.0930	48.8	Tb927.7.6960
UBC4/PEX4	Ubiquitin E2	LmxM.07.0850	20	Tb927.8.920
UBC5	Ubiquitin E2	LmxM.22.0610	28.2	Tb927.7.2540
UBC6	Ubiquitin E2	LmxM.33.1555	18.4	Tb927.4.2710
UBC7	Ubiquitin E2	LmxM.24.2130	17	Tb927.8.6090
UBC8	Ubiquitin E2	LmxM.31.0700	26.3	Tb927.11.13940
UBC9	SUMO E2	LmxM.02.0390	17.1	Tb927.2.2460
UBC10	Ubiquitin E2	LmxM.32.2770	26.1	Tb927.2.3720
UBC11	Ubiquitin E2	LmxM.33.0900	31.7	Tb927.4.3190, Tb927.4.3460
UBC12	Nedd8 E2	LmxM.24.1710	21.6	Tb927.8.6510

UBC13	Ubiquitin E2	LmxM.34.1300	16.7	Tb927.5.1000
UBC14	Ubiquitin E2	LmxM.24.2140	36.4	Not identified
UEV1	Ubiquitin E2 variant	LmxM.13.1580	16	Tb927.11.3310
HECT1	HECT E3 ligase	LmxM.36.6340	455.4	Tb927.10.8390
HECT2	HECT E3 ligase	LmxM.29.0910	153	Tb927.6.2370
HECT3	HECT E3 ligase	LmxM.07.0280	666.2	Tb927.8.1590
HECT4	HECT E3 ligase	LmxM.13.1470	592.1	Tb927.11.3390
HECT5	HECT E3 ligase	LmxM.36.4370	276.8	Tb11.v5.0817, Tb927.10.9750
HECT6	HECT E3 ligase	LmxM.26.2370	421.9	Tb927.9.1770
HECT7	HECT E3 ligase	LmxM.31.1090	178.7	Tb927.11.14330
HECT8	HECT E3 ligase	LmxM.31.3930	453.9	Tb927.11.16260
HECT9	HECT E3 ligase	LmxM.33.3960	149.3	Tb927.4.770
HECT10	HECT E3 ligase	LmxM.34.2450	250.9	Tb927.9.13360
HECT11	HECT E3 ligase	LmxM.34.5390	732.6	Tb927.4.310
HECT12	HECT E3 ligase	LmxM.34.4000	147.1	Not identified
HECT13	HECT E3 ligase	LmxM.33.3400	36.3	Not identified
HECT14	HECT E3 ligase	LmxM.26.2650	63.5	Tb927.9.1350
RBR1	RBR E3 ligase	LmxM.29.2170	58.1	Tb927.6.3780
Not given	RING-type	LmxM.15.1410	52.8	Tb927.9.5260
Not given	RING-type	LmxM.21.0023	12.2	Tb927.10.1810
Not given	RING-type	LmxM.24.1610	13.1	Not identified
Not given	RING-type	LmxM.34.0660	133.9	Tb927.10.3800
Not given	RING-type	LmxM.34.4500	9.4	Tb927.9.10170
Not given	RING-type	LmxM.01.0430	81.2	Tb927.9.4050
Not given	RING-type	LmxM.02.0140	94.1	Tb927.2.2360
Not given	RING-type	LmxM.03.0010	104.9	Not identified
Not given	RING-type	LmxM.04.0540	63.7	Not identified
Not given	RING-type	LmxM.04.0640	35.7	Not identified
Not given	RING-type	LmxM.07.0370	96.5	Not identified
Not given	RING-type	LmxM.08.1091	41.1	Tb927.5.2920
Not given	RING-type	LmxM.08.1215	56.3	Tb927.5.3070
Not given	RING-type	LmxM.09.0140	57.3	Tb927.11.12190
Not given	RING-type	LmxM.09.0350	88.4	Not identified
Not given	RING-type	LmxM.09.0430	51.9	Tb927.11.12440
Not given	RING-type	LmxM.09.1210	44.9	Not identified
Not given	RING-type	LmxM.10.0440	17.6	Not identified
Not given	RING-type	LmxM.10.1140	39.3	Tb927.8.4570
Not given	RING-type	LmxM.12.0100	32	Tb927.6.1190

Not given	RING-type	LmxM.12.1240	96	Tb927.1.4520
Not given	RING-type	LmxM.25.0740	122.7	Tb927.11.750
Not given	RING-type	LmxM.25.2230	38	Tb11.v5.0818, Tb927.3.2340
Not given	RING-type	LmxM.25.2290	33.2	Tb927.3.2410
Not given	RING-type	LmxM.26.1170	55.2	Tb927.7.770
Not given	RING-type	LmxM.26.1560	204.2	Tb927.7.1090
Not given	RING-type	LmxM.27.0570	59.9	Tb11.v5.0388, Tb927.11.1190
Not given	RING-type	LmxM.27.1200	44.1	Tb11.1410, Tb927.11.1810
Not given	RING-type	LmxM.28.0760	83	Tb927.11.8010
Not given	RING-type	LmxM.28.1300	45.9	Tb927.5.4280
Not given	RING-type	LmxM.28.1830	99.6	Tb927.11.8010
Not given	RING-type	LmxM.29.1230	78.8	Tb927.6.2710
Not given	RING-type	LmxM.30.2890	135.3	Tb927.8.7200
Not given	RING-type	LmxM.31.0560	19.8	Not identified
Not given	RING-type	LmxM.13.0230	44.9	Tb927.11.4560
Not given	RING-type	LmxM.16.0650	11.6	Tb927.5.3745
Not given	RING-type	LmxM.17.0030	21	Tb927.7.6190
Not given	RING-type	LmxM.17.0290	76.2	Not identified
Not given	RING-type	LmxM.17.0400	113.6	Not identified
Not given	RING-type	LmxM.18.1150	39.4	Tb927.10.12940
Not given	RING-type	LmxM.18.1570	16.9	Tb927.10.12460
Not given	RING-type	LmxM.19.1150	288.2	Tb11.v5.0394, Tb927.10.15750
Not given	RING-type	LmxM.36.1930	32.6	Not identified
Not given	RING-type	LmxM.36.2930	59.4	Not identified
Not given	RING-type	LmxM.36.3830	34	Tb927.11.9660
Not given	RING-type	LmxM.21.1295	28.2	Not identified
Not given	RING-type	LmxM.22.0060	84.8	Tb927.3.5640, Tb927.7.2050
Not given	RING-type	LmxM.22.0190	50.8	Not identified
Not given	RING-type	LmxM.23.0280	117.9	Not identified
Not given	RING-type	LmxM.23.1730	42.9	Tb927.8.3460
Not given	RING-type	LmxM.24.0080	55.3	Tb927.11.4860
Not given	RING-type	LmxM.24.0300	193.2	Tb927.11.5020
Not given	RING-type	LmxM.24.1380	44.1	Tb927.8.6850
Not given	RING-type	LmxM.24.1390	37.3	Tb927.8.6850
Not given	RING-type	LmxM.25.0340	72	Tb927.3.5390

Not given	RING-type	LmxM.34.2520	42.8	Tb927.9.13300
Not given	RING-type	LmxM.29.2360	60.8	Tb927.6.3640
Not given	RING-CH-type	LmxM.08_29.1630	135	Tb927.3.4220
Not given	RING-CH-type	LmxM.27.0120	70.1	Tb927.3.710
Not given	RING-CH-type	LmxM.30.0030	115.9	Not identified
Not given	RING-CH-type	LmxM.30.1920	140.1	Tb927.4.4880, Tb927.8.7580
Not given	U-box E3 ligase	LmxM.06.0510	71.2	Not identified
Not given	U-box E3 ligase	LmxM.13.0660	76	Tb927.11.4210
Not given	U-box E3 ligase	LmxM.26.1600	72.8	Not identified
Not given	U-box E3 ligase	LmxM.27.2480	53	Tb927.2.5240
Not given	U-box E3 ligase	LmxM.08_29.0780	66.8	Tb927.3.3560

Table 2. *Summary of Leishmania mexicana genes encoding ubiquitination and Ubl-conjugating enzymes identified by bioinformatics.*

3.2.2 Analysis of E1, E2 and E3 genes

Of the putative E1, E2 and E3 genes identified, the predicted molecular weights of encoded proteins range from between 115-127 kDa for E1s, 16-49 kDa for E2s, 147-733 kDa for HECT E3 ligases and 9-288 kDa for RING E3 ligases. Only one RBR-type E3 ligase, with a predicted molecular weight of 58 kDa, was identified. Therefore, the HECT E3 ligases appear to be the class of *L. mexicana* ubiquitination enzymes with both the greatest molecular weight range and the largest proteins at the higher end of their molecular weight range. All of the E1, E2 and HECT and RBR E3s identified had predicted orthologues in the closely related kinetoplastid *T. brucei* (identified using OrthoMCL) except for UBC14 and HECT12. UBC14 did, however, have a predicted orthologous gene in another kinetoplastid species, *T. cruzi* (CL Brener Non-Esmeraldo-like).

To analyse the presence of conserved catalytic residues in the *L. mexicana* E1, E2 and HECT E3 gene families, multiple sequence alignments of *L. mexicana* and human protein sequences were carried out using T-Coffee (Notredame, Higgins and Heringa, 2000). A partial alignment of UBA1a and UBA1b with human ubiquitin-activating E1 enzymes (Figure 5A) revealed conservation of the catalytic cysteine residue (C596 in UBA1a and C651 in UBA1b, equivalent to C632 in HsUBA1 (Xie, 2014)). Upon aligning the *L. mexicana* and human E2 sequences, the conserved catalytic cysteine residue was found in all *L. mexicana* E2s except for UEV1 (Figure 5B), suggesting that UEV1 is a

non-catalytic UEV family protein (Sancho *et al.*, 1998). Furthermore, the conserved HPN (His-Pro-Asn) motif, which is conserved in human E2s and which contains an asparagine residue that can be important for catalysis (Wu *et al.*, 2003; Jones *et al.*, 2019; Berndsen *et al.*, 2013), was found to be partially or completely missing in UBC3, UBC6, UBC11 and UBC14, as well as UEV1. When the HECT domains of *L. mexicana* HECT E3 ligases (identified using Interpro domain searches) and the HECT domain of four human E3 ligases were aligned, HECT E3s 1-12 were shown to contain the conserved catalytic cysteine residue. HECT13 and HECT14, in contrast, lacked a putative catalytic cysteine, consistent with the identification of a partial HECT domain in these sequences and suggesting that they may be pseudogenes or possess alternative, non-catalytic functions (Figure 5C).

The high degree of substrate specificity possessed by eukaryotic E3s is due in part to their protein-protein interactions domains (Metzger, Hristova and Weissman, 2012). In order to identify the domain structures of *L. mexicana* HECT and RBR E3s, the protein sequences were analysed using Interpro domain searches. All 12 HECT E3s (Figure 6) contained C-terminal HECT domains as is typical for this class of E3s (Metzger, Hristova and Weissman, 2012). In addition, numerous other domains were detected N-terminal to the HECT domains. HECT1 and HECT4 have large B30.2/SPRY (IPR001870) domains and HECT6, HECT8 and HECT11 have one or more SPRY domains (IPR003877). Both B30.2/SPRY and SPRY domains are likely to be protein interaction sites (Woo *et al.*, 2006). HECT6, HECT7 and HECT8 all contain zinc finger domains, with HECT6 and HECT8 containing ZZ-type zinc finger domains (IPR000433), thought to be protein-protein interaction domains (Legge *et al.*, 2004), and HECT7 containing a RanBP2-type zinc finger domain (IPR001876). HECT7 and HECT10 contain ARM domains (IPR011989, IPR016024) with protein or nucleic acid-binding potential and HECT8 contains a YVTN-like (IPR011044) region. HECT12 has both a tetratricopeptide repeat (TPR) domain (IPR013026) that could facilitate protein-protein interactions (Lamb, Tugendreich and Hieter, 1995) and a protein kinase domain (IPR000719), suggesting a dual function of this protein in phosphorylation and ubiquitination. No additional domains were detected for HECT2, HECT5 or HECT9. Aside from the previously identified RING and IBR domains, no domain structures were identified for RBR1.

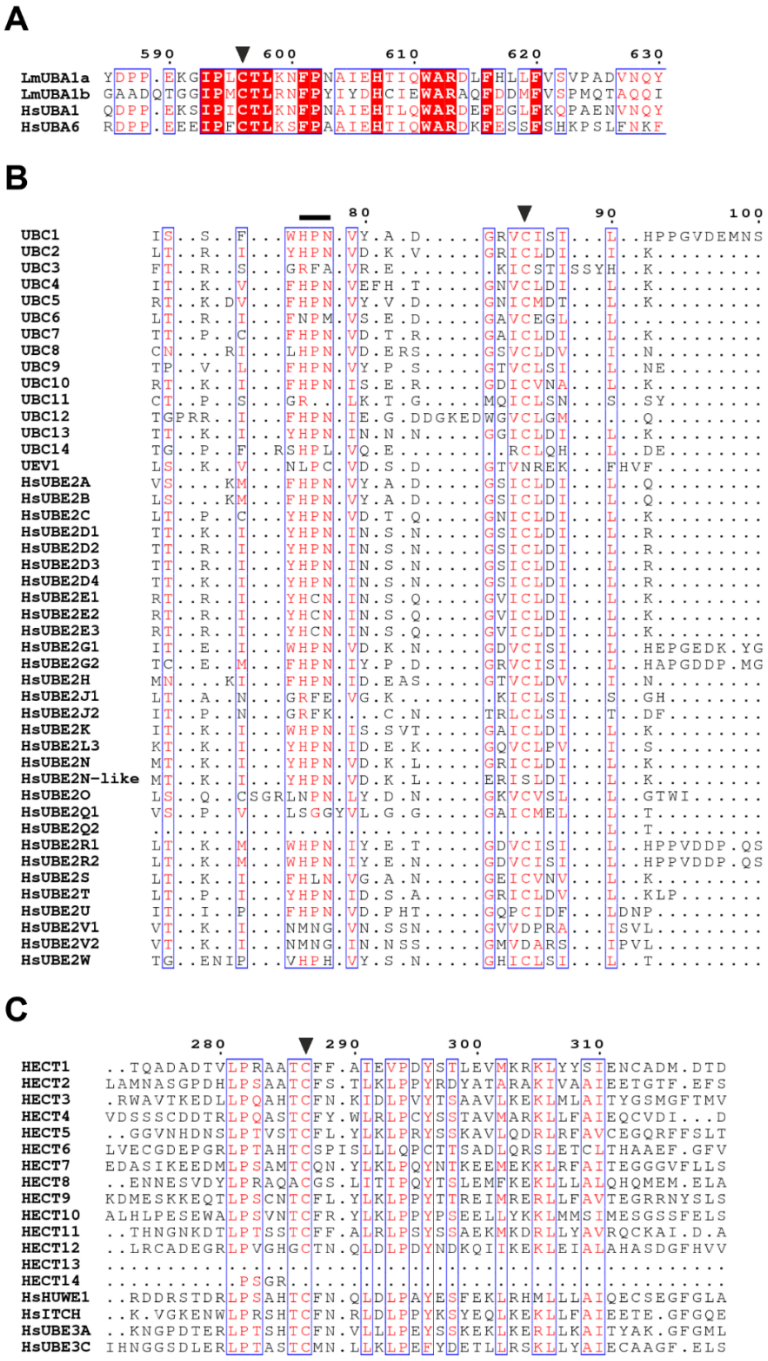

Figure 5. *Partial alignments of L. mexicana and H. sapiens protein sequences.* Residues in the local vicinity of **A** E1 ubiquitin-activating enzyme, **B** E2 ubiquitin-conjugating enzyme and **C** E3 ubiquitin ligase HECT domain catalytic residues are shown. Sequences obtained from TriTryDB (*L. mexicana*) and NCBI or UniProt (*H. sapiens*) were aligned using T-Coffee. Red boxes indicate amino acid identity, red characters show similarity within the highlighted group and blue frames highlight similarity across groups. Black bar indicates the position of the conserved HPN motif in E2 proteins and the black triangles highlight the conserved catalytic cysteine residues in all classes of protein. *L. mexicana* proteins are indicated with the prefix Lm and *H. sapiens* proteins with the prefix Hs. Where no prefix is given, sequences belong to *L. mexicana*.

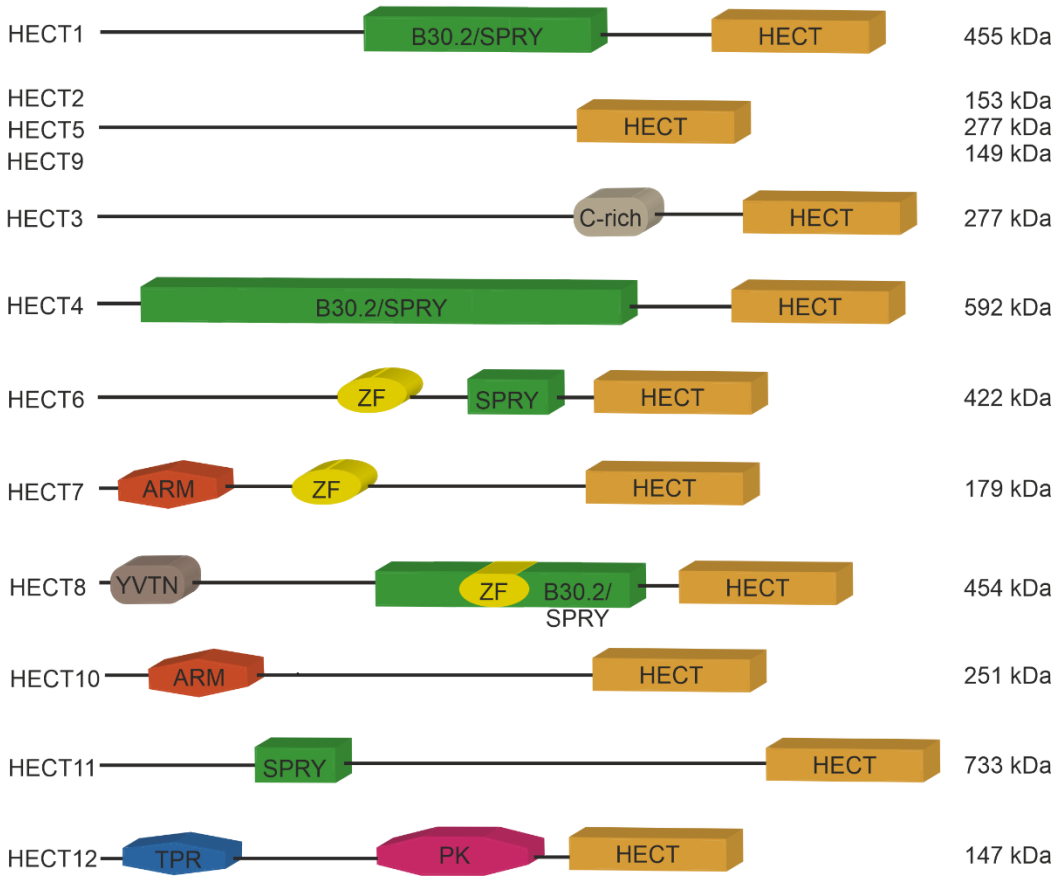

Figure 6. *Domain structures of L. mexicana HECT E3 ligases.* Interpro was used to identify domain structures in the protein sequences of HECTs 1-12. B30.2/SPRY (IPR001870), HECT (IPR000569), SPRY (IPR003877), zinc finger (ZF, IPR000433 or IPR001876), armadillo-like or armadillo-type (ARM, IPR011989 or IPR016024), tetratricopeptide repeat-containing (TPR, IPR013026) and protein kinase (PK, IPR000719) domains were identified. A cysteine-rich and YVTN-like (IPR011044) region were also found. Length of proteins is not to scale due to the large molecular weight range (147-733 kDa). Instead the molecular weights are indicated beside the proteins.

3.2.3 Localisation of *Leishmania* E1, E2 and HECT/RBR E3s

In an attempt to identify interesting proteins for future study and explore the interaction potential of the 4 E1, 15 E2 and 13 HECT/RBR E3 enzymes, the corresponding genes were endogenously tagged with mNeonGreen (Shaner *et al.*, 2013) in procyclic promastigotes using CRISPR-Cas9 (Beneke *et al.*, 2017). The mNeonGreen tag additionally includes a 3 x myc tag (henceforth referred to as myc-mNeonGreen). N-terminal tagging was applied for all genes except for UBA3, which was tagged at the C-

terminus. N-terminal tagging was deemed the best strategy for the HECT E3 ligases in particular as it was thought least likely to negatively affect the C-terminal catalytic HECT domain and thereby interfere with protein function. Notably, none of the genes of interest contained predicted N-terminal signal sequences. Following transfection with the appropriate sgDNAs (targeting the 5'- or 3'-end of the gene of interest for N- and C-terminal tagging respectively) and blasticidin resistance repair cassettes, cells were selected for cassette integration on the population level using blasticidin. In theory, this strategy would produce mixed populations of cells, with each cell containing between one and the maximum number of tagged alleles of the targeted gene.

Figure 7 contains representative live cell images for each tagged cell line in 3 channels: mNeonGreen, Hoechst 33342 and differential interference contrast. Hoechst 33342 stain was included in order to distinguish the nucleus and kinetoplast by virtue of its nucleic acid-binding capacity, enabling co-localisation imaging to be performed for these two organelles. The larger patch of stained DNA represents the nucleus whereas the smaller patch represents the kinetoplast. In this way, UBA1a, UBA1b and UBA3 were found to be localised to the cytoplasm, defined as distribution throughout the cell, including inside the nucleus and flagellum. In contrast, UBA2 signal was detected only in the nucleus, consistent with the finding that *T. brucei* SUMO is localised to the nucleus (Liao *et al.*, 2010). Of the 15 E2s, 11 were cytoplasmically localised whereas UBC3 was cytosolic, defined as being found in the main body of the cell but excluding organelles such as the nucleus. Although classified as cytoplasmic and cytosolic respectively, the distribution of UBC1/CDC34 and UBC3 was not even, instead showing a patchy or dotted appearance. UBC6 was found to be enriched in the kinetoplast although signal from myc-mNeonGreen-UBC6 was seen throughout the cytoplasm. Similarly, UBC9 was enriched in the nucleus although signal was seen in the cytosol, again consistent with the reported localisation of TbSUMO (Liao *et al.*, 2010).

UBA1a

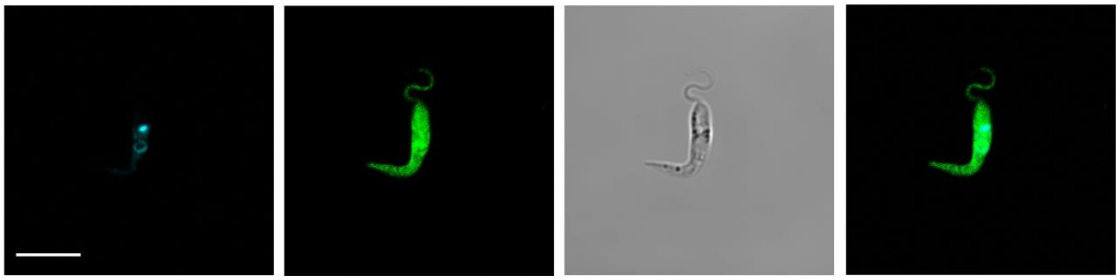

UBA1b

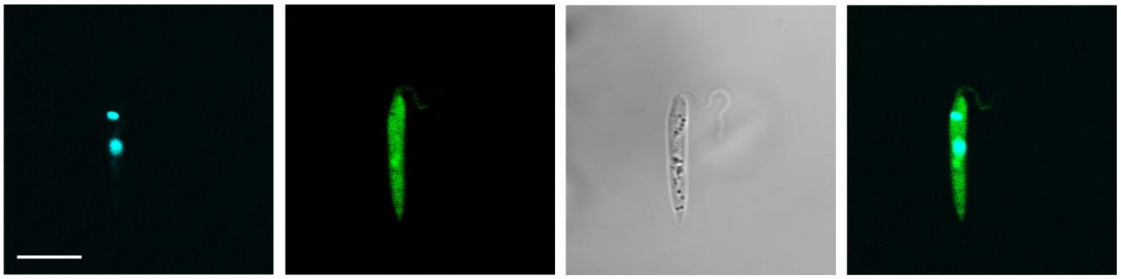

UBA2

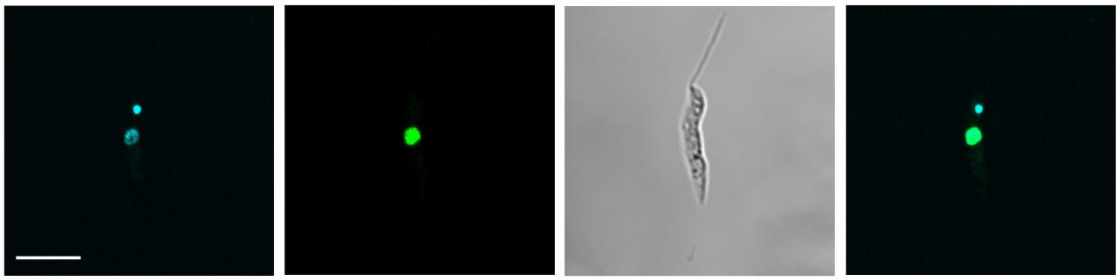

UBA3

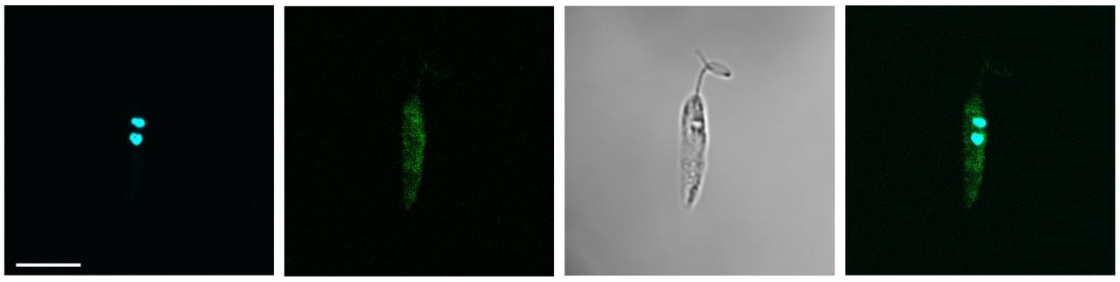

UBC1/CDC34

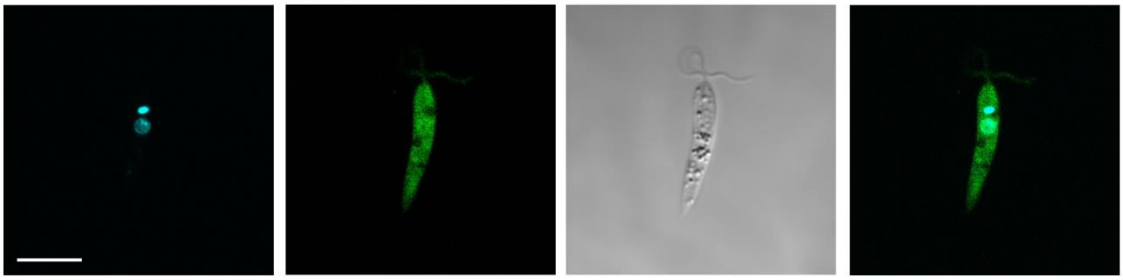

UBC2

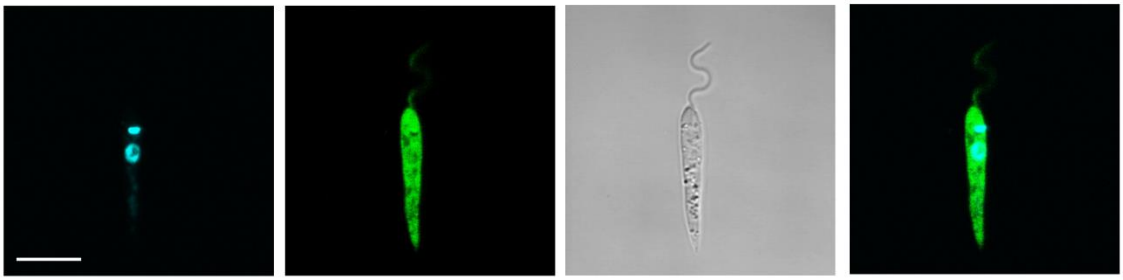

UBC3

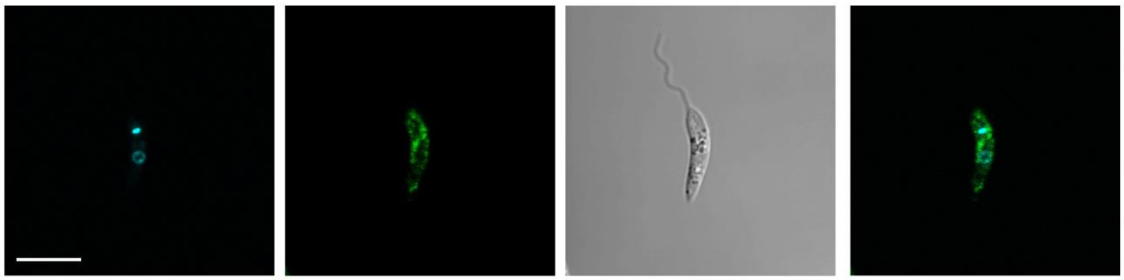

UBC4/PEX4

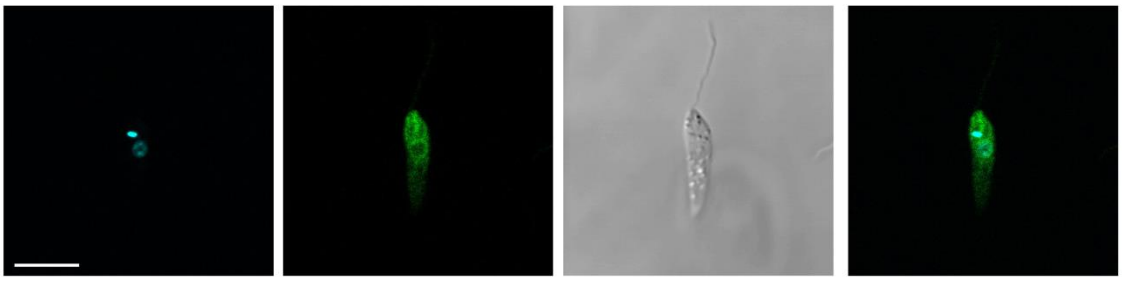

UBC5

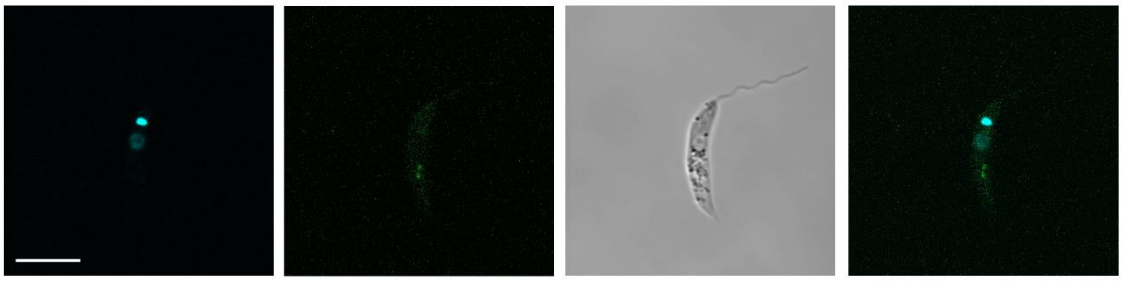

UBC6

UBC7

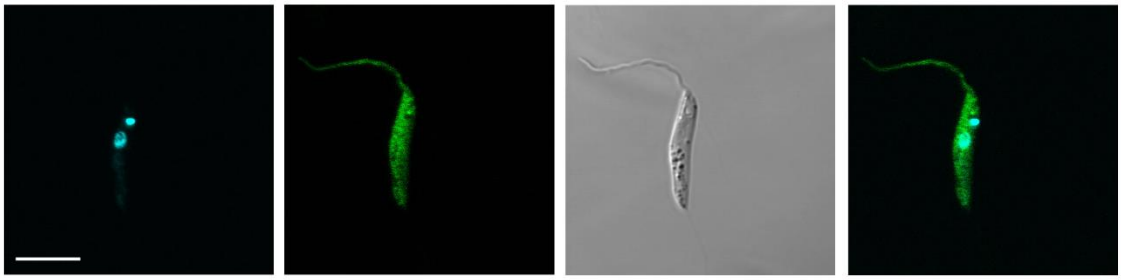

UBC8

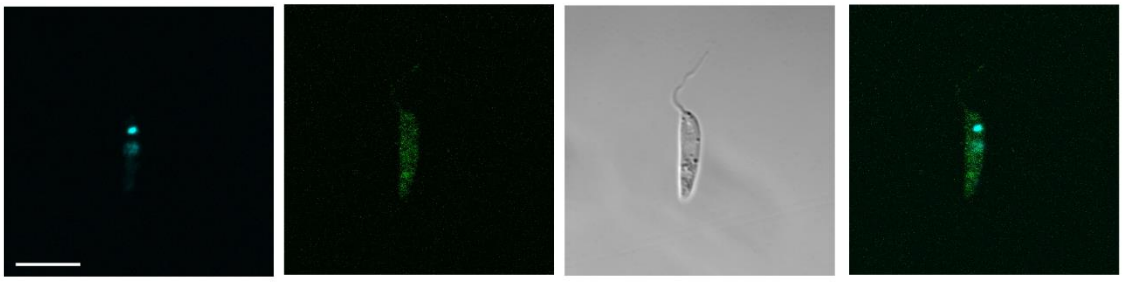

UBC9

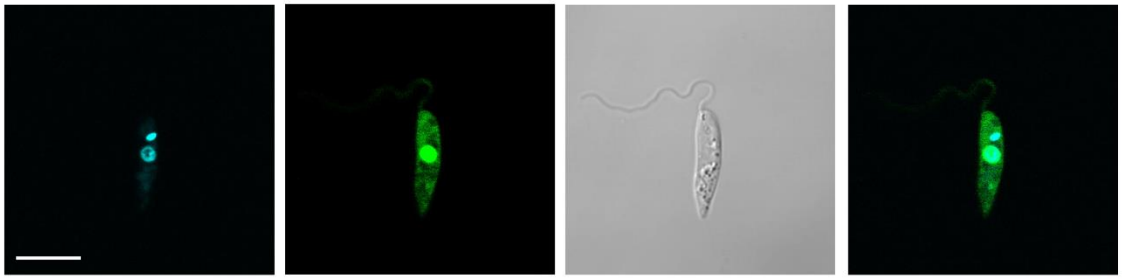

UBC10

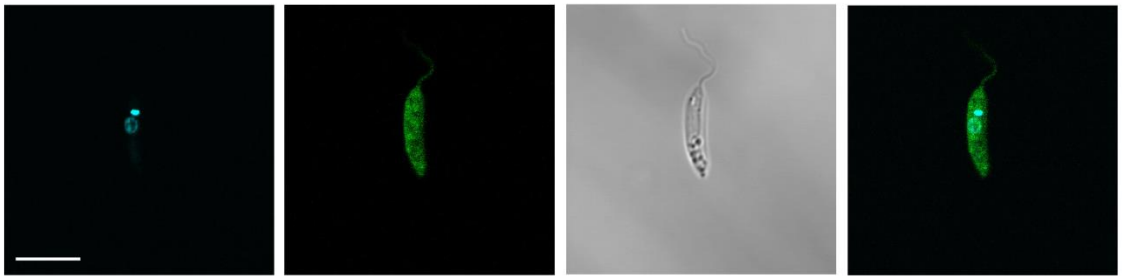

UBC11

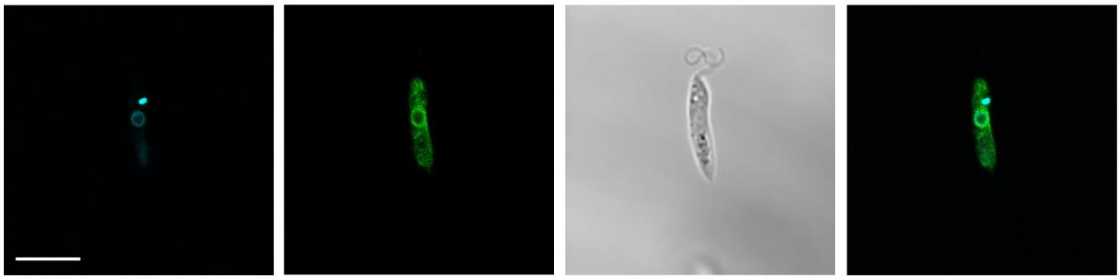

UBC12

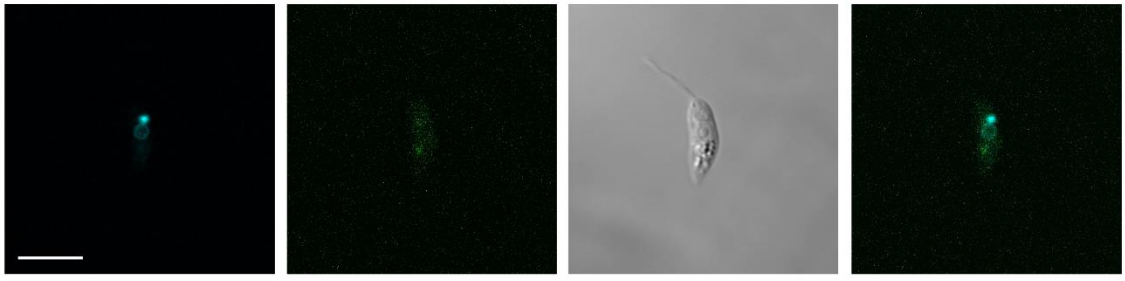

UBC13

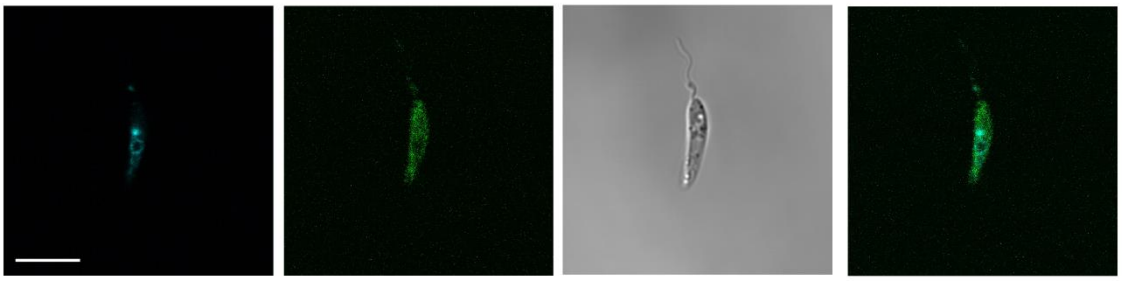

UBC14

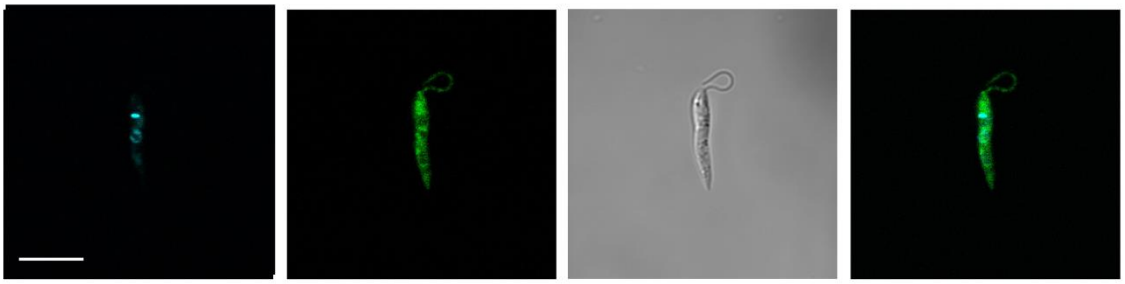

UEV1

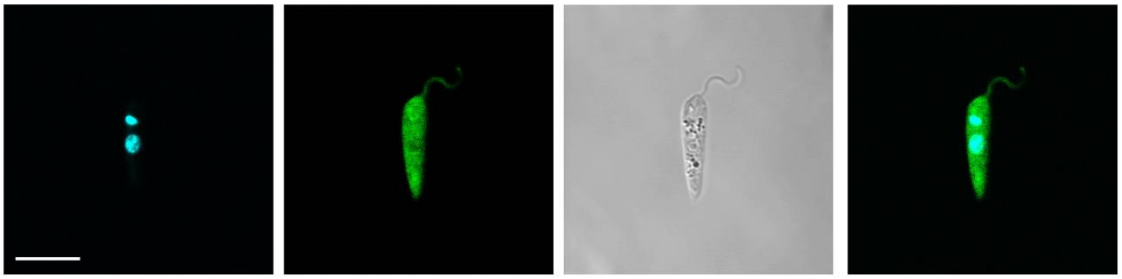

HECT1

HECT2

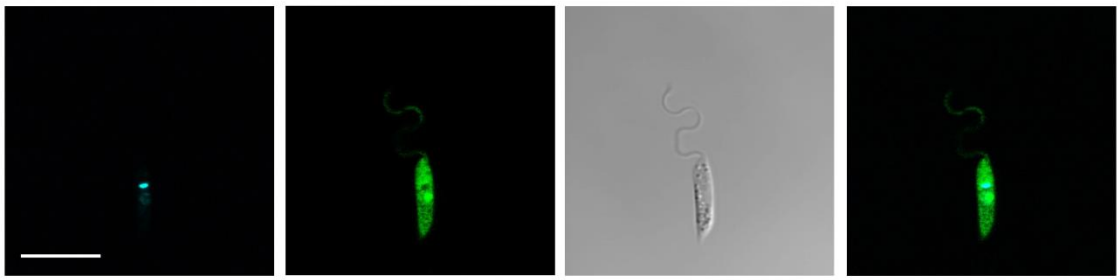

HECT3

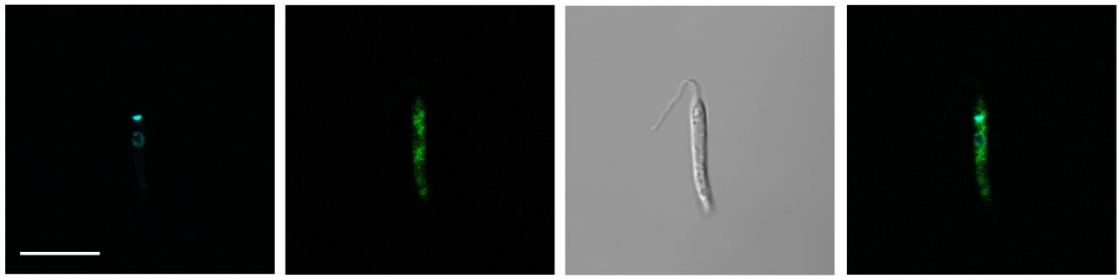

HECT4

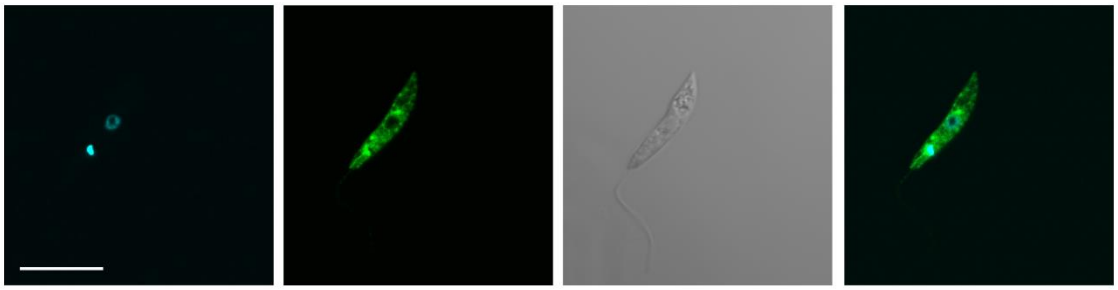

HECT5

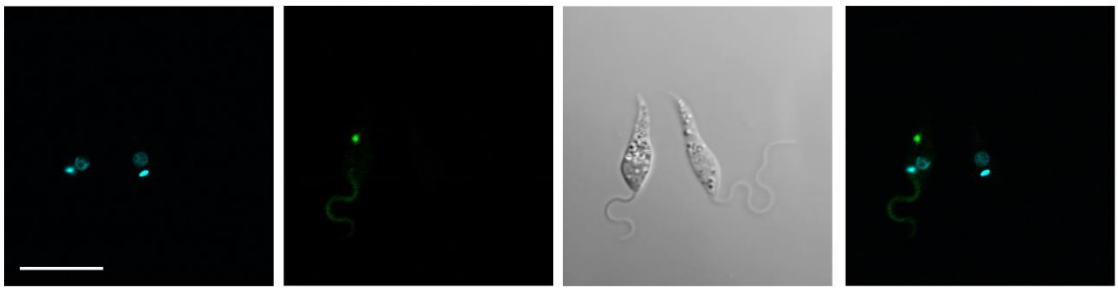

HECT6

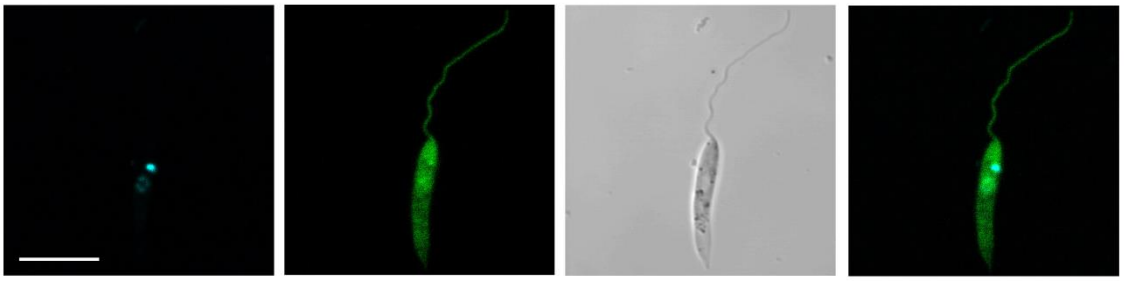

HECT7

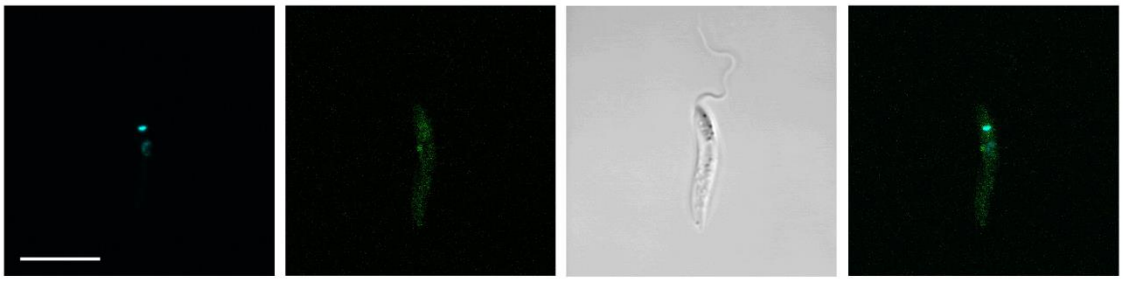

HECT8

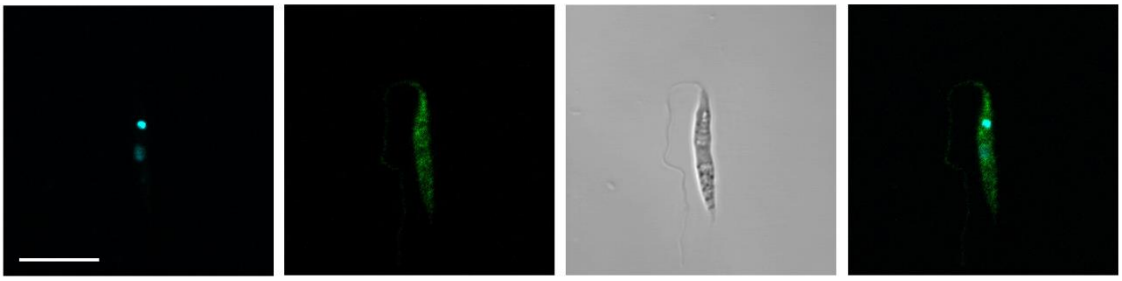

HECT9

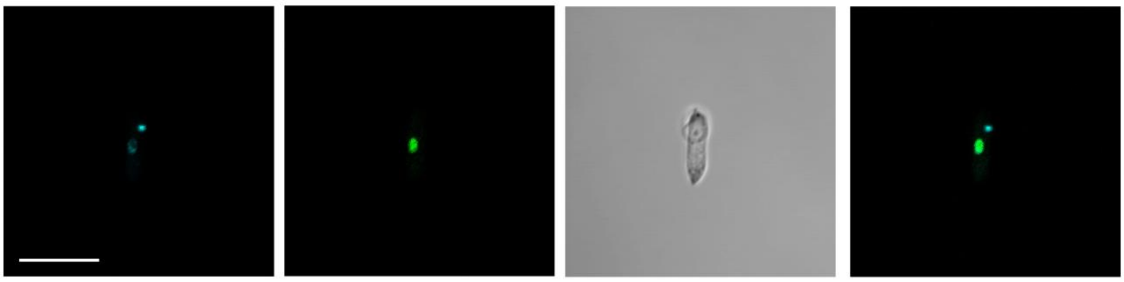

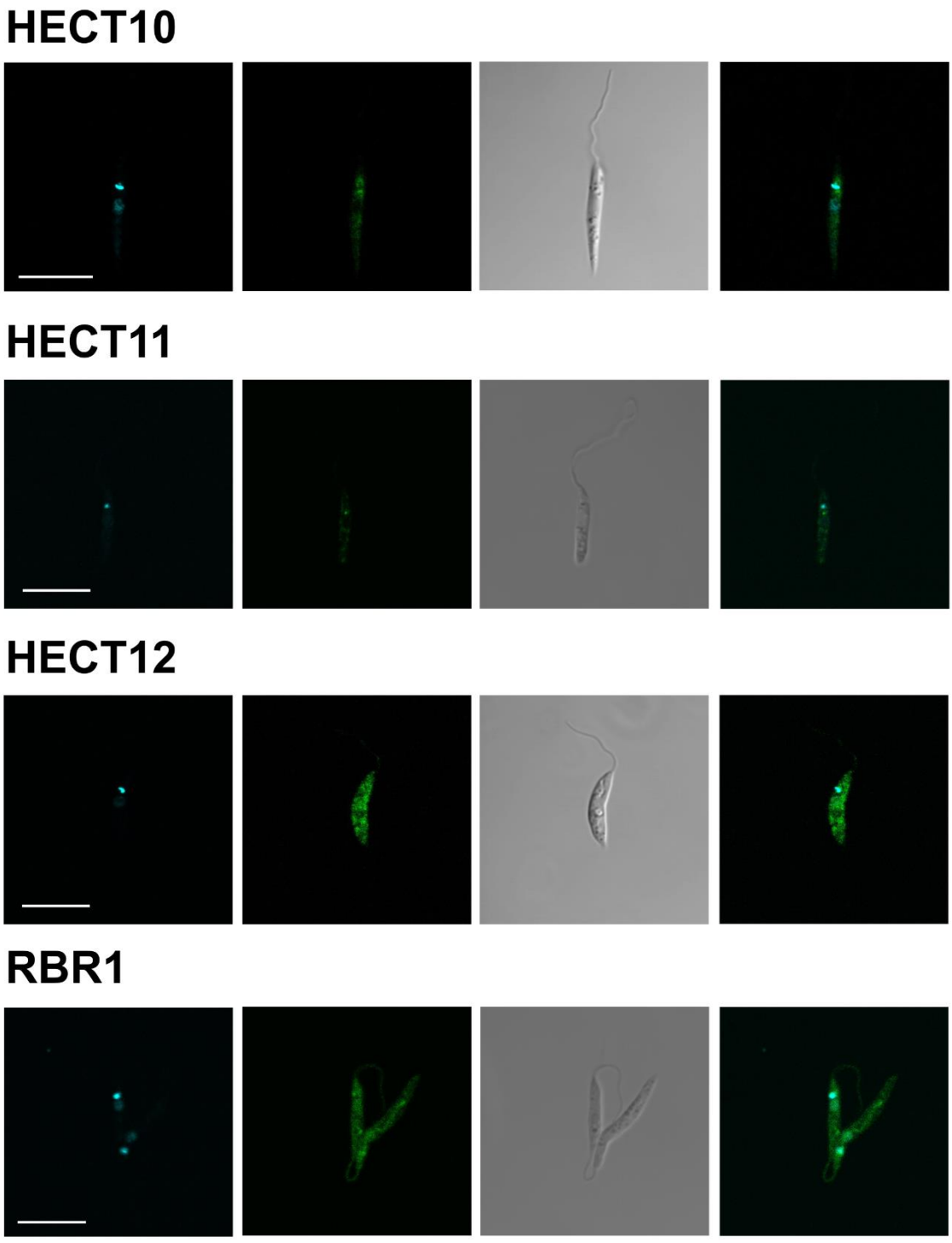

Figure 7. *Localisation of selected E1, E2 and E3 proteins in L. mexicana promastigotes.* Panels from left to right show Hoechst 33342 staining of the nucleus and kinetoplast, mNeonGreen signal of the tagged protein, a differential interference contrast image and a merged Hoechst/mNeonGreen image. Scale bars represent 10 µm.

Of the 12 HECT E3 ligases, 4 were cytoplasmically localised and 4 (HECT1, HECT8, HECT10 and HECT11) were cytosolic. Of these, HECT1, HECT3 and HECT11 have a patchy or dotted distribution and HECT12 was found to be enriched just anterior of the kinetoplast, around the region of the basal body (Halliday *et al.*, 2019). Less common localisations observed included HECT9, found in the nucleus, and HECT4, which showed a reticular pattern resembling the mitochondrion (Halliday *et al.*, 2019). Additionally, HECT5 was found localised to a single dot posterior to the nucleus, with some (less than half) of the cells showing flagellar localisation. RBR1 was enriched in the kinetoplast but also found throughout the rest of the cell. The localisations described here are summarised diagrammatically in Figure 8.

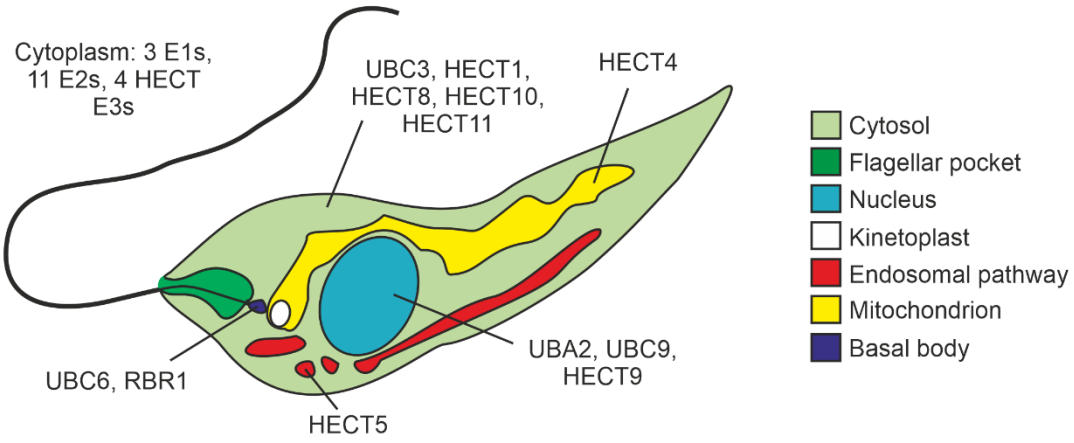

Figure 8. *Summary of E1, E2 and HECT/RBR E3 localisations in L. mexicana.* Compartment(s) containing the most prominent mNeonGreen signal for each tagged protein are indicated.

3.2.4 Generation of a null mutant E1, E2 and HECT/RBR E3 library

In order to investigate the role of ubiquitination, SUMOylation and Neddylation genes in the life cycle of *L. mexicana*, the 4 E1, 15 E2, 12 HECT E3 and 1 RBR E3 genes were targeted for deletion in procyclic promastigotes using CRISPR-Cas9 (Beneke *et al.*, 2017). In contrast to the endogenous tagging strategy, however, two sgDNAs targeting the 5'- and 3'-UTRs and two types of repair cassette (containing two different antibiotic resistance markers) were typically used for integration into the targeted gene locus. Additionally, repair cassettes were designed to contain unique 12 nt barcodes (upstream of the 30 nt homology region) that could allow for the identification of individual null mutant lines in a pooled context.

Three rounds of transfection were performed in order to reduce the likelihood of not obtaining a null mutant line due to technical failure. This meant that unless a null mutant line was successfully generated, PCRs and transfections were carried out three times for each gene of interest. Null mutant lines were validated using PCRs to detect removal of the gene of interest (amplification of ~500 bp region within the gene of interest) and integration of the blasticidin resistance repair cassette (amplification of the ~800 bp region between the 5'-UTR of the gene and the blasticidin resistance repair cassette) (Figure 9A). After two rounds of transfection, null mutants were generated for all genes except UBA1a, UBC3, UBC7, UBC12, UBC13 and HECT3 (Figure 9B). Given the unusually large size of the HECT3 gene (18.6 kbp), the largest of the *L. mexicana* HECT E3s, it was decided to redesign the 5' and 3' sgDNA primers and the 5' cassette primer in order to target only the first 8 kbp of the gene for editing. This was done in the hope of increasing the efficiency of cassette integration by homologous recombination (which may have been very low over the original 19 kbp distance) and with the aim of removing the ATG start codon required for translation. The first round of transfection with sgDNA and repair cassettes amplified using the new primers successfully produced a HECT3 null mutant. A third round of transfection, an attempt to produce null mutants that had still not been generated, did not produce any new null mutants. Although drug resistant clones were obtained for UBA1a, UBC3, UBC7 and UBC12, they still contained the gene of interest (Figure 9C). Since these mutants were resistant to both blasticidin and puromycin (suggesting that deletion of at least two alleles of the gene of interest has occurred), gene duplication events are likely to have occurred to allow the parasite to retain the gene, highlighting the importance of these genes for promastigote survival. No mutant clones were obtained for UBC13 so a technical failure in the CRISPR-Cas9 procedure cannot be ruled out. Δ*hect12* was generated and confirmed (using similar methods) by Carolina Catta-Preta.

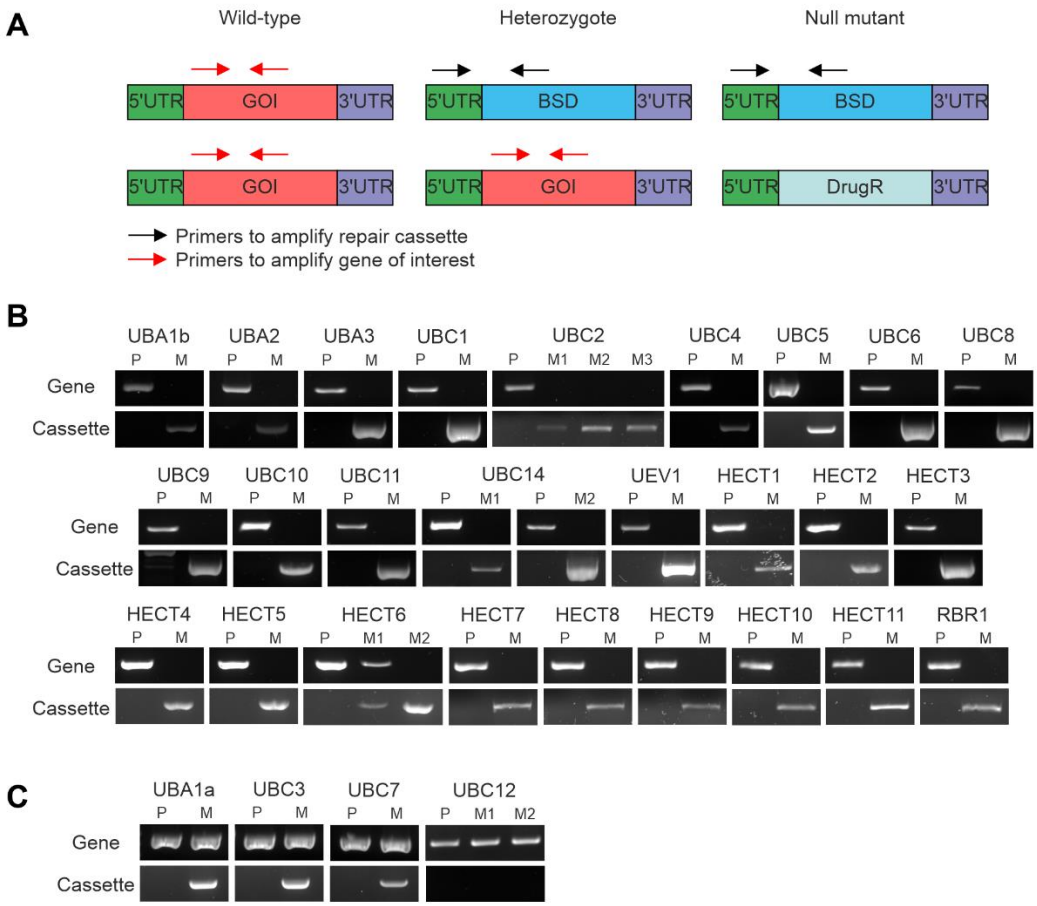

Figure 9. *Confirmation of the null mutant library*. **A** Schematic of PCRs performed to identify null mutants from heterozygotes or mutants with additional gene copies. Primers were designed to amplify regions within the gene of interest (GOI, red primers) and between the 5'-UTR of the gene and the blasticidin resistance repair cassette of the edited DNA (black primers). **B** PCRs performed on genomic DNA from parental (P) and mutant (M) cells are shown for genes that were deleted successfully. **C** PCRs performed on genomic DNA from parental (P) and mutant (M) cells are shown for genes that could not be deleted (no mutant clones were obtained for UBC13).

The ability to generate null mutants for all genes except UBA1a, UBC3, UBC7, UBC12 and UBC13 suggests that 1 out of 2 ubiquitin E1s and 3 out of 13 ubiquitin E2s may be essential in promastigotes. Interestingly, a null mutant was successfully generated for UBA3 (putative Nedd8 E1) despite UBC12 (putative Nedd8 E2) appearing to be essential. This could indicate the existence of an additional Nedd8 E1 that is capable of loading UBC12 or suggest that the essential function of UBC12 is independent of its role in Neddylation. None of the SUMOylation, HECT E3 or RBR E3 genes were essential in promastigotes, as evidenced by the successful generation of null mutants for these genes.

3.2.5 Activity profiling of null mutant lines

To confirm the generation of null mutants at the level of protein activity (and to identify active ubiquitination enzymes in *L. mexicana* cell lysates), an activity-based triple-E probe was used (Mulder *et al.*, 2016). This probe, based on the human ubiquitin sequence but with the C-terminal Gly76 replaced with dehydroalanine (Ub-Dha), can pass between E1 ubiquitin-activating, E2 ubiquitin-conjugating and cysteine-dependent (HECT/RBR) E3 ubiquitin ligase enzymes through sequential trans-thioesterification reactions, although there has been no reported use in *L. mexicana* (Figure 4). Importantly, at each stage in the cascade, Ub-Dha can become covalently bound to the active site cysteine of ubiquitination enzymes, enabling their subsequent detection. It was proposed that this probe would likely interact with *Leishmania* E1, E2 and HECT/RBR E3 enzymes since *Leishmania* ubiquitin only has 2 amino acid substitutions relative to human ubiquitin (Figure 10). Initially, optimisations for lysis buffer detergent, probe concentration, ATP concentration, $MgCl_2$ concentration, incubation time and temperature were performed. Figure 11 shows the profiling of Cas9 T7 and Δ*uba1b* promastigote lysates with Cy5-tagged triple-E probe (Cy5-Ub-Dha). The predicted molecular weights of UBA1b and Cy5-Ub-Dha are 127.6 kDa and 9.1 kDa respectively. Therefore, the expected molecular weight for UBA1b bound to probe is 136.7 kDa. A protein is detected at the expected size for the Cas9 T7 sample but is absent in the Δ*uba1b* sample, providing further evidence that a Δ*uba1b* mutant has been successfully generated. This finding also suggests that UBA1b is active in *L. mexicana* promastigotes. Additionally, that a protein of around 150 kDa is present in the Δ*uba1b* but not the wild-type InstantBlue™-stained sample may indicate that UBA1b regulates the abundance of this protein. Also visible are polymeric forms of Cy5-Ub-Dha, seen in the Cy5 image, but not the InstantBlue™ stain of the same gel. Since the predicted molecular weights of *L. mexicana* ubiquitin E2s range between 16-49 kDa, these polymers would likely interfere with E2 identification using Cy5-Ub-Dha. Furthermore, based on the banding pattern seen in Cas9 T7 cells, the large (147-733 kDa) HECT E3 ligases also appear to be mostly absent, perhaps because they are difficult to separate on an SDS-PAGE gel. For these two reasons, in addition to the poor reproducibility of sample profiling seen with this probe, extensive profiling of the null mutant library was not performed.

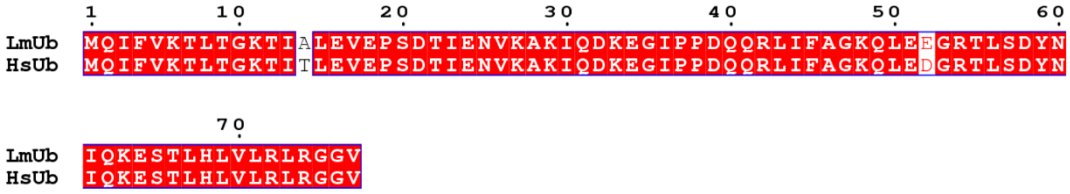

Figure 10. *Alignment of L. mexicana and H. sapiens ubiquitin protein sequences.* Red boxes indicate amino acid identity, red characters show similarity within the highlighted group and blue frames highlight similarity across groups.

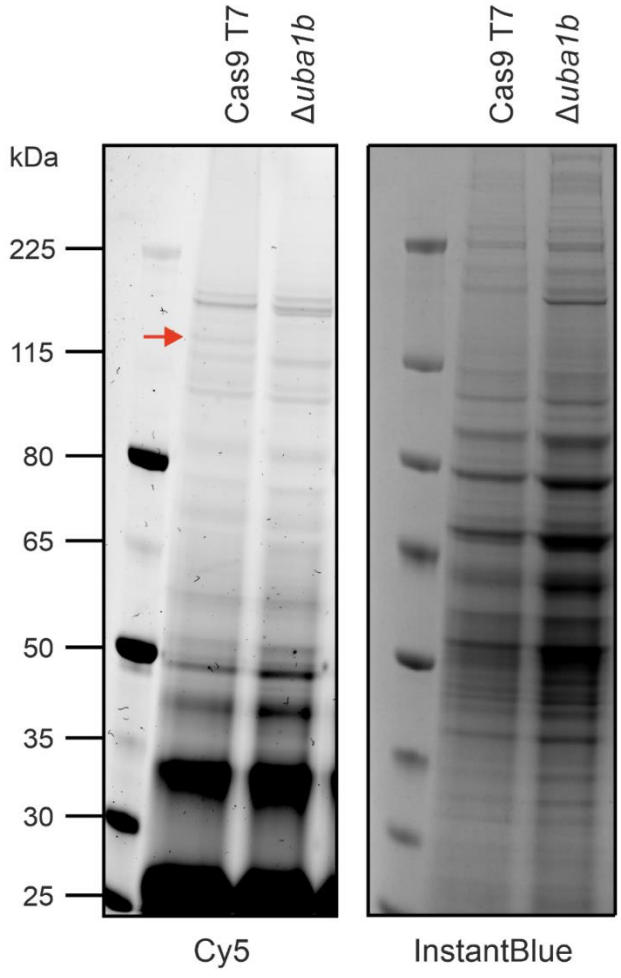

Figure 11. *Activity-based profiling of Cas9 T7 and Δuba1b cell lysates.* Cells were lysed in lysis buffer containing Cy5-Ub-Dha triple-E probe and then incubated with ATP and $MgCl_2$ for 1 h at 37°C. Fluorescence imaging in the Cy5 channel and InstantBlue™ staining of the same gel are shown. Red arrow indicates the position of UBA1b.

3.2.6 Bar-seq screen for defects in differentiation and infection

Given the large amount of time and resources that phenotyping 27 (3 E1, 11 E2 and 13 E3) null mutants individually would require, a bar-seq strategy was instead utilised to assess the role of ubiquitination, SUMOylation and Neddylation genes in the life cycle of *L. mexicana*. Bar-seq methods involve the parallel phenotyping of pools of mutants using next-generation sequencing (Smith *et al.*, 2009), for which purpose unique 12 nt barcodes had been inserted into individual null mutants. Our bar-seq screen aimed to identify genes required for differentiation and infection and that may be of interest for further study. To achieve this, 58 promastigote-stage null mutants, including 3 E1, 10 E2 (excluding Δ*ubc5*, which was obtained following initiation of the screen) and 13 E3 null mutants were pooled in equal proportions and in 6 replicate samples. Pooled promastigote (PRO) cultures were grown for 7 d and then induced to form axenic amastigotes (AXA) or used to purify metacyclic stage promastigotes (META). Purified metacyclic cells were used to infect macrophages (inMAC) in culture or mice using footpad injection (FP). At the time points indicated in Figure 12A, DNA was extracted to allow for amplification of the barcoded regions by PCR and quantitative analysis by next generation sequencing.

To analyse fitness phenotypes of the null mutant lines, the number of reads for each barcode were first divided by the total number of reads for expected barcodes at each experimental stage and data averaged across the 6 replicates. Upon matching barcodes back to their respective null mutant lines, changes in the average proportional representation of these lines were used to infer changes in fitness. Unpaired t-tests using the Holm-Šídák multiple comparison method were performed between adjacent time points in order to assess statistically significant loss-of-fitness. Gain-of-fitness phenotypes could not be analysed confidently due to the fact that there is a higher likelihood for null mutant lines to exhibit decreased, rather than increased, fitness during the experiment (which would lead to a proportional increase in the remaining null mutant lines, mimicking gain-of-fitness). Tests of statistical significance were only performed between adjacent time points due to the potential for null mutant lines to cumulatively acquire fitness changes throughout the duration of the experiment, enabling the experimental period linked with a particular viability defect to be correctly identified. This experiment was first described in Damianou *et al.* (2020).

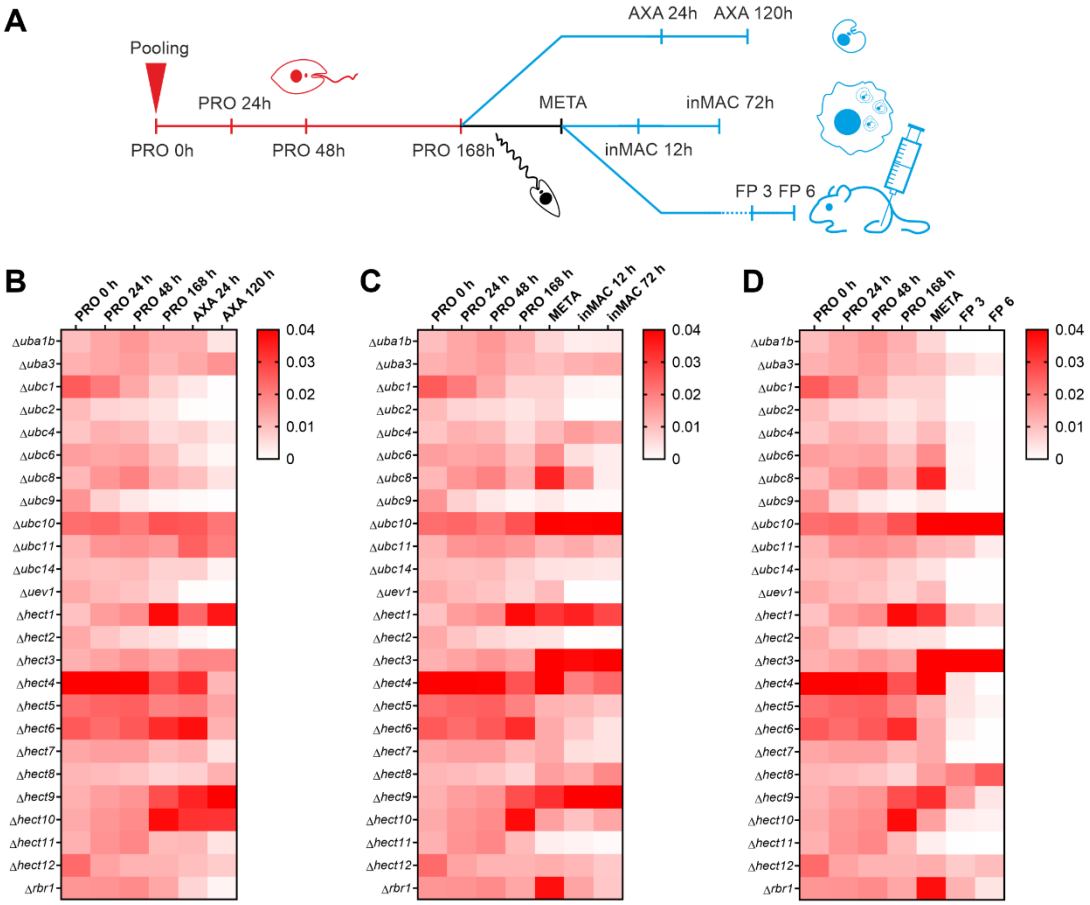

Figure 12. *Life cycle phenotyping of ubiquitination gene null mutants.* Fifty-eight null mutant lines, including 3 E1, 11 E2 and 13 E3 null mutants, were pooled (n = 6) as procyclic promastigotes and grown to stationary phase. Cells were then induced to differentiate into axenic amastigotes *in vitro* or metacyclic promastigotes purified and used to infect macrophages or mice. **A** Experimental workflow showing the time points at which DNA was extracted for barcode amplification and next generation sequencing. The heat maps for promastigote to **B** axenic amastigote, **C** macrophage infection or **D** mouse infection experiments show the average proportional representation of each null mutant at each experimental time point, calculated by dividing the number of reads for null mutant-specific barcodes by the total number of reads for expected barcodes. Samples included represent promastigote time-point zero (PRO 0 h), early-log phase (PRO 24 h), mid-log phase (PRO 48 h), late-log phase (PRO 72 h), stationary phase (PRO 168 h), early axenic amastigote differentiation (AXA 24 h), post-axenic amastigote differentiation (AXA 120 h), purified metacyclic promastigotes (META), early macrophage infection (inMAC 12 h), late macrophage infection (inMAC 72 h), 3 week mouse footpad infection (FP 3) and 6 week mouse footpad infection (FP 6).

The bar-seq experimental data are summarised in Figure 12B-D in heat maps displaying the proportional representation of each null mutant line at each experimental time point,

with a gradient of white to red representing proportions ranging between zero and 0.04 (or above) respectively. For Δ*uba2*, only 2.6 x 10^6, instead of 4 x 10^6 cells, were added to the pools due to the poor prior growth of this cell line. Furthermore, the associated barcode was not detected in all of the PRO 0 h time points, prompting the decision to exclude this cell line from the analysis. Between the PRO 0 h and PRO 168 h samples, there was no complete loss of any null mutant line from the populations, although several loss-of-fitness phenotypes (decreases in proportional representation within the population) were observed between adjacent timepoints (<0.05, unpaired t-test, Holm-Šídák method, S4 Table, Damianou *et al.* (2020)). For example, reduced fitness was seen at two or more promastigote time points for Δ*ubc9*, Δ*hect2* and Δ*hect12.* No loss-of-fitness phenotypes were observed between the PRO 168 h and META samples or between the PRO 168 h and AXA 24 h samples.

Within both the AXA 24 h-AXA 120 h and META-inMAC 12 h intervals, loss-of-fitness was observed for 10 null mutants: Δ*uba1b,* Δ*ubc2,* Δ*ubc6,* Δ*ubc8,* Δ*ubc9,* Δ*uev1,* Δ*hect2,* Δ*hect4*, Δ*hect7* and Δ*rbr1,* demonstrating good correlation between these two experiments. Of these, strong defects (>3-fold decrease in fitness) were observed for Δ*ubc1/cdc34*, Δ*ubc2,* Δ*uev1* and Δ*hect2*. In addition, Δ*ubc4/pex4,* Δ*ubc11, Δubc14,* Δ*hect5,* Δ*hect6,* Δ*hect11* and Δ*hect12* showed loss-of-fitness between the AXA 24 h and AXA 120 h samples and Δ*hect10* showed a reduction in fitness between the META and inMAC 12 h samples. Further loss-of-fitness for Δ*ubc8* and Δ*rbr1* was observed between inMAC 12 h and inMAC 72 h. All null mutant lines that showed loss-of-fitness defects in the axenic amastigote and macrophage samples also had compromised fitness in the mouse, although many of phenotypes observed were more severe. Specifically, Δ*uba1b,* Δ*ubc1/cdc34,* Δ*ubc2,* Δ*ubc9,* Δ*ubc14*, Δ*uev1,* Δ*hect2,* Δ*hect7* and Δ*hect11* had at least 20-fold reductions in fitness between the META and FP 3 samples. Additionally, Δ*uba3* and Δ*hect1* showed small decreases in fitness during this interval. Notably, Δ*ubc1/cdc34*, Δ*ubc2*, Δ*uev1* and Δ*hect2* showed the most dramatic and consistent loss-of-fitness phenotypes, including >5-fold, >25-fold and >200-fold decreases in fitness across the axenic amastigote, macrophage infection and mouse infection experiments respectively (calculated between the PRO 168 h/META sample and the experimental endpoints). A pBLAST search revealed that HECT2 is related to human UBE3C (28% query cover, 35.3% identity, $1e^{-64}$ E value), a HECT E3 ligase that ubiquitinates proteasome substrates to enhance proteasomal processivity (Chu *et al.*, 2013). Overall, Δ*ubc2* and Δ*uev1* had the most severe phenotypes with reductions in fitness of 50-fold in the axenic amastigote, 200-fold in the macrophage and a complete loss-of-fitness (to zero) in the mouse.

3.2.7 Validation of defects in amastigote differentiation

One of the caveats of the bar-seq experiment is that some null mutant lines could be affected by the presence of other null mutant lines in the population. For example, there may be competition for environmental resources that prevents a less well-adapted null mutant line from surviving, even though it may survive well on its own. Therefore, to validate the phenotypes observed in the pooled context of the bar-seq experiment, a cell viability assay was carried out during the axenic differentiation of individual null mutant lines from promastigotes to amastigotes. The viability assay used relies on the cell permeable, oxidation-reduction indicator resazurin which, upon exposure to cellular metabolic reduction, undergoes a colour change (due to the conversion of resazurin to resorufin) that results in fluorescence emission at 590 nm. Measurements of the fluorescence intensity of null mutant lines relative to a parental control cell line (Cas9 T7) were used to provide a measure of cell viability.

Figure 13A and B show the viability assays (average of sextuplicate samples and 2 individual experiments except for Δ*hect4* and Δ*rbr1*) for the E1 and E2 null mutants and E3 null mutants respectively. Strongly decreased viability compared to Cas9 T7 at 48 h and/or 120 h into differentiation was observed for Δ*ubc1/cdc34,* Δ*ubc2,* Δ*uev1,* Δ*hect2,* Δ*hect7*, Δ*hect10*, Δ*hect11* and Δ*rbr1* (significance confirmed by unpaired t-test, $p<0.05$ except for Δ*rbr1*). Since extreme loss-of-fitness was observed for Δ*ubc1/cdc34*, Δ*ubc2*, Δ*uev1* and Δ*hect2* in the bar-seq experiment, this shows that the strongest phenotypes could be replicated with the viability assay. The data also goes some way to confirm the phenotypes of Δ*hect7*, Δ*hect11* and Δ*rbr1,* also shown to exhibit loss-of-fitness in the AXA bar-seq. Δ*hect10*, however, showed strong representation in the AXA bar-seq, despite showing loss-of-fitness in the inMAC stages. Additionally, a number of less pronounced loss-of-fitness phenotypes observed in the bar-seq were not detected by the viability assay, suggesting a differential sensitivity for these techniques. Figure 13C shows the results of the two independent experiments (average shown in B) plotted for Δ*hect3* and Δ*hect5*. A standard deviation of >0.4 for relative viability values was observed at two time points for these null mutant lines, indicating a large discrepancy between the phenotypes observed in the two independent experiments.

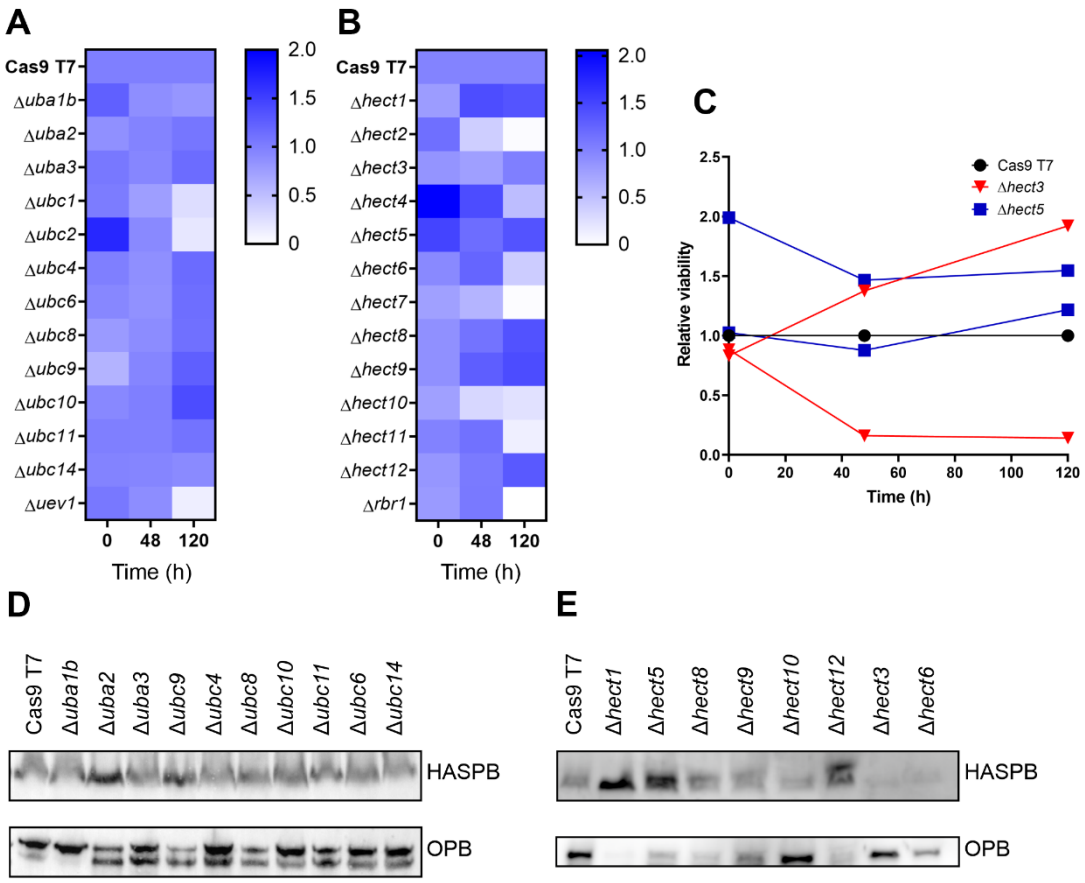

Figure 13. *Individual analysis of null mutant line differentiation into axenic amastigotes.* **A** and **B** Relative viability (compared to the Cas9 T7 parental cell line) of E1 and E2 and HECT/RBR E3 null mutant lines respectively at 0, 48 and 120 h into promastigote to axenic amastigote differentiation. Following an 8 h incubation with resazurin, fluorescence intensities at 590 nm were obtained, background corrected and averaged between replicates for each sample. Relative viabilities were then calculated by dividing the average fluorescence intensity obtained for each cell line by the fluorescence intensity obtained for the Cas9 T7 cell line at the equivalent time point. Relative viability is indicated on a scale of 0 (white, no viability) to 2 (blue, viability 2 times greater than the Cas9 T7 cell line at the equivalent time point). Data are an average of two independent experiments, each with 6 replicates. **C** Data from the two independent experiments represented in **B** are shown separately for Δ*hect3* and Δ*hect5*. **D** and **E** HASPB immunoblots performed on E1 and E2 and HECT/RBR E3 null mutant cell lysates respectively at 120 h into axenic amastigote differentiation. Cas9 T7 was included as a positive control and anti-oligopeptidase B (OPB) used as a loading control.

For all null mutants surviving 120 h into differentiation (determined by checking for intact cells under a light microscope), Western blot analysis was performed using hydrophilic acylated surface protein B (HASPB) antibody, a marker for *L. mexicana* amastigotes

(Nugent *et al.*, 2004; Depledge *et al.*, 2010), to determine whether the cells had differentiated successfully. For all null mutant lines tested, HASPB expression was seen, confirming the ability of these null mutant lines to differentiate into amastigotes. Δ*ubc1/cdc34*, Δ*ubc2*, Δ*uev1*, Δ*hect2*, Δ*hect7* and Δ*hect11* were not analysed due to the absence of cells for those null mutant lines at 120 h. Additionally, Δ*hect4* and Δ*rbr1* were not analysed as their phenotypes had not been confirmed with repeat viability assays.

3.3 Discussion

3.3.1 E1, E2 and E3 genes in *L. mexicana*

Trypanosomatids are amongst the most ancient of eukaryotes and possess some highly divergent biochemistry, for example compartmentalisation of the glycolytic pathway or mRNA trans-splicing (Hannaert *et al.*, 2003; Donelson, Gardner and El-Sayed, 1999). Despite this, our bioinformatic analysis of the *L. mexicana* genome revealed numerous ubiquitin conjugation system components: 2 ubiquitin E1, 13 ubiquitin E2 and 79 E3 ligase genes, including 12 HECT E3s, 1 RBR E3, 5 U-box RING E3s and 4 RING-CH-type E3s. These numbers are similar to those of another single-celled eukaryote, *S. cerevisiae*, which has 1 E1, 11 E2s and 60-100 E3s, of which 5 are HECT E3s, 2 are RBR E3s, 2 are U-box E3s and at least one is a RING CH-type E3 (Finley *et al.*, 2012; Lin, Li and Shu, 2019). In contrast, humans have 2 E1s, 40 E2s and over 600 E3s, of which 28 are HECT E3s, around 15 are RBR E3s, 9 are U-box E3s and 11 are RING CH-type E3s (Lorenz *et al.*, 2013; Scheffner and Kumar, 2014; Eisenhaber *et al.*, 2007; Li *et al.*, 2008; Lin, Li and Shu, 2019). These numbers reveal that *Leishmania* may have a greater proportion of HECT E3s than *S. cerevisiae* or humans, suggesting an expansion of this gene family in the *Leishmania* lineage.

Although we identified nearly 100 putative ubiquitination genes in *L. mexicana*, there were some limitations to our bioinformatic approach. For example, it may have been possible to overlook genes that are particularly divergent from the selected Interpro domain search profiles. However, that the numbers of ubiquitination genes found in *L. mexicana* are similar to those found in *S. cerevisiae* makes it likely that the majority of *L. mexicana* E1, E2 and E3 genes were identified. The identification of SUMO and Nedd8 E1s and E2s using ubiquitin E1 or E2 search profiles respectively also supports this, since it suggests that our ubiquitin E1 and E2 search criteria were somewhat lenient. A second limitation was that we were unable to distinguish between E3s that act as monomers, dimers or multi-subunit complexes, such as those found in CRL complexes,

due to the complexity of predicting protein-protein interactions. For example, the identification of RING E3s found in cullin-RING complexes would require a detailed understanding of the protein-protein interactions that occur between the relevant RING E3s and substrate adaptor proteins (Metzger, Hristova and Weissman, 2012; Deshaies and Joazeiro, 2009). An estimation of the number of multi-subunit complexes could alternatively be made, however, by searching the *L. mexicana* genome for adaptor proteins such as F box, SOCS box, VHL box, or BTB domain proteins (Deshaies and Joazeiro, 2009).

Alignments of the relevant protein families revealed that UBA1a-b, UBC1-14 and HECT1-12 contained putative catalytic cysteine residues, suggesting they are likely to encode functional ubiquitination proteins. UEV1, in contrast, lacks a catalytic cysteine residue and was identified as part of the non-catalytic UEV family (Sancho *et al.*, 1998). Of the remaining putative ubiquitin E2s identified, 4 (UBC3, UBC6, UBC11 and UBC14) were missing the conserved asparagine residue thought to be important for E2 catalysis (Wu *et al.*, 2003; Jones *et al.*, 2019; Berndsen *et al.*, 2013). For these proteins, the missing asparagine residue may indicate non-canonical methods of E2 catalysis. Of the ubiquitination genes identified, only one gene, *HECT12*, was not found in either *T. brucei* or *T. cruzi*, suggesting that it may have a *Leishmania*-specific function. Additionally, we identified a putative SUMO E1 catalytic subunit (UBA2), a Nedd8 E1 catalytic subunit (UBA3), a SUMO E2 (UBC9) and a Nedd8 E2 (UBC12), although E1, E2 and E3 genes for ubiquitin-like modifiers were not extensively searched for. Despite this, previous characterisation of the *T. brucei* orthologues of UBA2 and UBC9 by *in vitro* SUMOylation assays, and UBA3 and UBC12 by affinity purification of Nedd8 lend further weight to their proposed functions (Ye *et al.*, 2015; Liao *et al.*, 2017).

Protein domain analysis of HECTs 1-12 and RBR1 revealed that 9 HECT E3s contained additional domains or other sequence features N-terminal to their (C-terminal) HECT domains. Most of the domains identified were putative protein-protein interaction domains such as SPRY and ZZ-type zinc finger domains, although some, such as the ARM domains found in HECT7 and HECT10, have protein or nucleic-acid binding potential. In addition to its ARM domain, HECT7 contains a RanBP2-type zinc finger domain. This is similar to the zinc finger domain that is found in human RanBP2, a SUMO E3 ligase, and binds to Ran (Pichler *et al.*, 2002; Yaseen and Blobel, 1999). Human RanBP2, however, unlike *L. mexicana* HECT7, is neither a HECT E3 nor RING E3. Instead, its catalytic activity originates from a predominantly unstructured region of the protein and, unlike the case for HECT E3s, is independent of the cysteine residues within

it (Pichler *et al.*, 2004). In future studies, it would be interesting to see whether HECT7 also displays SUMOylation activity and, if so, whether this activity is dependent on the putative catalytic cysteine identified in the alignment (Figure 5C). To the knowledge of the author, a true SUMO HECT E3 ligase has not yet been described in any species. The protein-protein interaction domains identified in this chapter could be sites of substrate interaction and may help to regulate substrate specificity (Metzger, Hristova and Weissman, 2012). Conversely, HECT2, HECT3, HECT5 and HECT9, for which no protein-protein interaction domains were identified, may interact with substrates through domains with evolutionarily divergent protein sequences or as yet uncharacterised protein motifs.

Following the domain analysis of *L. mexicana* HECT E3 ligases, HECT12 was identified as a dual protein kinase and HECT E3 ligase. There is known to be substantial interplay between phosphorylation and ubiquitination in eukaryotic cells. For example, activated protein kinases can trigger a negative feedback loop that results in their own ubiquitination and degradation, either through the proteasome or lysosome (Lu and Hunter, 2009). A good example of this is the regulation of human ERK2 by MEKK1, another dual protein kinase/E3 ligase, which occurs in the MAPK signalling pathway. Following stress-induced ERK2 activation, MEKK1 ubiquitinates ERK2, resulting in its degradation by the proteasome (Lu *et al.*, 2002). Conversely, E3 ligase activity can be regulated by phosphorylation. A well-studied example of this involves Cbl E3 ligases, which ubiquitinate and thereby regulate receptor tyrosine kinases by triggering their degradation. In addition, these receptor tyrosine kinases can phosphorylate Cbl E3s on a tyrosine residue (Tyr371 in c-Cbl) in the linker helix region, causing a conformational change that increases Cbl activity (Zheng, Tweten and Mensa-Wilmot, 2005). Investigations into the possible regulation of the HECT12 protein kinase domain by the HECT E3 ligase domain, or vice versa, would be an interesting area for further study. These could begin, for example, by determining whether the protein kinase domain of HECT12 is modified by ubiquitination and, if so, whether this is dependent on the putative catalytic cysteine of the HECT12 HECT domain.

3.3.2 Localisations of E1, E2 and HECT/RBR E3 enzymes in *L. mexicana*

Analysis of mNeonGreen-tagged E1, E2 and HECT/RBR E3 genes revealed that most (18 out of 32) proteins had a cytoplasmic localisation. Proteins identified as localising to the cytosol included UBC3, HECT1, HECT8, HECT10 and HECT11. However, of the cytoplasmic and cytosolic proteins identified, UBC1/CDC34, UBC3, HECT1, HECT3 and

HECT11 had a patchy or dotted distribution. Many of these patterns are difficult to distinguish from those typical of small cytoplasmic organelles such as lipid droplets, acidocalcisomes, glycosomes or RNA granules (Halliday *et al.*, 2019), highlighting the need for future co-localisation studies to fully confirm the localisation of these proteins. UBA2 and UBC9, a predicted SUMO E1 and E2 catalytic subunit respectively, had nuclear localisations, illustrated by their co-localisation with the larger of two patches of DNA stained with Hoechst 33342. This lends more weight to their putative identities, since *T. brucei* SUMO, human UBA2 (SUMO E1) and *S. cerevisiae* UBC9 (SUMO E2) all localise to the nucleus (Liao *et al.*, 2010; Azuma *et al.*, 2001; Huh *et al.*, 2003). HECT9 was also found to be localised to the nucleus, suggesting it may play a role in nuclear processes such as regulating gene transcription, DNA replication or DNA repair. Although UBC6 and RBR1 were found throughout the cytoplasm, they were strongly enriched in the kinetoplast, suggesting a possible role in kinetoplast function. Similarly, HECT12, enriched in the basal body area, may play a role in basal body function. Although the localisation patterns of HECT4 and HECT5 resemble the mitochondrion and part of the endocytic system respectively, these would need to be confirmed using co-localisation techniques, for example by staining cells with MitoTracker™ or FM™ 4-64 respectively (Halliday *et al.*, 2019). Increased confidence of protein localisation could also be achieved by obtaining localisation data for both N- and C-terminally tagged proteins. This could help to identify proteins for which addition of the N- or C-terminal tag had led to protein misfolding, since disrupted and non-disrupted proteins may show different localisations. The finding that HECT5 was localised to the flagellum in some cells could be followed up by determining whether the presence of HECT5 is linked to flagellum age. For example, if HECT5 were found to be present only in newly-formed flagella, it would suggest a role for HECT5 in flagellum assembly. This could be achieved by looking for co-localisation with known flagellum assembly factors.

3.3.3 Importance of E1, E2 and E3 genes in the *L. mexicana* life cycle

Previous work has underscored the importance of the ubiquitination system in *Leishmania* by demonstrating both the essentiality of the parasite proteasome and a key role for DUBs in the life cycle of this parasite (Khare *et al.*, 2016; Wyllie *et al.*, 2019; Damianou *et al.*, 2020). The generation of a select ubiquitination gene null mutant library revealed that 1 out of 2 ubiquitin E1s and 3 out of 13 ubiquitin E2s could not be deleted and therefore may be essential in promastigotes. A similar proportion (4 out of 20) cysteine peptidase DUBs were shown to be essential in promastigotes, suggesting a comparable degree of redundancy in DUB function (Damianou *et al.*, 2020). UBC12, a

putative Nedd8-conjugating enzyme, also appears to be essential in promastigotes, suggesting it may function independently of the Nedd8 E1 catalytic subunit UBA3, which is non-essential in promastigotes. This could be due to the presence of an additional Nedd8 E1 catalytic subunit or a Neddylation-independent function of UBC12. In contrast, none of the HECT or RBR E3 ligases were essential in promastigotes, likely attributable to an increased substrate specificity and redundancy in function that characterises E3 ligases (Iconomou and Saunders, 2016). Until the requirement for RING and U-box E3 ligases has also been determined, however, general conclusions regarding the essentiality of E3 ligases in promastigotes cannot be made. Further investigation into the essential requirement for UBA1a, UBC3, UBC7, UBC12 and UBC13 in promastigotes, for example via the generation of facilitated or conditional null mutants, will be required to validate the relevant null mutants (Jones *et al.*, 2018). This is of particular interest for UBA1a, since *L. major* UBA1a and human UBA1 exhibit differential inhibition by TAK-243, suggesting that *Leishmania* UBA1a-selective inhibitors could be developed (Boer and Bijlmakers, 2019).

Originally, the triple-E activity-based probe (Mulder *et al.*, 2016) was selected to allow the confirmation of E1, E2 and HECT/RBR null mutants at the level of enzyme activity. This analysis, which involves the parallel profiling of parental and mutant cell lines, permits the identification of proteins in a gel representing ubiquitination enzymes bound to the probe (present in the parental sample but not in null mutant samples). By identifying specific ubiquitination enzymes in this way, it can be determined whether these enzymes are catalytically active in parasite lysates. This method was used to validate the generation of a UBA1b null mutant and show that this E1 is active in promastigote cell lysates. However, for a number of reasons, extensive analyses of the null mutant library using Cy5-Ub-Dha were not carried out. Firstly, polymeric Cy5-Ub-Dha forms observed in the sample preparation were deemed likely to interfere with the identification of active E2 enzymes. Secondly, *L. mexicana* HECT E3 ligases, which have large molecular weights, appeared difficult to identify using the probe. Finally, despite considerable experimental optimisation, inconsistent probe labelling was often seen between parallel lanes in an experiment, meaning it could be difficult to reliably identify differences in sample banding pattern and/or intensity. It is unlikely that the poor performance of this probe in *L. mexicana* lysates is due to the differences between human and *Leishmania* ubiquitin since another ubiquitin-based probe, Cy5-Ub-PRG (Ekkebus *et al.*, 2013), has been used to successfully profile DUB activity in *Leishmania* lysates (Damianou *et al.*, 2020). In the future, other activity-based probes for Cys-

dependent and Cys-independent ubiquitination enzymes (discussed in section 3.1.2) could be tested to determine their usefulness in *Leishmania*.

In interpreting our bar-seq data, it was reasoned that since null mutants were more likely to exhibit decreases in proportional representation as the experiments progressed, our analysis should be limited to the identification of loss-of-fitness phenotypes. This is because decreases in the relative abundance of a subset of null mutant lines in the population would lead to an increase in the proportional representation of the remaining null mutant lines, potentially mimicking gain-of-fitness phenotypes. Despite this limitation, the bar-seq approach allowed us to identify numerous fitness phenotypes associated with the promastigote and amastigote life cycle stages. In particular, loss-of-fitness was identified for more than one interval between promastigote time points for Δ*ubc9*, hinting at a role for SUMOylation (UBC9), and *Δhect2* and *Δhect12*, for HECT E3-mediated ubiquitination, in promastigote growth and/or survival. These genes were not absolutely required for survival, however, given our ability to detect Δ*ubc9*, Δ*hect2* and Δ*hect12* in the metacyclic promastigote samples. Also of interest was the high degree of correlation between the data from the axenic amastigote, macrophage and mouse infection experiments, supporting previous findings that only small transcriptomic differences exist between axenic and intracellular amastigotes (Fiebig, Kelly and Gluenz, 2015). The strong phenotypes observed for Δ*ubc1/cdc34*, Δ*ubc2*, Δ*uev1* and Δ*hect2* in the amastigote stages suggest an important role for these genes in the successful transformation from promastigote to amastigote. Since Δ*hect2* also showed loss-of-fitness in the promastigote stage, the effect of HECT2 deletion on cell survival/proliferation may be a more general one. For example, if the function of human UBE3C is shared with HECT2, then the build-up of harmful, incompletely-degraded proteasome substrates during the life cycle could explain the requirement for HECT2 in amastigotes and the more subtle effect of HECT2 deletion on promastigotes (Chu *et al.*, 2013). Notably, the observed requirement for UBC1/CDC34 during *L. mexicana* mouse infection mirrors the finding that TbCDC34 is required for infection of mice with bloodstream form *T. brucei* (Rojas *et al.*, 2017). Additionally, the human orthologues of both UBC2 and UEV1 (UBE2N and UBE2V1 respectively) have been implicated in the differentiation of various human cell types, perhaps pointing to a general role for these protein families in differentiation processes (Sancho *et al.*, 1998; Wu *et al.*, 2009; Zhang *et al.*, 2017; Lentucci *et al.*, 2017). Since both ubiquitination and deubiquitination enzymes have been found to be essential in the promastigote to amastigote transition, interplay between the activities of E2/E3s (UBC1/CDC34, UBC2, UEV1 and HECT2) and DUBs (DUB4, DUB7 and DUB13) could be crucial for maintaining an optimal abundance

and/or state of modification of protein targets that are required for differentiation. Δ*uba1b*, Δ*ubc14*, Δ*hect7* and Δ*hect11* were lost at later stages and Δ*ubc9* showed cumulative loss throughout the experiments, suggesting that the deleted genes are required for normal amastigote proliferation, including during mouse infection.

Using a cell viability assay, we were able to recreate the extreme loss-of-fitness phenotypes observed for Δ*ubc1/cdc34*, Δ*ubc2*, Δ*uev1* and Δ*hect2* during axenic amastigote differentiation in the bar-seq experiment. This demonstrates that our bar-seq approach is a valid way of identifying strong defects in promastigote-amastigote differentiation. Some, but not all, more subtle loss-of-fitness phenotypes were also recreated in the viability assay, including those seen for Δ*hect7*, Δ*hect11* and Δ*rbr1*. Our inability to recreate all relevant bar-seq phenotypes with the viability assay may suggest that bar-seq is a more sensitive method for identifying loss-of-fitness phenotypes, perhaps due to its use of next-generation sequencing technologies. Alternatively, this discrepancy could be explained by the fact that there were only two (and in some cases one) biological experimental replicate, which could make it more difficult to identify statistically significant differences between samples. It is also possible that the pooled context of the bar-seq experiment generates more false positive results, since competition for resources could lead to the loss of cell lines in co-culture. Given that some cell lines, in particular Δ*hect3* and Δ*hect5*, had fairly variable results between repeat biological experiments, it would be useful to obtain at least 3 biological replicates to be confident of the phenotypes observed. The bar-seq experiment, in contrast, utilised 6 biological replicates.

Another important difference between the bar-seq and viability assay experiments concerns the method of data analysis. For the bar-seq data, adjacent time points were compared using an unpaired t-test and corrections for multiple comparisons, resulting in a more stringent statistical analysis. For the viability assay, in contrast, viability was calculated relative to the parental Cas9 T7 cell line and unpaired t-tests performed between the 0 h and 120 h time points without correction for multiple comparisons. Since more loss-of-fitness phenotypes were observed with the bar-seq experiment than the viability assay, however, the correction for multiple comparisons does not appear to be too stringent. It is also important to consider that the viability assay measures metabolic activity of cells whereas the bar-seq experiment measures the relative abundance of DNA barcodes. This difference may explain why Δ*hect10* showed a viability defect in the individual assessment despite strong representation in the AXA bar-seq. This is because Δ*hect10* cells might differentiate but persist in a

metabolically inactive state. Interestingly, our HASPB blot showed that Δ*hect10* is able to differentiate into amastigotes, in support of this interpretation.

In summary, E1, E2 and E3 genes in the *L. mexicana* genome were successfully identified and characterised using bioinformatics. Although the localisation of most of the E1, E2 and HECT/RBR E3 proteins was shown to be cytoplasmic or cytosolic, there are a number of more restricted localisations that require further confirmation and investigation. The finding that many E1, E2 and E3 genes are required for either the successful transformation from promastigote to amastigote or normal proliferation during mouse infection adds significantly to the body of evidence demonstrating the importance of the ubiquitination system in the differentiation and intracellular survival of *L. mexicana.*

4 Biochemical and structural analysis of UBC2-UEV1

4.1 Introduction

4.1.1 Introducing human UBE2N and its orthologues

Ubiquitination is catalysed by the sequential action of E1, E2 and E3 enzymes. Despite their place in the centre of the cascade, E2 enzymes have been reported to confer priming versus chain-building control and chain link specificity, making them key players in determining the overall effect of ubiquitin modifications (Stewart *et al.*, 2016). Good examples of this are human UBE2N and *S. cerevisiae* Ubc13, orthologous E2s with Lys63-linked chain-forming ability (Christensen, Brzovic and Klevit, 2007; David *et al.*, 2010). For UBE2N/Ubc13 to exert its catalytic activity, interaction with UEV family proteins is required. UEVs are similar in sequence and structure to canonical E2 enzymes yet lack the conserved cysteine residue required for catalysis (Sancho *et al.*, 1998). In humans, 2 UEVs, UBE2V1 (Uev1 in *S. cerevisiae*) and UBE2V2 (Mms2 in *S. cerevisiae*), exist and can form heterodimers with UBE2N/Ubc13 (Hofmann and Pickart, 1999; Hofmann and Pickart, 2001). Notably, UBE2V1 and UBE2V2 differ in their chain assembly activities – UBE2V1 causes polyubiquitination whereas UBE2V2 directs di-ubiquitin formation, with the difference in activity attributable to an additional 30 amino acids at the N-terminus of UBE2V1 (Andersen *et al.*, 2005). In rice (*Oryza sativa*), four different UEVs exist and differ in length, post-translational modification, strength of interaction with OsUBE2N, chain assembly activity, subcellular localisation and expression level. Existence of this variation suggests that regulation of UEV partner may be an important way to control UBE2N activity (Wang *et al.*, 2017). Variation in UEV function has also been observed for different (tomato) UEVs in Fen-mediated programmed cell death in *Nicotiana benthamiana* (Mural *et al.*, 2013; Hamera *et al.*, 2014).

Lys63-linked chains generated by human UBE2N and UBE2V1/UBE2V2 have been linked to inflammatory signalling (Wu and Karin, 2015) and DNA damage response pathways (Lee *et al.*, 2017). In the latter case, when double-stranded DNA breaks are formed, the E3 ligase RNF8 is recruited to sites of damage and co-operates with UBE2N-UBE2V2 to polyubiquitinate histone H1 (Thorslund *et al.*, 2015). Binding of these Lys63-linked chains by RNF168 results in the monoubiquitination of histone H2A. This modification is associated with 53BP1 recruitment and DNA repair by non-homologous end-joining (NHEJ) (Nakada, 2016; Lee *et al.*, 2017). Other roles for UBE2N include, but

are not limited to, influences on ER-associated degradation, thymidine synthesis and mitotic checkpoint control (Hodge, Spyracopoulos and Glover, 2016). Interestingly, decreased expression of UBE2V1 has been shown to be important for the differentiation of HT-29-M6 intestinal mucosecretory cells (Sancho *et al.*, 1998). Conversely, UBE2V1 facilitates the differentiation of osteosarcoma cells by promoting the Smurf1-mediated ubiquitination and degradation of the transcription factor Smad1. This effect of UBE2V1 is independent of UBE2N (Zhang *et al.*, 2017). A role for UBE2N in haematopoiesis, including B cell development, has also been proposed (Wu *et al.*, 2009; Lentucci *et al.*, 2017).

Due to its role in inflammatory signalling, host UBE2N is often targeted by pathogens. For example, Lys63-linked ubiquitination of the human E3 ligases cIAP1/2 and TRAF6 is decreased during *Leishmania donovani* infection and probably attributable to reduced association with LdUBE2N. This results in reduced signalling through Toll-like receptor 4, allowing the parasite to subvert the host immune response (Gupta *et al.*, 2014). A similar example is seen during *Leishmania amazonensis* infection, in which upregulation of the UBE2N miRNA let-7e is proposed to influence the expression of genes involved in NO production and TLR pathway signalling, leading to subversion of the host immune response (Muxel *et al.*, 2018). Similarly, the *Toxoplasma gondii* virulence factor ROP18 (a Ser/Thr protein kinase) positively influences host UBE2N degradation (Yang *et al.*, 2017). In *Shigella flexneri* infection, the effector protein OspI deaminates Q100 of UBE2N, leading to reduced TRAF6 ubiquitination and NF-κB signalling through the diacylglycerol axis (Sanada *et al.*, 2012). Comparably, non-canonical ubiquitination of UBE2N at K92 or K94 by *Legionella pneumophila* MavC broadly reduces NF-κB pathway activation (Gan *et al.*, 2019).

4.1.2 Structure of UBE2N and its orthologues

Structurally, E2s consist of conserved UBC domains of around 150 amino acids in length with or without N- or C-terminal extensions. UBE2V1 has an N-terminal extension whereas UBE2N and UBE2V2 lack either extension (Wenzel, Stoll and Klevit, 2011). During Lys63-linked chain synthesis, UBE2N/Ubc13 becomes charged with a donor ubiquitin bound to the catalytic cysteine, C87. The acceptor ubiquitin is then positioned by non-covalent interactions with the UEV protein to allow K63 to undergo nucleophilic attack of the thioester, subsequently forming an isopeptide bond (McKenna *et al.*, 2001; Eddins *et al.*, 2006). In UBE2N, the conserved asparagine residue of the HPN motif is N79 (Wu *et al.*, 2003). When UBE2N and UBE2V2 interact, F13 of UBE2V2 fits into a

hydrophobic pocket of UBE2N formed by E55, F57 and R70 like a key in a keyhole (Pastushok *et al.*, 2005). Other important protein-protein interaction sites include the E1/E3 interaction site of UBE2N, proposed to be on loops 4 and 7 of the N-terminal helix (Wenzel, Stoll and Klevit, 2011). In humans, UBE2N interacts with several E3s including BIRC2, CHIP, RNF8 and ZNRF2 (Bertrand *et al.*, 2008; Zhang *et al.*, 2005; Plans *et al.*, 2006). In *S. cerevisiae*, at least two residues of Mms2 (I62 and S32) are critical for the non-covalent interaction with ubiquitin (Pastushok, Spyracopoulos and Xiao, 2007).

4.1.3 Aims

In the previous chapter, the L. mexicana orthologues of human UBE2N and UBE2V1/2, UBC2 and UEV1 respectively, were shown to be essential for promastigote to amastigote differentiation and mouse infection. In this chapter, the biochemical and structural features of UBC2 and UEV1 are explored in detail. Specifically, this chapter aimed to determine the following features of UBC2 and UEV1: their structure, which E1s and E3s they can interact with, whether they are catalytically active and what types of ubiquitin modification (if any) they form.

4.2 Results

4.2.1 UBC2 and UEV1 sequence analysis

To find out more about UBC2 and UEV1, the most probable orthologues of *L. mexicana* UBC2 (LmxM.04.0680) and UEV1 (LmxM.13.1580) were identified in the *T. brucei*, *S. cerevisiae* and human genomes using protein BLAST searches. For UBC2, these were determined to be Tb927.9.8000 (TbUBC2), ScUBC13 and HsUBE2N respectively, with the identity of TbUBC2 further confirmed using the OrthoMCL data in TriTrypDB. For UEV1, these were determined to be Tb927.11.3310 (TbUEV1), ScMMS2, HsUBE2V1 and HsUBE2V2. The identified orthologues were then aligned with UBC2 and UEV1. Figure 14A shows that there is a high level of conservation between UBC2 and its orthologues. Specifically, UBC2 shares 77%, 66% and 70% amino acid identity with the equivalent *T. brucei, S. cerevisiae* and human proteins respectively. Such a high level of shared identity suggests that the functions of UBC2 are likely to be well-conserved. In contrast, UEV1 is less well conserved with its orthologues, sharing 70%, 54% and 47% identity with the equivalent *T. brucei, S. cerevisiae* and human proteins respectively (Figure 14B). Consequently, there may be more functional divergence within this gene family. In humans, UBE2N and UBE2V1/V2 form a heterodimeric complex specific for

K63-linked ubiquitination and have been linked to inflammatory signalling (Wu and Karin, 2015) and DNA damage response pathways (Lee *et al.*, 2017).

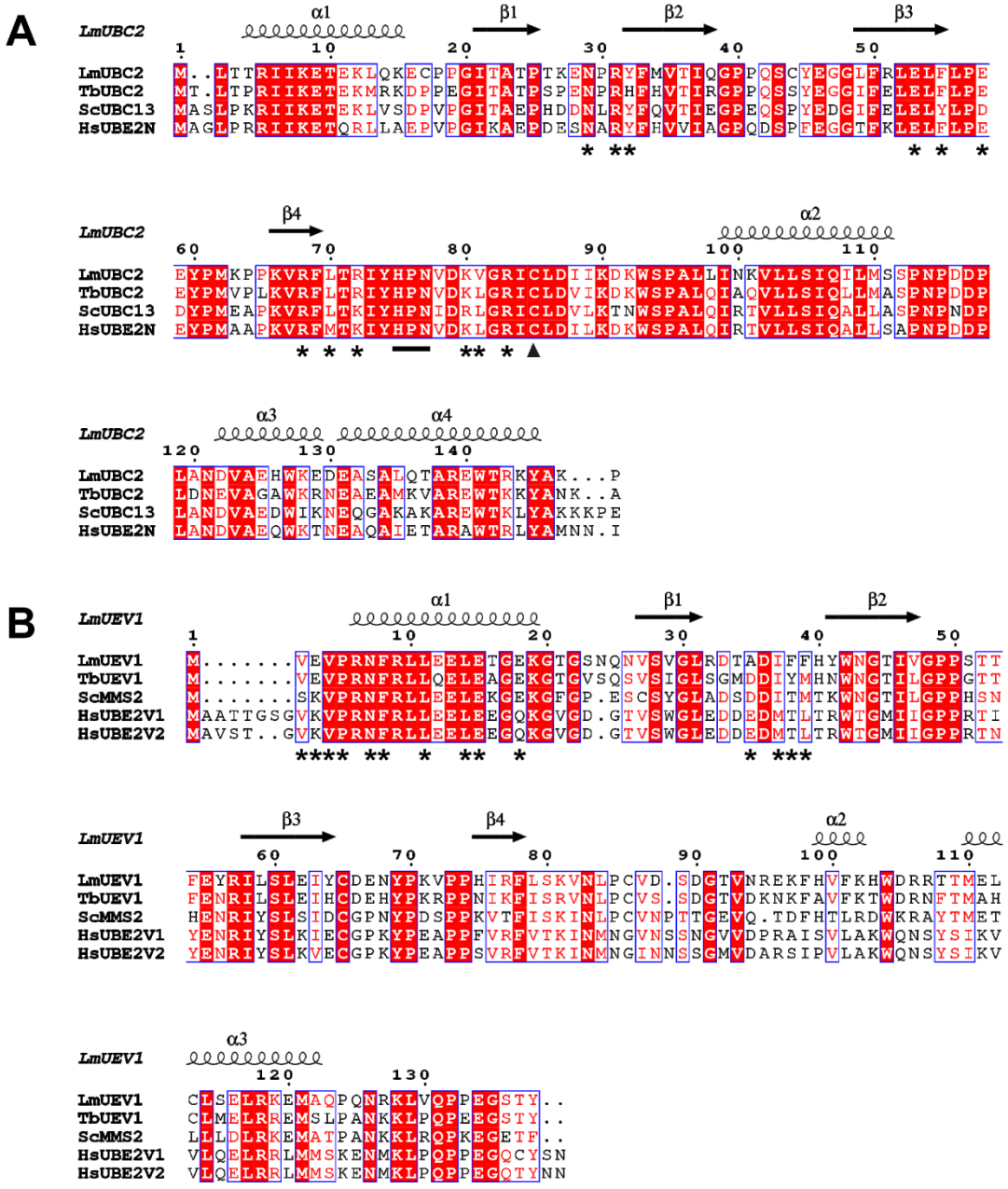

Figure 14. *Alignments of LmUBC2 and LmUEV1 with selected orthologues.* Sequence alignment and structural annotation were performed using T-Coffee and ESPript 3.0 respectively for **A** LmUBC2 and **B** LmUEV1. Red boxes indicate amino acid identity, red characters show similarity within the highlighted group and blue frames highlight similarity across groups. Positions of the UBC2 HPN motif and catalytic cysteine are shown by a black line and triangle respectively. Secondary structures derived from the crystallised *L. mexicana* UBC2-UEV1 heterodimer (Figure 21) are represented above the sequence alignment with helices represented by spirals and beta

sheets by arrows. Asterisks denote important interface residues in the *L. mexicana* complex. *Lm, Leishmania mexicana; Tb, Trypanosoma brucei; Sc, Saccharomyces cerevisiae; Hs, Homo sapiens.*

UBC2 and *UEV1* encode proteins of 148 and 138 amino acids in length respectively, corresponding to predicted molecular weights of 17 kDa and 16 kDa. Based on the alignment in Figure 14A, the putative catalytic cysteine of UBC2 is C85, equivalent to C87 in ScUBC13 and C87 in HsUBE2N (Motegi *et al.*, 2006). UBC2 also contains an HPN motif found 10 amino acids N-terminal of C86. HPN motifs are conserved in active E2 enzymes, where the asparagine residue can contribute to catalysis (Wu *et al.*, 2003; Berndsen *et al.*, 2013; Jones *et al.*, 2019). All of the proteins in the UEV1 alignment (Figure 14B) lack catalytic cysteine residues and HPN motifs, consistent with UEV1 being part of the noncatalytic UEV family of E2s (Sancho *et al.*, 1998). To perform the UEV1 alignment, isoform 3 (canonical sequence in UniProtKB) of UBE2V1 was used as this is the most similar isoform to UEV1. However, UBE2V1 is predicted to have numerous isoforms produced by alternative splicing. For example, a 30 residue N-terminal extension of isoform 2 (UEV-1A) relative to UBE2V2 has previously been shown to account for their differing functions (Andersen *et al.*, 2005). Since UEV1 lacks such an N-terminal extension, it could be predicted to be more similar in function to UBE2V2 than UBE2V1.

4.2.2 Expression and purification of recombinant UBA1a, UBC2 and UEV1

In order to characterise UBC2 and UEV1 at a biochemical and structural level, recombinant UBC2 and UEV1 were generated. Since UBC2 is a putative E2 ubiquitin-conjugating enzyme, an E1 ubiquitin-activating enzyme would also be required in order to study its ubiquitination activity. For this purpose, UBA1a (LmxM.23.0550), a putative E1 proposed to be essential in the promastigote stage, was selected. Two putative E1s (UBA1a and UBA1b) exist in *L. mexicana*, and, like TbUBA1a and TbUBA1b, are more closely related to HsUBA1 than HsUBA6 (Boer and Bijlmakers, 2019). Specifically, *L. mexicana* UBA1a and UBA1b share 36% and 33% amino acid identity with HsUBA1 respectively and 28% identity with each other. Based on its higher shared identity with HsUBA1 and potential essentiality, it was reasoned that UBA1a would be most likely to show a broad E2 specificity (comparable to that of HsUBA1) and therefore be capable of loading ubiquitin onto UBC2 (Jin *et al.*, 2007; David *et al.*, 2010).

Initially, UBA1a, UBC2 and UEV1 sequences were codon-optimised for *E. coli* expression and cloned into expression vectors containing N-terminal 6xHis tags with or without one of the following solubility-enhancing tags: MBP, GST or Im9 (Shevket *et al.*, 2018). Expression tests were then performed for *E. coli* transformed with the UBA1a and UBC2 expression plasmids in both LB and auto-induction media. To do this, protein expression was induced with IPTG (LB media) or high density cell growth (auto-induction media) and cultures allowed to grow before cells were lysed in sample buffer and run on an SDS-PAGE gel. Successful expression of UBA1a and UBC2 was seen following growth of all tested strains in both types of media Figure 15 (left and centre). Little difference in yield was seen between the two media conditions, however, the presence of a solubility tag appeared to improve UBC2 yield. Due to the relative ease of generating LB media compared to auto-induction media and the smaller molecular weight of Im9 compared to MBP and GST (which may therefore be less likely to interfere with protein folding), it was decided to express UBA1a, UBC2 and UEV1 as Im9 fusion proteins using LB as the growth medium. It was later shown that Im9-tagging of UEV1 improved yield in a similar manner to Im9-UBC2 (Figure 15, right). Representative gels showing the induction of protein expression in cultures used for scaled-up expression and purification are shown in Figure 16.

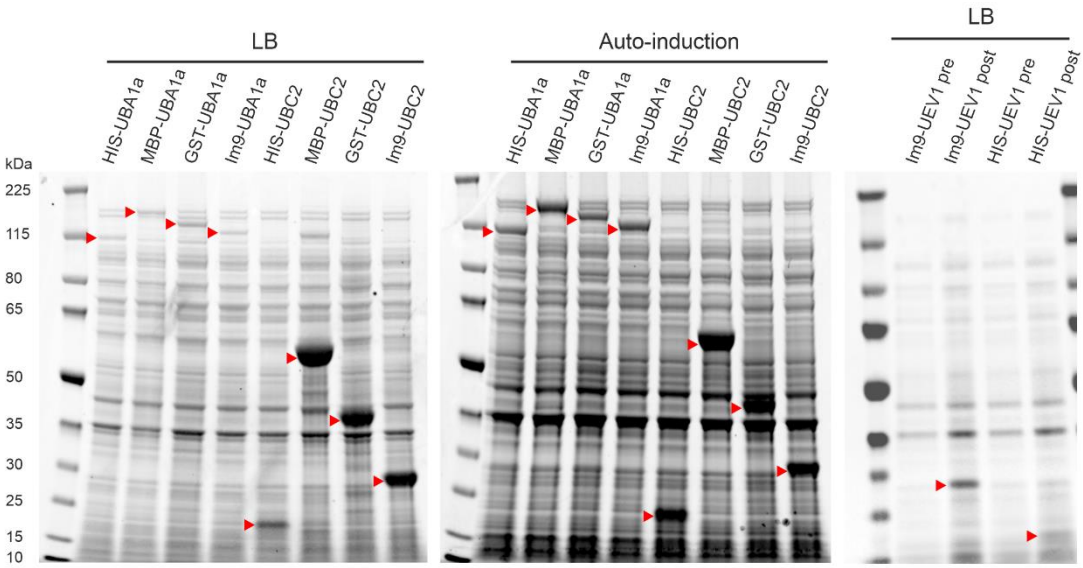

Figure 15. *E. coli protein expression tests for L. mexicana UBA1a, UBC2 and UEV1. E. coli* containing N-terminally 6xHis-tagged UBA1a, UBC2 and UEV1 expression vectors (with or without additional MBP, GST or Im9 solubility tags) were grown in LB or auto-induction medium. Following induction of protein expression with IPTG (LB media) or high density cell growth (auto-induction media) and further growth for 24 h at 20°C, aliquots of *E. coli* culture were heated with

reducing sample buffer, run on a gel and stained with InstantBlue™. Red arrows indicate the positions of the tagged proteins of interest. Pre, before IPTG induction; post, after IPTG induction and further growth.

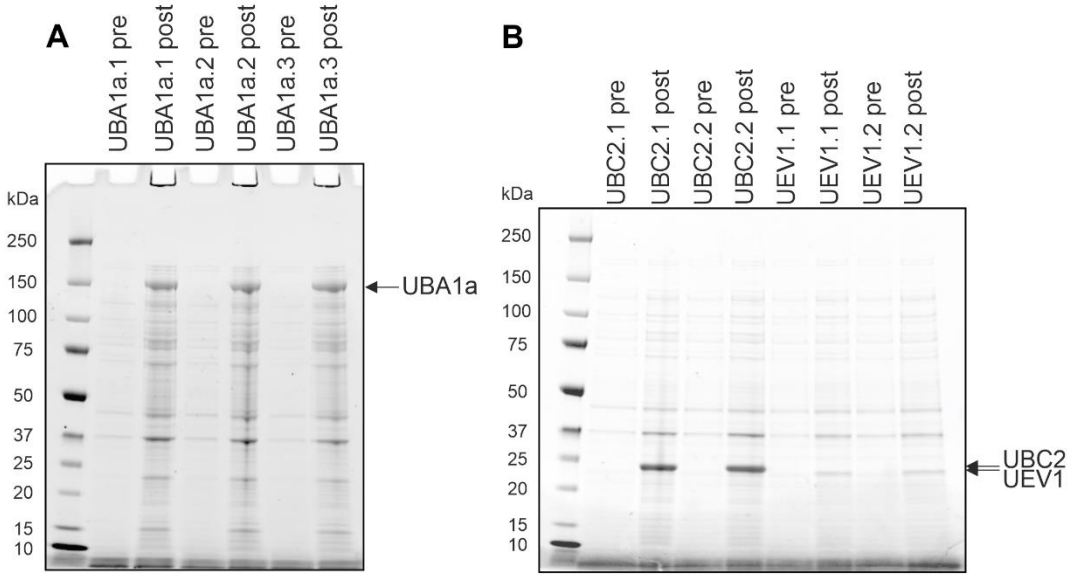

Figure 16. *Induction of L. mexicana UBA1a, UBC2 and UEV1 protein expression in E. coli.* Protein samples from *E. coli* containing N-terminal 6xHis- and Im9-tagged UBA1a, UBC2 or UEV1 are shown pre- and post-induction (and subsequent growth) with IPTG. Numbers indicate *E. coli* samples grown in different culture flasks. Data are representative of two rounds of protein expression.

Protein purification was typically carried out using two rounds of nickel affinity chromatography and one round of size-exclusion chromatography (Figure 17 and Figure 18). After the first round of nickel affinity chromatography, the His-Im9 tag was cleaved from all 3 proteins, leaving an additional 3 amino acids (Gly, Pro, Ala) at the N-terminus. The successful cleavage of the Im9-tag is indicated by a downwards shift in the molecular weight of the protein of interest between the Pre-H3C and Post-H3C samples (Figure 17B and Figure 18C and D). Following the final purification step, all 3 proteins showed a good level of purity as assessed by InstantBlue™ staining (Figure 19A). For UBC2 and UEV1, no additional protein bands were detected whereas the UBA1a sample contained extra proteins at around 74 and 100 kDa. These appeared below UBA1a, suggesting the presence of co-purified protein and/or UBA1a degradation products.

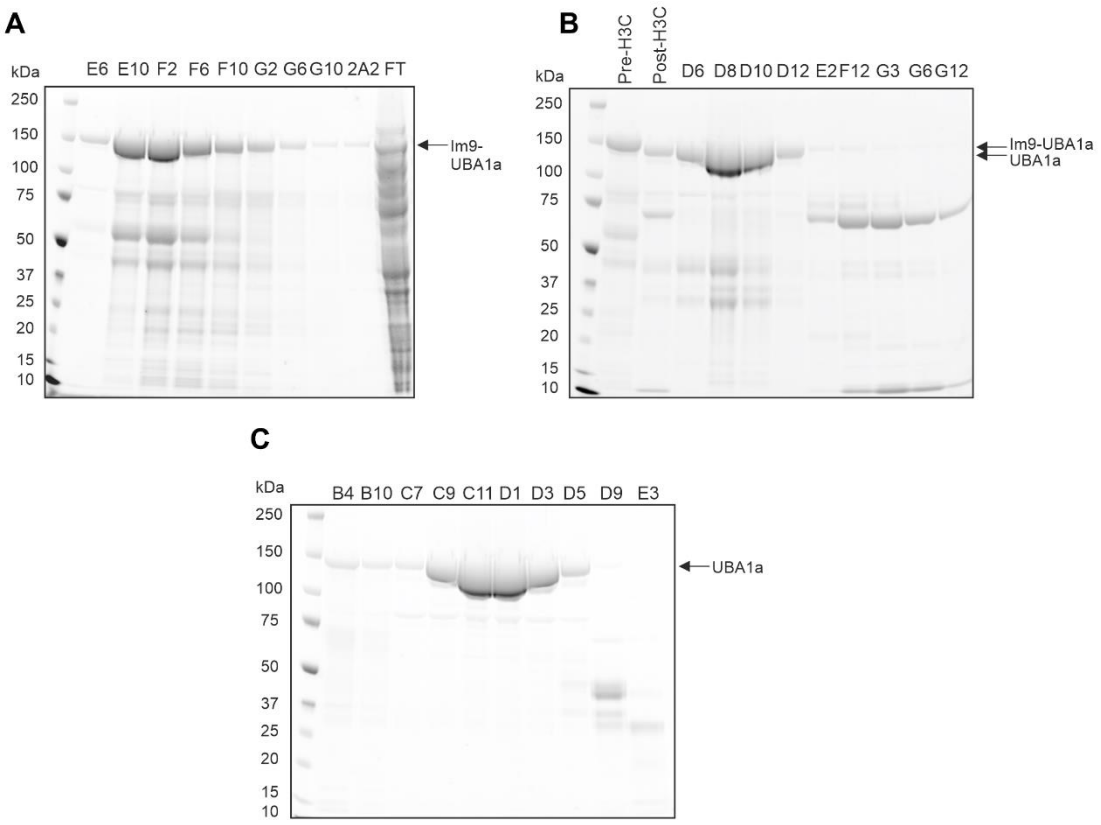

Figure 17. *Purification of L. mexicana UBA1a from E. coli.* **A** Fractions collected from the initial nickel affinity purification of Im9-6xHis-UBA1a expressed in LB. **B** Fractions collected during the second nickel affinity purification of UBA1a following Im9-His tag cleavage. Pre- and post-tag cleavage (Pre-H3C and Post-H3C samples respectively) samples are also included. **C** UBA1a fractions collected following size-exclusion chromatography. Data are representative of two rounds of protein expression. FT, flow-through.

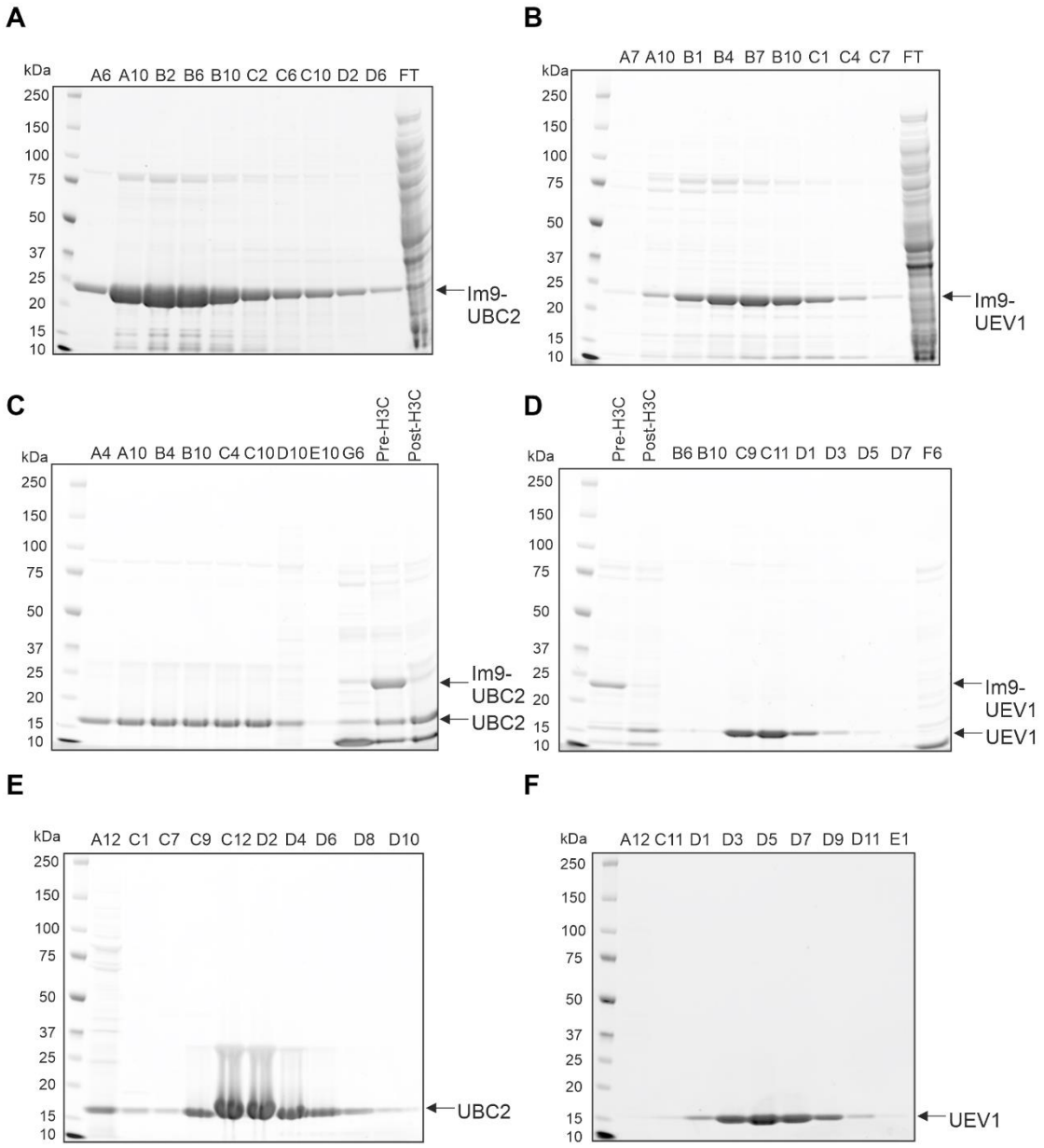

Figure 18. *Purification of L. mexicana UBC2 and UEV1 from E. coli.* **A** and **B** Fractions collected from the initial nickel affinity purification of Im9-6xHis-UBC2 and Im9-6xHis-UEV1 respectively expressed in LB. **C** and **D** Fractions collected during the second nickel affinity purifications of UBC2 and UEV1 respectively following Im9-His tag cleavage. Pre- and post-tag cleavage (Pre-H3C and Post-H3C samples respectively) samples are also included. **E** and **F** UBC2 and UEV1 fractions respectively collected following size-exclusion chromatography. Data are representative of two rounds of protein expression. FT, flow-through.

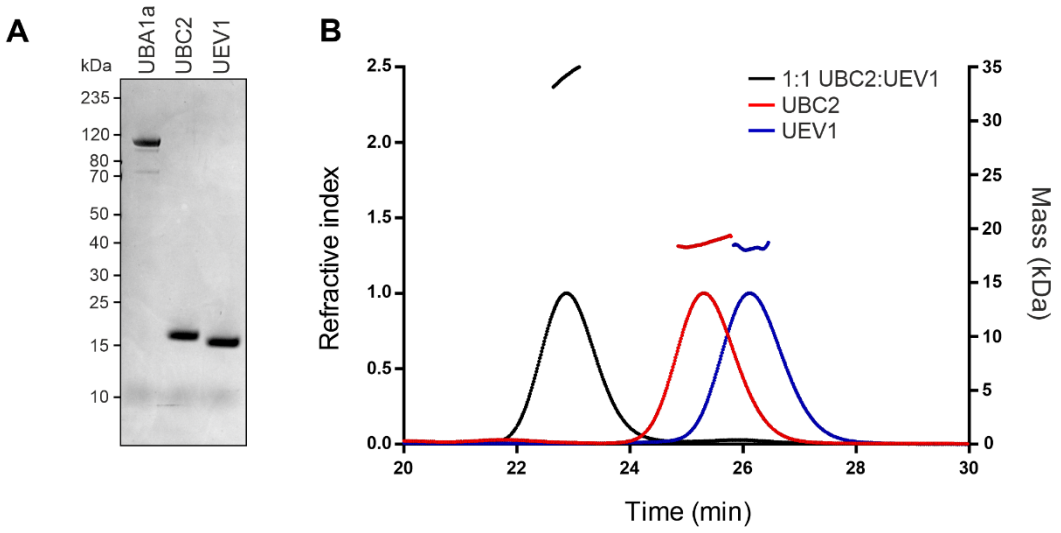

Figure 19. *UBC2 and UEV1 form a stable heterodimer in vitro.* **A** SDS-PAGE gel showing recombinant UBA1a, UBC2 and UEV1 stained with InstantBlue™ stain. Proteins were expressed in *E. coli* and purified by nickel affinity and size-exclusion chromatography. 1 µg of each protein was loaded onto the gel. **B** Elution profiles of UBC2, UEV1 and a 1:1 molar mix of UBC2-UEV1 presented as changes in refractive index over time. Curved lines show changes in refractive index for UBC2-UEV1 (black), UBC2 (red) and UEV1 (blue). The expected mass (as estimated from light scattering data) in kDa is indicated by a dashed line above the peak corresponding to each protein sample.

4.2.3 UBC2 and UEV1 form a stable heterodimer *in vitro*

The orthologues of UBC2 and UEV1 in *T. brucei*, *S. cerevisiae* and humans have previously been shown to form a heterodimeric complex (Crozier *et al.*, 2017; Hofmann and Pickart, 1999; McKenna *et al.*, 2001; Ulrich and Jentsch, 2000). To test whether this was also true in *L. mexicana*, a SEC-MALLS approach was used. SEC-MALLS involves the separation of protein samples in a size-exclusion column followed by measurements of refractive index (used to monitor sample exiting the column) and light scattering (used to estimate the molar mass). The chromatograms in Figure 19B show peaks in the refractive index representing the purified UBC2 and UEV1 samples at 25 and 26 minutes respectively. Measurement of both the refractive index and multi-angle laser light scattering allowed an estimation of the molecular weights of the recombinant proteins at 18.7 kDa and 18.2 kDa for UBC2 and UEV1 respectively. These values are close to the predicted molecular weights of 17 kDa for UBC2 and 16 kDa for UEV1. That both of these proteins eluted as a single peak is indicative of them existing in monomeric form while also reflecting the high quality of the protein preparations. When UBC2 and UEV1

were mixed in an equimolar ratio, an elution peak was seen at 23 min, indicating the presence of a higher molecular weight species (estimated at 34.2 kDa). Given that no peaks were seen representing UBC2 and UEV1 monomers, it can be assumed that all protein material in this sample existed in heterodimeric UBC2-UEV1 complexes. Therefore, *L. mexicana* UBC2 and UEV1 readily associate to form a heterodimeric UBC2-UEV1 complex.

4.2.4 Structure of the UBC2-UEV1 heterodimer

To investigate the conservation and interactions of UBC2 and UEV1 at the structural level, crystals of their complex and of UBC2 alone were sought. Initially, three commercially available screens were used to search for appropriate crystallisation conditions: PACT premier™ (Molecular Diagnostics), Crystal Screen HT™ (Hampton) and INDEX™ (Hampton). Crystals of UBC2-UEV1 took 2 days to grow in 0.1 M Bis-Tris propane, pH 7.5, 0.2 M sodium formate and 20% PEG (Figure 20, crystal 1) or this buffer plus 0.05% dimethylformamide (DMF) (Figure 20, crystal 2). A bright signal was seen in the UV channel for crystal 1, suggesting it was likely to be formed from protein. No crystals of UBC2 alone had formed after 2 months. UBC2-UEV1 crystals were sent for data collection at the Diamond Light Source, with the best crystal yielding a dataset extending to 1.7 Å spacing. The structure was subsequently solved by molecular replacement using the coordinates of the human UBE2N-UBE2V2 complex (PDB ID: 1J7D) as the search model (Moraes *et al.*, 2001). There were two UBC2-UEV1 heterodimers in the crystallographic asymmetric unit. These structures were found to be highly similar following superposition of chains representing UBC2, UEV1 or the UBC2-UEV1 heterodimer, with RMSDs of 0.32 Å, 0.74 Å and 1.13 Å for 146, 132 and 276 equivalent atoms respectively. Since residues Gly20 to Asn24 are poorly defined in the electron density maps for one of the UEV1 chains, the alternative UBC2-UEV1 heterodimer was the focus of our analysis.

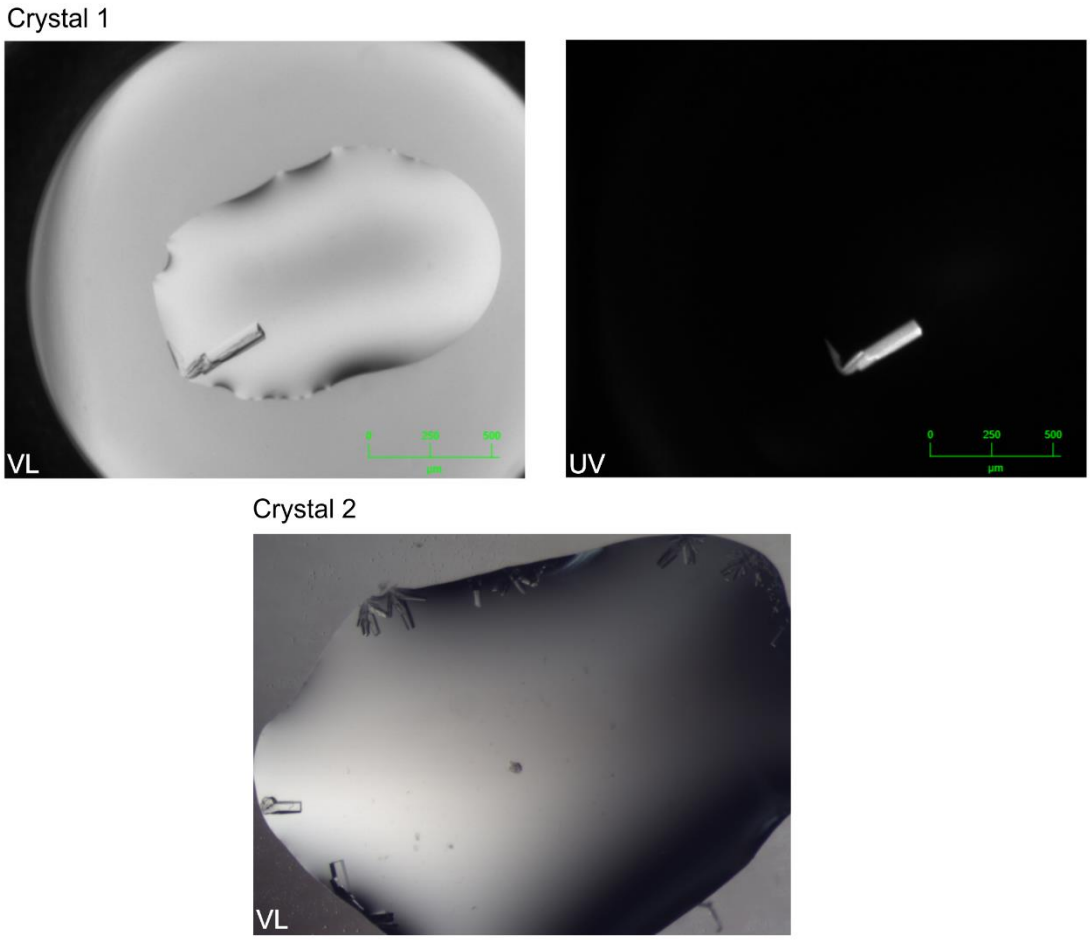

Figure 20. *UBC2-UEV1 crystals*. Crystal 1 was grown in 0.1 M Bis-Tris propane, pH 7.5, 0.2 M sodium formate and 20% PEG in a 96-well sitting drop format and crystal 2 in the same buffer with 0.05% DMF as an additive in a 24-well plate hanging drop format. For both crystals, 6.6 mg mL^{-1} of UBC2-UEV1 prepared in equimolar amounts was mixed in a 1:1 ratio with screening solution. VL, visible light; UV, ultraviolet.

Like its *S. cerevisiae* and human orthologues, UBC2 has a canonical E2 structure of a 4-stranded antiparallel β-sheet flanked by 4 α-helices (Figure 21A). UEV1 has a similar arrangement, but its polypeptide chain is shorter and the prominent pair of α-helices at the C-terminus of UBC2 (α3 and α4) are missing from UEV1. Similar to *S. cerevisiae* Mms2, but not human UBE2V1 or UBE2V2, the N-terminus of UEV1 has a shorter segment preceding the first α-helix (Figure 14B). Superposing UBC2 with human UBE2N, UEV1 with human UBE2V2 or the UBC2-UEV1 and UBE2N-UBE2V2 heterodimers (Figure 22A) gives RMSDs of 0.82, 1.15 and 1.13 Å for 147, 135 and 271 equivalent atoms respectively, demonstrating a high level of structural conservation between these orthologues. The conserved active site residues, His75, Pro76, Asn77 and Cys85, are found between strand β4 and helix α of UBC2, with the thiol group of

Cys85 projecting out of the catalytic cleft (Figure 21B). The high level of sequence conservation around these residues is reflected in the close proximity of their superposed catalytic clefts.

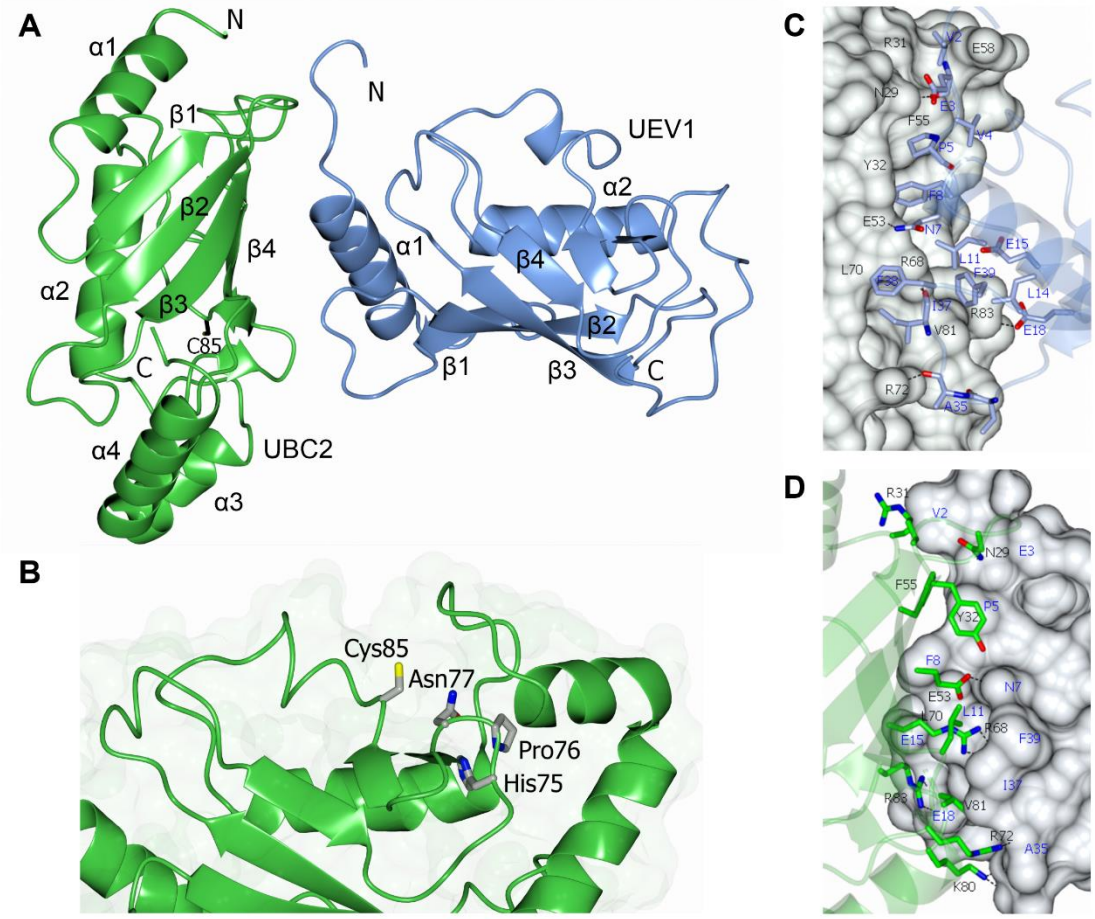

Figure 21. *Structure of the UBC2-UEV1 heterodimer.* **A** Ribbon diagram showing the crystal structure of UBC2 (green) and UEV1 (blue) in complex. The location of the N- and C-termini are highlighted along with the numbering of alpha helices (α) and beta strands (β). **B** Zoom-in of the conserved catalytic residues in UBC2. The HPN motif and proposed catalytic cysteine are shown as cylinders coloured by atom (red, oxygen; blue, nitrogen; yellow, sulphur). **C-D** Zoom-in of interface between UBC2 and UEV1 with UBC2 or UEV1 as a surface fill model respectively. Amino acid residues are shown as cylinders coloured by atom (red, oxygen; blue, nitrogen). Hydrogen bonds are denoted by dashed lines.

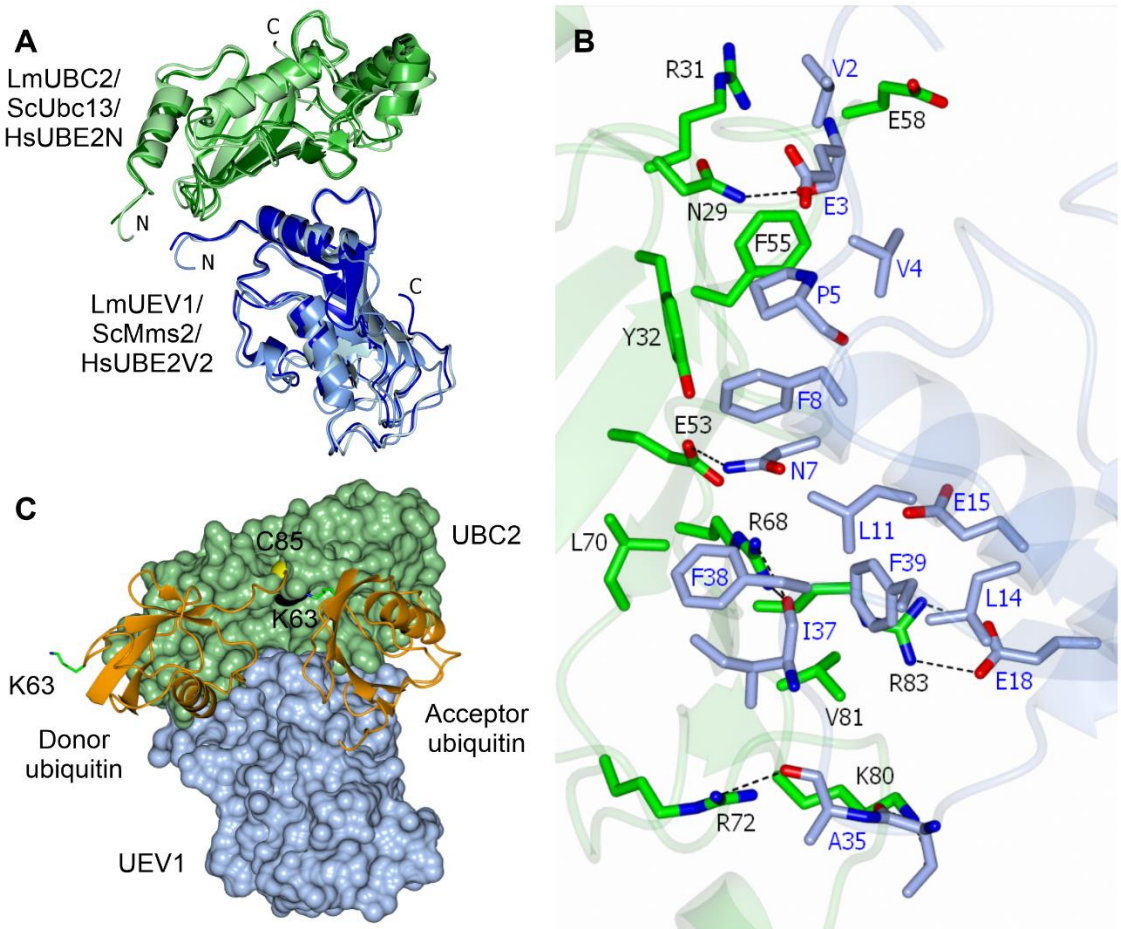

Figure 22. *Structural analysis of the UBC2-UEV1 heterodimer.* **A** Superposition of chains A and B for UBC2-UEV1 (dark green and dark blue, PDB ID: 6ZM3), HsUBE2N-UBE2V2 (darker green and darker blue, PDB ID: 1J7D) and ScUbc13-Mms2 (light green and light blue, PDB ID: 1JAT). Locations of the N- and C-termini are shown. **B** Zoom-in of the interface between UBC2 and UEV1 showing residues thought to contribute most significantly to complex formation according to analysis in the program PISA (Krissinel and Henrick, 2007). Residues are labelled in black for UBC2 and blue for UEV1. Residues are coloured by atom (red, oxygen; blue, nitrogen). Hydrogen bonds are denoted by dashed lines. **C** Superposition of UBC2-UEV1 onto the structure of the UBE2N-UBE2V2-Ub complex (PDB ID: 2GMI) (Eddins *et al.*, 2006) showing UBC2 (green) and UEV1 (blue) as space fill models and the positions of acceptor and donor ubiquitins (orange ribbons) obtained from the UBE2N-UBE2V2-Ub structure. C85 is represented by black (carbon) and yellow (sulphur) spheres. K63 of ubiquitin is highlighted as cylinders coloured by atom (blue, nitrogen).

4.2.5 Analysis of the UBC2-UEV1 interface

The interface between UBC2 and UEV1 involves the β2, β3 and β4 sheets and the loops following β1, β3 and β4 of UBC2 and the N-terminus, α1 helix and loop following β1 of UEV1 (Figure 21C-D and Figure 22B). The buried surface area of this interface is 1,466 $Å^2$. The core of the interface contains a number of hydrophobic residues (Tyr32, Phe55, Leu70 and Val81 of UBC2 and Pro5, Phe8, Leu11, Leu14 and Phe39 of UEV1) that contribute strongly to the interaction. Hydrophobic residues are highly conserved at these positions (Figure 14), illustrating the importance of the associated hydrophobic interactions for complex formation. These hydrophobic interactions are complemented by a number of polar intermolecular interactions, mostly notably those between the side chains of Glu53 of UBC2 and Asn7 of UEV1 and Arg68 of UBC2 and the main chain carbonyl oxygen of Ile37 of UEV1. Both of these interactions are conserved in the human UBE2N-UBE2V2 structure, although Met is present in UBE2V2 in place of Ile. Notably, a salt bridge is formed between Arg83 of UBC2 and Glu18 of UEV1. Although these residues are conserved in *S. cerevisiae*, human UBE2V1/2 has Gln in place of Glu. In human UBE2V2, Asp38 and Glu39 residues provide hydrogen bonds for the interaction interface. These are replaced by Thr and Ala (at positions 34 and 35 respectively) in UEV1.

4.2.6 Ubiquitin transfer occurs between UBA1a and UBC2 *in vitro*

To assess whether UBA1a, UBC2 and UEV1 are an active E1, active E2 and inactive E2 variant respectively, recombinant proteins were tested in thioester intermediate assays. In such assays, Cys-dependent ubiquitination enzymes (E1, E2 and HECT/RBR E3s) are provided with the necessary components (usually ATP, ubiquitin, E1 and E2 enzymes if required) to allow them to form a thioester bond with ubiquitin, and the thioester intermediate is identified by looking for the appearance of a lower mobility protein species. The absence of this species under reducing conditions, which break the thioester bond, can be used to confirm the presence of a thioester intermediate.

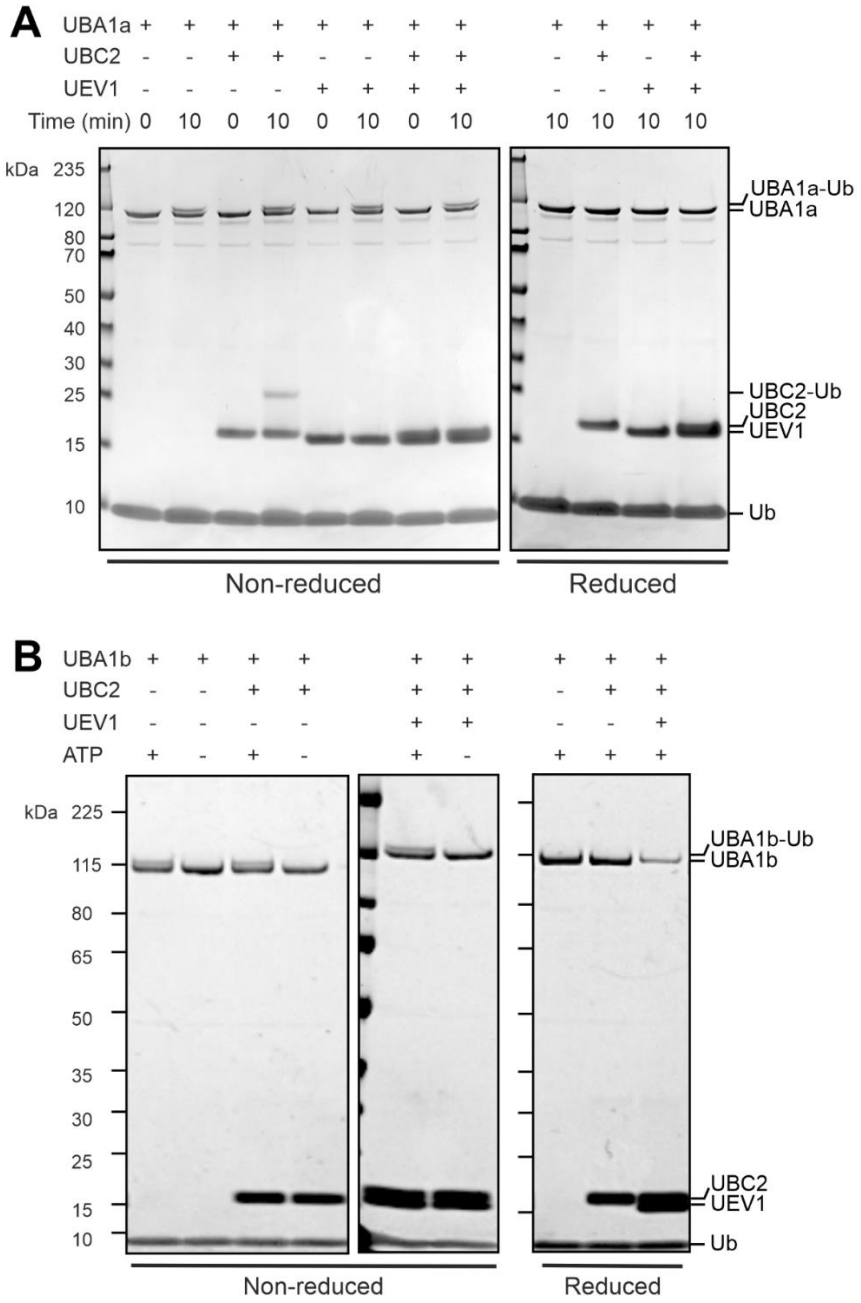

Figure 23. *UBA1a and UBC2 cooperate in ubiquitin transfer in vitro.* **A** Thioester assay demonstrating the ability of UBA1a and UBC2 to form thioester bonds with ubiquitin. UBA1a, ubiquitin and ATP were incubated with UBC2 and UEV1 as indicated in ubiquitination assay buffer for up to 10 min at room temperature. Samples were treated with either reducing or non-reducing sample buffer and visualised by SDS-PAGE with InstantBlue™ stain. **B** UBA1b and ubiquitin were incubated with UBC2, UEV1 and ATP as indicated in ubiquitination assay buffer for 30 min at 30°C. Samples were treated with either reducing or non-reducing sample buffer and visualised by SDS-PAGE with InstantBlue™ stain. Data shown are representative of two or more experiments.

Figure 23A shows the results of incubating UBA1a, UBC2 and UEV1 in different combinations along with ubiquitin and ATP. In these assays, human ubiquitin, which has 2 amino acid substitutions relative to *L. mexicana* ubiquitin, was used. When UBA1a was present under non-reducing conditions, the appearance of a UBA1a~Ub thioester intermediate (at around 125 kDa) was observed over time. Under reducing conditions, this intermediate was lost, confirming the presence of thioester-linked UBA1a~Ub. When UBA1a and UBC2 were combined under non-reducing conditions, the appearance of an additional protein band at 26 kDa was observed, suggesting the transfer of ubiquitin between UBA1a and UBC2 to form thioester-linked UBC2~Ub. This protein complex was lost under reducing conditions, confirming its identity as a UBC2~Ub thioester intermediate. In contrast, when UBA1a and UEV1 were combined, no lower mobility species of UEV1 were observed, suggesting that UEV1 is unable to receive ubiquitin from UBA1a. When UBA1a, UBC2 and UEV1 were combined, no UBC2~Ub thioester intermediate was observed. It was reasoned that UEV1 could prevent UBC2 from binding ubiquitin or, alternatively, that the presence of UEV1 facilitates the release of ubiquitin from UBC2 or its transfer onto substrate(s) in solution. Conversely, the alternative *L. mexicana* ubiquitin E1, UBA1b (obtained from Daniel Harris, University of Glasgow), was unable to transfer ubiquitin to UBC2, despite being capable of forming thioester-linked UBA1b~Ub (Figure 23B). UBA1b was also unable to transfer ubiquitin onto UEV1, showing that ubiquitin cannot be loaded onto UEV1 by either of the two *L. mexicana* ubiquitin E1 enzymes. These results support the identities of UBA1a, UBC2 and UEV1 as an active E1 ubiquitin-activating enzyme, active E2 ubiquitin-conjugating enzyme and inactive E2 variant respectively.

4.2.7 UBC2 and UEV1 conjugate ubiquitin *in vitro*

Previous *in vitro* studies have demonstrated the ability of *S. cerevisiae* UBC13 and MMS2 and their human counterparts to promote the formation of K63-linked ubiquitin chains in the absence of E3 enzyme (Wu *et al.*, 2003; Andersen *et al.*, 2005; Hofmann and Pickart, 1999; McKenna *et al.*, 2001; Pastushok *et al.*, 2005). To test whether the *L. mexicana* enzymes share this ability, different combinations of UBC2 and UEV1 were incubated with UBA1a, ubiquitin and ATP and di-ubiquitin formation monitored by immunoblotting for mono- and poly-ubiquitinated conjugates (all ubiquitinated proteins) and K63-linked ubiquitin under reducing conditions. This approach was chosen in order to distinguish between UBC2, UEV1 and di-ubiquitin, which all have similar molecular weights. In the ubiquitin conjugate blot, di-ubiquitin formation was observed after 30 minutes in the presence of UBC2 and UEV1 and increased by 90 minutes (Figure 24A).

In contrast, di-ubiquitin formation was not observed in the absence of either UBC2 or UEV1, suggesting that both proteins are required for di-ubiquitin formation. An additional protein that may represent tri-ubiquitin was also observed above di-ubiquitin at the 90 minute time point, suggesting that higher order chains may be being assembled. Additionally, since the reducing conditions would disrupt any UBC2-Ub thioester intermediates, the protein at around 26 kDa in samples containing UBC2 may represent auto-ubiquitinated UBC2. Comparably, *in vitro* auto-ubiquitination of human UBE2N on K92, equivalent to K90 in UBC2, has been observed (McKenna *et al.*, 2001). Auto-ubiquitinated UBA1a also appears to be present at the top of the blot.

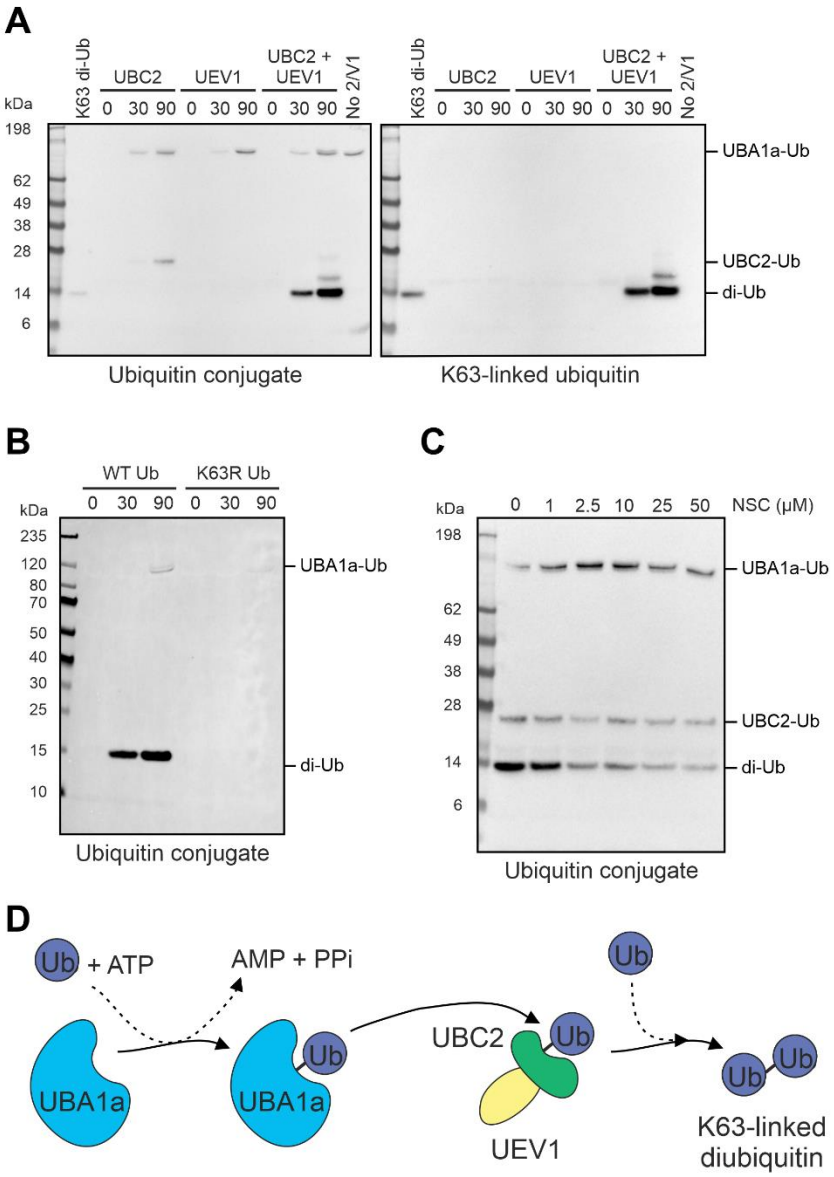

Figure 24. *Di-ubiquitin formation assays.* **A** UBA1a, ubiquitin and ATP were incubated with UBC2 and UEV1 as indicated in ubiquitination assay buffer for up to 90 min at 37°C. Reactions were

visualised by immunoblotting with either ubiquitin conjugate or K63-linked ubiquitin antibodies. **B** Di-ubiquitin formation assay performed as in **A** but with wild-type ubiquitin substituted for K63R ubiquitin where shown. **C** UBC2 and UEV1 were pre-incubated with UBE2N inhibitor NSC697923 at the concentrations indicated for 15 min prior to setting up a di-ubiquitin formation assay as in **A**. For **B** and **C**, samples were treated with reducing sample buffer prior to SDS-PAGE and immunoblotting with ubiquitin conjugate antibody. Data shown in **A**-**C** are representative of two or more experiments. No 2/V1, no UBC2 or UEV1. **D** Schematic summarising the findings of Figure 23 and Figure 24. UBA1a activates ubiquitin in an ATP-dependent manner, allowing ubiquitin to bind to the active site of UBA1a via a thioester linkage. Ubiquitin is then transferred to UBC2 (green) which, when present in complex with UEV1 (yellow), can generate free K63-linked ubiquitin chains.

Since *S. cerevisiae* UBC13 and MMS2 and their human orthologues have been shown to specifically form K63-linked ubiquitin chains (Hofmann and Pickart, 1999; McKenna *et al.*, 2001), the reactions described above were additionally probed with a K63 linkage-specific antibody. The right-hand panel in Figure 24A shows that K63-linked ubiquitin conjugates are formed by UBC2-UEV1. Furthermore, UBC2 and UEV1 were unable to conjugate K63R mutant ubiquitin, demonstrating the essential requirement for K63 of ubiquitin in the formation of free ubiquitin chains by UBC2-UEV1 (Figure 24B). Pre-incubation of UBC2 with between 1 µM and 25 µM of UBE2N inhibitor NSC697923 reduced di-ubiquitin formation in a concentration-dependent manner, showing that K63-linked ubiquitin chain formation is dependent upon UBC2 catalytic activity (Figure 24C). That NSC697923 was likely to inhibit UBC2 was rationalised based on the fact that 4 residues that were mutated to make UBE2N resistant to NSC697923 are also found in UBC2 (Hodge *et al.*, 2015). Complete inhibition of di-ubiquitin formation was not achieved, perhaps due to an insufficiently long incubation time for UBC2 with NSC697923. These experiments demonstrate that UBC2 and UEV1 can form free K63-linked ubiquitin chains *in vitro*.

The crystal structure of *S. cerevisiae* Ubc13-Mms2 covalently linked to a donor ubiquitin molecule revealed the structural basis of K63 linkage specificity in ubiquitin chain formation. In this structure, Mms2 directs the K63 residue of a putative acceptor ubiquitin into the Ubc13 active site, where it can attack Gly76 of the donor ubiquitin bound to the Ubc13 active site cysteine to form an isopeptide bond (Eddins *et al.*, 2006). An overlay of this structure (PDB ID: 2GMI) with the UBC2-UEV1 structure allowed the positions of the donor and acceptor ubiquitins relative to the *L. mexicana* complex to be revealed (Figure 22C). This provides a model of the quaternary complex without significant steric clashes and suggests that the same strategy is used to confer Lys63-linkage specificity

in *L. mexicana* and *S. cerevisiae*. In support of this, two Mms2 residues shown to be required for acceptor ubiquitin binding in the *S. cerevisiae* Ubc13-Mms2-Ub structure, Ser27 and Thr44, are conserved in *L. mexicana* UEV1 (Ser28 and Thr45 respectively).

4.2.8 UBC2 can cooperate with human E3s to allow polyubiquitination *in vitro*

As the cognate E3s for UBC2 and UEV1 have not yet been identified, human E3s known to catalyse ubiquitination in coordination with UBE2N were tested for their ability to similarly cooperate with UBC2 and/or UEV1. The reasons for doing this were threefold. Firstly, to investigate whether UBC2 could carry out the typical E2 role of facilitating ubiquitin transfer to substrates via E3 enzymes. Secondly, in the hope of making inferences about *L. mexicana* E3s that could be part of the UBC2 ubiquitination cascade and, lastly, to explore the conservation of E2-E3 interactions between *L. mexicana* and humans. For this purpose, two RING E3 ligases, BIRC2 and RNF8, were selected for testing on the basis that they are known to interact with human UBE2N (Bertrand *et al.*, 2008; Plans *et al.*, 2006; Lok *et al.*, 2012). In humans, BIRC2 has wide-ranging roles including in regulating apoptosis and cell proliferation (Bertrand *et al.*, 2008; Samuel *et al.*, 2005) and RNF8 has well-characterised roles in DNA damage signalling (Kolas *et al.*, 2007; Mailand *et al.*, 2007; Huen *et al.*, 2007). In addition, HUWE1, a HECT E3 ligase that is not known or predicted to interact with UBE2N, was also chosen for comparison (Kar *et al.*, 2012). All recombinant E3s used were GST-tagged and, with the exception of HUWE1 that was N-terminally truncated, full-length.

Figure 25 shows the ubiquitination profiles observed for BIRC2, RNF8 or HUWE1 incubated with different combinations of UBC2 and UEV1 in reactions containing UBA1a, ubiquitin and ATP. When BIRC2 or RNF8 were incubated with UBC2 in the absence of UEV1, a prominent pattern of polyubiquitination was seen (upper panel). Based on the K63-linked ubiquitin and GST blots (middle and lower panels respectively), the polyubiquitination observed was not K63-linked and occurred both as a result of E3 auto-ubiquitination and of free chain formation and/or ubiquitination of other proteins (such as UBA1a, UBC2 or UEV1) in solution. When BIRC2 or RNF8 were incubated with UEV1 in the absence of UBC2, polyubiquitination did not occur. However, a single protein was present in the ubiquitin conjugate blot at around 130 kDa, likely representing ubiquitinated UBA1a (as observed in Figure 24A-C). Similarly, polyubiquitination was not observed when BIRC2 or RNF8 were incubated with both UBC2 and UEV1. In these samples, however, di-ubiquitin formation was notably increased, suggesting that UEV1 is able to regulate UBC2 such that it switches its activity between facilitating

polyubiquitination by E3s and forming K63-linked ubiquitin chains in complex with UEV1. In contrast, polyubiquitination was observed when either UBC2, UEV1 or UBC2 and UEV1 were combined with HUWE1, suggesting that physical interaction between E2s and HUWE1 may be required for HUWE1 activity. Alternatively, the truncated nature of the recombinant HUWE1 protein, which lacks its UBA and WWE protein-protein interaction domains, may have encouraged non-specific interaction with and ubiquitin transfer from UBA1a. No ubiquitin conjugates were observed in the absence of both UBC2 and UEV1.

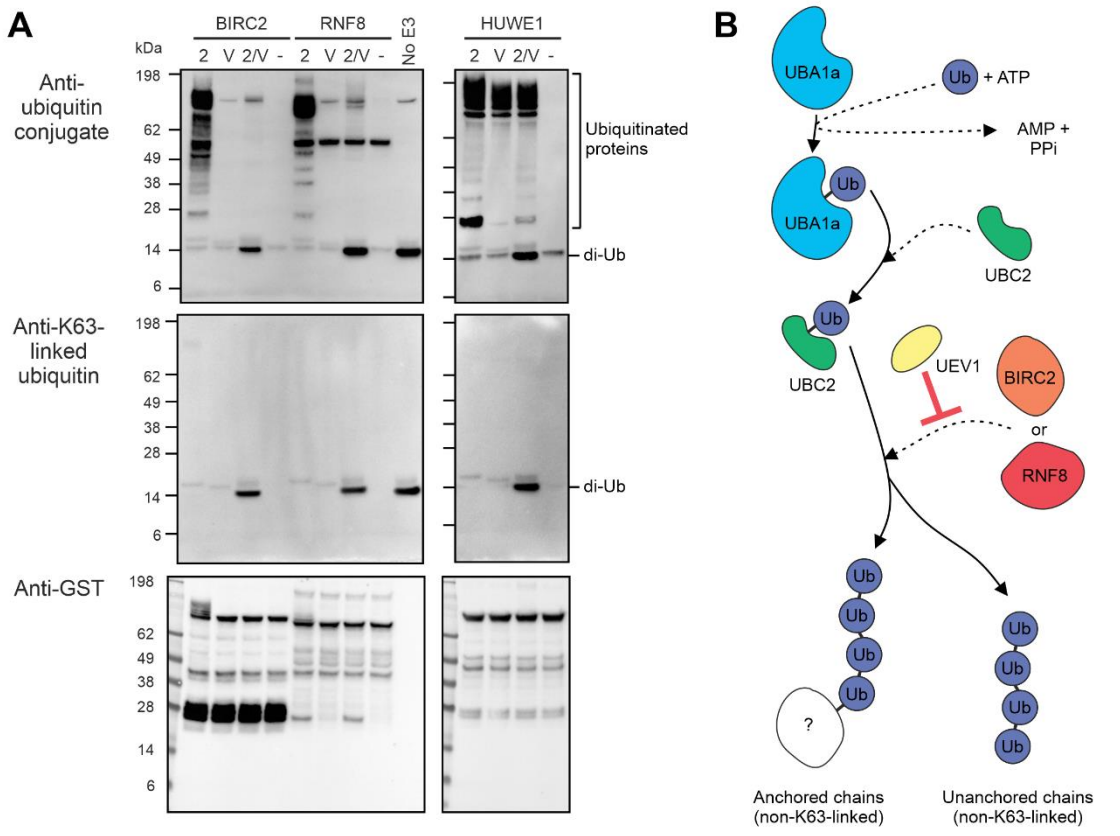

Figure 25. *Cooperation of UBC2 with human E3s in in vitro polyubiquitination.* **A** UBA1a, ubiquitin and ATP were incubated with UBC2, UEV1 and human E3s (BIRC2, RNF8 and HUWE1) as indicated in ubiquitination assay buffer for 1 h at 30°C. Reactions were visualised by immunoblotting with either ubiquitin conjugate, K63-linked ubiquitin or GST antibodies as shown. 2, UBC2; V1, UEV1; -, no UBC2 or UEV1; no E3, no BIRC2, RNF8 or HUWE1. **B** Schematic summarising the findings of **A**. UBA1a activates ubiquitin in an ATP-dependent manner, allowing ubiquitin to bind to the active site of UBA1a via a thioester linkage. Ubiquitin is then transferred to UBC2 which can, by interacting with the human E3s BIRC2 and RNF8, form non-K63-linked polyubiquitin chains. UEV1 inhibits this association, presumably via its interaction with UBC2.

4.2.9 UBC2-UEV1 can extend ubiquitin chains on human CHIP

In order to further interrogate the functional conservation between *Leishmania* and human enzymes, the ability of UBC2 to extend ubiquitin chains on the human U-box E3/E4 ligase CHIP was investigated. *In vitro* monoubiquitination of CHIP by UBE2W can be followed by the extension of ubiquitin chains by UBE2N-UBE2V1 and provides an example of a pair of cooperating E2s with distinct chain initiation and elongation functions (Soss *et al.*, 2011; Zhang *et al.*, 2005; Ye and Rape, 2009). To simplify the experimental setup and interpretation of results, it was decided to select a single E1 enzyme to facilitate ubiquitin transfer to both human UBE2W and *L. mexicana* UBC2. In a thioester assay, *L. mexicana* UBA1a was shown to be equally competent at transferring ubiquitin to UBE2W as human UBA1 (Figure 26A) and was therefore selected for use in subsequent experiments. In addition to the reducible UBE2W-Ub thioester bands observed, an additional, non-reducible band was observed following incubation of E1 and E2 enzymes. This is likely to be N-terminally ubiquitinated UBE2W (Tatham *et al.*, 2013; Scaglione *et al.*, 2013).

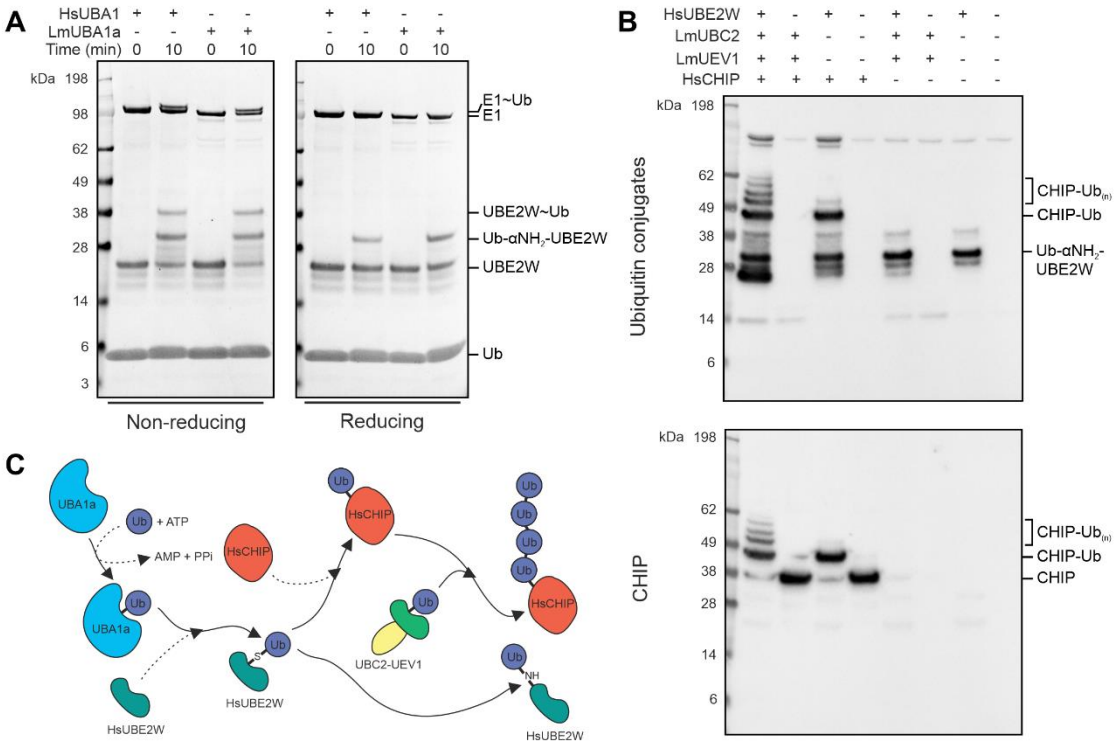

Figure 26. *Ubiquitin chain extension activity of UBC2-UEV1.* **A** Thioester assay showing ubiquitin transfer to UBE2W from both human UBA1 and *L. mexicana* UBA1a. UBE2W, ubiquitin and ATP were incubated with human UBA1 or *L. mexicana* UBA1a as indicated in ubiquitination assay buffer for up to 10 min at room temperature. Samples were treated with either reducing or non-

reducing sample buffer and visualised by SDS-PAGE with InstantBlue™ stain. **B** UBA1a, ubiquitin and ATP were incubated with UBC2, UEV1, human UBE2W and human CHIP as indicated in ubiquitination assay buffer for 1 h at 30°C. Reactions were visualised by immunoblotting with either ubiquitin conjugate or CHIP antibodies as shown. **C** Schematic summarising **A-B**. UBA1a activates ubiquitin in an ATP-dependent manner, allowing ubiquitin to bind to the active site of UBA1a via a thioester linkage. Ubiquitin is then transferred to HsUBE2W which monoubiquitinates HsCHIP. Alternatively, HsUBE2W can ubiquitinate its own N-terminus. Once primed with monoubiquitin, UBC2-UEV1 can extend ubiquitin chains on HsCHIP. Lm, *Leishmania mexicana*; Hs, *Homo sapiens*. Where species is not indicated, proteins are from *L. mexicana*.

When *L. mexicana* UBC2 and UEV1 were incubated with human UBE2W and CHIP in the presence of E1, ubiquitin and ATP, polyubiquitinated CHIP was observed (Figure 26B). When UBE2W was absent from this reaction, no CHIP ubiquitination or free chain formation was seen. Alternatively, when UBC2 and UEV1 were absent, only monoubiquitinated CHIP was observed, suggesting that UBE2W is priming CHIP with a single ubiquitin modification that can then be extended by UBC2 and UEV1. In this respect, UBC2 and UEV1 behave in a similar manner to human UBE2N-UBE2V1 (Soss *et al.*, 2011). The absence of free chain formation in the presence of UBC2, UEV1 and CHIP, however, is in contrast to what was reported for human UBE2N-UBE2V1 and CHIP (Soss *et al.*, 2011; Zhang *et al.*, 2005). In reactions where UBE2W was present but CHIP was absent, a strong band at around 34 kDa was observed, likely corresponding to N-terminally ubiquitinated UBE2W as in Figure 26A (Tatham *et al.*, 2013; Scaglione *et al.*, 2013).

4.2.10 Bioinformatic prediction of UBC2-interacting E3s

In order to make predictions of UBC2-interacting E3s in *L. mexicana*, reciprocal pBLAST searches of human BIRC2, RNF8 and CHIP were performed. Table 3 shows that, within the *L. mexicana* genome, BIRC2 is most similar to LmxM.36.3830, a putative RING-type E3 ligase. Similarly, the top hit for a pBLAST search of LmxM.36.3830 against the human genome was BIRC2. Despite this match, the query cover for both of these searches was very low (≤25%), making it likely that these proteins have different functions. These differences may include their E2 interactions, substrate specificities or ubiquitin chain formation activities. Unlike for BIRC2, reciprocal pBLASTs of RNF8 and CHIP did not identify the original query sequence, making it unlikely that an *L. mexicana* orthologue was successfully identified. Notably, LmxM.34.4000, the protein that was identified as being most similar (within the *L. mexicana* genome) to human CHIP, was shown to be a putative protein kinase and HECT E3 ligase. This similarity is due to the presence of a

TPR domain in both CHIP and LmxM.34.4000, rather than the E3 ligase and kinase domains of these proteins (Ballinger *et al.*, 1999).

Query sequence	Top hit	Identity (%)	Query cover (%)	E value
BIRC2	LmxM.36.3830	48.9	8	$8e^{-08}$
LmxM.36.3830	BIRC2	48.9	25	$6e^{-08}$
RNF8	LmxM.28.1830	29.5	19	$2e^{-05}$
LmxM.28.1830	HLTF	28.7	77	$1e^{-70}$
CHIP	LmxM.34.4000	31.0	37	$3e^{-13}$
LmxM.34.4000	SLK	25.5	20	$1e^{-23}$

Table 3. *Identification of potential UBC2-interacting E3s in L. mexicana.* Human BIRC2, RNF8 and CHIP protein sequences were BLASTed against the *L. mexicana* genome and the protein sequences of the top hits BLASTed back against the human genome. *Leishmania* proteins are represented by their gene IDs.

4.3 Discussion

4.3.1 Ubiquitination activity of UBC2-UEV1

The observation that UBC2 and UEV1 form a heterodimer was not unexpected since the *T. brucei*, *S. cerevisiae* and human orthologues of UBC2 and UEV1 form a complex (Crozier *et al.*, 2017; Hofmann and Pickart, 1999; McKenna *et al.*, 2001; Ulrich and Jentsch, 2000). That UBC2 and UEV1 form a heterodimer is also consistent with the similar loss-of-fitness phenotypes observed for Δ*ubc2* and Δ*uev1* during promastigote to amastigote differentiation, detailed in the previous chapter. Notably, UBC2 was found to exist as a monomer *in vitro*. This property is similar to HsUBE2N but contrasts with ScUbc13, which is a homodimer *in vitro* (Hofmann and Pickart, 1999). Given that dimerisation does not affect the ability of another human E2, UBE2W, to transfer ubiquitin, this difference may not be physiologically relevant (Vittal *et al.*, 2013). It is also possible (yet unlikely due to the small size of the extension), that the additional 3 amino acid residues at the N-terminus of the recombinant UBC2 protein prevent homodimer formation.

Subsequent biochemical characterisation of UBC2 and UEV1 revealed that UBA1a and UBC2 are a functional ubiquitin E1-E2 pair. This demonstrates a level of specificity for E1-E2 interactions in *L. mexicana*, since UBA1b cannot similarly transfer ubiquitin to UBC2. This is despite both UBA1a and UBA1b being more closely related to human

UBA1 than UBA6. That UBA1a and UBA1b appear to have unique functions is interesting since there is no obvious requirement for two ubiquitin E1s in other single-celled eukaryotes. *S. cerevisiae*, for example, possesses only one ubiquitin E1 (Finley *et al.*, 2012). A differential requirement for UBA1a and UBA1b is further supported by the likelihood that UBA1a, but not UBA1b, is an essential gene in promastigotes. One avenue for future investigation would be determining why two E1s are required in *Leishmania*. For example, does UBA1b, like human UBA6, conjugate other Ubls in addition to ubiquitin (Chiu, Sun and Chen, 2007)? Another interesting line of investigation would be determining whether UBA1a could be validated as a potential drug target for treating leishmaniasis. For this purpose, an inducible UBA1a null mutant could be generated using the DiCre system and used to investigate whether triggering the deletion of *UBA1a* with rapamycin leads to promastigote cell death (Duncan *et al.*, 2016). Additionally, an indication of whether UBA1a is essential for establishing infection could be obtained by infecting mice with rapamycin-treated stationary phase promastigotes. If UBA1a proved to be essential for both promastigote viability and establishing mouse infection, this would provide a good rationale for the development of UBA1a inhibitors. Encouragingly, *L. major* UBA1a is resistant to inhibition by the human E1 inhibitor TAK-243, suggesting that UBA1a-selective inhibitors could be developed (Boer and Bijlmakers, 2019).

The finding that UBC2 and UEV1 are highly conserved at both the sequence and structural level suggests that their function may be shared between distantly related species. For example, the fact that UEV1 is more similar in sequence to HsUBE2V2 and ScMMS2 than to HsUBE2V1 hints at a possible function for UEV1 in DNA damage repair (Andersen *et al.*, 2005). The UBC2-UEV1 heterodimer, like its *S. cerevisiae* and human orthologues, is able to form K63-linked ubiquitin chains *in vitro*. Since most of the chains produced by UBC2-UEV1 in our *in vitro* assays were di-ubiquitin, this supports the suggestion that UEV1 is more similar to human UBE2V2, which forms di-ubiquitin *in vitro*, than isoform 2 of UBE2V1, which forms polyubiquitin chains (Wu *et al.*, 2003; Andersen *et al.*, 2005; Hofmann and Pickart, 1999; McKenna *et al.*, 2001; Pastushok *et al.*, 2005). Indeed, it would be interesting to see whether the di-ubiquitin formation activity of UBC2-UEV1 could be altered by adding the human UBE2V1 N-terminal sequence onto UEV1, since it would inform on the importance of the N-terminal region of UEV1 for determining ubiquitin chain-forming activity (di-ubiquitin versus longer chain formation). In the di-ubiquitin formation assay, however, the conjugation of higher-order chains, thought to represent tri-ubiquitin, were additionally observed. This suggests that UBC2-UEV1 is capable of producing lengthier ubiquitin chains, albeit in smaller quantities. Since UBC2

and UEV1 share 77% and 70% amino acid identity with their *T. brucei* orthologues respectively, the biochemical properties of UBC2-UEV1 are expected to be conserved between these species. In the future, whether UBC2 and UEV1 play a role in *Leishmania* DNA repair processes could be investigated by exposing Cas9 T7 parental, Δ*ubc2* and Δ*uev1* cells to increasing doses of UV irradiation or the DNA alkylating agent methyl methanesulfonate (MMS), and determining whether Δ*ubc2* and Δ*uev1* are more sensitive to DNA damage (for example as measured using a phospho-histone H2A.X antibody, a marker of double-stranded DNA damage) or cell death than the Cas9 T7 line under these conditions (Zhao *et al.*, 2007; Prakash and Prakash, 1977; Rogakou *et al.*, 1998).

Given the dual requirement for UBC2 and UEV1 during promastigote and amastigote differentiation, it is likely that the ubiquitination activity of UBC2-UEV1 plays a role in the promastigote to amastigote transition. This could involve K63-linked di-ubiquitin formation and/or cooperation with E3 ligases to form K63-linked polyubiquitin chains. In order to identify the E3 ligases downstream of UBC2-UEV1, affinity purification proteomics could be used. Following the generation of recombinant E3 proteins, *in vitro* ubiquitination assays could be performed to test for the cooperation of UBC2-UEV1 with these E3s in ubiquitin chain formation. Identification of the substrates of such E3s, for which various methods have been described, would help to tease apart the role of UBC2-UEV1 in the differentiation process. One common approach is to compare the ubiquitinome of a wild-type cell line to an E3 null mutant or overexpression line using Gly–Gly (diGly) remnant affinity purification, which utilises antibodies recognising the diGly remnant on the ε-amine of lysine following digestion of ubiquitinated proteins with trypsin (Iconomou and Saunders, 2016). Potential substrates could then be validated using co-immunoprecipitation, *in vitro* ubiquitination assays and by Western blot comparing the amount of ubiquitinated putative substrate protein in E3 null mutant or overexpression cell lines relative to a control line. Ideally, these experiments would be carried out during promastigote to amastigote differentiation. However, this might not be possible if the E3 of interest is essential for the differentiation process.

For our *in vitro* experiments, human BIRC2 and RNF8 provided useful tools for examining the activity of UBC2 in the absence of available *Leishmania* E3s. These experiments showed that both BIRC2 and RNF8 can form polyubiquitin chains (non-K63-linked) in a UBC2-dependent manner. Intriguingly, UEV1 inhibited this reaction by switching UBC2 activity towards unanchored K63-linked di-ubiquitin formation. This ability of UEV1 could allow UBC2 to flip between direct (covalent attachment of ubiquitin

to substrates) and indirect (unanchored ubiquitin chain binding to regulated proteins) mechanisms of regulating other proteins as well as between sets of protein targets, depending on the availability of UEV1. For this reason, it would be interesting to investigate whether the relative expression of UBC2 and UEV1 changes during the lifecycle of *L. mexicana*. The proposed role for UEV1 in specifying K63-linked chain formation is further supported by the observation that polyubiquitin chains produced in the presence of UBC2 and BIRC2 or RNF8 are not K63-linked. In support of our finding that UBC2 acts alone with RNF8, human UBE2V1 and UBE2V2 have been shown to be dispensable for the function of UBE2N and RNF8 in DNA damage signalling (Huen *et al.*, 2008). Conversely, the formation of polyubiquitin chains on human CHIP was seen in the presence of both UBC2 and UEV1, demonstrating that, in certain contexts (perhaps dependent on E3 pairing), the UBC2-UEV1 heterodimer can form poly-ubiquitin chains. In this example, K63-linked ubiquitin chains could be formed in a manner similar to that described for rat RNF4, where, due to interactions between the RING domain and UBE2N/UBC2, the donor ubiquitin is held in a 'folded-back' conformation poised for nucleophilic attack by K63 of the acceptor ubiquitin bound to UBE2V2/UEV1 (Plechanovová *et al.*, 2012; Branigan *et al.*, 2015). For this reason, it would be useful to determine (using a K63-linked ubiquitin blot) whether the ubiquitin chains produced by UBC2-UEV1 and CHIP are K63-linked. The ability of UBC2-UEV1 to extend ubiquitin chains on CHIP illustrates the potential for UBC2-UEV1 to act in coordination with other E2s in *L. mexicana*, although an E2 with such a role has yet to be identified.

The physiological role of ubiquitin chains generated by *Leishmania* UBC2-UEV1 is currently unknown and an important area for further investigation. However, previous research has shown that free ubiquitin chains are present in both *S. cerevisiae* and human cells and that their levels (in *S. cerevisiae*) increase following heat shock, DNA damage or oxidative stress (Braten *et al.*, 2012). Furthermore, unanchored K63-linked chains generated by the human E3 ligases TRAF6 and TRIM32 have been shown to interact with and activate protein kinases (Di Rienzo *et al.*, 2019; Xia *et al.*, 2009) and unanchored K48-linked chains can inhibit the proteasome (Piotrowski *et al.*, 1997), demonstrating that free ubiquitin chains can perform regulatory functions. Do the unanchored K63-linked di-ubiquitin chains generated by UBC2-UEV1 have similar regulatory roles? Curiously, *S. cerevisiae* HUL5, the E3 ligase partly responsible for free chain formation upon stress induction (Braten *et al.*, 2012), is related to *L. mexicana* HECT2 (45% query cover, 32.6% identity, E value: $5e^{-47}$). This raises the possibility that HECT2 is involved in the response to environmental stresses that trigger the promastigote to amastigote transition and may explain the requirement for HECT2 in

amastigotes. Exploring the potential interaction between UBC2-UEV1 or HECT2 and protein kinases involved in stress responses is an interesting avenue for further study. Alternatively, the K63-linked di-ubiquitin chains generated by UBC2-UEV1 in the *in vitro* assays may not be physiologically relevant. Instead, UBC2-UEV1 may preferentially associate with E3 ligases to facilitate the formation of poly-ubiquitin chains. The identification of UBC2 and UEV1 in an interactome of *L. mexicana* DUB2, which is able to cleave K63-linked di-ubiquitin *in vitro*, suggests a possible interplay between these proteins in the regulation of K63-linked ubiquitin chains (Damianou *et al.*, 2020). This interaction remains to be validated, however, which could be achieved by co-immunoprecipitation.

Based on low query cover and/or the inability to identify the original query sequence in reciprocal pBLAST searches, it can be concluded that the attempts to identify UBC2-interacting E3s in *L. mexicana* were unsuccessful. This shows that although UBC2 and UEV1 are highly conserved between *L. mexicana* and humans, human BIRC2, RNF8 and CHIP are not. Therefore, the E3s that interact with UBC2 in *L. mexicana* may be highly divergent from those in humans and could, dependent on whether they are essential for the parasite, present good opportunities for drug target validation. Since RING and U-box E3 ligases act as molecular scaffolds, inhibitors of these E3 classes would need to disrupt protein-protein (for example E2-E3 or E3-substrate) interactions or trigger protein degradation (PROTACs). Additionally, the implied divergence of *L. mexicana* E3s suggests that they may have novel, parasite-specific functions.

4.3.2 Structural insights into UBC2-UEV1

The X-ray crystal structure of the UBC2-UEV1 heterodimer revealed high conservation of the UBC2 active site and UBC2-UEV1 interface, highlighting the importance of these features in the function of this complex across diverse eukaryotes. This high level of conservation also means that, despite the possibility that UBC2 and UEV1 may be essential in the amastigote stage, UBC2-UEV1 would not be a good drug target. This is because it would be highly difficult to develop specific active site or protein-protein interaction inhibitors to inhibit the catalytic activity of UBC2 or the interaction between UBC2 and UEV1 respectively. Instead, the identification of E3 ligases and substrates of UBC2-UEV1 that are also essential for promastigote-amastigote differentiation may be a better source of potential drug targets.

The structural modelling of UBC2-UEV1 in complex with donor and acceptor ubiquitins, together with the conservation of key UEV1 residues that are required for acceptor ubiquitin interaction, are consistent with a role for UEV1 in dictating K63-linked chain specificity by correctly orienting the acceptor ubiquitin (Eddins *et al.*, 2006). In contrast, the donor ubiquitin is thought to exhibit flexible positioning around the covalent Cys85 linkage (Eddins *et al.*, 2006; Branigan *et al.*, 2015). Since UBC2 and UEV1 exhibit such high degrees of conservation at both the structural and functional level, the finding that the nature of UBC2 activity can be regulated by UEV1 has implications for orthologous proteins in other species.

5 Identification of UBC2- and UEV1-interacting proteins

5.1 Introduction

5.1.1 The complexity of ubiquitin networks

Due to the complexity of the ubiquitin system, cataloguing the interactions that occur between system components, or the components responsible for a particular ubiquitin modification, can be very challenging. For example, a huge number of proteins are required for ubiquitin networks to function and may include E1s, E2s, E3s, E4s, DUBs, substrates and proteins with ubiquitin-binding domains that physically interact with ubiquitinated substrates to elicit an effect (Husnjak and Dikic, 2012). Complicating things further, E1s can perform ubiquitination activity in concert with multiple E2s, E2s can act with multiple E3s, E3s can act with multiple E2s and substrate proteins may be modified by more than one E3 ligase or DUB. Furthermore, interactions between the different components, such as E2s and E3s or E3s and substrates, as well as ubiquitin modifications themselves, can be very transient and therefore difficult to detect (Iconomou and Saunders, 2016; Kliza and Husnjak, 2020). The identification of E3 substrates, in particular, is made additionally problematic by low affinity interactions between E3s and their targets, the possibility that some ubiquitinated substrates will be removed from the cell by proteasomal degradation and the fact that only a subpopulation of substrate protein in a cell may contain the modification of interest (Kliza and Husnjak, 2020).

5.1.2 Methods for studying ubiquitin networks

Multiple methods exist for identifying components of ubiquitin networks, although most have focused on the identification of E3 ligase substrates. These include yeast two-hybrid screening, *in vitro* ubiquitination assays, protein microarrays, global protein stability profiling, differential expression proteomics, affinity purification proteomics, ubiquitin ligase trapping and proximity labelling (Iconomou and Saunders, 2016). The development of diGly affinity proteomics, which exploit the diGly remnant found at the C-terminus of Ubls following digestion with trypsin and which can be used for the enrichment of ubiquitin substrates by immunopurification, has been particularly useful in the field (Xu, Paige and Jaffrey, 2010; Kliza and Husnjak, 2020). Also of note is the development of BioID, a proximity labelling technique involving the fusion of a promiscuous biotin ligase (BirA*) to the protein of interest. In the presence of biotin, BirA*

biotinylates proteins in the close vicinity of the fusion protein, permitting their detection using affinity purification and mass spectrometry (Roux *et al.*, 2012). Demonstrating the applications of this technique to the identification of ubiquitin substrates, Coyaud *et al.* (2015) used a combined strategy involving proteasomal inhibition and BioID to identify 50 putative substrates of the $SCF^{\beta\text{-}TrCP1/2}$ E3 ligase. More recently, TurboID and miniTurbo, mutant versions of BirA* that work over a greater temperature range and have shorter labelling times, have been developed. Of these, TurboID offers the advantage of the highest biotinylation activity whereas miniTurbo has the lowest background activity (Branon *et al.*, 2018).

In the past, affinity purification proteomics methods have been used to identify components of the *S. cerevisiae* APC/C complex and networks associated with SCF E3s (Zachariae *et al.*, 1998; Yoon *et al.*, 2002; Seol *et al.*, 1999; Seol, Shevchenko and Deshaies, 2001). Putative E2-E3 interactions have also been identified using yeast two-hybrid screening and include those involving human UBE2N, UBE2V1 and UBE2V2 (Markson *et al.*, 2009; van Wijk *et al.*, 2009; Christensen, Brzovic and Klevit, 2007). Due to the low affinity of most RING-E2 interactions, these can be difficult to detect using affinity purification approaches. However, some E3s, including gp78, Rad18 and AO7, contain regions outside their RING domain responsible for binding to E2s that have permitted the detection of E2-E3 interactions using this technique (Metzger *et al.*, 2014).

5.1.3 Aims

This chapter aimed to lend insight into existing cooperation between UBC2-UEV1 and *Leishmania* E3s and the roles of UBC2 and UEV1 in promastigote and amastigote biology. To this end, the selection of a cross-linking affinity purification proteomics approach for the identification of UBC2 and UEV1 interaction partners followed by the identification of UBC2 and UEV1 interactomes in *Leishmania* promastigotes and amastigotes will be described.

5.2 Results

5.2.1 Selection of affinity purification strategy

In order to further interrogate the roles of UBC2-UEV1 in *Leishmania*, it was decided to identify the interactomes of these proteins. Initially, both affinity purification and proximity labelling techniques were considered. For these purposes, the N-terminally myc-

mNeonGreen-tagged cell lines used for localisation imaging and miniTurbo- and TurboID-tagged cell lines were tested. The TurboID- and miniTurbo- lines were generated using the same primers and CRISPR-Cas9 strategy used for N-terminal myc-mNeonGreen tagging and all tags were attached to the target protein by a flexible GS linker (GSGSGSGSGS) (Beneke *et al.*, 2017; Beneke and Gluenz, 2019). Since both UBC2 and UEV1 are essential for promastigote-amastigote differentiation, the ability of tagged cell lines to differentiate from promastigotes to amastigotes can inform on the effect of tags on protein function. These effects were assessed using a cell viability assay, the data from which are presented in Figure 27A. Relative to the Cas9 T7 parental line, *myc-mNeonGreen-UBC2*, *miniTurbo-UBC2*, *TurboID-UBC2*, *miniTurbo-UEV1* and *TurboID-UEV1* all showed dramatically reduced viability at 48 h and 120 h following initiation of promastigote-amastigote differentiation. In contrast, *myc-mNeonGreen-UEV1* maintained similar viability to the Cas9 T7 cell line throughout differentiation. However, since the myc-*mNeonGreen-UEV1* cell line was generated using only a single repair cassette containing a blasticidin resistance marker and population level antibiotic selection, wild-type *UEV1* alleles may have been retained in the population, potentially explaining the lack of effect of the myc-mNeonGreen tag on cell viability. Overall, these results suggest that all three types of tag (myc-mNeonGreen, miniTurbo and TurboID) can disrupt UBC2 and/or UEV1 function, making them unsuitable for the identification of UBC2- and UEV1-interacting partners.

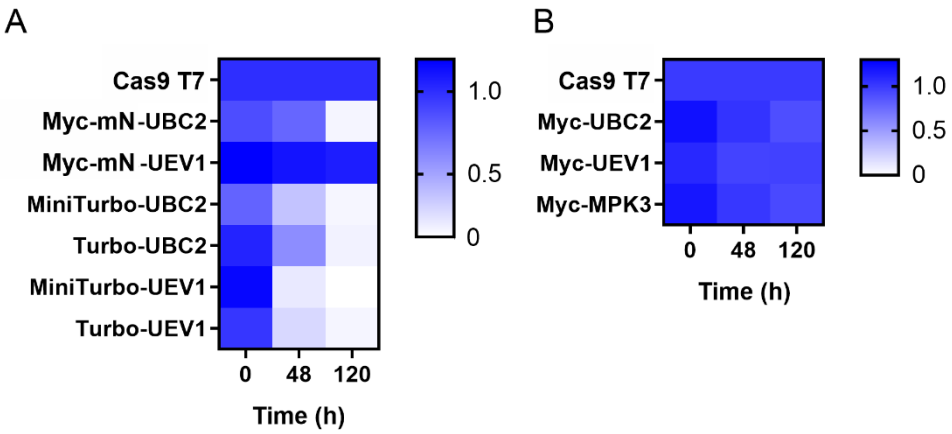

Figure 27. *Viability of tagged cell lines during promastigote to amastigote differentiation.* Relative viability of **A** myc-mNeonGreen- (Myc-mN-), TurboID- (Turbo), miniTurbo- and **B** myc-tagged lines respectively at 0, 48 and 120 h into promastigote to axenic amastigote differentiation. Following an 8 h incubation with resazurin, fluorescence intensities at 590 nm were obtained, background corrected and averaged between replicates for each sample. Relative viabilities were then calculated by dividing the average fluorescence intensity obtained for each cell line by the

fluorescence intensity obtained for the Cas9 T7 cell line at the equivalent time point. Relative viability is indicated on a scale of 0 (white, no viability) to 1.2 (blue, viability 1.2 times greater than the Cas9 T7 cell line at the equivalent time point). Data are an average of two independent experiments, each with 6 replicates.

Since the molecular weights of the myc-mNeonGreen, TurboID and miniTurbo tags are 32 kDa, 35 kDa and 28 kDa respectively (Branon *et al.*, 2018), it may be that any form of large, N-terminal tag is incompatible with UBC2 or UEV1 function. For this reason, UBC2 and UEV1 cell lines with only an N-terminal 3 x myc tag (connected to the target protein by a flexible GS linker) were generated. MPK3 (LmxM.10.0490) was also tagged to enable enrichment of UBC2- and UEV1-specific interactors in affinity purification proteomics experiments, on the assumption that most, if not all, MPK3 interacting partners are different from those of UBC2 and UEV1. Two repair cassettes containing different antibiotic resistance markers (blasticidin and puromycin) were used to tag both alleles of the targeted genes, ensuring that tests of cell viability would inform on potential disruption of UBC2 or UEV1 function by the 3 x myc tag. As can be seen in Figure 27B, all three myc-tagged cell lines showed similar viability to the parental Cas9 T7 cell line 120 h into promastigote-amastigote differentiation, suggesting the 3 x myc tag does not disrupt UBC2 or UEV1 function.

5.2.2 Confirming localisation of UBC2 and UEV1

Since the myc-mNeonGreen tag used to provide localisation information on UBC2 and UEV1 appears to disrupt their function, it may also interfere with their localisation. To increase the level of certainty surrounding the localisation of UBC2 and UEV1, C-terminal tagging with mNeonGreen-myc was performed with two repair cassettes containing different antibiotic resistance markers (blasticidin and puromycin) and the resulting cell lines imaged. Unlike the cell line in which UBC2 was N-terminally tagged with mNeonGreen, these cell lines showed similar viabilities to the Cas9 T7 parental line throughout promastigote to amastigote differentiation (Figure 28A), suggesting that the C-terminal tag has no effect on either UBC2 or UEV1 function. The expression of UBC2-mNeonGreen-myc (predicted molecular weight 49 kDa) and UEV1-mNeonGreen-myc (predicted molecular weight 48 kDa) was also confirmed at the protein level by Western blotting with an anti-myc antibody (Figure 28B). Fluorescence images of live cells indicated cytoplasmic localisations for both UBC2 and UEV1 (Figure 28C), as was observed for the N-terminally myc-mNeonGreen-tagged proteins. This finding lends increased confidence to the proposal that UBC2 and UEV1 are cytoplasmically localised.

Despite the implication that C-terminal mNeonGreen-myc tags do not affect UBC2 or UEV1 function, the 3 x myc tag (without mNeonGreen) was selected for use in immunoprecipitation experiments based on the rationale that the large mNeonGreen-myc tag was more likely to interfere with the ability of UBC2 and UEV1 to bind their interacting partners than the 3 x myc tag.

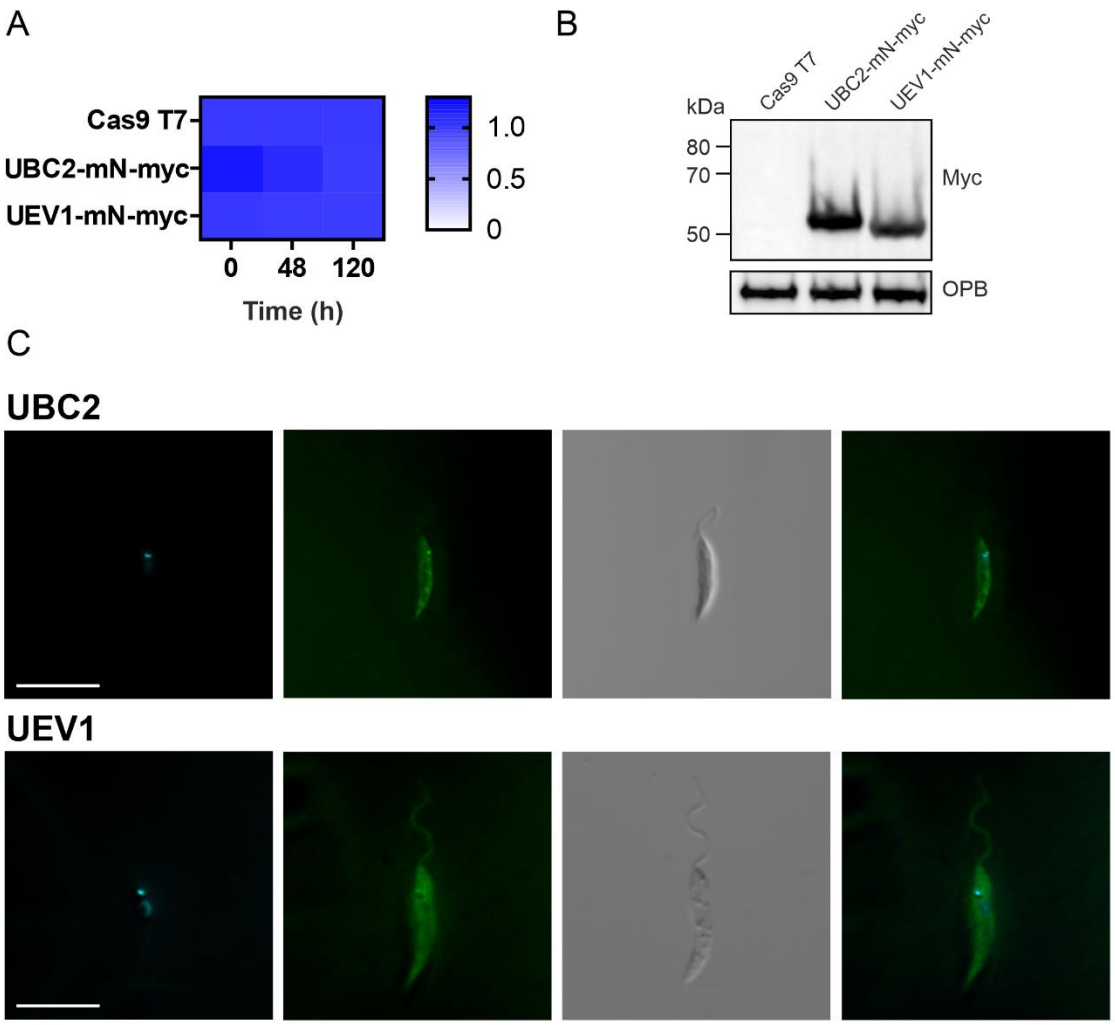

Figure 28. *Localisation of C-terminally tagged UBC2 and UEV1.* **A** Viability of C-terminally mNeonGreen-myc- tagged UBC2 (UBC2-mN-myc) and UEV1 (UEV1-mN-myc) cell lines at 0, 48 and 120 h into promastigote to axenic amastigote differentiation. Following an 8 h incubation with resazurin, fluorescence intensities at 590 nm were obtained, background corrected and averaged between replicates for each sample. Relative viabilities were then calculated by dividing the average fluorescence intensity obtained for each cell line by the fluorescence intensity obtained for the Cas9 T7 cell line at the equivalent time point. Relative viability is indicated on a scale of 0 (white, no viability) to 1.2 (blue, viability 1.2 times greater than the Cas9 T7 cell line at the equivalent time point). Data are an average of two independent experiments, each with 6 replicates. **B** Anti-myc and anti-OPB (loading control) Western blots of the Cas9 T7 parental cell

line and mNeonGreen-myc-tagged UBC2 and UEV1 cell lines. **C** Live cell imaging panels from left to right show Hoechst 33342 staining of the nucleus and kinetoplast, mNeonGreen signal of the tagged protein, a differential interference contrast image and a merged Hoechst/mNeonGreen image. Scale bars represent 10 µm.

5.2.3 Validation of tagged cell lines

Prior to carrying out immunoprecipitations on the myc-tagged cell lines, validation was carried out at the DNA and protein level. Figure 29A shows the PCR amplification of DNA from *myc-MPK3*, *myc-UBC2* and *myc-UEV1* cell lines, specifically the region between the 5'-UTR of the targeted gene and the gene itself. In the parental Cas9 T7 line, only small DNA fragments of around 300 bp are seen, representing the unedited gene regions. In the *myc-UBC2* and *myc-UEV1* mutants, these DNA fragments are absent and replaced by bands at around 1,600 bp and 1,800 bp, representing amplification of the inserted blasticidin or puromycin repair cassettes respectively. In the *myc-MPK3* mutant, both the small and larger fragments are visible, suggesting the existence of more than two alleles of the gene. Overall, these results confirm the successful complete allele-tagging of UBC2 and UEV1 (important for interpreting the cell viability data) and the successful tagging of at least two alleles of MPK3.

At the protein level, *myc-MPK3*, *myc-UBC2* and *myc-UEV1* were shown to be expressed in both promastigotes and amastigotes (Figure 29B), demonstrating the potential for immunoprecipitations to be performed in both of these life cycle stages. Additionally, 120 h following the initiation of promastigote-amastigote differentiation, all three myc-tagged cell lines (in addition to the Cas9 T7 parental line) showed expression of HASPB (Figure 29C), a marker of the amastigote life cycle stage (Nugent *et al.*, 2004; Depledge *et al.*, 2010). This latter result complements the viability assay in demonstrating the ability of the myc-tagged cell lines to successfully differentiate from promastigotes to amastigotes.

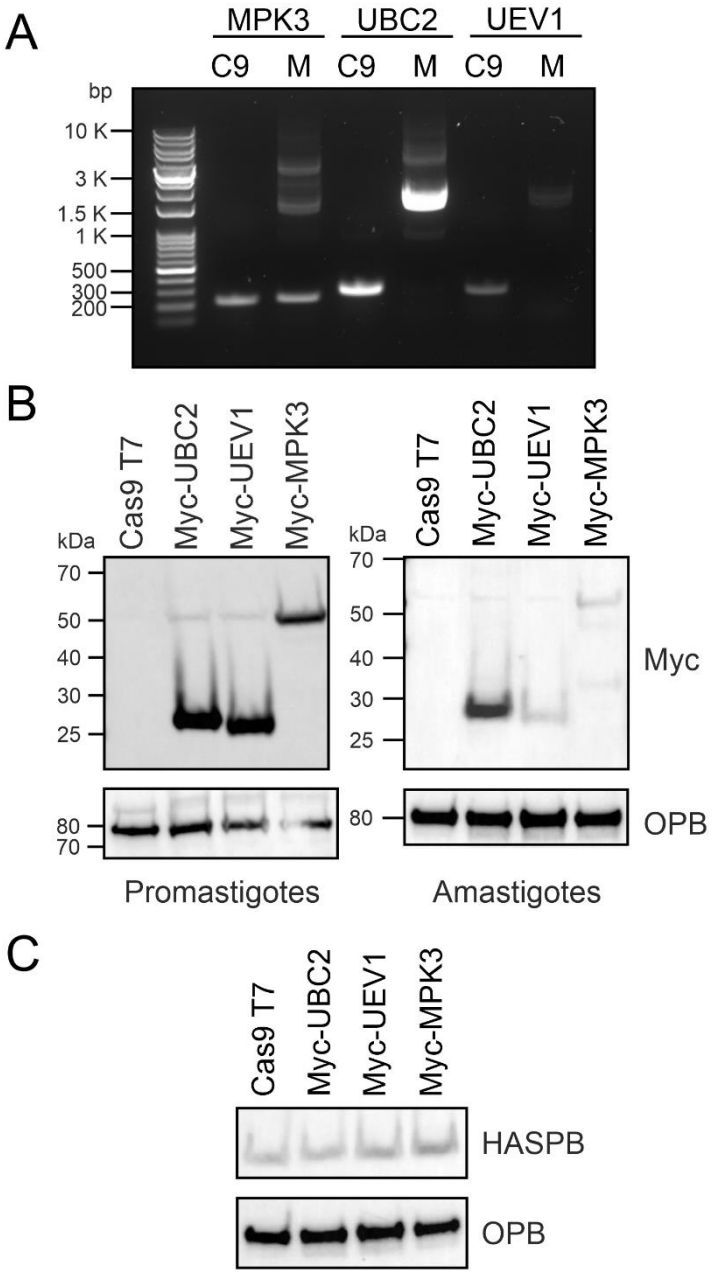

Figure 29. *Validation of myc-tagged cell lines.* **A** PCR amplification of the region between the 5'-UTR of the gene and the gene itself. Without the tagging repair cassette, this fragment should be around 300 bp and with the cassette it should be around 1,600 (blasticidin resistance) or 1,800 bp (puromycin resistance). C9, Cas9 T7 parental line; M, mutant line; bp, base pairs. The targeted gene is indicated above the gel image. **B** Anti-myc and anti-OPB (loading control) Western blots showing the expression of myc-tagged proteins in promastigotes and amastigotes. **C** Anti-HASPB and anti-OPB Western blots indicating the ability of tagged cell lines to differentiate into amastigotes. For all blot samples, protein from 3.6 x 10^6 cells was run per well.

5.2.4 UBC2 and UEV1 interactomes in promastigotes

In order to identify the interacting partners of UBC2 and UEV1 in promastigotes, a cross-linking affinity purification proteomics approach was used. Summarily, this involved the chemical cross-linking of promastigote cells expressing myc-MPK3, myc-UBC2 or myc-UEV1, the subsequent immunoprecipitation of myc-tagged proteins and their binding partners using anti-myc beads and the identification and quantification of proteins using mass spectrometry. The use of a chemical crosslinker was included in order to “fix” protein interactions to allow the identification of more weakly- or transiently-interacting proteins. This was thought to be particularly relevant to the identification of interactions between UBC2 and RING E3s, since RING E3:E2 interactions are often of low affinity (Metzger *et al.*, 2014). The protein gel in Figure 30 shows the relative amounts of myc-tagged protein present in the total (T) and unbound (U) fractions during the immunoprecipitation step. The general trend is that the band representing the unbound fraction appears less intense than that representing the total material, suggesting that the beads are binding myc-tagged proteins in the samples. This difference is not obvious for all samples, however, which may be due to variation in the viscosity of the protein samples, leading to their differential migration in the SDS-PAGE gels. Despite this, a clear band was seen representing one twentieth of the material eluted from the anti-myc beads, illustrating that a sufficient amount of protein was present for subsequent processing steps.

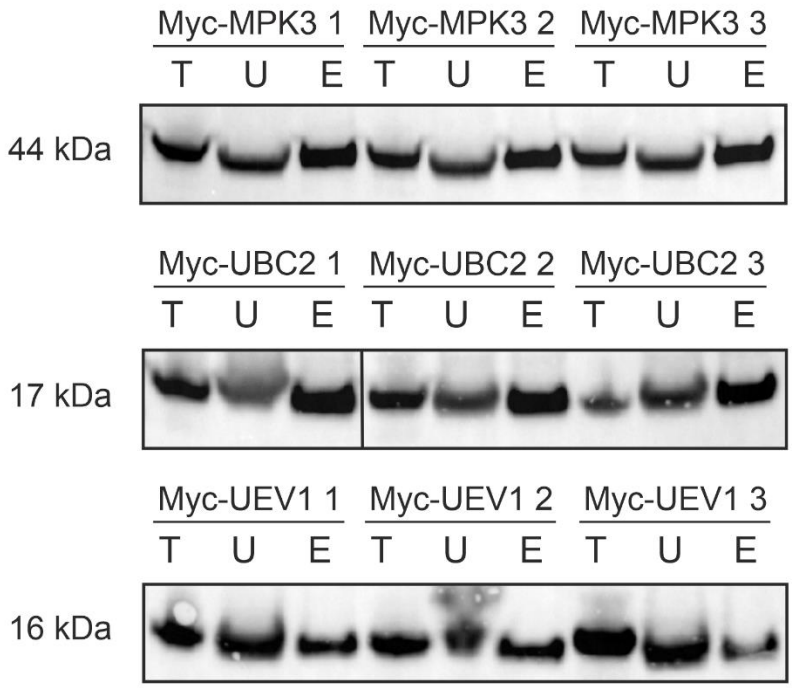

Figure 30. *Immunoprecipitation of myc-tagged proteins in promastigotes.* Anti-myc Western blot of the total (T), unbound (U) and eluted (E) fractions. Equivalent amounts of the total and unbound fractions were run for each sample. One twentieth of the eluted material was run alongside. Samples were prepared in triplicate (1, 2 and 3) for each myc-tagged protein. Molecular weights of the proteins of interest are shown on the left hand side.

Following the reduction, alkylation and digestion (with trypsin) of the proteins, peptides were desalted and loaded onto the mass spectrometer. After peptide identification and protein quantification, differences in protein abundance between the myc-UBC2 and myc-MPK3 or myc-UEV1 and myc-MPK3 samples were used to infer specific UBC2 and/or UEV1 interactors. To perform this analysis, two strategies were taken. First, pairwise ANOVA tests (with the null hypothesis that protein abundance is equal between groups) were performed in PEAKS Studio. Since these analyses use peptide-level data, they provide higher sensitivity for detecting differences between highly abundant proteins (since these proteins will tend to have higher peptide counts). Second, SAINTq analysis of protein-level data was used to identify enrichment in the myc-UBC2 or myc-UEV1 samples versus the myc-MPK3 samples. Compared to the analysis in PEAKS Studio, SAINTq analysis gives greater weighting to proteins that have very low or no abundance in the myc-MPK3 samples. Since we are assuming in our analysis that UBC2 and UEV1 have (at least some) different interacting partners to MPK3, this is likely to be the most biologically relevant strategy. However, where few peptides are detected for a specific protein, the chance of false positive identification is enhanced.

For analysis of the promastigote proteomics data, significant enrichment was defined by a P-value of less than 0.05 or a false discovery rate of less than 5% for the PEAKS Studio and SAINTq analyses respectively. In the myc-UBC2 samples, 18 and 23 proteins were identified as significantly enriched using the PEAKS Studio and SAINTq analysis methods respectively (Table 4 and Table 5 respectively). Of these, 13 proteins were identified in both analyses (Figure 31). One of these was the bait protein (UBC2) and 8 were proteins associated with the ubiquitin system, including UEV1, ubiquitin (LmxM.09.0891, LmxM.30.2030 and LmxM.30.1900; all peptides matching ubiquitin fusion proteins matched to the N-terminal ubiquitin portion only), UBC13 and 3 RING-type E3 ligases (LmxM.24.1380, LmxM.18.1150 and LmxM.24.0080). For the purposes of this work, the RING E3 ligases were named RING-type E3 ligase 1-3 (RING1-3) for LmxM.24.1380, LmxM.18.1150 and LmxM.24.0080 respectively. The remaining 4 proteins were a hypothetical protein (LmxM.26.2490), an aldose 1-epimerase-like protein, an LSD1-like protein and isocitrate dehydrogenase.

Accession	**-10logP**	**Fold change UBC2/MPK3**	**Description**
LmxM.24.1380*	39.3	1000.0	RING-type E3 ligase 1
LmxM.34.1300*	34.8	7.2	UBC13
LmxM.26.2490*	32.9	30.0	hypothetical protein
LmxM.23.0430*	32.7	19.8	aldose 1-epimerase-like protein
LmxM.13.1580*	26.9	288.0	UEV1
LmxM.11.0630	21.8	1.6	aminopeptidase
LmxM.04.0680*	19.1	422.8	UBC2
LmxM.18.1150*	16.9	311.4	RING-type E3 ligase 2
LmxM.34.4850	16.7	1.2	proteasome alpha 1 subunit
LmxM.30.1395*	16.0	251.0	LSD1-like protein
LmxM.10.0290*	15.6	12.8	isocitrate dehydrogenase
LmxM.36.3100	15.2	1.2	ATP synthase
LmxM.14.1160	15.1	1.5	enolase
LmxM.24.0080*	14.2	91.2	RING-type E3 ligase 3
LmxM.09.0891*	13.8	47.9	polyubiquitin
LmxM.30.2030*	13.8	47.9	ubiquitin-fusion protein 2

LmxM.30.1900*	13.8	47.9	ubiquitin-fusion protein 1
LmxM.25.2010	13.3	2.1	2,4-dihydroxyhept-2-ene-1,7-dioic acid aldolase

Table 4. *Proteins enriched in UBC2 versus MPK3 promastigote immunoprecipitations, as analysed in PEAKS Studio.* A P-value of 0.05 was used as the cut-off. P-values were obtained from an ANOVA of peptide-level data. An asterisk indicates proteins that were found in both the PEAKS Studio and SAINTq analyses for this dataset.

Accession	**BFDR**	**Peptide Count**	**Description**
LmxM.04.0680*	0	33	UBC2
LmxM.08_29.2160	0	10	rab-GDP dissociation inhibitor
LmxM.13.1580*	0	26	UEV1
LmxM.24.0080*	0	12	RING-type E3 ligase 3
LmxM.30.1395*	0	6	LSD1-like protein
LmxM.30.2560	0	2	hypothetical protein
LmxM.34.1300*	0	2	UBC13
LmxM.14.1320	0.0001	2	serine hydroxymethyltransferase
LmxM.26.2490*	0.002	62	hypothetical protein
LmxM.24.1380*	0.0037	7	RING-type E3 ligase 1
LmxM.10.0290*	0.0051	4	isocitrate dehydrogenase
LmxM.23.0430*	0.0063	11	aldose 1-epimerase-like protein
LmxM.34.2090	0.0082	2	kinesin
LmxM.10.0910	0.0099	2	Rab11 GTPase
LmxM.32.2300	0.0122	2	udp-glc 4'-epimerase
LmxM.09.0891*	0.0143	4	polyubiquitin
LmxM.30.1900*	0.0143	4	ubiquitin-fusion protein 1
LmxM.30.2030*	0.0143	4	ubiquitin-fusion protein 2
LmxM.18.1150*	0.0209	10	RING-type E3 ligase 2
LmxM.05.0030	0.0233	2	small GTP-binding protein
LmxM.34.3700	0.0272	6	Gim5A
LmxM.23.0200	0.0362	2	endoribonuclease L-PSP
LmxM.33.3670	0.0447	10	vacuolar ATP synthase catalytic subunit a

Table 5. *Proteins enriched in UBC2 versus MPK3 promastigote immunoprecipitations, as analysed by protein-level analysis in SAINTq.* A 5% false discovery rate was used as the cut-off.

BFDR, Bayesian false discovery rate. An asterisk indicates proteins that were found in both the PEAKS Studio and SAINTq analyses for this dataset.

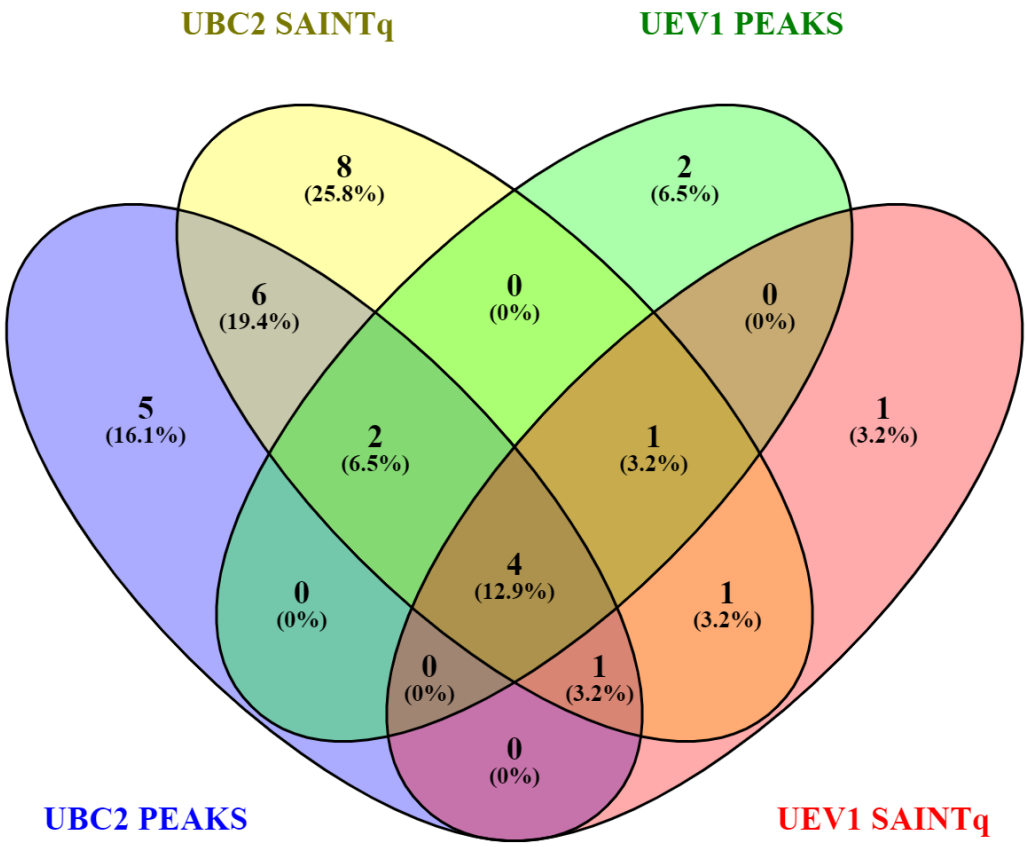

Figure 31. *Overlap between promastigote datasets.* Venn diagram illustrating the overlap between interacting partners identified for UBC2 and UEV1 in the promastigote stage using PEAKS Studio and SAINTq analysis methods.For the myc-UEV1 samples, 9 and 8 proteins were identified as significantly enriched by PEAKS Studio and SAINTq respectively (Table 6 and Table 7 respectively), with 5 proteins identified in both analyses (Figure 31). These included the bait protein (UEV1), UBC2, a rab-GDP dissociation inhibitor, UBC13 and isocitrate dehydrogenase. 4 proteins were found in the PEAKS Studio and SAINTq analyses of both UBC2 and UEV1: UBC2, UEV1, UBC13 and isocitrate dehydrogenase. This suggests that UBC2 and UEV1 interact in promastigote cells and share some of the same interacting partners. Additionally, the good correlation

observed between proteins identified in the PEAKS Studio and SAINTq analyses suggest that the input data are reliable.

Accession	-10logP	Fold change UEV1/MPK3	Description
LmxM.23.0430	46.1	1000.0	aldose 1-epimerase-like protein
LmxM.24.1380	45.1	1000.0	RING-type E3 ligase 1
LmxM.08_29.2160*	41.4	24.1	rab-GDP dissociation inhibitor
LmxM.13.1580*	24.3	433.0	UEV1
LmxM.34.1300*	20.2	5.1	UBC13
LmxM.04.0680*	19.2	125.4	UBC2
LmxM.36.3840	15.7	2.4	glycyl tRNA synthetase
LmxM.16.0950	14.0	1.7	sucrose-phosphate synthase-like protein
LmxM.10.0290*	13.4	6.2	isocitrate dehydrogenase

Table 6. *Proteins enriched in UEV1 versus MPK3 promastigote immunoprecipitations, as analysed in PEAKS Studio.* A P-value of 0.05 was used as the cut-off. P-values were obtained from an ANOVA of peptide-level data. An asterisk indicates proteins that were found in both the PEAKS Studio and SAINTq analyses for this dataset.

Accession	BFDR	Peptide Count	Description
LmxM.04.0680*	0	33	UBC2
LmxM.08_29.2160*	0	10	rab-GDP dissociation inhibitor
LmxM.13.1580*	0	26	UEV1
LmxM.34.1300*	0.0008	2	UBC13
LmxM.28.0890	0.0037	2	ribonucleoside-diphosphate reductase large chain
LmxM.10.0290*	0.0071	4	isocitrate dehydrogenase
LmxM.26.2490	0.0255	62	hypothetical protein
LmxM.34.2090	0.048	2	kinesin

Table 7. *Proteins enriched in UEV1 versus MPK3 promastigote immunoprecipitations, as analysed by protein-level analysis in SAINTq.* A 5% false discovery rate was used as the cut-off. BFDR, Bayesian false discovery rate. An asterisk indicates proteins that were found in both the PEAKS Studio and SAINTq analyses for this dataset.

The proposed interactomes of UBC2 and UEV1, as identified using SAINTq analysis, are shown in Figure 32. The SAINTq analysis data were selected due to the greater weighting that SAINTq analysis (versus PEAKS Studio analysis) gives to proteins that have very low or no abundance in the myc-MPK3 samples. However, peptide counts should also be considered when assessing the level of confidence in specific interactors. In the figure, UBC2 is shown to associate with multiple ubiquitin system proteins and proteins associated with intracellular transport (Rab11 GTPase, small GTP-binding protein, rab-GDP dissociation inhibitor and kinesin), carbohydrate metabolism (aldose 1-epimerase-like protein and udp-glc 4'epimerase), organic substance metabolism (isocitrate dehydrogenase) and drug metabolism (vacuolar ATP synthase catalytic subunit a). UEV1 shares interactions with UBC13, rab-GDP dissociation inhibitor, kinesin and isocitrate dehydrogenase and additionally interacts with the large chain of ribonucleoside-diphosphate reductase, which generates deoxyribonucleotides for DNA synthesis (Elledge, Zhou and Allen, 1992). The identification of key processes associated with UBC2 and UEV1 interacting partners was facilitated by gene ontology (GO) enrichment in TriTrypDB. UBC2 and UEV1 also both interact with a hypothetical protein, LmxM.26.2490, and UBC2 interacts with serine hydroxymethyltransferase, LmxM.30.2560, LSD1-like protein, Gim5A and endoribonuclease L-PSP. Of these, the ubiquitin system proteins, LmxM.30.2560, LSD1-like protein, and udp-glc 4'epimerase were most enriched in the UBC2 versus the MPK3 immunoprecipitations. Of these, UEV1, all 3 RING E3 ligases, ubiquitin and the LSD1-like protein had high peptide counts, suggesting they are high confidence interacting partners of UBC2.

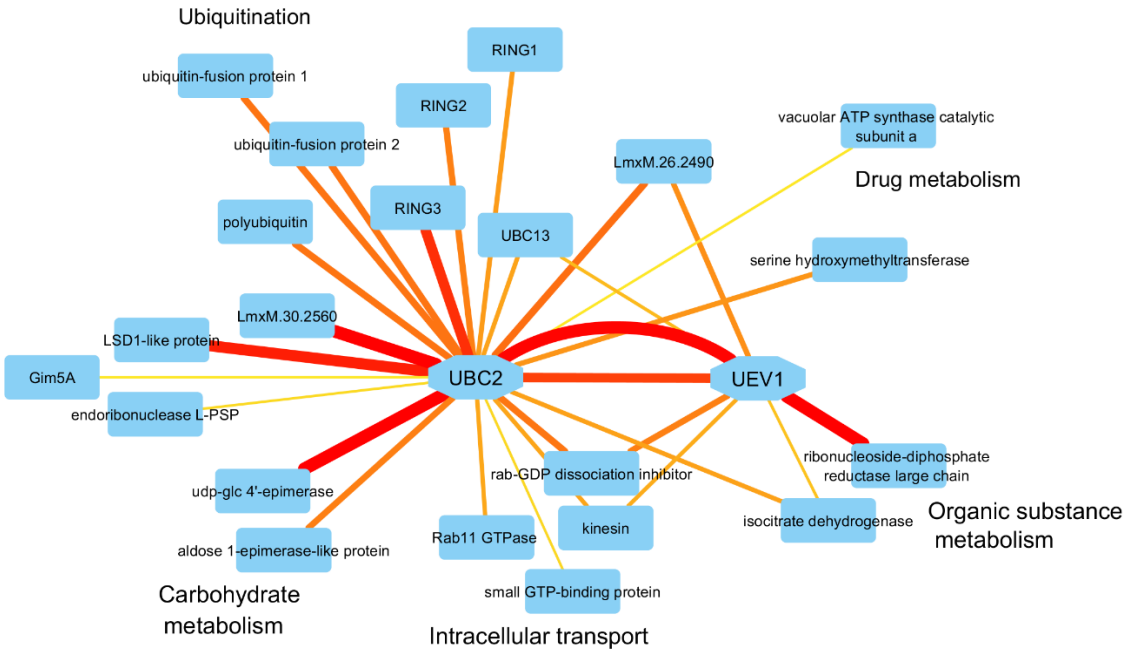

Figure 32. *UBC2 and UEV1 interactomes in L. mexicana promastigotes.* Putative interacting partners of UBC2 and UEV1 as determined by protein-level SAINTq analysis (data in Table 5 and Table 7). Thickness and colours of edges are proportional to the log2 fold change between the protein abundances in UBC2 or UEV1 versus MPK3 immunoprecipitation samples, where yellow represents ≤2 and red, ≥10. Key cellular processes (identified using GO term analysis and literature searching) with which proteins or putative proteins are associated are indicated next to the relevant nodes.

5.2.5 UBC2 and UEV1 interactomes in amastigotes

To identify the interacting partners of UBC2 and UEV1 in amastigotes, a similar cross-linking affinity purification proteomics approach was used. Stationary phase promastigote cells were transferred into amastigote medium and harvested following 120 h of growth at 33°C with 5% CO_2. A key difference in the protocol for amastigote versus promastigote sample processing was the addition of extra protease inhibitors to counteract the higher peptidase activity found in amastigote cells (Besteiro *et al.*, 2007). The protein gel in Figure 33 shows the relative amounts of myc-tagged protein present in the total and unbound fractions during the immunoprecipitation of amastigote lysates. The depletion of myc-tagged material in the unbound fraction is most apparent for the myc-MPK3 samples. However, there was still a sufficient amount of protein present in the eluted fractions for subsequent processing and mass spectrometry analysis.

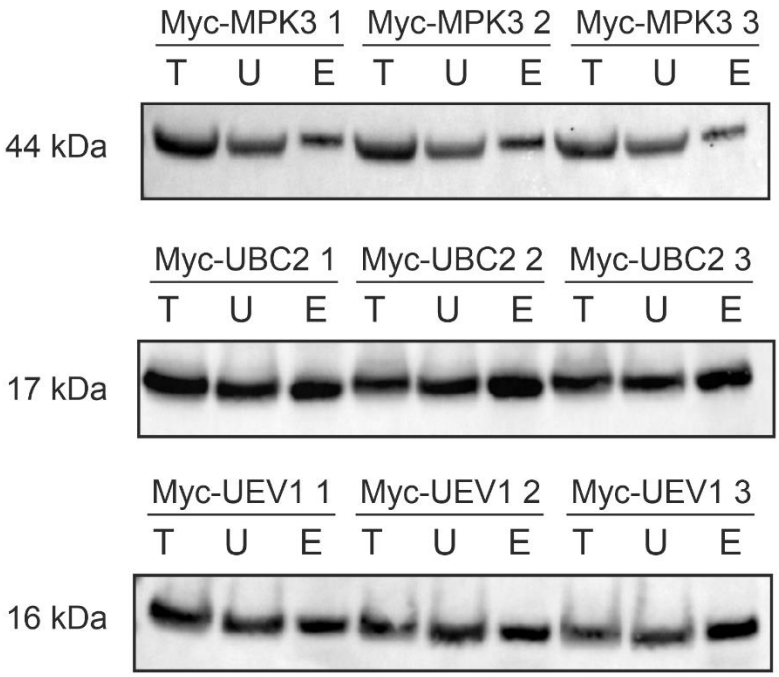

Figure 33. *Immunoprecipitation of myc-tagged proteins in amastigotes.* Anti-myc Western blot of the total (T), unbound (U) and eluted (E) fractions. Equivalent amounts of the total and unbound fractions were run for each sample. One twentieth of the eluted material was run alongside. Samples were prepared in triplicate (1, 2 and 3) for each myc-tagged protein. Molecular weights of the proteins of interest are shown on the left hand side.

As for the promastigote data, both pairwise ANOVA tests (performed in PEAKS Studio) and protein-level SAINTq analysis were performed on the amastigote data but a P-value cut-off of 0.01 was used for the PEAKS Studio analysis. Using the PEAKS Studio and SAINTq analysis methods (Table 8 and Table 9 respectively), 10 and 24 proteins were identified as significantly enriched in the myc-UBC2 samples respectively. However, in contrast to the high level of crossover observed for analyses of the promastigote data, only 4 proteins were identified in both amastigote data analyses (Figure 34). Of these, one was the bait protein (UBC2) and the others were UEV1, RING3 and a vacuolar ATPase subunit-like protein. Of the proteins identified in only one analysis, multiple were associated with the vacuolar ATPase (LmxM.33.3670 and LmxM.28.2430 in the PEAKS Studio analysis and LmxM.31.0920 in the SAINTq analysis). Both forms of analysis identified components of the proteasome (LmxM.19.1120 and LmxM.21.1700 and LmxM.31.1200 in the PEAKS Studio and LmxM.31.0920 in the SAINTq analyses respectively). Also identified in the SAINTq analysis and with high peptide counts were a nonspecific nucleoside hydrolase, an oxidoreductase and lanosterol 14-alpha-demethylase. Between the SAINTq-analysed promastigote and amastigote interactome

datasets for UBC2, only 3 proteins were shared (Figure 35). These were the UBC2 bait, UEV1 and RING3.

Accession	-10logP	Fold change UBC2/MPK3	Description
LmxM.24.0080*	51.28	1000.0	RING-type E3 ligase 3
LmxM.16.1370	42.49	1000.0	hypothetical protein
LmxM.05.1140*	28.76	3.3	vacuolar ATPase subunit-like protein
LmxM.04.0680*	27.76	13.5	UBC2
LmxM.19.1120	26.05	8.0	proteasome regulatory non-ATP-ase subunit
LmxM.33.3670	24.19	1.7	vacuolar ATP synthase catalytic subunit a
LmxM.21.1700	23.11	2.6	proteasome alpha 2 subunit
LmxM.28.2430	22.74	2.0	vacuolar ATP synthase subunit b
LmxM.13.1580*	21.74	35.5	UEV1
LmxM.27.1895	20.05	1.4	hypothetical protein

Table 8. *Proteins enriched in UBC2 versus MPK3 amastigote immunoprecipitations, as analysed in PEAKS Studio.* A P-value of 0.01 was used as the cut-off. P-values were obtained from an ANOVA of peptide-level data. An asterisk indicates proteins that were found in both the PEAKS Studio and SAINTq analyses for this dataset.

Accession	BFDR	Peptide Count	Description
LmxM.04.0680*	0	27	UBC2
LmxM.13.1580*	0	19	UEV1
LmxM.24.0080*	0	3	RING-type E3 ligase 3
LmxM.25.0220	0	2	hypothetical protein
LmxM.29.2720	0	2	GRAM domain containing protein
LmxM.30.2150	0	2	prostaglandin f2-alpha synthase
LmxM.31.0920	0	2	vacuolar proton-ATPase-like protein
LmxM.33.1415	0	4	d-isomer specific 2-hydroxyacid dehydrogenase-like protein
LmxM.18.1580	0.0001	24	nonspecific nucleoside hydrolase
LmxM.36.4170	0.0001	8	oxidoreductase
LmxM.34.0620	0.0013	3	hypothetical protein
LmxM.30.0480b	0.0049	2	hypothetical protein

LmxM.13.0220	0.0084	3	small Rab GTP binding protein
LmxM.05.1140*	0.012	10	vacuolar ATPase subunit-like protein
LmxM.11.1100	0.0157	22	lanosterol 14-alpha-demethylase
LmxM.34.1110	0.0201	2	Rdx family
LmxM.26.0240	0.0245	2	eukaryotic translation initiation factor 4E
LmxM.36.2820	0.0288	2	hypothetical protein
LmxM.30.1400	0.0327	2	hypothetical protein
LmxM.31.1200	0.0379	3	proteasome regulatory non-ATP-ase subunit
LmxM.34.4820	0.0435	3	histidine phosphatase superfamily
LmxM.19.0150	0.0491	3	protein kinase

Table 9. *Proteins enriched in UBC2 versus MPK3 amastigote immunoprecipitations, as analysed by protein-level analysis in SAINTq.* A 5% false discovery rate was used as the cut-off. BFDR, Bayesian false discovery rate. An asterisk indicates proteins that were found in both the PEAKS Studio and SAINTq analyses for this dataset.

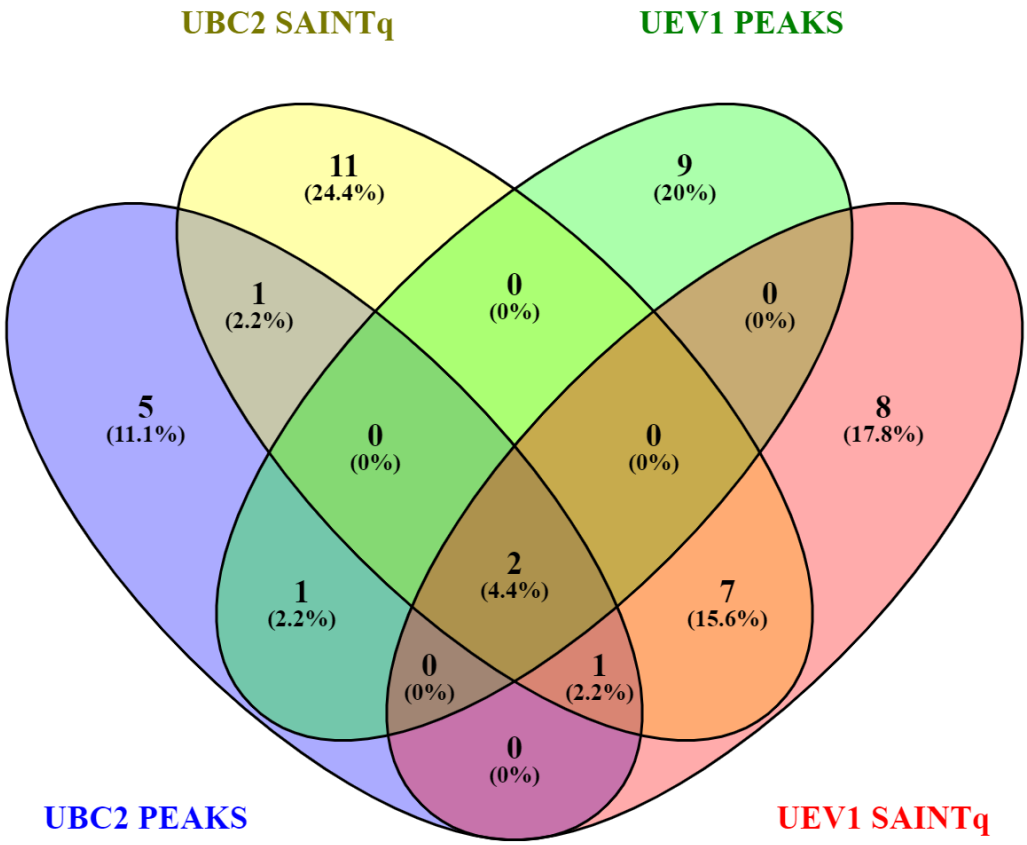

Figure 34. *Overlap between amastigote datasets.* Venn diagram illustrating the overlap between interacting partners identified for UBC2 and UEV1 in the amastigote stage using PEAKS Studio and SAINTq analysis methods.

For the myc-UEV1 samples, 12 and 18 proteins were identified as significantly enriched by PEAKS Studio and SAINTq respectively (Table 10 and Table 11 respectively), with only 2 proteins identified in both analyses (Figure 34). These were the bait (UEV1) and UBC2. Like for UBC2, vacuolar ATPase-related proteins were detected by both analyses (LmxM.28.2430 in the PEAKS Studio and LmxM.31.0920 in the SAINTq analyses). Many of the other proteins identified in the PEAKS Studio analysis were associated with carbohydrate metabolism (hexokinase and phosphoglycerate kinase) or other metabolic processes (NADH-cytochrome b5 reductase, protein tyrosine phosphatase-like protein, alkyl dihydroxyacetonephosphate synthase and ATP-dependent zinc metallopeptidase).

Other proteins identified included thiol-dependent reductase 1 and spindle pole body protein 1. For the SAINTq analysis, additional proteins with high peptide counts included an oxidoreductase (also a UBC2 interactor), a protein kinase and a hypothetical protein (LmxM.26.0730). Between the SAINTq-analysed promastigote and amastigote interactome datasets for UEV1, only 2 proteins were shared (Figure 35). These were the UEV1 bait and UBC2. Only 2 proteins were found in the PEAKS Studio and SAINTq analyses of both UBC2 and UEV1: UBC2 and UEV1. This suggests that UBC2 and UEV1 interact in amastigote cells but may also have independent roles.

Accession	**-10logP**	**Fold change UEV1/MPK3**	**Description**
LmxM.21.0250	32.11	2.4	hexokinase
LmxM.28.2430	27.23	1.5	vacuolar ATP synthase subunit b
LmxM.16.0230	25.65	1.1	protein tyrosine phosphatase-like
LmxM.29.0120	25.16	2.4	alkyl dihydroxyacetonephosphate synthase
LmxM.13.1580*	24.69	37.3	UEV1
LmxM.28.1570	24.04	2.5	hydrolase
LmxM.32.0240	23.17	1.6	thiol-dependent reductase 1
LmxM.29.3380	22.69	4.1	phosphoglycerate kinase
LmxM.31.1500	21.55	1.9	ATP-dependent zinc metallopeptidase
LmxM.13.1060	20.65	2.0	NADH-cytochrome b5 reductase
LmxM.36.3780	20.35	1.5	spindle pole body protein 1
LmxM.04.0680*	19.79	3.8	UBC2

Table 10. *Proteins enriched in UEV1 versus MPK3 amastigote immunoprecipitations, as analysed in PEAKS Studio.* A P-value of 0.01 was used as the cut-off. P-values were obtained from an ANOVA of peptide-level data. An asterisk indicates proteins that were found in both the PEAKS Studio and SAINTq analyses for this dataset.

Accession	**BFDR**	**Peptide Count**	**Description**
LmxM.13.1580*	0	19	UEV1
LmxM.25.0220	0	2	hypothetical protein

LmxM.26.0730	0	5	hypothetical protein
LmxM.29.2720	0	2	GRAM domain containing protein
LmxM.30.0480b	0	2	hypothetical protein
LmxM.17.0725	0.0001	4	guanosine monophosphate reductase
LmxM.36.2820	0.0002	2	hypothetical protein
LmxM.11.0040	0.0003	3	ABC transporter
LmxM.34.1110	0.0036	2	Rdx family
LmxM.36.4170	0.0067	8	oxidoreductase
LmxM.31.0920	0.0099	2	vacuolar proton-ATPase-like protein
LmxM.09.1020	0.0134	3	CDC50/LEM3 family
LmxM.21.1560	0.0193	2	hypothetical protein
LmxM.24.0080	0.0267	3	RING-type E3 ligase 3
LmxM.33.0030	0.0332	11	protein kinase
LmxM.30.0180	0.0393	2	hypothetical protein
LmxM.04.0680*	0.0448	27	UBC2
LmxM.32.0830	0.0498	4	2 4-dienoyl-coa reductase fadh1

Table 11. *Proteins enriched in UEV1 versus MPK3 amastigote immunoprecipitations, as analysed by protein-level analysis in SAINTq.* A 5% false discovery rate was used as the cut-off. BFDR, Bayesian false discovery rate. An asterisk indicates proteins that were found in both the PEAKS Studio and SAINTq analyses for this dataset.

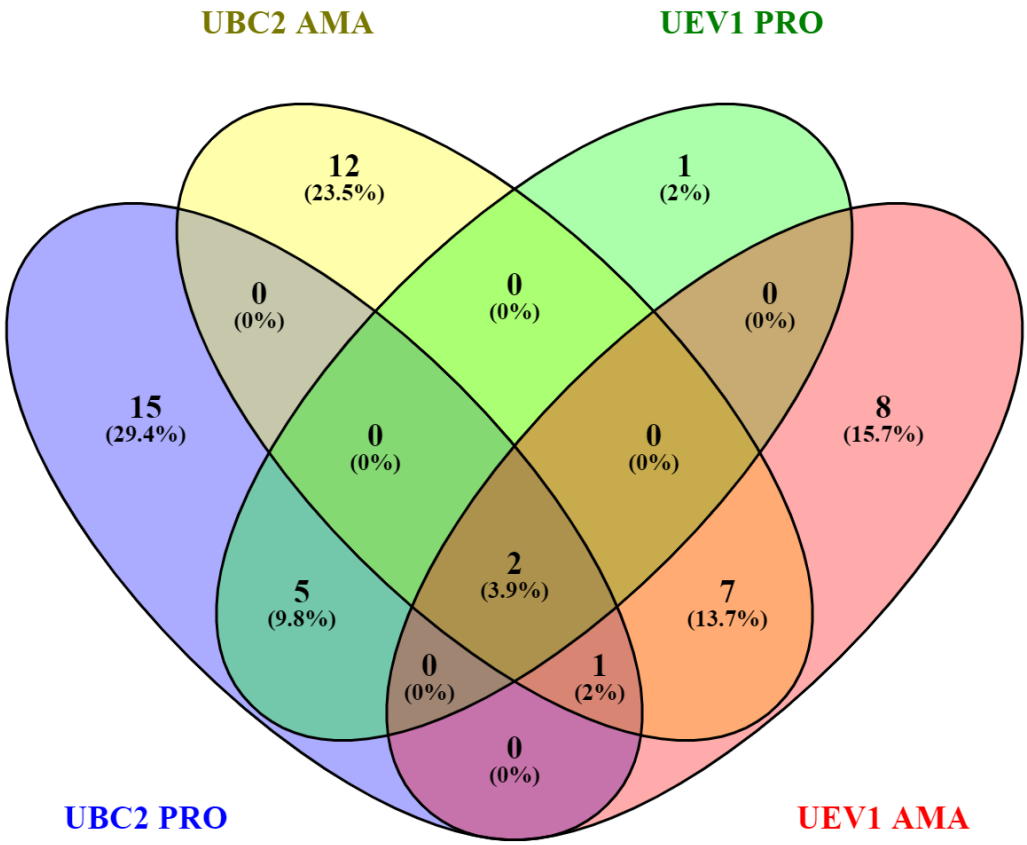

Figure 35. *Overlap between promastigote and amastigote datasets.* Venn diagram illustrating the overlap between interacting partners identified for UBC2 and UEV1 in promastigotes and amastigotes using the SAINTq analysis method.

5.3 Discussion

The finding that myc-mNeonGreen-, TurboID- and miniTurbo- tagged UBC2 and UEV1 cell lines are mostly unable to differentiate from promastigotes to amastigotes demonstrates that the N-terminal tagging of UBC2 or UEV1 with large protein tags is problematic. This discovery will be relevant for the future study of these proteins, in which C-terminal or small N-terminal (such as the 3 x myc) tags should be favoured. C-terminal mNeonGreen-tagged UBC2 and UEV1 showed cytoplasmic localisations which were confirmed by the cytoplasmic localisations of N-terminal mNeonGreen-tagged UBC2 and

UEV1, despite the evidence of the latter proteins having disrupted function. These results provide strong evidence for the cytoplasmic localisation of UBC2 and UEV1 which are further supported by the expectation that, given the ability of UBC2 and UEV1 to form a heterodimeric complex, these proteins would localise to the same cellular compartment(s).

The demonstration that myc-UBC2, myc-UEV1 and myc-MPK3 cell lines were viable and express HASPB 120 h into promastigote to amastigote differentiation showed that they were suitable for investigating the interacting partners of UBC2 and UEV1 in both promastigotes and amastigotes. For this purpose, UBC2 and UEV1 interacting partners were identified using cross-linking affinity purification proteomics. Several limitations to affinity purification proteomics strategies exist and must be considered when interpreting the related data. Firstly, the addition of a tag to the bait protein could disrupt the binding of interacting partners, depending on the location, size and structure of the tag. In the case of UBC2, for example, the N-terminal tag is positioned near E1 and E3 binding surfaces, making it possible that the tag could interfere with E1 and/or E3 binding (Stewart *et al.*, 2016). In selecting a small 3 x myc tag, connected to the protein of interest by a flexible linker, it was hoped that any disruption of protein-protein interactions would be minimal. However, disruption of E1 binding by the myc tag could account for the fact that no E1 enzymes were identified in any of the affinity purification proteomics experiments. Alternatively, it may be that E1-UBC2 interactions are too weak and/or transient to be detected using this method. Since the tagging approach used results in the expression of the gene of interest being controlled by non-endogenous regulatory elements, the level of protein expression may also differ from that in unedited cells. This has the potential to influence the function of the protein, including its protein-protein interactions. However, since the main aim of these experiments was to provide information on potential interacting partners that could be further validated by co-immunoprecipitation, this was not considered to be problematic.

Despite the limitations of the affinity purification proteomics strategy, multiple proteins were identified as enriched in the myc-UBC2 and myc-UEV1 samples relative to the myc-MPK3 sample by analyses in PEAKS Studio and SAINTq. However, since these analyses rely on comparisons with the myc-MPK3 samples, it is possible that, if MPK3 and UBC2 and/or UEV1 share some of the same interacting partners, some UBC2 and/or UEV1 interactors may not have been identified. In both life cycle stages and in both myc-UBC2 and myc-UEV1 samples, UBC2 and UEV1 were found to interact with one another, supporting the finding that these proteins form a stable heterodimeric complex

in vitro. Given the ability of UBC2 to form a thioester bond with and transfer ubiquitin *in vitro*, it was not surprising to see ubiquitin in the list of UBC2 interactors. More interestingly, the identification of UBC13 (which may be essential in promastigotes) suggests that UBC2 and UBC13 may have distinct but complementary E2 activities, similar to those exhibited by human UBE2W and UBE2N-UBE2V1 (Soss *et al.*, 2011; Zhang *et al.*, 2005; Ye and Rape, 2009). RING1, RING2 and RING3, also UBC2 interactors, may be responsible for the transfer of ubiquitin from UBC2 (with or without UEV1) to substrates or may themselves be ubiquitinated by UBC2. Notably, none of the UBC2-interacting E3s matched the top hits in the protein BLAST searches for *L. mexicana* orthologues of human BIRC2, RNF8 and CHIP described in chapter 2.

Some (or all) of the UBC2 interactors identified in promastigotes may be UBC2 or UBC2-UEV1 substrates. These include aldose 1-epimerase-like protein, udp-glc 4'epimerase and isocitrate dehydrogenase, which point to roles for UBC2 in the regulation of cellular respiration; aldose 1-epimerase is responsible for the conversion of aldoses (such as glucose) between their α- and β-forms, udp-glc 4'epimerase catalyses the reversible conversion of UDP-galactose to UDP-glucose and isocitrate dehydrogenase plays a role in the citric acid cycle (Poolman *et al.*, 1990; Frey, 1996). Such regulation could be achieved through ubiquitin modifications influencing the catalytic activity, localisation or degradation of target proteins, for example by contributing to the formation of branched K48/K63 ubiquitin chains (Ohtake *et al.*, 2018). UBC2 may also regulate gene expression, as hinted at by its interaction with an LSD1-like protein in promastigotes. In humans, LSD1 is primarily responsible for the demethylation of mono- and dimethyl histone 3 lysine 4 (H3K4) and, interestingly, its aberrant activity has been linked with increased glycolytic activity in cancer cells (Sakamoto *et al.*, 2015). Consequently, facilitating ubiquitination of the LSD1-like protein may be an additional way in which UBC2 regulates cellular respiration. The identification of a large number of proteins linked to intracellular transport (in the SAINTq analysis) suggests that UBC2 may regulate these processes. Indeed, the *S. cerevisiae* and *C. elegans* homologues of UBC2 have recently been shown to regulate membrane protein sorting (Renz *et al.*, 2020; Zhang *et al.*, 2018). Additionally, the interaction of UBC2 with the vacuolar ATP synthase, components of which were identified in a screen for *T. brucei* isometamidium resistance, suggests a role for UBC2 in trypanosomal drug resistance (Baker *et al.*, 2015). Since K63 ubiquitin modifications provide signals for plasma membrane protein internalisation and other intracellular trafficking steps, the ubiquitination of the vacuolar ATPase by UBC2 could be proposed to influence its trafficking (Erpapazoglou, Walker and Haguenauer-Tsapis, 2014). In *T. brucei*, the Gim5A protein (also found to interact

with UBC2) is a glycosomal membrane protein essential for the survival of bloodstream-form trypanosomes (Maier *et al.*, 2001). Whether UBC2 is involved in the trafficking of Gim5A to the glycosomal membrane is an additional area for future investigation. Two hypothetical proteins, LmxM.26.2490 and LmxM.30.2560, are also strongly enriched in the myc-UBC2 samples. To uncover the function of these proteins, detailed phenotypic studies could be carried out on LmxM.26.2490 and LmxM.30.2560 null mutant cells (provided that these genes are not essential).

The fact that UEV1 shares interactions with LmxM.26.2490, UBC13, rab-GDP dissociation inhibitor, kinesin and isocitrate dehydrogenase in promastigotes makes it highly likely that these are true UBC2-UEV1 interactors, while also suggesting that UEV1 cooperates with UBC2 in regulating cellular respiration and intracellular transport. In the future, it would be interesting to test whether UBC13 has ubiquitin chain initiation functions that complement the chain building activity of UBC2-UEV1. However, to achieve this, a substrate (and possibly the E3 partners) of both proteins would first need to be identified to allow for testing in *in vitro* ubiquitination assays. That more interacting partners, including RING E3 ligases, were identified for UBC2 than UEV1 raises the question of whether UBC2 modifies substrates in the absence of UEV1 in cells. This possibility is particularly intriguing given the ability of UBC2 to cooperate with human E3s to form non-K63-linked ubiquitin chains in the absence of UEV1 *in vitro*. Alternatively, this difference could be due to the strength and/or and positioning of interacting partner binding on the UBC2-UEV1 complex.

Unlike for the promastigote interactome data, there was little crossover between the PEAKS Studio and SAINTq analyses of the amastigote interactome data. When combined with the finding that the only UBC2 and UEV1 interactors shared between both analyses and the promastigote and amastigote datasets were UEV1 and RING3 and UEV1 respectively, it should be concluded that this dataset is not very reliable. Despite this, some insight can be gleaned from the data. For example, proteasome components were identified as UBC2 interacting partners in both analyses, suggesting that UBC2 ubiquitinates proteins brought to the proteasome for degradation. Furthermore, the identification of RING3 as a UBC2 interactor in both promastigotes and amastigotes suggests it may be a specific E3 partner of UBC2 in multiple *Leishmania* life cycle stages. This is supported by the identification of RING3 as a UEV1 interacting partner in the amastigote SAINTq analysis.

In addition to the ubiquitin system interactors, four proteins associated with the vacuolar ATPase were identified as UBC2 interactors in either the PEAKS Studio or SAINTq amastigote analyses. This supports the previous finding that a vacuolar ATPase subunit is a UBC2 interactor in promastigotes and is further supported by the identification of vacuolar ATPase components as UEV1 interactors in amastigotes. The oxidoreductase identified in both the UBC2 and UEV1 samples in amastigotes may be a true interacting partner and potential UEV1 interactors were identified that have roles in carbohydrate metabolism, contributing to the hypothesis that UBC2-UEV1 plays a role in regulating cellular respiration. The identification of a protein kinase as a potential UEV1 interactor is also of interest, since it suggests an interplay between phosphorylation and ubiquitin modifications in this pathway. Ideally, the amastigote interactome experiment should be repeated, this time with 4 or more replicates per cell line, in order to compensate for the higher variability between samples which may have led to problems in the PEAKS Studio and SAINTq analyses. This should allow for the more confident identification of UBC2 and UEV1 interacting proteins in amastigotes.

To determine which UBC2 and UEV1 interacting partners are substrates of ubiquitination carried out by UBC2 or UBC2-UEV1, the ubiquitination status of identified interacting partners could be investigated in Δ*ubc2*, Δ*uev1* and Cas9 T7 (control) cells by immunoprecipitating myc-tagged putative substrates and quantifying the level of protein ubiquitination by anti-ubiquitin Western blot. Clearly, this would only be possible in promastigotes due to the inability of Δ*ubc2* and Δ*uev1* cell lines to differentiate into amastigotes. An alternative approach that could be used for testing interacting partners from either the promastigote or amastigote stages is the use of *in vitro* ubiquitination assays. However, for this to be as physiologically relevant as possible, the E3 ligase responsible for the transfer of ubiquitin from UBC2 to the substrate protein would also need to be included. For this reason, the next step in the study of UBC2-UEV1 function in *Leishmania* should be the investigation of E3 partners.

To distinguish between E3s that carry out ubiquitination in cooperation with UBC2 versus E3s that are substrates of UBC2, a number of experiments can be carried out. Firstly, the interactions between UBC2 and/or UEV1 with RING1, RING2 and RING3 should be validated by co-immunoprecipitation, to confirm that these are true UBC2- and/or UEV1-interacting partners and do not represent false-positive identifications. Second, attempts to express and purify these proteins should be made, starting in *E. coli*. If these are successful, then the E3s can then be tested in *in vitro* ubiquitination assays, similar to those described in the previous chapter, to determine whether the E3s form ubiquitin

chains in the presence of UBA1a, UBC2, UEV1, ubiquitin and ATP. Whether UEV1 is required for the formation of such ubiquitin chains, and whether the chains formed are K63-linked, should also be investigated. Once the E3 partners of UBC2 and UEV1 have been identified, it would be interesting to test whether these are also essential in amastigotes (and therefore may be responsible for the essentiality of UBC2 and UEV1 in promastigote to amastigote differentiation) and whether the identification of their localisation by endogenous tagging with mNeonGreen can reveal anything about their functions. Overall, this chapter provides a good starting point for further investigations into the function of UBC2 and UEV1 in *Leishmania*, such as the identification of E3 partners and putative substrates.

6 General discussion

The generation of a null mutant library, combined with bar-seq analysis of the E1, E2 and HECT/RBR E3 null mutants allowed the identification of 5 genes that may be essential in promastigotes, 4 that are required for successful promastigote-amastigote differentiation and an additional 5 that are required for normal proliferation during mouse infection. These findings underscore the relative ease (compared to the profiling of individual null mutant lines) with which bar-seq analysis of CRISPR-Cas9-generated null mutant libraries can be applied to reliably phenotype a large number of mutants. This strategy is of particular relevance to the study of *Leishmania* since, until recently, only a small proportion of *Leishmania* genes (around 200) had been subjected to genetic target validation (Jones *et al.*, 2018). Correspondingly, bar-seq methods are already gaining traction in the field, with similar experiments having been used to dissect flagellar function and the roles of DUBs and protein kinases in the life cycle of *L. mexicana* (Beneke *et al.*, 2019; Damianou *et al.*, 2020; Baker *et al.*, 2020). Provided that an appropriate assay is available to detect the phenotype of interest and the caveats of bar-seq (such as difficulties in detecting gain-of-fitness phenotypes) are carefully considered, bar-seq techniques offer huge promise for the large scale analysis of *Leishmania* gene essentiality and function.

Given the crucial role that the ubiquitin system plays in protein degradation, the requirement for multiple ubiquitination and deubiquitination genes in the life cycle of *L. mexicana* could be generally explained by the need to balance ubiquitination and deubiquitination activities inside cells (Damianou *et al.*, 2020). In the promastigote and amastigote stages, the maintenance of key proteins at the required level of abundance may be crucial for maintaining internal promastigote- and amastigote-specific processes respectively. Additionally, the changes in gene expression required for promastigote-amastigote differentiation could be achieved by increases or decreases in ubiquitin-dependent protein degradation and may be facilitated by enzymes such as HECT2, which is essential for this transition. To identify some of the critical proteins that are ubiquitinated during promastigote-amastigote differentiation, diGly affinity purification proteomics could be used to compare the ubiquitinome in Cas9 T7 versus HECT2 overexpressing cell lines in samples collected midway through the differentiation process (Iconomou and Saunders, 2016). Alternatively, tandem-repeated ubiquitin-binding entities (TUBEs) specific for K48-linked ubiquitin, rather than diGly antibodies, could be used for the affinity purification. These offer multiple advantages: a high affinity to ubiquitin and the ability to distinguish between K48-linked ubiquitin (associated with

proteasomal degradation) and other types of ubiquitin linkage (Hjerpe *et al.*, 2009). However, TUBEs are also known to protect ubiquitinated proteins from both proteasomal degradation and DUB activity, which could make it difficult to identify the differences between samples from different genetic backgrounds. Since the ubiquitin chain specificity of HECT2 is also unknown at this stage, the author would recommend taking a diGly affinity purification approach.

Due to time constraints, only E1, E2 and HECT/RBR E3 genes were targeted for null mutant generation and subsequent analysis by bar-seq. To gain a more complete picture of the role of ubiquitination in the life cycle of *Leishmania*, it would be useful to carry out a similar analysis of the putative RING-type, RING-CH-type and U-box E3 ligases that were identified by bioinformatics analysis. In parallel, RING and U-box E3 proteins could be tagged with mNeonGreen to observe their intracellular localisation, potentially providing clues as to their cellular function. Ideally, imaging would be performed on both N- and C-terminally tagged cell lines to provide a high level of confidence in the observed protein localisations. Such studies are likely to be more informative than the localisation imaging of E1 and E2 enzymes described in chapter 2 since, relative to E1 and E2 enzymes, RING E3s may have more restricted localisations reflecting their more specific functions. To facilitate detailed follow-up studies of selected RING E3s, photocrosslinking activity-based probes, which have been shown to report on the activity of the human RING E3s RNF4 and c-Cbl, could be tested in *Leishmania* cell lysates (Mathur *et al.*, 2020). However, in order for the protein of interest to be reliably identified, E3-specific antibodies or epitope-tagged E3s would be required. The finding that *Leishmania* UBA1a can transfer ubiquitin to human UBE2W and that *Leishmania* UBC2 can cooperate with human E3s also has relevance for the future study of *Leishmania* E3 ligases. This is because it suggests that, even in the absence of identified *Leishmania* E1 and E2 partners, *in vitro* E3 activity assays could be set up using human E1 and E2 enzymes, allowing detailed biochemical analysis, such as structure-function studies, to be carried out.

The study of *Leishmania* RING E3 ligases is also relevant to the development of PROTACs for use in trypanosomatids. PROTACs, which trigger the selective degradation of target proteins, are useful tools because they enable the rapid removal of all target protein functions, not just those related to enzymatic activity, and often show greater selectivity compared to traditional inhibitors (Sun *et al.*, 2019). By identifying and performing structural studies on *Leishmania* E3s that add degradative (for example K48-linked) ubiquitin modifications to proteins, small molecule ligands could be designed that

specifically target these E3s. PROTACs can then be produced by connecting the E3 ligand to a target protein ligand via a linker. Provided that cell permeable trypanosomatid PROTACs can be developed, they would be an extremely useful research tool and may even hold therapeutic potential. In particular, PROTAC-induced degradation of target proteins could aid the study of essential proteins in *Leishmania* cells. This would be especially useful in studies of the amastigote stage, since current inducible gene deletion techniques (DiCre) cannot be effectively utilised in amastigotes (Duncan *et al.*, 2016). With PROTACs currently in clinical trials for the treatment of multiple cancers and both academic and industrial labs becoming increasingly invested in the field of targeted protein degradation, it will be interesting to see what benefits they can bring to the study of trypanosomatids (Mullard, 2019; Sun *et al.*, 2019).

Although the discovery of essential roles for UBC2 and UEV1 may not be surprising given the high levels of structural and functional (at the biochemical level) conservation that they exhibit, the fact that they are essential in amastigotes but not promastigotes suggests that they may play a role in biology unique to the parasite. Notably, the finding that potential UBC2/UBC2-UEV1 substrates include proteins linked to cellular respiration fits well with the fact that genes related to glycolysis and the citric acid cycle are upregulated in promastigotes versus amastigotes (Fiebig, Kelly and Gluenz, 2015). This is because it suggests that UBC2/UBC2-UEV1 downregulates the activity of glycolytic and citric acid cycle enzymes during promastigote-amastigote differentiation. This could occur, for example, through the addition of ubiquitin modifications that alter enzymatic activity and/or act as degradative signals. Although UBC2-UEV1 forms K63-linked ubiquitin chains *in vitro*, the finding that UBC2 can cooperate with human E3s to form non-K63-linked ubiquitin chains shows that UBC2 activity could be associated with the formation of multiple ubiquitin chain types on substrates, and therefore both non-degradative and degradative roles. Other potential substrates of UBC2/UBC2-UEV1 include proteins associated with intracellular transport, complementing the fact that genes related to amastins, vesicular transport and lysosomal activity are upregulated in amastigotes versus promastigotes. This is because it suggests a role for UBC2 and UEV1 in regulating the changes in the surface proteome that occur during the differentiation process (Saxena *et al.*, 2007; Fiebig, Kelly and Gluenz, 2015; Inbar *et al.*, 2017; Ruy *et al.*, 2019). This could be tested by comparing the surface expression of stage-specific membrane proteins (for example using flow cytometry) following promastigote-amastigote differentiation in the presence or absence of a sublethal dose of NSC697923. Furthermore, the association between UBC2 and UEV1 and vacuolar ATPase proteins suggests that UBC2-UEV1 is involved in the cellular response to pH

changes in the external environment (Forgac, 2007). During promastigote-amastigote differentiation, *Leishmania* must adapt to a more acidic environment (De Pablos, Ferreira and Walrad, 2016); this could be achieved in part through the regulation of vacuolar ATPase trafficking.

Since UBC2-UEV1 appears intractable as a drug target, investigations into essential E3 partners or substrates of UBC2-UEV1 could provide a future source of potential drug targets for validation. RINGs 1-3 and the UBC2/UEV1 interacting partners involved in cellular respiration and intracellular transport provide a good starting point for drug target identification. Additionally, uncovering what types of ubiquitin linkage are formed by UBC2 in combination with *Leishmania* E3s will be important both for understanding the functions of these modifications and identifying E3 ligases that produce degradative modifications. Such E3s would be useful for the development of PROTACs in *Leishmania*. From this point of view, RING2 may be the most interesting to investigate, since RING1 and RING3 were identified as potential interacting partners of both UBC2 and UEV1 whereas RING2 was only identified as a UBC2 interactor. This suggests that RING2 could act together with UBC2 in the absence of UEV1 and may produce non-K63-linked ubiquitin modifications. However, these findings do not exclude the possibility that RING1 and RING3 are able to produce non-K63-linked ubiquitin modifications when partnered with UBC2 alone.

Through carrying out the work described in this thesis, a broad overview of *Leishmania* E1, E2 and E3 enzymes has been obtained. Not only have the E1, E2 and E3 genes of *L. mexicana* been bioinformatically identified but multiple endogenously-tagged and null mutant cell lines have been generated, providing a valuable resource for the further study of *Leishmania* ubiquitination enzymes. Additionally, the gene essentiality data presented here should enable researchers to identify candidate drug targets for follow-up studies. A role for UBC2 and UEV1 in regulating promastigote-amastigote differentiation has also been established, highlighting the importance of ubiquitination in *Leishmania* cell biology.

In terms of methodology, this work also offers considerable value. The bar-seq strategy, for example, could be utilised to profile additional null mutant libraries, leading to a more complete view of gene essentiality in the *L. mexicana* life cycle. Furthermore, despite previous reports that E2:E3 interactions are difficult to identify using affinity proteomics methods (Metzger *et al.*, 2014), the affinity purification proteomics approach described here was able to identify putative E3 interacting partners of UBC2. Therefore, this method could be used in future to identify the E3 partners of other *Leishmania* E2s.

Despite the crucial role that ubiquitination and deubiquitination enzymes play in *Leishmania* differentiation and the potential for targeting these enzymes in the development of new anti-leishmanial therapies, the *Leishmania* ubiquitination system is critically understudied. In providing a comprehensive summary of ubiquitination genes in *L. mexicana* and insights into the biochemical analysis of *Leishmania* E1, E2 and E3s, this work offers an excellent starting point for the future study of these enzymes. By utilising a wide array of advanced tools originally developed for the study of the human and *S. cerevisiae* ubiquitin systems, including diGly antibodies, TUBEs and PROTACs, a more complete view of the system will be gained, facilitating the identification of features and roles unique to *Leishmania* biology while also generating new opportunities for the treatment of leishmaniasis.

Abbreviations

aa	amino acids
ABP	activity-based probe
APC/C	anaphase promoting complex/cyclosome
Apo-L1	apolipoprotein-L1
AQP1	aquaglyceroporin 1
Atg12	autophagy-related protein 12
Atg8	autophagy-related protein 8
ATP	adenosine triphosphate
BirA*	promiscuous biotin ligase
BLAST	basic local alignment search tool
BSF	bloodstream form
Cas9	CRISPR-associated protein 9
CHIP	C-terminus of Hsc70-interacting protein
CL	cutaneous leishmaniasis
CRISPR	clustered regularly interspaced short palindromic repeats
CRL	cullin RING ligase
crRNA	short CRISPR RNA
DALYs	disability adjusted life years
DMF	dimethylformamide
DNA	deoxyribonucleic acid
DNDi	Drugs for Neglected Diseases initiative
dNTP	deoxynucleotide triphosphate
DSP	dithiobis(succinimidyl propionate)
DUB	deubiquitinating enzyme
E1	E1 ubiquitin-activating enzyme
E2	E2 ubiquitin-conjugating enzyme
E3	E3 ubiquitin ligase
ERAD	endoplasmic reticulum-associated degradation
FAT10	HLA-F adjacent transcript 10
FAZ	flagellar attachment zone
FBS	fetal bovine serum
FDA	United States Food and Drug Administration
GO	gene ontology
GOI	gene of interest
GST	glutathione S-transferase

HASPB	hydrophilic acylated surface protein B
HECT	homologous to E6AP C-terminus
IAP	inhibitor of apoptosis
ID	identification
Im9	*E. coli* immunity protein of colicin E9
IPTG	isopropyl β-D-1-thiogalactopyranoside
ISG	invariant surface glycoprotein
ISG15	interferon-stimulated gene 15
JAMM/MPN+	JAB1/MPN/MOV34 metalloenzyme
kb	kilobases
kDa	kilodalton
kDNA	kinetoplast DNA
LB	Luria broth
LC-MS/MS	liquid chromatography with tandem mass spectrometry
MBP	maltose binding protein
MCL	mucocutaneous leishmaniasis
MINDY	motif interacting with Ub-containing novel DUB family
MMS	methyl methanesulfonate
MoeB	molybdopterin biosynthetic enzyme B
mRNA	messenger ribonucleic acid
Nedd8	neural precursor cell expressed developmentally down-regulated 8
NHEJ	non-homologous end joining
nt	nucleotides
NTD	neglected tropical disease
OPB	oligopeptidase B
OTU	ovarian tumour protease
PAM	protospacer adjacent motif
PBS	phosphate buffered saline
PCF	procyclic form
PCNA	proliferating cell nuclear antigen
PCR	polymerase chain reaction
PDB	Protein Data Bank
RBR	ring-between-ring
RCC1	regulator of chromatin condensation 1
RING	really interesting new gene
RIP	receptor interacting protein
RNA	ribonucleic acid

RNAi	ribonucleic acid interference
SCF	Skp, cullin, F-box containing
SCFC	SKP1-CUL1-F-box ubiquitin ligase complex
SDS-PAGE	sodium dodecyl sulphate-polyacrylamide gel electrophoresis
SEC	size-exclusion chromatography
SEC-MALLS	size exclusion chromatography-multi-angle laser light scattering
sgDNA	single guide DNA
sgRNA	single guide RNA
SPRING	secretory protein with a RING finger domain
SUMO	small ubiquitin-like modifier
T7 RNAP	T7 RNA polymerase
TBS	Tris-Buffered Saline
TCA	tricarboxylic acid
TCEP	tris(2-carboxyethyl)phosphine
TEAB	triethylammonium bicarbonate buffer
TFA	trifluoroacetic acid
tracrRNA	trans-activating crRNA
TUBE	tandem ubiquitin binding entity
UBA	ubiquitin-associated
Ubl	ubiquitin-like modifier
UCH	ubiquitin C-terminal hydrolase
UEV	ubiquitin E2 variant
Ufm1	ubiquitin-fold modifier 1
Urm1	ubiquitin-related modifier 1
USP	ubiquitin-specific protease
VL	visceral leishmaniasis
VSG	variant surface glycoprotein
ZUFSP	zinc finger with UFM1-specific peptidase domain protein

References

Abdul Rehman, S. A., Kristariyanto, Y. A., Choi, S. Y., Nkosi, P. J., Weidlich, S., Labib, K., Hofmann, K. and Kulathu, Y. (2016) 'MINDY-1 Is a Member of an Evolutionarily Conserved and Structurally Distinct New Family of Deubiquitinating Enzymes', *Mol Cell,* 63(1), pp. 146-55.

Adli, M. (2018) 'The CRISPR tool kit for genome editing and beyond', *Nat Commun,* 9(1), pp. 1911.

Alcolea, P. J., Alonso, A., Molina, R., Jiménez, M., Myler, P. J. and Larraga, V. (2019) 'Functional genomics in sand fly-derived Leishmania promastigotes', *PLoS Negl Trop Dis,* 13(5), pp. e0007288.

Alsford, S., Eckert, S., Baker, N., Glover, L., Sanchez-Flores, A., Leung, K. F., Turner, D. J., Field, M. C., Berriman, M. and Horn, D. (2012) 'High-throughput decoding of antitrypanosomal drug efficacy and resistance', *Nature,* 482(7384), pp. 232-6.

Alsford, S., Turner, D. J., Obado, S. O., Sanchez-Flores, A., Glover, L., Berriman, M., Hertz-Fowler, C. and Horn, D. (2011) 'High-throughput phenotyping using parallel sequencing of RNA interference targets in the African trypanosome', *Genome Res,* 21(6), pp. 915-24.

Alvar, J., Aparicio, P., Aseffa, A., Den Boer, M., Cañavate, C., Dedet, J. P., Gradoni, L., Ter Horst, R., López-Vélez, R. and Moreno, J. (2008) 'The relationship between leishmaniasis and AIDS: the second 10 years', *Clin Microbiol Rev,* 21(2), pp. 334-59, table of contents.

Alvar, J., Yactayo, S. and Bern, C. (2006) 'Leishmaniasis and poverty', *Trends Parasitol,* 22(12), pp. 552-7.

Alvarez, V. E., Kosec, G., Sant'Anna, C., Turk, V., Cazzulo, J. J. and Turk, B. (2008) 'Autophagy is involved in nutritional stress response and differentiation in Trypanosoma cruzi', *J Biol Chem,* 283(6), pp. 3454-64.

An, H. and Statsyuk, A. V. (2016) 'Facile synthesis of covalent probes to capture enzymatic intermediates during E1 enzyme catalysis', *Chem Commun (Camb),* 52(12), pp. 2477-80.

Andersen, P. L., Zhou, H., Pastushok, L., Moraes, T., McKenna, S., Ziola, B., Ellison, M. J., Dixit, V. M. and Xiao, W. (2005) 'Distinct regulation of Ubc13 functions by the two ubiquitin-conjugating enzyme variants Mms2 and Uev1A', *J Cell Biol,* 170(5), pp. 745-55.

Aravind, L. and Koonin, E. V. (2000) 'The U box is a modified RING finger - a common domain in ubiquitination', *Curr Biol,* 10(4), pp. R132-4.

Atayde, V. D., Aslan, H., Townsend, S., Hassani, K., Kamhawi, S. and Olivier, M. (2015) 'Exosome Secretion by the Parasitic Protozoan Leishmania within the Sand Fly Midgut', *Cell Rep,* 13(5), pp. 957-67.

Azevedo, C. S., Guido, B. C., Pereira, J. L., Nolasco, D. O., Corrêa, R., Magalhães, K. G., Motta, F. N., Santana, J. M., Grellier, P. and Bastos, I. M. (2017) 'Revealing a Novel Otubain-Like Enzyme from Leishmania infantum with Deubiquitinating Activity toward K48-Linked Substrate', *Front Chem,* 5, pp. 13.

Azuma, Y., Tan, S. H., Cavenagh, M. M., Ainsztein, A. M., Saitoh, H. and Dasso, M. (2001) 'Expression and regulation of the mammalian SUMO-1 E1 enzyme', *FASEB J,* 15(10), pp. 1825-7.

Bajaj, R., Ambaru, B. and Gupta, C. M. (2020) 'Deciphering the role of UBA-like domains in intraflagellar distribution and functions of myosin XXI in Leishmania', *PLoS One,* 15(4), pp. e0232116.

Baker, N., Catta-Preta, C. M. C., Neish, R., Sadlova, J., Powell, B., Alves-Ferreira, E. V. C., Geoghegan, V., Carnielli, J. B. T., Newling, K., Hughes, C., Vojtkova, B., Anand, J., Mihut, A., Walrad, P. B., Wilson, L. G., Pitchford, J. W., Volf, P. and Mottram, J. C. (2020) 'Systematic functional analysis of Leishmania protein kinases identifies regulators of differentiation and survival', *bioRxiv*, pp. 2020.09.06.279091.

Baker, N., Hamilton, G., Wilkes, J. M., Hutchinson, S., Barrett, M. P. and Horn, D. (2015) 'Vacuolar ATPase depletion affects mitochondrial ATPase function, kinetoplast dependency, and drug sensitivity in trypanosomes', *Proc Natl Acad Sci U S A,* 112(29), pp. 9112-7.
Ballinger, C. A., Connell, P., Wu, Y., Hu, Z., Thompson, L. J., Yin, L. Y. and Patterson, C. (1999) 'Identification of CHIP, a novel tetratricopeptide repeat-containing protein that interacts with heat shock proteins and negatively regulates chaperone functions', *Mol Cell Biol,* 19(6), pp. 4535-45.
Banerjee, I., Miyake, Y., Nobs, S. P., Schneider, C., Horvath, P., Kopf, M., Matthias, P., Helenius, A. and Yamauchi, Y. (2014) 'Influenza A virus uses the aggresome processing machinery for host cell entry', *Science,* 346(6208), pp. 473-7.
Barak, E., Amin-Spector, S., Gerliak, E., Goyard, S., Holland, N. and Zilberstein, D. (2005) 'Differentiation of Leishmania donovani in host-free system: analysis of signal perception and response', *Mol Biochem Parasitol,* 141(1), pp. 99-108.
Baranes-Bachar, K., Levy-Barda, A., Oehler, J., Reid, D. A., Soria-Bretones, I., Voss, T. C., Chung, D., Park, Y., Liu, C., Yoon, J. B., Li, W., Dellaire, G., Misteli, T., Huertas, P., Rothenberg, E., Ramadan, K., Ziv, Y. and Shiloh, Y. (2018) 'The Ubiquitin E3/E4 Ligase UBE4A Adjusts Protein Ubiquitylation and Accumulation at Sites of DNA Damage, Facilitating Double-Strand Break Repair', *Mol Cell,* 69(5), pp. 866-878.e7.
Barrangou, R., Fremaux, C., Deveau, H., Richards, M., Boyaval, P., Moineau, S., Romero, D. A. and Horvath, P. (2007) 'CRISPR provides acquired resistance against viruses in prokaryotes', *Science,* 315(5819), pp. 1709-12.
Bates, P. A., Robertson, C. D., Tetley, L. and Coombs, G. H. (1992) 'Axenic cultivation and characterization of Leishmania mexicana amastigote-like forms', *Parasitology,* 105 (Pt 2), pp. 193-202.
Beattie, L. and Kaye, P. M. (2011) 'Leishmania-host interactions: what has imaging taught us?', *Cell Microbiol,* 13(11), pp. 1659-67.
Beneke, T., Demay, F., Hookway, E., Ashman, N., Jeffery, H., Smith, J., Valli, J., Becvar, T., Myskova, J., Lestinova, T., Shafiq, S., Sadlova, J., Volf, P., Wheeler, R. J. and Gluenz, E. (2019) 'Genetic dissection of a Leishmania flagellar proteome demonstrates requirement for directional motility in sand fly infections', *PLoS Pathog,* 15(6), pp. e1007828.
Beneke, T. and Gluenz, E. (2019) 'LeishGEdit: A Method for Rapid Gene Knockout and Tagging Using CRISPR-Cas9', *Methods Mol Biol,* 1971, pp. 189-210.
Beneke, T. and Gluenz, E. (2020) 'Bar-seq strategies for the LeishGEdit toolbox', *bioRxiv*, pp. 2020.03.19.998856.
Beneke, T., Madden, R., Makin, L., Valli, J., Sunter, J. and Gluenz, E. (2017) 'A CRISPR Cas9 high-throughput genome editing toolkit for kinetoplastids', *R Soc Open Sci,* 4(5), pp. 170095.
Bern, C., Maguire, J. H. and Alvar, J. (2008) 'Complexities of assessing the disease burden attributable to leishmaniasis', *PLoS Negl Trop Dis,* 2(10), pp. e313.
Berndsen, C. E., Wiener, R., Yu, I. W., Ringel, A. E. and Wolberger, C. (2013) 'A conserved asparagine has a structural role in ubiquitin-conjugating enzymes', *Nat Chem Biol,* 9(3), pp. 154-6.
Bertrand, M. J., Milutinovic, S., Dickson, K. M., Ho, W. C., Boudreault, A., Durkin, J., Gillard, J. W., Jaquith, J. B., Morris, S. J. and Barker, P. A. (2008) 'cIAP1 and cIAP2 facilitate cancer cell survival by functioning as E3 ligases that promote RIP1 ubiquitination', *Mol Cell,* 30(6), pp. 689-700.
Bessat, M., Knudsen, G., Burlingame, A. L. and Wang, C. C. (2013) 'A minimal anaphase promoting complex/cyclosome (APC/C) in Trypanosoma brucei', *PLoS One,* 8(3), pp. e59258.
Besteiro, S., Williams, R. A., Coombs, G. H. and Mottram, J. C. (2007) 'Protein turnover and differentiation in Leishmania', *Int J Parasitol,* 37(10), pp. 1063-75.
Besteiro, S., Williams, R. A., Morrison, L. S., Coombs, G. H. and Mottram, J. C. (2006) 'Endosome sorting and autophagy are essential for differentiation and virulence of Leishmania major', *J Biol Chem,* 281(16), pp. 11384-96.

Bhattacharya, A., Corbeil, A., do Monte-Neto, R. L. and Fernandez-Prada, C. (2020) 'Of Drugs and Trypanosomatids: New Tools and Knowledge to Reduce Bottlenecks in Drug Discovery', *Genes (Basel),* 11(7).
Boer, D. R. and Bijlmakers, M. J. (2019) 'Differential Inhibition of Human and Trypanosome Ubiquitin E1S by TAK-243 Offers Possibilities for Parasite Selective Inhibitors', *Sci Rep,* 9(1), pp. 16195.
Branigan, E., Carlos Penedo, J. and Hay, R. T. (2020) 'Ubiquitin transfer by a RING E3 ligase occurs from a closed E2~ubiquitin conformation', *Nat Commun,* 11(1), pp. 2846.
Branigan, E., Plechanovová, A., Jaffray, E. G., Naismith, J. H. and Hay, R. T. (2015) 'Structural basis for the RING-catalyzed synthesis of K63-linked ubiquitin chains', *Nat Struct Mol Biol,* 22(8), pp. 597-602.
Branon, T. C., Bosch, J. A., Sanchez, A. D., Udeshi, N. D., Svinkina, T., Carr, S. A., Feldman, J. L., Perrimon, N. and Ting, A. Y. (2018) 'Efficient proximity labeling in living cells and organisms with TurboID', *Nat Biotechnol,* 36(9), pp. 880-887.
Braten, O., Shabek, N., Kravtsova-Ivantsiv, Y. and Ciechanover, A. (2012) 'Generation of free ubiquitin chains is up-regulated in stress and facilitated by the HECT domain ubiquitin ligases UFD4 and HUL5', *Biochem J,* 444(3), pp. 611-7.
Brooks, D. R., Denise, H., Westrop, G. D., Coombs, G. H. and Mottram, J. C. (2001) 'The stage-regulated expression of Leishmania mexicana CPB cysteine proteases is mediated by an intercistronic sequence element', *J Biol Chem,* 276(50), pp. 47061-9.
Brzovic, P. S., Lissounov, A., Christensen, D. E., Hoyt, D. W. and Klevit, R. E. (2006) 'A UbcH5/ubiquitin noncovalent complex is required for processive BRCA1-directed ubiquitination', *Mol Cell,* 21(6), pp. 873-80.
Bushell, E., Gomes, A. R., Sanderson, T., Anar, B., Girling, G., Herd, C., Metcalf, T., Modrzynska, K., Schwach, F., Martin, R. E., Mather, M. W., McFadden, G. I., Parts, L., Rutledge, G. G., Vaidya, A. B., Wengelnik, K., Rayner, J. C. and Billker, O. (2017) 'Functional Profiling of a Plasmodium Genome Reveals an Abundance of Essential Genes', *Cell,* 170(2), pp. 260-272.e8.
Callis, J. (2014) 'The ubiquitination machinery of the ubiquitin system', *Arabidopsis Book,* 12, pp. e0174.
Carnielli, J. B. T., Crouch, K., Forrester, S., Silva, V. C., Carvalho, S. F. G., Damasceno, J. D., Brown, E., Dickens, N. J., Costa, D. L., Costa, C. H. N., Dietze, R., Jeffares, D. C. and Mottram, J. C. (2018) 'A Leishmania infantum genetic marker associated with miltefosine treatment failure for visceral leishmaniasis', *EBioMedicine,* 36, pp. 83-91.
Castro, R., Scott, K., Jordan, T., Evans, B., Craig, J., Peters, E. L. and Swier, K. (2006) 'The ultrastructure of the parasitophorous vacuole formed by Leishmania major', *J Parasitol,* 92(6), pp. 1162-70.
Cayla, M., Rachidi, N., Leclercq, O., Schmidt-Arras, D., Rosenqvist, H., Wiese, M. and Späth, G. F. (2014) 'Transgenic analysis of the Leishmania MAP kinase MPK10 reveals an auto-inhibitory mechanism crucial for stage-regulated activity and parasite viability', *PLoS Pathog,* 10(9), pp. e1004347.
Ceccarelli, D. F., Tang, X., Pelletier, B., Orlicky, S., Xie, W., Plantevin, V., Neculai, D., Chou, Y. C., Ogunjimi, A., Al-Hakim, A., Varelas, X., Koszela, J., Wasney, G. A., Vedadi, M., Dhe-Paganon, S., Cox, S., Xu, S., Lopez-Girona, A., Mercurio, F., Wrana, J., Durocher, D., Meloche, S., Webb, D. R., Tyers, M. and Sicheri, F. (2011) 'An allosteric inhibitor of the human Cdc34 ubiquitin-conjugating enzyme', *Cell,* 145(7), pp. 1075-87.
Chan, C. H., Morrow, J. K., Li, C. F., Gao, Y., Jin, G., Moten, A., Stagg, L. J., Ladbury, J. E., Cai, Z., Xu, D., Logothetis, C. J., Hung, M. C., Zhang, S. and Lin, H. K. (2013) 'Pharmacological inactivation of Skp2 SCF ubiquitin ligase restricts cancer stem cell traits and cancer progression', *Cell,* 154(3), pp. 556-68.
Chaugule, V. K., Burchell, L., Barber, K. R., Sidhu, A., Leslie, S. J., Shaw, G. S. and Walden, H. (2011) 'Autoregulation of Parkin activity through its ubiquitin-like domain', *EMBO J,* 30(14), pp. 2853-67.

Chauhan, D., Tian, Z., Nicholson, B., Kumar, K. G., Zhou, B., Carrasco, R., McDermott, J. L., Leach, C. A., Fulcinniti, M., Kodrasov, M. P., Weinstock, J., Kingsbury, W. D., Hideshima, T., Shah, P. K., Minvielle, S., Altun, M., Kessler, B. M., Orlowski, R., Richardson, P., Munshi, N. and Anderson, K. C. (2012) 'A small molecule inhibitor of ubiquitin-specific protease-7 induces apoptosis in multiple myeloma cells and overcomes bortezomib resistance', *Cancer Cell,* 22(3), pp. 345-58.
Chen, Z. J. and Sun, L. J. (2009) 'Nonproteolytic functions of ubiquitin in cell signaling', *Mol Cell,* 33(3), pp. 275-86.
Chiu, Y. H., Sun, Q. and Chen, Z. J. (2007) 'E1-L2 activates both ubiquitin and FAT10', *Mol Cell,* 27(6), pp. 1014-23.
Christensen, C. B., Jørgensen, L., Jensen, A. T., Gasim, S., Chen, M., Kharazmi, A., Theander, T. G. and Andresen, K. (2000) 'Molecular characterization of a Leishmania donovanii cDNA clone with similarity to human 20S proteasome a-type subunit', *Biochim Biophys Acta,* 1500(1), pp. 77-87.
Christensen, D. E., Brzovic, P. S. and Klevit, R. E. (2007) 'E2-BRCA1 RING interactions dictate synthesis of mono- or specific polyubiquitin chain linkages', *Nat Struct Mol Biol,* 14(10), pp. 941-8.
Chu, B. W., Kovary, K. M., Guillaume, J., Chen, L. C., Teruel, M. N. and Wandless, T. J. (2013) 'The E3 ubiquitin ligase UBE3C enhances proteasome processivity by ubiquitinating partially proteolyzed substrates', *J Biol Chem,* 288(48), pp. 34575-87.
Chung, W. L., Leung, K. F., Carrington, M. and Field, M. C. (2008) 'Ubiquitylation is required for degradation of transmembrane surface proteins in trypanosomes', *Traffic,* 9(10), pp. 1681-97.
Clague, M. J., Heride, C. and Urbé, S. (2015) 'The demographics of the ubiquitin system', *Trends Cell Biol,* 25(7), pp. 417-26.
Clayton, C. E. (2016) 'Gene expression in Kinetoplastids', *Curr Opin Microbiol,* 32, pp. 46-51.
Cowtan, K. (2006) 'The Buccaneer software for automated model building. 1. Tracing protein chains', *Acta Crystallogr D Biol Crystallogr,* 62(Pt 9), pp. 1002-11.
Coyaud, E., Mis, M., Laurent, E. M., Dunham, W. H., Couzens, A. L., Robitaille, M., Gingras, A. C., Angers, S. and Raught, B. (2015) 'BioID-based Identification of Skp Cullin F-box (SCF)β-TrCP1/2 E3 Ligase Substrates', *Mol Cell Proteomics,* 14(7), pp. 1781-95.
Crozier, T. W. M., Tinti, M., Larance, M., Lamond, A. I. and Ferguson, M. A. J. (2017) 'Prediction of Protein Complexes in Trypanosoma brucei by Protein Correlation Profiling Mass Spectrometry and Machine Learning', *Mol Cell Proteomics,* 16(12), pp. 2254-2267.
Cull, B., Prado Godinho, J. L., Fernandes Rodrigues, J. C., Frank, B., Schurigt, U., Williams, R. A., Coombs, G. H. and Mottram, J. C. (2014) 'Glycosome turnover in Leishmania major is mediated by autophagy', *Autophagy,* 10(12), pp. 2143-57.
Cunningham, C. N., Baughman, J. M., Phu, L., Tea, J. S., Yu, C., Coons, M., Kirkpatrick, D. S., Bingol, B. and Corn, J. E. (2015) 'USP30 and parkin homeostatically regulate atypical ubiquitin chains on mitochondria', *Nat Cell Biol,* 17(2), pp. 160-9.
Currier, R. B., Cooper, A., Burrell-Saward, H., MacLeod, A. and Alsford, S. (2018) 'Decoding the network of Trypanosoma brucei proteins that determines sensitivity to apolipoprotein-L1', *PLoS Pathog,* 14(1), pp. e1006855.
Damasceno, J. D., Reis-Cunha, J., Crouch, K., Beraldi, D., Lapsley, C., Tosi, L. R. O., Bartholomeu, D. and McCulloch, R. (2020) 'Conditional knockout of RAD51-related genes in Leishmania major reveals a critical role for homologous recombination during genome replication', *PLoS Genet,* 16(7), pp. e1008828.
Damianou, A., Burge, R. J., Catta-Preta, C. M. C., Geoghegan, V., Nievas, Y. R., Newling, K., Brown, E., Burchmore, R., Rodenko, B. and Mottram, J. C. (2020) 'Essential roles for deubiquitination in Leishmania life cycle progression', *PLoS Pathog,* 16(6), pp. e1008455.
David, Y., Ziv, T., Admon, A. and Navon, A. (2010) 'The E2 ubiquitin-conjugating enzymes direct polyubiquitination to preferred lysines', *J Biol Chem,* 285(12), pp. 8595-604.

de Diego, J. L., Katz, J. M., Marshall, P., Gutiérrez, B., Manning, J. E., Nussenzweig, V. and González, J. (2001) 'The ubiquitin-proteasome pathway plays an essential role in proteolysis during Trypanosoma cruzi remodeling', *Biochemistry,* 40(4), pp. 1053-62.
de Menezes, J. P., Guedes, C. E., Petersen, A. L., Fraga, D. B. and Veras, P. S. (2015) 'Advances in Development of New Treatment for Leishmaniasis', *Biomed Res Int,* 2015, pp. 815023.
de Pablos, L. M., Ferreira, T. R., Dowle, A. A., Forrester, S., Parry, E., Newling, K. and Walrad, P. B. (2019) 'The mRNA-bound Proteome of Leishmania mexicana: Novel Genetic Insight into an Ancient Parasite', *Mol Cell Proteomics,* 18(7), pp. 1271-1284.
De Pablos, L. M., Ferreira, T. R. and Walrad, P. B. (2016) 'Developmental differentiation in Leishmania lifecycle progression: post-transcriptional control conducts the orchestra', *Curr Opin Microbiol,* 34, pp. 82-89.
Depledge, D. P., MacLean, L. M., Hodgkinson, M. R., Smith, B. A., Jackson, A. P., Ma, S., Uliana, S. R. and Smith, D. F. (2010) 'Leishmania-specific surface antigens show sub-genus sequence variation and immune recognition', *PLoS Negl Trop Dis,* 4(9), pp. e829.
Deshaies, R. J. and Joazeiro, C. A. (2009) 'RING domain E3 ubiquitin ligases', *Annu Rev Biochem,* 78, pp. 399-434.
Deveau, H., Barrangou, R., Garneau, J. E., Labonté, J., Fremaux, C., Boyaval, P., Romero, D. A., Horvath, P. and Moineau, S. (2008) 'Phage response to CRISPR-encoded resistance in Streptococcus thermophilus', *J Bacteriol,* 190(4), pp. 1390-400.
Di Rienzo, M., Antonioli, M., Fusco, C., Liu, Y., Mari, M., Orhon, I., Refolo, G., Germani, F., Corazzari, M., Romagnoli, A., Ciccosanti, F., Mandriani, B., Pellico, M. T., De La Torre, R., Ding, H., Dentice, M., Neri, M., Ferlini, A., Reggiori, F., Kulesz-Martin, M., Piacentini, M., Merla, G. and Fimia, G. M. (2019) 'Autophagy induction in atrophic muscle cells requires ULK1 activation by TRIM32 through unanchored K63-linked polyubiquitin chains', *Sci Adv,* 5(5), pp. eaau8857.
Diao, J., Zhang, Y., Huibregtse, J. M., Zhou, D. and Chen, J. (2008) 'Crystal structure of SopA, a Salmonella effector protein mimicking a eukaryotic ubiquitin ligase', *Nat Struct Mol Biol,* 15(1), pp. 65-70.
Dillon, L. A., Okrah, K., Hughitt, V. K., Suresh, R., Li, Y., Fernandes, M. C., Belew, A. T., Corrada Bravo, H., Mosser, D. M. and El-Sayed, N. M. (2015) 'Transcriptomic profiling of gene expression and RNA processing during Leishmania major differentiation', *Nucleic Acids Res,* 43(14), pp. 6799-813.
Diwu, Y., Zhang, J., Li, M., Yang, X., Shan, F., Ma, H., Zhang, X., Liao, S. and Tu, X. (2020) 'Solution structure of TbUfm1 from Trypanosoma brucei and its binding to TbUba5', *J Struct Biol*, pp. 107580.
Donelson, J. E., Gardner, M. J. and El-Sayed, N. M. (1999) 'More surprises from Kinetoplastida', *Proc Natl Acad Sci U S A,* 96(6), pp. 2579-81.
Dostálová, A. and Volf, P. (2012) 'Leishmania development in sand flies: parasite-vector interactions overview', *Parasit Vectors,* 5, pp. 276.
Dove, K. K. and Klevit, R. E. (2017) 'RING-Between-RING E3 Ligases: Emerging Themes amid the Variations', *J Mol Biol,* 429(22), pp. 3363-3375.
Duncan, S. M., Jones, N. G. and Mottram, J. C. (2017) 'Recent advances in Leishmania reverse genetics: Manipulating a manipulative parasite', *Mol Biochem Parasitol,* 216, pp. 30-38.
Duncan, S. M., Myburgh, E., Philipon, C., Brown, E., Meissner, M., Brewer, J. and Mottram, J. C. (2016) 'Conditional gene deletion with DiCre demonstrates an essential role for CRK3 in Leishmania mexicana cell cycle regulation', *Mol Microbiol,* 100(6), pp. 931-44.
Durcan, T. M., Tang, M. Y., Pérusse, J. R., Dashti, E. A., Aguileta, M. A., McLelland, G. L., Gros, P., Shaler, T. A., Faubert, D., Coulombe, B. and Fon, E. A. (2014) 'USP8 regulates mitophagy by removing K6-linked ubiquitin conjugates from parkin', *EMBO J,* 33(21), pp. 2473-91.
Dworkin-Rastl, E., Shrutkowski, A. and Dworkin, M. B. (1984) 'Multiple ubiquitin mRNAs during Xenopus laevis development contain tandem repeats of the 76 amino acid coding sequence', *Cell,* 39(2 Pt 1), pp. 321-5.

Eddins, M. J., Carlile, C. M., Gomez, K. M., Pickart, C. M. and Wolberger, C. (2006) 'Mms2-Ubc13 covalently bound to ubiquitin reveals the structural basis of linkage-specific polyubiquitin chain formation', *Nat Struct Mol Biol,* 13(10), pp. 915-20.
Eisenhaber, B., Chumak, N., Eisenhaber, F. and Hauser, M. T. (2007) 'The ring between ring fingers (RBR) protein family', *Genome Biol,* 8(3), pp. 209.
Ekkebus, R., van Kasteren, S. I., Kulathu, Y., Scholten, A., Berlin, I., Geurink, P. P., de Jong, A., Goerdayal, S., Neefjes, J., Heck, A. J., Komander, D. and Ovaa, H. (2013) 'On terminal alkynes that can react with active-site cysteine nucleophiles in proteases', *J Am Chem Soc,* 135(8), pp. 2867-70.
Elia, A. E., Boardman, A. P., Wang, D. C., Huttlin, E. L., Everley, R. A., Dephoure, N., Zhou, C., Koren, I., Gygi, S. P. and Elledge, S. J. (2015) 'Quantitative Proteomic Atlas of Ubiquitination and Acetylation in the DNA Damage Response', *Mol Cell,* 59(5), pp. 867-81.
Elledge, S. J., Zhou, Z. and Allen, J. B. (1992) 'Ribonucleotide reductase: regulation, regulation, regulation', *Trends Biochem Sci,* 17(3), pp. 119-23.
Emsley, P., Lohkamp, B., Scott, W. G. and Cowtan, K. (2010) 'Features and development of Coot', *Acta Crystallogr D Biol Crystallogr,* 66(Pt 4), pp. 486-501.
Erpapazoglou, Z., Walker, O. and Haguenauer-Tsapis, R. (2014) 'Versatile roles of k63-linked ubiquitin chains in trafficking', *Cells,* 3(4), pp. 1027-88.
Fiebig, M., Kelly, S. and Gluenz, E. (2015) 'Comparative Life Cycle Transcriptomics Revises Leishmania mexicana Genome Annotation and Links a Chromosome Duplication with Parasitism of Vertebrates', *PLoS Pathog,* 11(10), pp. e1005186.
Field, M. C. and Carrington, M. (2009) 'The trypanosome flagellar pocket', *Nat Rev Microbiol,* 7(11), pp. 775-86.
Finley, D., Bartel, B. and Varshavsky, A. (1989) 'The tails of ubiquitin precursors are ribosomal proteins whose fusion to ubiquitin facilitates ribosome biogenesis', *Nature,* 338(6214), pp. 394-401.
Finley, D., Ulrich, H. D., Sommer, T. and Kaiser, P. (2012) 'The ubiquitin-proteasome system of Saccharomyces cerevisiae', *Genetics,* 192(2), pp. 319-60.
Fleischmann, J. and Campbell, D. A. (1994) 'Expression of the Leishmania tarentolae ubiquitin-encoding and mini-exon genes', *Gene,* 144(1), pp. 45-51.
Forgac, M. (2007) 'Vacuolar ATPases: rotary proton pumps in physiology and pathophysiology', *Nat Rev Mol Cell Biol,* 8(11), pp. 917-29.
Frey, P. A. (1996) 'The Leloir pathway: a mechanistic imperative for three enzymes to change the stereochemical configuration of a single carbon in galactose', *FASEB J,* 10(4), pp. 461-70.
Gan, N., Nakayasu, E. S., Hollenbeck, P. J. and Luo, Z. Q. (2019) 'Legionella pneumophila inhibits immune signalling via MavC-mediated transglutaminase-induced ubiquitination of UBE2N', *Nat Microbiol,* 4(1), pp. 134-143.
Gannavaram, S., Connelly, P. S., Daniels, M. P., Duncan, R., Salotra, P. and Nakhasi, H. L. (2012) 'Deletion of mitochondrial associated ubiquitin fold modifier protein Ufm1 in Leishmania donovani results in loss of β-oxidation of fatty acids and blocks cell division in the amastigote stage', *Mol Microbiol,* 86(1), pp. 187-98.
Gannavaram, S., Sharma, P., Duncan, R. C., Salotra, P. and Nakhasi, H. L. (2011) 'Mitochondrial associated ubiquitin fold modifier-1 mediated protein conjugation in Leishmania donovani', *PLoS One,* 6(1), pp. e16156.
Gasiunas, G., Barrangou, R., Horvath, P. and Siksnys, V. (2012) 'Cas9-crRNA ribonucleoprotein complex mediates specific DNA cleavage for adaptive immunity in bacteria', *Proc Natl Acad Sci U S A,* 109(39), pp. E2579-86.
Georgiadou, S. P., Makaritsis, K. P. and Dalekos, G. N. (2015) 'Leishmaniasis revisited: Current aspects on epidemiology, diagnosis and treatment', *J Transl Int Med,* 3(2), pp. 43-50.
Gersch, M., Gladkova, C., Schubert, A. F., Michel, M. A., Maslen, S. and Komander, D. (2017) 'Mechanism and regulation of the Lys6-selective deubiquitinase USP30', *Nat Struct Mol Biol,* 24(11), pp. 920-930.

Gill, G. (2004) 'SUMO and ubiquitin in the nucleus: different functions, similar mechanisms?', *Genes Dev,* 18(17), pp. 2046-59.
Gluenz, E., Höög, J. L., Smith, A. E., Dawe, H. R., Shaw, M. K. and Gull, K. (2010) 'Beyond 9+0: noncanonical axoneme structures characterize sensory cilia from protists to humans', *FASEB J,* 24(9), pp. 3117-21.
Gomes, A. R., Bushell, E., Schwach, F., Girling, G., Anar, B., Quail, M. A., Herd, C., Pfander, C., Modrzynska, K., Rayner, J. C. and Billker, O. (2015) 'A genome-scale vector resource enables high-throughput reverse genetic screening in a malaria parasite', *Cell Host Microbe,* 17(3), pp. 404-413.
González, J., Ramalho-Pinto, F. J., Frevert, U., Ghiso, J., Tomlinson, S., Scharfstein, J., Corey, E. J. and Nussenzweig, V. (1996) 'Proteasome activity is required for the stage-specific transformation of a protozoan parasite', *J Exp Med,* 184(5), pp. 1909-18.
Graeff, G. R., Steele, P. M., Peterson, C. L., Bennett, M. L. and Langer, P. J. (1993) 'Sequence of a Leishmania major gene encoding an ubiquitin fusion protein', *Gene,* 131(1), pp. 155-6.
Graham, S. H. and Liu, H. (2016) 'Life and death in the trash heap: The ubiquitin proteasome pathway and UCHL1 in brain aging, neurodegenerative disease and cerebral Ischemia', *Ageing Res Rev*.
Grau-Bové, X., Sebé-Pedrós, A. and Ruiz-Trillo, I. (2015) 'The eukaryotic ancestor had a complex ubiquitin signaling system of archaeal origin', *Mol Biol Evol,* 32(3), pp. 726-39.
Gualdrón-López, M., Chevalier, N., Van Der Smissen, P., Courtoy, P. J., Rigden, D. J. and Michels, P. A. M. (2013) 'Ubiquitination of the glycosomal matrix protein receptor PEX5 in Trypanosoma brucei by PEX4 displays novel features', *Biochim Biophys Acta,* 1833(12), pp. 3076-3092.
Gupta, P., Giri, J., Srivastav, S., Chande, A. G., Mukhopadhyaya, R., Das, P. K. and Ukil, A. (2014) 'Leishmania donovani targets tumor necrosis factor receptor-associated factor (TRAF) 3 for impairing TLR4-mediated host response', *FASEB J,* 28(4), pp. 1756-68.
Haglund, K. and Dikic, I. (2012) 'The role of ubiquitylation in receptor endocytosis and endosomal sorting', *J Cell Sci,* 125(Pt 2), pp. 265-75.
Halliday, C., Billington, K., Wang, Z., Madden, R., Dean, S., Sunter, J. D. and Wheeler, R. J. (2019) 'Cellular landmarks of Trypanosoma brucei and Leishmania mexicana', *Mol Biochem Parasitol,* 230, pp. 24-36.
Hamera, S., Mural, R. M., Liu, Y. and Zeng, L. (2014) 'The tomato ubiquitin-conjugating enzyme variant Suv, but not SlUev1C and SlUev1D regulates Fen-mediated programmed cell death in Nicotiana benthamiana', *Plant Signal Behav,* 9(10), pp. e973814.
Han, T. X., Xu, X. Y., Zhang, M. J., Peng, X. and Du, L. L. (2010) 'Global fitness profiling of fission yeast deletion strains by barcode sequencing', *Genome Biol,* 11(6), pp. R60.
Hannaert, V., Bringaud, F., Opperdoes, F. R. and Michels, P. A. (2003) 'Evolution of energy metabolism and its compartmentation in Kinetoplastida', *Kinetoplastid Biol Dis,* 2(1), pp. 11.
Hashimoto, M., Murata, E. and Aoki, T. (2010) 'Secretory protein with RING finger domain (SPRING) specific to Trypanosoma cruzi is directed, as a ubiquitin ligase related protein, to the nucleus of host cells', *Cell Microbiol,* 12(1), pp. 19-30.
Hermanns, T., Pichlo, C., Woiwode, I., Klopffleisch, K., Witting, K. F., Ovaa, H., Baumann, U. and Hofmann, K. (2018) 'A family of unconventional deubiquitinases with modular chain specificity determinants', *Nat Commun,* 9(1), pp. 799.
Hjerpe, R., Aillet, F., Lopitz-Otsoa, F., Lang, V., England, P. and Rodriguez, M. S. (2009) 'Efficient protection and isolation of ubiquitylated proteins using tandem ubiquitin-binding entities', *EMBO Rep,* 10(11), pp. 1250-8.
Hochstrasser, M. (2009) 'Origin and function of ubiquitin-like proteins', *Nature,* 458(7237), pp. 422-9.
Hodge, C. D., Edwards, R. A., Markin, C. J., McDonald, D., Pulvino, M., Huen, M. S., Zhao, J., Spyracopoulos, L., Hendzel, M. J. and Glover, J. N. (2015) 'Covalent Inhibition of Ubc13 Affects

Ubiquitin Signaling and Reveals Active Site Elements Important for Targeting', *ACS Chem Biol,* 10(7), pp. 1718-28.
Hodge, C. D., Spyracopoulos, L. and Glover, J. N. (2016) 'Ubc13: the Lys63 ubiquitin chain building machine', *Oncotarget,* 7(39), pp. 64471-64504.
Hofmann, R. M. and Pickart, C. M. (1999) 'Noncanonical MMS2-encoded ubiquitin-conjugating enzyme functions in assembly of novel polyubiquitin chains for DNA repair', *Cell,* 96(5), pp. 645-53.
Hofmann, R. M. and Pickart, C. M. (2001) 'In vitro assembly and recognition of Lys-63 polyubiquitin chains', *J Biol Chem,* 276(30), pp. 27936-43.
Hoppe, T. (2005) 'Multiubiquitylation by E4 enzymes: 'one size' doesn't fit all', *Trends Biochem Sci,* 30(4), pp. 183-7.
Huang, D. T., Hunt, H. W., Zhuang, M., Ohi, M. D., Holton, J. M. and Schulman, B. A. (2007) 'Basis for a ubiquitin-like protein thioester switch toggling E1-E2 affinity', *Nature,* 445(7126), pp. 394-8.
Huang, L., Kinnucan, E., Wang, G., Beaudenon, S., Howley, P. M., Huibregtse, J. M. and Pavletich, N. P. (1999) 'Structure of an E6AP-UbcH7 complex: insights into ubiquitination by the E2-E3 enzyme cascade', *Science,* 286(5443), pp. 1321-6.
Huang, X. and Dixit, V. M. (2016) 'Drugging the undruggables: exploring the ubiquitin system for drug development', *Cell Res,* 26(4), pp. 484-98.
Huen, M. S., Grant, R., Manke, I., Minn, K., Yu, X., Yaffe, M. B. and Chen, J. (2007) 'RNF8 transduces the DNA-damage signal via histone ubiquitylation and checkpoint protein assembly', *Cell,* 131(5), pp. 901-14.
Huen, M. S., Huang, J., Yuan, J., Yamamoto, M., Akira, S., Ashley, C., Xiao, W. and Chen, J. (2008) 'Noncanonical E2 variant-independent function of UBC13 in promoting checkpoint protein assembly', *Mol Cell Biol,* 28(19), pp. 6104-12.
Huh, W. K., Falvo, J. V., Gerke, L. C., Carroll, A. S., Howson, R. W., Weissman, J. S. and O'Shea, E. K. (2003) 'Global analysis of protein localization in budding yeast', *Nature,* 425(6959), pp. 686-91.
Huibregtse, J. M., Scheffner, M., Beaudenon, S. and Howley, P. M. (1995) 'A family of proteins structurally and functionally related to the E6-AP ubiquitin-protein ligase', *Proc Natl Acad Sci U S A,* 92(11), pp. 5249.
Hungria, V. T. M., Crusoé, E. Q., Bittencourt, R. I., Maiolino, A., Magalhães, R. J. P., Sobrinho, J. D. N., Pinto, J. V., Fortes, R. C., Moreira, E. S. and Tanaka, P. Y. (2019) 'New proteasome inhibitors in the treatment of multiple myeloma', *Hematol Transfus Cell Ther,* 41(1), pp. 76-83.
Husnjak, K. and Dikic, I. (2012) 'Ubiquitin-binding proteins: decoders of ubiquitin-mediated cellular functions', *Annu Rev Biochem,* 81, pp. 291-322.
Hutchins, A. P., Liu, S., Diez, D. and Miranda-Saavedra, D. (2013) 'The repertoires of ubiquitinating and deubiquitinating enzymes in eukaryotic genomes', *Mol Biol Evol,* 30(5), pp. 1172-87.
Hyer, M. L., Milhollen, M. A., Ciavarri, J., Fleming, P., Traore, T., Sappal, D., Huck, J., Shi, J., Gavin, J., Brownell, J., Yang, Y., Stringer, B., Griffin, R., Bruzzese, F., Soucy, T., Duffy, J., Rabino, C., Riceberg, J., Hoar, K., Lublinsky, A., Menon, S., Sintchak, M., Bump, N., Pulukuri, S. M., Langston, S., Tirrell, S., Kuranda, M., Veiby, P., Newcomb, J., Li, P., Wu, J. T., Powe, J., Dick, L. R., Greenspan, P., Galvin, K., Manfredi, M., Claiborne, C., Amidon, B. S. and Bence, N. F. (2018) 'A small-molecule inhibitor of the ubiquitin activating enzyme for cancer treatment', *Nat Med,* 24(2), pp. 186-193.
Iconomou, M. and Saunders, D. N. (2016) 'Systematic approaches to identify E3 ligase substrates', *Biochem J,* 473(22), pp. 4083-4101.
Inbar, E., Hughitt, V. K., Dillon, L. A., Ghosh, K., El-Sayed, N. M. and Sacks, D. L. (2017) 'The Transcriptome of Leishmania major Developmental Stages in Their Natural Sand Fly Vector', *mBio,* 8(2).

Iribarren, P. A., Di Marzio, L. A., Berazategui, M. A., De Gaudenzi, J. G. and Alvarez, V. E. (2018) 'SUMO polymeric chains are involved in nuclear foci formation and chromatin organization in Trypanosoma brucei procyclic forms', *PLoS One,* 13(2), pp. e0193528.
Jansen, R., Embden, J. D., Gaastra, W. and Schouls, L. M. (2002) 'Identification of genes that are associated with DNA repeats in prokaryotes', *Mol Microbiol,* 43(6), pp. 1565-75.
Jin, J., Li, X., Gygi, S. P. and Harper, J. W. (2007) 'Dual E1 activation systems for ubiquitin differentially regulate E2 enzyme charging', *Nature,* 447(7148), pp. 1135-8.
Jinek, M., Chylinski, K., Fonfara, I., Hauer, M., Doudna, J. A. and Charpentier, E. (2012) 'A programmable dual-RNA-guided DNA endonuclease in adaptive bacterial immunity', *Science,* 337(6096), pp. 816-21.
Jones, N. G., Catta-Preta, C. M. C., Lima, A. P. C. A. and Mottram, J. C. (2018) 'Genetically Validated Drug Targets in Leishmania: Current Knowledge and Future Prospects', *ACS Infect Dis,* 4(4), pp. 467-477.
Jones, W. M., Davis, A. G., Wilson, R. H., Elliott, K. L. and Sumner, I. (2019) 'A conserved asparagine in a ubiquitin-conjugating enzyme positions the substrate for nucleophilic attack', *J Comput Chem*.
Jonnalagadda, S., Butt, T. R., Marsh, J., Sternberg, E. J., Mirabelli, C. K., Ecker, D. J. and Crooke, S. T. (1987) 'Expression and accurate processing of yeast penta-ubiquitin in Escherichia coli', *J Biol Chem,* 262(36), pp. 17750-6.
Kar, G., Keskin, O., Nussinov, R. and Gursoy, A. (2012) 'Human proteome-scale structural modeling of E2-E3 interactions exploiting interface motifs', *J Proteome Res,* 11(2), pp. 1196-207.
Kariithi, H. M., Boeren, S., Murungi, E. K., Vlak, J. M. and Abd-Alla, A. M. (2016) 'A proteomics approach reveals molecular manipulators of distinct cellular processes in the salivary glands of Glossina m. morsitans in response to Trypanosoma b. brucei infections', *Parasit Vectors,* 9(1), pp. 424.
Keusekotten, K., Elliott, P. R., Glockner, L., Fiil, B. K., Damgaard, R. B., Kulathu, Y., Wauer, T., Hospenthal, M. K., Gyrd-Hansen, M., Krappmann, D., Hofmann, K. and Komander, D. (2013) 'OTULIN antagonizes LUBAC signaling by specifically hydrolyzing Met1-linked polyubiquitin', *Cell,* 153(6), pp. 1312-26.
Khare, S., Nagle, A. S., Biggart, A., Lai, Y. H., Liang, F., Davis, L. C., Barnes, S. W., Mathison, C. J., Myburgh, E., Gao, M. Y., Gillespie, J. R., Liu, X., Tan, J. L., Stinson, M., Rivera, I. C., Ballard, J., Yeh, V., Groessl, T., Federe, G., Koh, H. X., Venable, J. D., Bursulaya, B., Shapiro, M., Mishra, P. K., Spraggon, G., Brock, A., Mottram, J. C., Buckner, F. S., Rao, S. P., Wen, B. G., Walker, J. R., Tuntland, T., Molteni, V., Glynne, R. J. and Supek, F. (2016) 'Proteasome inhibition for treatment of leishmaniasis, Chagas disease and sleeping sickness', *Nature,* 537(7619), pp. 229-233.
Kim, H. C. and Huibregtse, J. M. (2009) 'Polyubiquitination by HECT E3s and the determinants of chain type specificity', *Mol Cell Biol,* 29(12), pp. 3307-18.
Kimblin, N., Peters, N., Debrabant, A., Secundino, N., Egen, J., Lawyer, P., Fay, M. P., Kamhawi, S. and Sacks, D. (2008) 'Quantification of the infectious dose of Leishmania major transmitted to the skin by single sand flies', *Proc Natl Acad Sci U S A,* 105(29), pp. 10125-30.
Kirchhoff, L. V., Kim, K. S., Engman, D. M. and Donelson, J. E. (1988) 'Ubiquitin genes in trypanosomatidae', *J Biol Chem,* 263(25), pp. 12698-704.
Kirisako, T., Kamei, K., Murata, S., Kato, M., Fukumoto, H., Kanie, M., Sano, S., Tokunaga, F., Tanaka, K. and Iwai, K. (2006) 'A ubiquitin ligase complex assembles linear polyubiquitin chains', *EMBO J,* 25(20), pp. 4877-87.
Klein, C. A., Droll, D. and Clayton, C. (2013) 'SUMOylation in Trypanosoma brucei', *PeerJ,* 1, pp. e180.
Kliza, K. and Husnjak, K. (2020) 'Resolving the Complexity of Ubiquitin Networks', *Front Mol Biosci,* 7, pp. 21.

Koegl, M., Hoppe, T., Schlenker, S., Ulrich, H. D., Mayer, T. U. and Jentsch, S. (1999) 'A novel ubiquitination factor, E4, is involved in multiubiquitin chain assembly', *Cell,* 96(5), pp. 635-44.
Kolas, N. K., Chapman, J. R., Nakada, S., Ylanko, J., Chahwan, R., Sweeney, F. D., Panier, S., Mendez, M., Wildenhain, J., Thomson, T. M., Pelletier, L., Jackson, S. P. and Durocher, D. (2007) 'Orchestration of the DNA-damage response by the RNF8 ubiquitin ligase', *Science,* 318(5856), pp. 1637-40.
Komander, D. and Rape, M. (2012) 'The ubiquitin code', *Annu Rev Biochem,* 81, pp. 203-29.
Krissinel, E. and Henrick, K. (2007) 'Inference of macromolecular assemblies from crystalline state', *J Mol Biol,* 372(3), pp. 774-97.
Kumar, P. and Wang, C. C. (2005) 'Depletion of anaphase-promoting complex or cyclosome (APC/C) subunit homolog APC1 or CDC27 of Trypanosoma brucei arrests the procyclic form in metaphase but the bloodstream form in anaphase', *J Biol Chem,* 280(36), pp. 31783-91.
Lamb, J. R., Tugendreich, S. and Hieter, P. (1995) 'Tetratrico peptide repeat interactions: to TPR or not to TPR?', *Trends Biochem Sci,* 20(7), pp. 257-9.
Laskay, T., van Zandbergen, G. and Solbach, W. (2003) 'Neutrophil granulocytes--Trojan horses for Leishmania major and other intracellular microbes?', *Trends Microbiol,* 11(5), pp. 210-4.
Laskay, T., van Zandbergen, G. and Solbach, W. (2008) 'Neutrophil granulocytes as host cells and transport vehicles for intracellular pathogens: apoptosis as infection-promoting factor', *Immunobiology,* 213(3-4), pp. 183-91.
Lechtenberg, B. C., Rajput, A., Sanishvili, R., Dobaczewska, M. K., Ware, C. F., Mace, P. D. and Riedl, S. J. (2016) 'Structure of a HOIP/E2~ubiquitin complex reveals RBR E3 ligase mechanism and regulation', *Nature,* 529(7587), pp. 546-50.
Lee, B. L., Singh, A., Mark Glover, J. N., Hendzel, M. J. and Spyracopoulos, L. (2017) 'Molecular Basis for K63-Linked Ubiquitination Processes in Double-Strand DNA Break Repair: A Focus on Kinetics and Dynamics', *J Mol Biol,* 429(22), pp. 3409-3429.
Legge, G. B., Martinez-Yamout, M. A., Hambly, D. M., Trinh, T., Lee, B. M., Dyson, H. J. and Wright, P. E. (2004) 'ZZ domain of CBP: an unusual zinc finger fold in a protein interaction module', *J Mol Biol,* 343(4), pp. 1081-93.
Lehane, M. J. (1997) 'Peritrophic matrix structure and function', *Annu Rev Entomol,* 42, pp. 525-50.
Leimkühler, S., Wuebbens, M. M. and Rajagopalan, K. V. (2001) 'Characterization of Escherichia coli MoeB and its involvement in the activation of molybdopterin synthase for the biosynthesis of the molybdenum cofactor', *J Biol Chem,* 276(37), pp. 34695-701.
Lentucci, C., Belkina, A. C., Cederquist, C. T., Chan, M., Johnson, H. E., Prasad, S., Lopacinski, A., Nikolajczyk, B. S., Monti, S., Snyder-Cappione, J., Tanasa, B., Cardamone, M. D. and Perissi, V. (2017) 'Inhibition of Ubc13-mediated Ubiquitination by GPS2 Regulates Multiple Stages of B Cell Development', *J Biol Chem,* 292(7), pp. 2754-2772.
Leung, K. F., Riley, F. S., Carrington, M. and Field, M. C. (2011) 'Ubiquitylation and developmental regulation of invariant surface protein expression in trypanosomes', *Eukaryot Cell,* 10(7), pp. 916-31.
Li, L., Stoeckert, C. J. and Roos, D. S. (2003) 'OrthoMCL: identification of ortholog groups for eukaryotic genomes', *Genome Res,* 13(9), pp. 2178-89.
Li, W., Bengtson, M. H., Ulbrich, A., Matsuda, A., Reddy, V. A., Orth, A., Chanda, S. K., Batalov, S. and Joazeiro, C. A. (2008) 'Genome-wide and functional annotation of human E3 ubiquitin ligases identifies MULAN, a mitochondrial E3 that regulates the organelle's dynamics and signaling', *PLoS One,* 3(1), pp. e1487.
Li, Z., Zou, C. B., Yao, Y., Hoyt, M. A., McDonough, S., Mackey, Z. B., Coffino, P. and Wang, C. C. (2002) 'An easily dissociated 26 S proteasome catalyzes an essential ubiquitin-mediated protein degradation pathway in Trypanosoma brucei', *J Biol Chem,* 277(18), pp. 15486-98.
Liao, S., Hu, H., Wang, T., Tu, X. and Li, Z. (2017) 'The Protein Neddylation Pathway in Trypanosoma brucei: FUNCTIONAL CHARACTERIZATION AND SUBSTRATE IDENTIFICATION', *J Biol Chem,* 292(3), pp. 1081-1091.

Liao, S., Wang, T., Fan, K. and Tu, X. (2010) 'The small ubiquitin-like modifier (SUMO) is essential in cell cycle regulation in Trypanosoma brucei', *Exp Cell Res,* 316(5), pp. 704-15.
Lin, D. Y., Diao, J. and Chen, J. (2012) 'Crystal structures of two bacterial HECT-like E3 ligases in complex with a human E2 reveal atomic details of pathogen-host interactions', *Proc Natl Acad Sci U S A,* 109(6), pp. 1925-30.
Lin, D. Y., Diao, J., Zhou, D. and Chen, J. (2011) 'Biochemical and structural studies of a HECT-like ubiquitin ligase from Escherichia coli O157:H7', *J Biol Chem,* 286(1), pp. 441-9.
Lin, H., Li, S. and Shu, H. B. (2019) 'The Membrane-Associated MARCH E3 Ligase Family: Emerging Roles in Immune Regulation', *Front Immunol,* 10, pp. 1751.
Lois, L. M. and Lima, C. D. (2005) 'Structures of the SUMO E1 provide mechanistic insights into SUMO activation and E2 recruitment to E1', *EMBO J,* 24(3), pp. 439-51.
Lok, G. T., Sy, S. M., Dong, S. S., Ching, Y. P., Tsao, S. W., Thomson, T. M. and Huen, M. S. (2012) 'Differential regulation of RNF8-mediated Lys48- and Lys63-based poly-ubiquitylation', *Nucleic Acids Res,* 40(1), pp. 196-205.
Lorenz, S., Cantor, A. J., Rape, M. and Kuriyan, J. (2013) 'Macromolecular juggling by ubiquitylation enzymes', *BMC Biol,* 11, pp. 65.
Love, K. R., Pandya, R. K., Spooner, E. and Ploegh, H. L. (2009) 'Ubiquitin C-terminal electrophiles are activity-based probes for identification and mechanistic study of ubiquitin conjugating machinery', *ACS Chem Biol,* 4(4), pp. 275-87.
Lowrie, D. J., Giffin, B. F. and Ventullo, R. M. (1993) 'The ubiquitin-ligase system in Trypanosoma brucei brucei', *Am J Trop Med Hyg,* 49(5), pp. 545-51.
Lu, X., Olsen, S. K., Capili, A. D., Cisar, J. S., Lima, C. D. and Tan, D. S. (2010) 'Designed semisynthetic protein inhibitors of Ub/Ubl E1 activating enzymes', *J Am Chem Soc,* 132(6), pp. 1748-9.
Lu, Z. and Hunter, T. (2009) 'Degradation of activated protein kinases by ubiquitination', *Annu Rev Biochem,* 78, pp. 435-75.
Lu, Z., Xu, S., Joazeiro, C., Cobb, M. H. and Hunter, T. (2002) 'The PHD domain of MEKK1 acts as an E3 ubiquitin ligase and mediates ubiquitination and degradation of ERK1/2', *Mol Cell,* 9(5), pp. 945-56.
Lv, Z., Rickman, K. A., Yuan, L., Williams, K., Selvam, S. P., Woosley, A. N., Howe, P. H., Ogretmen, B., Smogorzewska, A. and Olsen, S. K. (2017) 'S. pombe Uba1-Ubc15 Structure Reveals a Novel Regulatory Mechanism of Ubiquitin E2 Activity', *Mol Cell,* 65(4), pp. 699-714.e6.
López-Farfán, D., Bart, J. M., Rojas-Barros, D. I. and Navarro, M. (2014) 'SUMOylation by the E3 ligase TbSIZ1/PIAS1 positively regulates VSG expression in Trypanosoma brucei', *PLoS Pathog,* 10(12), pp. e1004545.
Machida, Y. J., Machida, Y., Chen, Y., Gurtan, A. M., Kupfer, G. M., D'Andrea, A. D. and Dutta, A. (2006) 'UBE2T is the E2 in the Fanconi anemia pathway and undergoes negative autoregulation', *Mol Cell,* 23(4), pp. 589-96.
Maier, A., Lorenz, P., Voncken, F. and Clayton, C. (2001) 'An essential dimeric membrane protein of trypanosome glycosomes', *Mol Microbiol,* 39(6), pp. 1443-51.
Mailand, N., Bekker-Jensen, S., Faustrup, H., Melander, F., Bartek, J., Lukas, C. and Lukas, J. (2007) 'RNF8 ubiquitylates histones at DNA double-strand breaks and promotes assembly of repair proteins', *Cell,* 131(5), pp. 887-900.
Manning-Cela, R., Jaishankar, S. and Swindle, J. (2006) 'Life-cycle and growth-phase-dependent regulation of the ubiquitin genes of Trypanosoma cruzi', *Arch Med Res,* 37(5), pp. 593-601.
Markson, G., Kiel, C., Hyde, R., Brown, S., Charalabous, P., Bremm, A., Semple, J., Woodsmith, J., Duley, S., Salehi-Ashtiani, K., Vidal, M., Komander, D., Serrano, L., Lehner, P. and Sanderson, C. M. (2009) 'Analysis of the human E2 ubiquitin conjugating enzyme protein interaction network', *Genome Res,* 19(10), pp. 1905-11.

Martínez-Calvillo, S., Yan, S., Nguyen, D., Fox, M., Stuart, K. and Myler, P. J. (2003) 'Transcription of Leishmania major Friedlin chromosome 1 initiates in both directions within a single region', *Mol Cell,* 11(5), pp. 1291-9.
Masuda, Y., Suzuki, M., Kawai, H., Hishiki, A., Hashimoto, H., Masutani, C., Hishida, T., Suzuki, F. and Kamiya, K. (2012) 'En bloc transfer of polyubiquitin chains to PCNA in vitro is mediated by two different human E2-E3 pairs', *Nucleic Acids Res,* 40(20), pp. 10394-407.
Mathur, S., Fletcher, A. J., Branigan, E., Hay, R. T. and Virdee, S. (2020) 'Photocrosslinking Activity-Based Probes for Ubiquitin RING E3 Ligases', *Cell Chem Biol,* 27(1), pp. 74-82.e6.
Mbang-Benet, D. E., Sterkers, Y., Morelle, C., Kebe, N. M., Crobu, L., Portalès, P., Coux, O., Hernandez, J. F., Meghamla, S., Pagès, M. and Bastien, P. (2014) 'The bacterial-like HslVU protease complex subunits are involved in the control of different cell cycle events in trypanosomatids', *Acta Trop,* 131, pp. 22-31.
McCall, L. I., Zhang, W. W. and Matlashewski, G. (2013) 'Determinants for the development of visceral leishmaniasis disease', *PLoS Pathog,* 9(1), pp. e1003053.
McClellan, A. J., Laugesen, S. H. and Ellgaard, L. (2019) 'Cellular functions and molecular mechanisms of non-lysine ubiquitination', *Open Biol,* 9(9), pp. 190147.
McGrath, J. P., Jentsch, S. and Varshavsky, A. (1991) 'UBA 1: an essential yeast gene encoding ubiquitin-activating enzyme', *EMBO J,* 10(1), pp. 227-36.
McKenna, S., Spyracopoulos, L., Moraes, T., Pastushok, L., Ptak, C., Xiao, W. and Ellison, M. J. (2001) 'Noncovalent interaction between ubiquitin and the human DNA repair protein Mms2 is required for Ubc13-mediated polyubiquitination', *J Biol Chem,* 276(43), pp. 40120-6.
McNicholas, S., Potterton, E., Wilson, K. S. and Noble, M. E. (2011) 'Presenting your structures: the CCP4mg molecular-graphics software', *Acta Crystallogr D Biol Crystallogr,* 67(Pt 4), pp. 386-94.
Metzger, M. B., Hristova, V. A. and Weissman, A. M. (2012) 'HECT and RING finger families of E3 ubiquitin ligases at a glance', *J Cell Sci,* 125(Pt 3), pp. 531-7.
Metzger, M. B., Pruneda, J. N., Klevit, R. E. and Weissman, A. M. (2014) 'RING-type E3 ligases: master manipulators of E2 ubiquitin-conjugating enzymes and ubiquitination', *Biochim Biophys Acta,* 1843(1), pp. 47-60.
Mi, J., Zhang, J., Liao, S. and Tu, X. (2018) 'Solution structure of a ubiquitin-like protein from Trypanosoma brucei', *Protein Sci,* 27(10), pp. 1831-1836.
Michel, M. A., Elliott, P. R., Swatek, K. N., Simicek, M., Pruneda, J. N., Wagstaff, J. L., Freund, S. M. and Komander, D. (2015) 'Assembly and specific recognition of k29- and k33-linked polyubiquitin', *Mol Cell,* 58(1), pp. 95-109.
Michels, P. A., Bringaud, F., Herman, M. and Hannaert, V. (2006) 'Metabolic functions of glycosomes in trypanosomatids', *Biochim Biophys Acta,* 1763(12), pp. 1463-77.
Misra, M., Kuhn, M., Löbel, M., An, H., Statsyuk, A. V., Sotriffer, C. and Schindelin, H. (2017) 'Dissecting the Specificity of Adenosyl Sulfamate Inhibitors Targeting the Ubiquitin-Activating Enzyme', *Structure,* 25(7), pp. 1120-1129.e3.
Moraes, T. F., Edwards, R. A., McKenna, S., Pastushok, L., Xiao, W., Glover, J. N. and Ellison, M. J. (2001) 'Crystal structure of the human ubiquitin conjugating enzyme complex, hMms2-hUbc13', *Nat Struct Biol,* 8(8), pp. 669-73.
Morales, M. A., Watanabe, R., Dacher, M., Chafey, P., Osorio y Fortéa, J., Scott, D. A., Beverley, S. M., Ommen, G., Clos, J., Hem, S., Lenormand, P., Rousselle, J. C., Namane, A. and Späth, G. F. (2010) 'Phosphoproteome dynamics reveal heat-shock protein complexes specific to the Leishmania donovani infectious stage', *Proc Natl Acad Sci U S A,* 107(18), pp. 8381-6.
Motegi, A., Sood, R., Moinova, H., Markowitz, S. D., Liu, P. P. and Myung, K. (2006) 'Human SHPRH suppresses genomic instability through proliferating cell nuclear antigen polyubiquitination', *J Cell Biol,* 175(5), pp. 703-8.
Mowbray, C. E., Braillard, S., Speed, W., Glossop, P. A., Whitlock, G. A., Gibson, K. R., Mills, J. E., Brown, A. D., Gardner, J. M., Cao, Y., Hua, W., Morgans, G. L., Feijens, P. B., Matheeussen, A.

and Maes, L. J. (2015) 'Novel Amino-pyrazole Ureas with Potent In Vitro and In Vivo Antileishmanial Activity', *J Med Chem,* 58(24), pp. 9615-24.
Mulder, M. P., Witting, K., Berlin, I., Pruneda, J. N., Wu, K. P., Chang, J. G., Merkx, R., Bialas, J., Groettrup, M., Vertegaal, A. C., Schulman, B. A., Komander, D., Neefjes, J., El Oualid, F. and Ovaa, H. (2016) 'A cascading activity-based probe sequentially targets E1-E2-E3 ubiquitin enzymes', *Nat Chem Biol,* 12(7), pp. 523-30.
Mullard, A. (2019) 'First targeted protein degrader hits the clinic', *Nat Rev Drug Discov*.
Mural, R. V., Liu, Y., Rosebrock, T. R., Brady, J. J., Hamera, S., Connor, R. A., Martin, G. B. and Zeng, L. (2013) 'The tomato Fni3 lysine-63-specific ubiquitin-conjugating enzyme and suv ubiquitin E2 variant positively regulate plant immunity', *Plant Cell,* 25(9), pp. 3615-31.
Murata, E., Hashimoto, M. and Aoki, T. (2008) 'Interaction between cFLIP and Itch, a ubiquitin ligase, is obstructed in Trypanosoma cruzi-infected human cells', *Microbiol Immunol,* 52(11), pp. 539-43.
Murshudov, G. N., Skubák, P., Lebedev, A. A., Pannu, N. S., Steiner, R. A., Nicholls, R. A., Winn, M. D., Long, F. and Vagin, A. A. (2011) 'REFMAC5 for the refinement of macromolecular crystal structures', *Acta Crystallogr D Biol Crystallogr,* 67(Pt 4), pp. 355-67.
Murshudov, G. N., Vagin, A. A. and Dodson, E. J. (1997) 'Refinement of macromolecular structures by the maximum-likelihood method', *Acta Crystallogr D Biol Crystallogr,* 53(Pt 3), pp. 240-55.
Mutomba, M. C. and Wang, C. C. (1998) 'The role of proteolysis during differentiation of Trypanosoma brucei from the bloodstream to the procyclic form', *Mol Biochem Parasitol,* 93(1), pp. 11-22.
Muxel, S. M., Acuña, S. M., Aoki, J. I., Zampieri, R. A. and Floeter-Winter, L. M. (2018) 'Toll-Like Receptor and miRNA-let-7e Expression Alter the Inflammatory Response in Leishmania amazonensis-Infected Macrophages', *Front Immunol,* 9, pp. 2792.
Muñoz, C., San Francisco, J., Gutiérrez, B. and González, J. (2015) 'Role of the Ubiquitin-Proteasome Systems in the Biology and Virulence of Protozoan Parasites', *Biomed Res Int,* 2015, pp. 141526.
Mwenechanya, R., Kovářová, J., Dickens, N. J., Mudaliar, M., Herzyk, P., Vincent, I. M., Weidt, S. K., Burgess, K. E., Burchmore, R. J. S., Pountain, A. W., Smith, T. K., Creek, D. J., Kim, D. H., Lepesheva, G. I. and Barrett, M. P. (2017) 'Sterol 14α-demethylase mutation leads to amphotericin B resistance in Leishmania mexicana', *PLoS Negl Trop Dis,* 11(6), pp. e0005649.
Nakada, S. (2016) 'Opposing roles of RNF8/RNF168 and deubiquitinating enzymes in ubiquitination-dependent DNA double-strand break response signaling and DNA-repair pathway choice', *J Radiat Res,* 57 Suppl 1, pp. i33-i40.
Nalawansha, D. A. and Crews, C. M. (2020) 'PROTACs: An Emerging Therapeutic Modality in Precision Medicine', *Cell Chem Biol,* 27(8), pp. 998-1014.
Ndubaku, C. and Tsui, V. (2015) 'Inhibiting the deubiquitinating enzymes (DUBs)', *J Med Chem,* 58(4), pp. 1581-95.
Neutzner, M. and Neutzner, A. (2012) 'Enzymes of ubiquitination and deubiquitination', *Essays Biochem,* 52, pp. 37-50.
Ng, L. G., Hsu, A., Mandell, M. A., Roediger, B., Hoeller, C., Mrass, P., Iparraguirre, A., Cavanagh, L. L., Triccas, J. A., Beverley, S. M., Scott, P. and Weninger, W. (2008) 'Migratory dermal dendritic cells act as rapid sensors of protozoan parasites', *PLoS Pathog,* 4(11), pp. e1000222.
Nguyen, L., Plafker, K. S., Starnes, A., Cook, M., Klevit, R. E. and Plafker, S. M. (2014) 'The ubiquitin-conjugating enzyme, UbcM2, is restricted to monoubiquitylation by a two-fold mechanism that involves backside residues of E2 and Lys48 of ubiquitin', *Biochemistry,* 53(24), pp. 4004-14.
Notredame, C., Higgins, D. G. and Heringa, J. (2000) 'T-Coffee: A novel method for fast and accurate multiple sequence alignment', *J Mol Biol,* 302(1), pp. 205-17.

Nugent, P. G., Karsani, S. A., Wait, R., Tempero, J. and Smith, D. F. (2004) 'Proteomic analysis of Leishmania mexicana differentiation', *Mol Biochem Parasitol,* 136(1), pp. 51-62.
Ohtake, F., Tsuchiya, H., Saeki, Y. and Tanaka, K. (2018) 'K63 ubiquitylation triggers proteasomal degradation by seeding branched ubiquitin chains', *Proc Natl Acad Sci U S A,* 115(7), pp. E1401-E1408.
Osaka, F., Saeki, M., Katayama, S., Aida, N., Toh-E, A., Kominami, K., Toda, T., Suzuki, T., Chiba, T., Tanaka, K. and Kato, S. (2000) 'Covalent modifier NEDD8 is essential for SCF ubiquitin-ligase in fission yeast', *EMBO J,* 19(13), pp. 3475-84.
Ozkan, E., Yu, H. and Deisenhofer, J. (2005) 'Mechanistic insight into the allosteric activation of a ubiquitin-conjugating enzyme by RING-type ubiquitin ligases', *Proc Natl Acad Sci U S A,* 102(52), pp. 18890-5.
Ozkaynak, E., Finley, D., Solomon, M. J. and Varshavsky, A. (1987) 'The yeast ubiquitin genes: a family of natural gene fusions', *EMBO J,* 6(5), pp. 1429-39.
Pace, D. (2014) 'Leishmaniasis', *J Infect,* 69 Suppl 1, pp. S10-8.
Pao, K. C., Stanley, M., Han, C., Lai, Y. C., Murphy, P., Balk, K., Wood, N. T., Corti, O., Corvol, J. C., Muqit, M. M. and Virdee, S. (2016) 'Probes of ubiquitin E3 ligases enable systematic dissection of parkin activation', *Nat Chem Biol,* 12(5), pp. 324-31.
Pao, K. C., Wood, N. T., Knebel, A., Rafie, K., Stanley, M., Mabbitt, P. D., Sundaramoorthy, R., Hofmann, K., van Aalten, D. M. F. and Virdee, S. (2018) 'Activity-based E3 ligase profiling uncovers an E3 ligase with esterification activity', *Nature*.
Park, J. E., Miller, Z., Jun, Y., Lee, W. and Kim, K. B. (2018) 'Next-generation proteasome inhibitors for cancer therapy', *Transl Res,* 198, pp. 1-16.
Pastushok, L., Moraes, T. F., Ellison, M. J. and Xiao, W. (2005) 'A single Mms2 "key" residue insertion into a Ubc13 pocket determines the interface specificity of a human Lys63 ubiquitin conjugation complex', *J Biol Chem,* 280(18), pp. 17891-900.
Pastushok, L., Spyracopoulos, L. and Xiao, W. (2007) 'Two Mms2 residues cooperatively interact with ubiquitin and are critical for Lys63 polyubiquitination in vitro and in vivo', *FEBS Lett,* 581(28), pp. 5343-8.
Paul, A. and Wang, B. (2017) 'RNF8- and Ube2S-Dependent Ubiquitin Lysine 11-Linkage Modification in Response to DNA Damage', *Mol Cell,* 66(4), pp. 458-472.e5.
Pearce, M. J., Mintseris, J., Ferreyra, J., Gygi, S. P. and Darwin, K. H. (2008) 'Ubiquitin-like protein involved in the proteasome pathway of Mycobacterium tuberculosis', *Science,* 322(5904), pp. 1104-7.
Pelzer, C., Kassner, I., Matentzoglu, K., Singh, R. K., Wollscheid, H. P., Scheffner, M., Schmidtke, G. and Groettrup, M. (2007) 'UBE1L2, a novel E1 enzyme specific for ubiquitin', *J Biol Chem,* 282(32), pp. 23010-4.
Peters, N. C., Egen, J. G., Secundino, N., Debrabant, A., Kimblin, N., Kamhawi, S., Lawyer, P., Fay, M. P., Germain, R. N. and Sacks, D. (2008) 'In vivo imaging reveals an essential role for neutrophils in leishmaniasis transmitted by sand flies', *Science,* 321(5891), pp. 970-4.
Petroski, M. D. and Deshaies, R. J. (2005) 'Function and regulation of cullin-RING ubiquitin ligases', *Nat Rev Mol Cell Biol,* 6(1), pp. 9-20.
Pichler, A., Gast, A., Seeler, J. S., Dejean, A. and Melchior, F. (2002) 'The nucleoporin RanBP2 has SUMO1 E3 ligase activity', *Cell,* 108(1), pp. 109-20.
Pichler, A., Knipscheer, P., Saitoh, H., Sixma, T. K. and Melchior, F. (2004) 'The RanBP2 SUMO E3 ligase is neither HECT- nor RING-type', *Nat Struct Mol Biol,* 11(10), pp. 984-91.
Pickart, C. M., Kasperek, E. M., Beal, R. and Kim, A. (1994) 'Substrate properties of site-specific mutant ubiquitin protein (G76A) reveal unexpected mechanistic features of ubiquitin-activating enzyme (E1)', *J Biol Chem,* 269(10), pp. 7115-23.
Piotrowski, J., Beal, R., Hoffman, L., Wilkinson, K. D., Cohen, R. E. and Pickart, C. M. (1997) 'Inhibition of the 26 S proteasome by polyubiquitin chains synthesized to have defined lengths', *J Biol Chem,* 272(38), pp. 23712-21.

Plans, V., Scheper, J., Soler, M., Loukili, N., Okano, Y. and Thomson, T. M. (2006) 'The RING finger protein RNF8 recruits UBC13 for lysine 63-based self polyubiquitylation', *J Cell Biochem,* 97(3), pp. 572-82.
Plechanovová, A., Jaffray, E. G., Tatham, M. H., Naismith, J. H. and Hay, R. T. (2012) 'Structure of a RING E3 ligase and ubiquitin-loaded E2 primed for catalysis', *Nature,* 489(7414), pp. 115-20.
Ponder, E. L. and Bogyo, M. (2007) 'Ubiquitin-like modifiers and their deconjugating enzymes in medically important parasitic protozoa', *Eukaryot Cell,* 6(11), pp. 1943-52.
Ponte-Sucre, A., Gamarro, F., Dujardin, J. C., Barrett, M. P., López-Vélez, R., García-Hernández, R., Pountain, A. W., Mwenechanya, R. and Papadopoulou, B. (2017) 'Drug resistance and treatment failure in leishmaniasis: A 21st century challenge', *PLoS Negl Trop Dis,* 11(12), pp. e0006052.
Poolman, B., Royer, T. J., Mainzer, S. E. and Schmidt, B. F. (1990) 'Carbohydrate utilization in Streptococcus thermophilus: characterization of the genes for aldose 1-epimerase (mutarotase) and UDPglucose 4-epimerase', *J Bacteriol,* 172(7), pp. 4037-47.
Potterton, L., Agirre, J., Ballard, C., Cowtan, K., Dodson, E., Evans, P. R., Jenkins, H. T., Keegan, R., Krissinel, E., Stevenson, K., Lebedev, A., McNicholas, S. J., Nicholls, R. A., Noble, M., Pannu, N. S., Roth, C., Sheldrick, G., Skubak, P., Turkenburg, J., Uski, V., von Delft, F., Waterman, D., Wilson, K., Winn, M. and Wojdyr, M. (2018) 'CCP4i2: the new graphical user interface to the CCP4 program suite', *Acta Crystallogr D Struct Biol,* 74(Pt 2), pp. 68-84.
Prakash, L. and Prakash, S. (1977) 'Isolation and characterization of MMS-sensitive mutants of Saccharomyces cerevisiae', *Genetics,* 86(1), pp. 33-55.
Proto, W. R., Jones, N. G., Coombs, G. H. and Mottram, J. C. (2014) 'Tracking autophagy during proliferation and differentiation of Trypanosoma brucei', *Microb Cell,* 1(1), pp. 9-20.
Pruneda, J. N., Smith, F. D., Daurie, A., Swaney, D. L., Villén, J., Scott, J. D., Stadnyk, A. W., Le Trong, I., Stenkamp, R. E., Klevit, R. E., Rohde, J. R. and Brzovic, P. S. (2014) 'E2~Ub conjugates regulate the kinase activity of Shigella effector OspG during pathogenesis', *EMBO J,* 33(5), pp. 437-49.
Pulvino, M., Liang, Y., Oleksyn, D., DeRan, M., Van Pelt, E., Shapiro, J., Sanz, I., Chen, L. and Zhao, J. (2012) 'Inhibition of proliferation and survival of diffuse large B-cell lymphoma cells by a small-molecule inhibitor of the ubiquitin-conjugating enzyme Ubc13-Uev1A', *Blood,* 120(8), pp. 1668-77.
Rahighi, S., Ikeda, F., Kawasaki, M., Akutsu, M., Suzuki, N., Kato, R., Kensche, T., Uejima, T., Bloor, S., Komander, D., Randow, F., Wakatsuki, S. and Dikic, I. (2009) 'Specific recognition of linear ubiquitin chains by NEMO is important for NF-kappaB activation', *Cell,* 136(6), pp. 1098-109.
Renz, C., Albanèse, V., Tröster, V., Albert, T. K., Santt, O., Jacobs, S. C., Khmelinskii, A., Léon, S. and Ulrich, H. D. (2020) 'Ubc13-Mms2 cooperates with a family of RING E3 proteins in budding yeast membrane protein sorting', *J Cell Sci,* 133(10).
Reynolds, D., Cliffe, L., Förstner, K. U., Hon, C. C., Siegel, T. N. and Sabatini, R. (2014) 'Regulation of transcription termination by glucosylated hydroxymethyluracil, base J, in Leishmania major and Trypanosoma brucei', *Nucleic Acids Res,* 42(15), pp. 9717-29.
Rivkin, E., Almeida, S. M., Ceccarelli, D. F., Juang, Y. C., MacLean, T. A., Srikumar, T., Huang, H., Dunham, W. H., Fukumura, R., Xie, G., Gondo, Y., Raught, B., Gingras, A. C., Sicheri, F. and Cordes, S. P. (2013) 'The linear ubiquitin-specific deubiquitinase gumby regulates angiogenesis', *Nature,* 498(7454), pp. 318-24.
Robert, X. and Gouet, P. (2014) 'Deciphering key features in protein structures with the new ENDscript server', *Nucleic Acids Res,* 42(Web Server issue), pp. W320-4.
Robertson, C. D. (1999) 'The Leishmania mexicana proteasome', *Mol Biochem Parasitol,* 103(1), pp. 49-60.
Robinson, D. G., Chen, W., Storey, J. D. and Gresham, D. (2014) 'Design and analysis of Bar-seq experiments', *G3 (Bethesda),* 4(1), pp. 11-8.

Rogakou, E. P., Pilch, D. R., Orr, A. H., Ivanova, V. S. and Bonner, W. M. (1998) 'DNA double-stranded breaks induce histone H2AX phosphorylation on serine 139', *J Biol Chem,* 273(10), pp. 5858-68.
Rogers, M. E. (2012) 'The role of leishmania proteophosphoglycans in sand fly transmission and infection of the Mammalian host', *Front Microbiol,* 3, pp. 223.
Rogers, M. E. and Bates, P. A. (2007) 'Leishmania manipulation of sand fly feeding behavior results in enhanced transmission', *PLoS Pathog,* 3(6), pp. e91.
Rogers, M. E., Chance, M. L. and Bates, P. A. (2002) 'The role of promastigote secretory gel in the origin and transmission of the infective stage of Leishmania mexicana by the sandfly Lutzomyia longipalpis', *Parasitology,* 124(Pt 5), pp. 495-507.
Rogers, M. E., Ilg, T., Nikolaev, A. V., Ferguson, M. A. and Bates, P. A. (2004) 'Transmission of cutaneous leishmaniasis by sand flies is enhanced by regurgitation of fPPG', *Nature,* 430(6998), pp. 463-7.
Rojas, F., Koszela, J., Búa, J., Llorente, B., Burchmore, R., Auer, M., Mottram, J. C. and Téllez-Iñón, M. T. (2017) 'The ubiquitin-conjugating enzyme CDC34 is essential for cytokinesis in contrast to putative subunits of a SCF complex in Trypanosoma brucei', *PLoS Negl Trop Dis,* 11(6), pp. e0005626.
Rosenzweig, D., Smith, D., Opperdoes, F., Stern, S., Olafson, R. W. and Zilberstein, D. (2008) 'Retooling Leishmania metabolism: from sand fly gut to human macrophage', *FASEB J,* 22(2), pp. 590-602.
Rotin, D. and Kumar, S. (2009) 'Physiological functions of the HECT family of ubiquitin ligases', *Nat Rev Mol Cell Biol,* 10(6), pp. 398-409.
Roux, K. J., Kim, D. I., Raida, M. and Burke, B. (2012) 'A promiscuous biotin ligase fusion protein identifies proximal and interacting proteins in mammalian cells', *J Cell Biol,* 196(6), pp. 801-10.
Ruiz-González, M. X. and Marín, I. (2006) 'Proteasome-related HslU and HslV genes typical of eubacteria are widespread in eukaryotes', *J Mol Evol,* 63(4), pp. 504-12.
Ruy, P. C., Monteiro-Teles, N. M., Miserani Magalhães, R. D., Freitas-Castro, F., Dias, L., Aquino Defina, T. P., Rosas De Vasconcelos, E. J., Myler, P. J. and Kaysel Cruz, A. (2019) 'Comparative transcriptomics in Leishmania braziliensis: disclosing differential gene expression of coding and putative noncoding RNAs across developmental stages', *RNA Biol,* 16(5), pp. 639-660.
Sacks, D. L. and Perkins, P. V. (1985) 'Development of infective stage Leishmania promastigotes within phlebotomine sand flies', *Am J Trop Med Hyg,* 34(3), pp. 456-9.
Sakamoto, A., Hino, S., Nagaoka, K., Anan, K., Takase, R., Matsumori, H., Ojima, H., Kanai, Y., Arita, K. and Nakao, M. (2015) 'Lysine Demethylase LSD1 Coordinates Glycolytic and Mitochondrial Metabolism in Hepatocellular Carcinoma Cells', *Cancer Res,* 75(7), pp. 1445-56.
Samuel, T., Okada, K., Hyer, M., Welsh, K., Zapata, J. M. and Reed, J. C. (2005) 'cIAP1 Localizes to the nuclear compartment and modulates the cell cycle', *Cancer Res,* 65(1), pp. 210-8.
Sanada, T., Kim, M., Mimuro, H., Suzuki, M., Ogawa, M., Oyama, A., Ashida, H., Kobayashi, T., Koyama, T., Nagai, S., Shibata, Y., Gohda, J., Inoue, J., Mizushima, T. and Sasakawa, C. (2012) 'The Shigella flexneri effector OspI deamidates UBC13 to dampen the inflammatory response', *Nature,* 483(7391), pp. 623-6.
Sancho, E., Vilá, M. R., Sánchez-Pulido, L., Lozano, J. J., Paciucci, R., Nadal, M., Fox, M., Harvey, C., Bercovich, B., Loukili, N., Ciechanover, A., Lin, S. L., Sanz, F., Estivill, X., Valencia, A. and Thomson, T. M. (1998) 'Role of UEV-1, an inactive variant of the E2 ubiquitin-conjugating enzymes, in in vitro differentiation and cell cycle behavior of HT-29-M6 intestinal mucosecretory cells', *Mol Cell Biol,* 18(1), pp. 576-89.
Sangenito, L. S., Gonçalves, D. S., Seabra, S. H., d'Avila-Levy, C. M., Santos, A. L. and Branquinha, M. H. (2016) 'HIV aspartic peptidase inhibitors are effective drugs against the trypomastigote form of the human pathogen Trypanosoma cruzi', *Int J Antimicrob Agents,* 48(4), pp. 440-4.

Sato, Y., Yoshikawa, A., Yamashita, M., Yamagata, A. and Fukai, S. (2009) 'Structural basis for specific recognition of Lys 63-linked polyubiquitin chains by NZF domains of TAB2 and TAB3', *EMBO J,* 28(24), pp. 3903-9.
Savoia, D., Allice, T. and Tovo, P. A. (2005) 'Antileishmanial activity of HIV protease inhibitors', *Int J Antimicrob Agents,* 26(1), pp. 92-4.
Saxena, A., Lahav, T., Holland, N., Aggarwal, G., Anupama, A., Huang, Y., Volpin, H., Myler, P. J. and Zilberstein, D. (2007) 'Analysis of the Leishmania donovani transcriptome reveals an ordered progression of transient and permanent changes in gene expression during differentiation', *Mol Biochem Parasitol,* 152(1), pp. 53-65.
Scaglione, K. M., Basrur, V., Ashraf, N. S., Konen, J. R., Elenitoba-Johnson, K. S., Todi, S. V. and Paulson, H. L. (2013) 'The ubiquitin-conjugating enzyme (E2) Ube2w ubiquitinates the N terminus of substrates', *J Biol Chem,* 288(26), pp. 18784-8.
Scheffner, M. and Kumar, S. (2014) 'Mammalian HECT ubiquitin-protein ligases: biological and pathophysiological aspects', *Biochim Biophys Acta,* 1843(1), pp. 61-74.
Scheffner, M., Nuber, U. and Huibregtse, J. M. (1995) 'Protein ubiquitination involving an E1-E2-E3 enzyme ubiquitin thioester cascade', *Nature,* 373(6509), pp. 81-3.
Schulman, B. A. and Harper, J. W. (2009) 'Ubiquitin-like protein activation by E1 enzymes: the apex for downstream signalling pathways', *Nat Rev Mol Cell Biol,* 10(5), pp. 319-31.
Seol, J. H., Feldman, R. M., Zachariae, W., Shevchenko, A., Correll, C. C., Lyapina, S., Chi, Y., Galova, M., Claypool, J., Sandmeyer, S., Nasmyth, K. and Deshaies, R. J. (1999) 'Cdc53/cullin and the essential Hrt1 RING-H2 subunit of SCF define a ubiquitin ligase module that activates the E2 enzyme Cdc34', *Genes Dev,* 13(12), pp. 1614-26.
Seol, J. H., Shevchenko, A. and Deshaies, R. J. (2001) 'Skp1 forms multiple protein complexes, including RAVE, a regulator of V-ATPase assembly', *Nat Cell Biol,* 3(4), pp. 384-91.
Serafim, T. D., Coutinho-Abreu, I. V., Oliveira, F., Meneses, C., Kamhawi, S. and Valenzuela, J. G. (2018) 'Sequential blood meals promote Leishmania replication and reverse metacyclogenesis augmenting vector infectivity', *Nat Microbiol,* 3(5), pp. 548-555.
Shaner, N. C., Lambert, G. G., Chammas, A., Ni, Y., Cranfill, P. J., Baird, M. A., Sell, B. R., Allen, J. R., Day, R. N., Israelsson, M., Davidson, M. W. and Wang, J. (2013) 'A bright monomeric green fluorescent protein derived from Branchiostoma lanceolatum', *Nat Methods,* 10(5), pp. 407-9.
Sharma, V., Sharma, P., Selvapandiyan, A. and Salotra, P. (2016) 'Leishmania donovani-specific Ub-related modifier-1: an early endosome-associated ubiquitin-like conjugation in Leishmania donovani', *Mol Microbiol,* 99(3), pp. 597-610.
Shevket, S. H., Gonzalez, D., Cartwright, J. L., Kleanthous, C., Ferguson, S. J., Redfield, C. and Mavridou, D. A. I. (2018) 'The CcmC–CcmE interaction during cytochrome c maturation by System I is driven by protein–protein and not protein–heme contacts', *J Biol Chem,* 293(43), pp. 16778-16790.
Shlomai, J. (2004) 'The structure and replication of kinetoplast DNA', *Curr Mol Med,* 4(6), pp. 623-47.
Sidik, S. M., Huet, D., Ganesan, S. M., Huynh, M. H., Wang, T., Nasamu, A. S., Thiru, P., Saeij, J. P. J., Carruthers, V. B., Niles, J. C. and Lourido, S. (2016) 'A Genome-wide CRISPR Screen in Toxoplasma Identifies Essential Apicomplexan Genes', *Cell,* 166(6), pp. 1423-1435.e12.
Siegel, T. N., Hekstra, D. R., Kemp, L. E., Figueiredo, L. M., Lowell, J. E., Fenyo, D., Wang, X., Dewell, S. and Cross, G. A. (2009) 'Four histone variants mark the boundaries of polycistronic transcription units in Trypanosoma brucei', *Genes Dev,* 23(9), pp. 1063-76.
Silva-Jardim, I., Horta, M. F. and Ramalho-Pinto, F. J. (2004) 'The Leishmania chagasi proteasome: role in promastigotes growth and amastigotes survival within murine macrophages', *Acta Trop,* 91(2), pp. 121-30.
Singh, N., Kumar, M. and Singh, R. K. (2012) 'Leishmaniasis: current status of available drugs and new potential drug targets', *Asian Pac J Trop Med,* 5(6), pp. 485-97.
Sluimer, J. and Distel, B. (2018) 'Regulating the human HECT E3 ligases', *Cell Mol Life Sci,* 75(17), pp. 3121-3141.

Smit, J. J. and Sixma, T. K. (2014) 'RBR E3-ligases at work', *EMBO Rep,* 15(2), pp. 142-54.
Smith, A. M., Heisler, L. E., Mellor, J., Kaper, F., Thompson, M. J., Chee, M., Roth, F. P., Giaever, G. and Nislow, C. (2009) 'Quantitative phenotyping via deep barcode sequencing', *Genome Res,* 19(10), pp. 1836-42.
Smith, A. M., Heisler, L. E., St Onge, R. P., Farias-Hesson, E., Wallace, I. M., Bodeau, J., Harris, A. N., Perry, K. M., Giaever, G., Pourmand, N. and Nislow, C. (2010) 'Highly-multiplexed barcode sequencing: an efficient method for parallel analysis of pooled samples', *Nucleic Acids Res,* 38(13), pp. e142.
Sollelis, L., Ghorbal, M., MacPherson, C. R., Martins, R. M., Kuk, N., Crobu, L., Bastien, P., Scherf, A., Lopez-Rubio, J. J. and Sterkers, Y. (2015) 'First efficient CRISPR-Cas9-mediated genome editing in Leishmania parasites', *Cell Microbiol,* 17(10), pp. 1405-12.
Soss, S. E., Yue, Y., Dhe-Paganon, S. and Chazin, W. J. (2011) 'E2 conjugating enzyme selectivity and requirements for function of the E3 ubiquitin ligase CHIP', *J Biol Chem,* 286(24), pp. 21277-86.
Spratt, D. E., Walden, H. and Shaw, G. S. (2014) 'RBR E3 ubiquitin ligases: new structures, new insights, new questions', *Biochem J,* 458(3), pp. 421-37.
Stanley, M., Han, C., Knebel, A., Murphy, P., Shpiro, N. and Virdee, S. (2015) 'Orthogonal thiol functionalization at a single atomic center for profiling transthiolation activity of E1 activating enzymes', *ACS Chem Biol,* 10(6), pp. 1542-54.
Stempin, C. C., Rojas Marquez, J. D., Ana, Y. and Cerban, F. M. (2017) 'GRAIL and Otubain-1 are Related to T Cell Hyporesponsiveness during Trypanosoma cruzi Infection', *PLoS Negl Trop Dis,* 11(1), pp. e0005307.
Stephen, A. G., Trausch-Azar, J. S., Handley-Gearhart, P. M., Ciechanover, A. and Schwartz, A. L. (1997) 'Identification of a region within the ubiquitin-activating enzyme required for nuclear targeting and phosphorylation', *J Biol Chem,* 272(16), pp. 10895-903.
Steverding, D. (2006) 'Ubiquitination of plasma membrane ectophosphatase in bloodstream forms of Trypanosoma brucei', *Parasitol Res,* 98(2), pp. 157-61.
Stewart, M. D., Ritterhoff, T., Klevit, R. E. and Brzovic, P. S. (2016) 'E2 enzymes: more than just middle men', *Cell Res,* 26(4), pp. 423-40.
Sun, X., Gao, H., Yang, Y., He, M., Wu, Y., Song, Y., Tong, Y. and Rao, Y. (2019) 'PROTACs: great opportunities for academia and industry', *Signal Transduct Target Ther,* 4, pp. 64.
Sunter, J. and Gull, K. (2017) 'Shape, form, function and Leishmania pathogenicity: from textbook descriptions to biological understanding', *Open Biol,* 7(9).
Sutherst, R. W. (2004) 'Global change and human vulnerability to vector-borne diseases', *Clin Microbiol Rev,* 17(1), pp. 136-73.
Swaney, D. L., Rodríguez-Mias, R. A. and Villén, J. (2015) 'Phosphorylation of ubiquitin at Ser65 affects its polymerization, targets, and proteome-wide turnover', *EMBO Rep,* 16(9), pp. 1131-44.
Swatek, K. N. and Komander, D. (2016) 'Ubiquitin modifications', *Cell Res,* 26(4), pp. 399-422.
Swindle, J., Ajioka, J., Eisen, H., Sanwal, B., Jacquemot, C., Browder, Z. and Buck, G. (1988) 'The genomic organization and transcription of the ubiquitin genes of Trypanosoma cruzi', *EMBO J,* 7(4), pp. 1121-7.
Taherbhoy, A. M., Schulman, B. A. and Kaiser, S. E. (2012) 'Ubiquitin-like modifiers', *Essays Biochem,* 52, pp. 51-63.
Tanaka, K. (2009) 'The proteasome: overview of structure and functions', *Proc Jpn Acad Ser B Phys Biol Sci,* 85(1), pp. 12-36.
Tatham, M. H., Plechanovová, A., Jaffray, E. G., Salmen, H. and Hay, R. T. (2013) 'Ube2W conjugates ubiquitin to α-amino groups of protein N-termini', *Biochem J,* 453(1), pp. 137-45.
Taylor, N. C. and McGouran, J. F. (2019) 'Strategies to Target Specific Components of the Ubiquitin Conjugation/Deconjugation Machinery', *Front Chem,* 7, pp. 914.
Taylor, S. V., Kelleher, N. L., Kinsland, C., Chiu, H. J., Costello, C. A., Backstrom, A. D., McLafferty, F. W. and Begley, T. P. (1998) 'Thiamin biosynthesis in Escherichia coli.

Identification of ThiS thiocarboxylate as the immediate sulfur donor in the thiazole formation', *J Biol Chem,* 273(26), pp. 16555-60.
Teo, G., Koh, H., Fermin, D., Lambert, J. P., Knight, J. D., Gingras, A. C. and Choi, H. (2016) 'SAINTq: Scoring protein-protein interactions in affinity purification - mass spectrometry experiments with fragment or peptide intensity data', *Proteomics,* 16(15-16), pp. 2238-45.
Thomas, S., Green, A., Sturm, N. R., Campbell, D. A. and Myler, P. J. (2009) 'Histone acetylations mark origins of polycistronic transcription in Leishmania major', *BMC Genomics,* 10, pp. 152.
Thorslund, T., Ripplinger, A., Hoffmann, S., Wild, T., Uckelmann, M., Villumsen, B., Narita, T., Sixma, T. K., Choudhary, C., Bekker-Jensen, S. and Mailand, N. (2015) 'Histone H1 couples initiation and amplification of ubiquitin signalling after DNA damage', *Nature,* 527(7578), pp. 389-93.
Tokumoto, M., Nagahama, Y. and Tokumoto, T. (2000) 'Molecular cloning of cDNA encoding a ubiquitin-activating enzyme (E1) from goldfish (Carassius auratus) and expression analysis of the cloned gene', *Biochim Biophys Acta,* 1492(1), pp. 259-63.
TriTrypDB (2020) *Kinetoplastid Informatics Resources* (Accessed: 28 Aug 2020).
Tsigankov, P., Gherardini, P. F., Helmer-Citterich, M., Späth, G. F., Myler, P. J. and Zilberstein, D. (2014) 'Regulation dynamics of Leishmania differentiation: deconvoluting signals and identifying phosphorylation trends', *Mol Cell Proteomics,* 13(7), pp. 1787-99.
Tunes, L. G., Morato, R. E., Garcia, A., Schmitz, V., Steindel, M., Corrêa-Junior, J. D., Dos Santos, H. F., Frézard, F., de Almeida, M. V., Silva, H., Moretti, N. S., de Barros, A. L. B. and do Monte-Neto, R. L. (2020) 'Preclinical Gold Complexes as Oral Drug Candidates to Treat Leishmaniasis Are Potent Trypanothione Reductase Inhibitors', *ACS Infect Dis,* 6(5), pp. 1121-1139.
Turnbull, A. P., Ioannidis, S., Krajewski, W. W., Pinto-Fernandez, A., Heride, C., Martin, A. C. L., Tonkin, L. M., Townsend, E. C., Buker, S. M., Lancia, D. R., Caravella, J. A., Toms, A. V., Charlton, T. M., Lahdenranta, J., Wilker, E., Follows, B. C., Evans, N. J., Stead, L., Alli, C., Zarayskiy, V. V., Talbot, A. C., Buckmelter, A. J., Wang, M., McKinnon, C. L., Saab, F., McGouran, J. F., Century, H., Gersch, M., Pittman, M. S., Marshall, C. G., Raynham, T. M., Simcox, M., Stewart, L. M. D., McLoughlin, S. B., Escobedo, J. A., Bair, K. W., Dinsmore, C. J., Hammonds, T. R., Kim, S., Urbé, S., Clague, M. J., Kessler, B. M. and Komander, D. (2017) 'Molecular basis of USP7 inhibition by selective small-molecule inhibitors', *Nature,* 550(7677), pp. 481-486.
Télles, S., Abate, T., Slezynger, T. C. and Henríquez, D. A. (1999) 'Trypanosoma cruzi and human ubiquitin are immunologically distinct proteins despite only three amino acid difference in their primary sequence', *FEMS Immunol Med Microbiol,* 24(2), pp. 123-30.
Ueda-Nakamura, T., da Conceição Rocha Sampaio, M., Cunha-e-Silva, N. L., Traub-Cseko, Y. M. and de Souza, W. (2002) 'Expression and processing of megasome cysteine proteinases during Leishmania amazonensis differentiation', *Parasitol Res,* 88(4), pp. 332-7.
Ulrich, H. D. and Jentsch, S. (2000) 'Two RING finger proteins mediate cooperation between ubiquitin-conjugating enzymes in DNA repair', *EMBO J,* 19(13), pp. 3388-97.
Um, J. W. and Chung, K. C. (2006) 'Functional modulation of parkin through physical interaction with SUMO-1', *J Neurosci Res,* 84(7), pp. 1543-54.
Vagin, A. and Teplyakov, A. (1997) 'MOLREP: an Automated Program for Molecular Replacement', *Journal of Applied Crystallography,* 30(6), pp. 1022-1025.
Van den Kerkhof, M., Mabille, D., Chatelain, E., Mowbray, C. E., Braillard, S., Hendrickx, S., Maes, L. and Caljon, G. (2018) 'In vitro and in vivo pharmacodynamics of three novel antileishmanial lead series', *Int J Parasitol Drugs Drug Resist,* 8(1), pp. 81-86.
van der Veen, A. G. and Ploegh, H. L. (2012) 'Ubiquitin-like proteins', *Annu Rev Biochem,* 81, pp. 323-57.
van Griensven, J., Diro, E., Lopez-Velez, R., Boelaert, M., Lynen, L., Zijlstra, E., Dujardin, J. C. and Hailu, A. (2013) 'HIV-1 protease inhibitors for treatment of visceral leishmaniasis in HIV-co-infected individuals', *Lancet Infect Dis,* 13(3), pp. 251-9.

van Wijk, S. J., de Vries, S. J., Kemmeren, P., Huang, A., Boelens, R., Bonvin, A. M. and Timmers, H. T. (2009) 'A comprehensive framework of E2-RING E3 interactions of the human ubiquitin-proteasome system', *Mol Syst Biol,* 5, pp. 295.
Vassilev, L. T., Vu, B. T., Graves, B., Carvajal, D., Podlaski, F., Filipovic, Z., Kong, N., Kammlott, U., Lukacs, C., Klein, C., Fotouhi, N. and Liu, E. A. (2004) 'In vivo activation of the p53 pathway by small-molecule antagonists of MDM2', *Science,* 303(5659), pp. 844-8.
Vittal, V., Wenzel, D. M., Brzovic, P. S. and Klevit, R. E. (2013) 'Biochemical and structural characterization of the ubiquitin-conjugating enzyme UBE2W reveals the formation of a noncovalent homodimer', *Cell Biochem Biophys,* 67(1), pp. 103-10.
Volf, P., Hajmova, M., Sadlova, J. and Votypka, J. (2004) 'Blocked stomodeal valve of the insect vector: similar mechanism of transmission in two trypanosomatid models', *Int J Parasitol,* 34(11), pp. 1221-7.
Wang, H., La Russa, M. and Qi, L. S. (2016) 'CRISPR/Cas9 in Genome Editing and Beyond', *Annu Rev Biochem,* 85, pp. 227-64.
Wang, Q., Zang, Y., Zhou, X. and Xiao, W. (2017) 'Characterization of four rice UEV1 genes required for Lys63-linked polyubiquitination and distinct functions', *BMC Plant Biol,* 17(1), pp. 126.
Wauer, T., Swatek, K. N., Wagstaff, J. L., Gladkova, C., Pruneda, J. N., Michel, M. A., Gersch, M., Johnson, C. M., Freund, S. M. and Komander, D. (2015) 'Ubiquitin Ser65 phosphorylation affects ubiquitin structure, chain assembly and hydrolysis', *EMBO J,* 34(3), pp. 307-25.
Weber, E., Rothenaigner, I., Brandner, S., Hadian, K. and Schorpp, K. (2017) 'A High-Throughput Screening Strategy for Development of RNF8-Ubc13 Protein-Protein Interaction Inhibitors', *SLAS Discov,* 22(3), pp. 316-323.
Wei, Y., Hu, H., Lun, Z. R. and Li, Z. (2014) 'Centrin3 in trypanosomes maintains the stability of a flagellar inner-arm dynein for cell motility', *Nat Commun,* 5, pp. 4060.
Wenzel, D. M., Lissounov, A., Brzovic, P. S. and Klevit, R. E. (2011) 'UBCH7 reactivity profile reveals parkin and HHARI to be RING/HECT hybrids', *Nature,* 474(7349), pp. 105-8.
Wenzel, D. M., Stoll, K. E. and Klevit, R. E. (2011) 'E2s: structurally economical and functionally replete', *Biochem J,* 433(1), pp. 31-42.
Wertz, I. E., O'Rourke, K. M., Zhou, H., Eby, M., Aravind, L., Seshagiri, S., Wu, P., Wiesmann, C., Baker, R., Boone, D. L., Ma, A., Koonin, E. V. and Dixit, V. M. (2004) 'De-ubiquitination and ubiquitin ligase domains of A20 downregulate NF-kappaB signalling', *Nature,* 430(7000), pp. 694-9.
Wetmore, K. M., Price, M. N., Waters, R. J., Lamson, J. S., He, J., Hoover, C. A., Blow, M. J., Bristow, J., Butland, G., Arkin, A. P. and Deutschbauer, A. (2015) 'Rapid quantification of mutant fitness in diverse bacteria by sequencing randomly bar-coded transposons', *mBio,* 6(3), pp. e00306-15.
Wheeler, R. J., Gluenz, E. and Gull, K. (2015) 'Basal body multipotency and axonemal remodelling are two pathways to a 9+0 flagellum', *Nat Commun,* 6, pp. 8964.
Wheeler, R. J., Sunter, J. D. and Gull, K. (2016) 'Flagellar pocket restructuring through the Leishmania life cycle involves a discrete flagellum attachment zone', *J Cell Sci,* 129(4), pp. 854-67.
Whiting, C. C., Su, L. L., Lin, J. T. and Fathman, C. G. (2011) 'GRAIL: a unique mediator of CD4 T-lymphocyte unresponsiveness', *FEBS J,* 278(1), pp. 47-58.
Wickliffe, K. E., Williamson, A., Meyer, H. J., Kelly, A. and Rape, M. (2011) 'K11-linked ubiquitin chains as novel regulators of cell division', *Trends Cell Biol,* 21(11), pp. 656-63.
Wiener, R., DiBello, A. T., Lombardi, P. M., Guzzo, C. M., Zhang, X., Matunis, M. J. and Wolberger, C. (2013) 'E2 ubiquitin-conjugating enzymes regulate the deubiquitinating activity of OTUB1', *Nat Struct Mol Biol,* 20(9), pp. 1033-9.
Williams, R. A., Mottram, J. C. and Coombs, G. H. (2013) 'Distinct roles in autophagy and importance in infectivity of the two ATG4 cysteine peptidases of Leishmania major', *J Biol Chem,* 288(5), pp. 3678-90.

Williams, R. A., Smith, T. K., Cull, B., Mottram, J. C. and Coombs, G. H. (2012) 'ATG5 is essential for ATG8-dependent autophagy and mitochondrial homeostasis in Leishmania major', *PLoS Pathog,* 8(5), pp. e1002695.
Williams, R. A., Tetley, L., Mottram, J. C. and Coombs, G. H. (2006) 'Cysteine peptidases CPA and CPB are vital for autophagy and differentiation in Leishmania mexicana', *Mol Microbiol,* 61(3), pp. 655-74.
Williams, R. A., Woods, K. L., Juliano, L., Mottram, J. C. and Coombs, G. H. (2009) 'Characterization of unusual families of ATG8-like proteins and ATG12 in the protozoan parasite Leishmania major', *Autophagy,* 5(2), pp. 159-72.
Windheim, M., Peggie, M. and Cohen, P. (2008) 'Two different classes of E2 ubiquitin-conjugating enzymes are required for the mono-ubiquitination of proteins and elongation by polyubiquitin chains with a specific topology', *Biochem J,* 409(3), pp. 723-9.
Winter, G., Lobley, C. M. and Prince, S. M. (2013) 'Decision making in xia2', *Acta Crystallogr D Biol Crystallogr,* 69(Pt 7), pp. 1260-73.
Wong, S. and Campbell, D. A. (1989) 'A polyubiquitin gene from Trypanosoma brucei', *Mol Biochem Parasitol,* 37(1), pp. 147-50.
Wong, S., Elgort, M. G., Gottesdiener, K. and Campbell, D. A. (1992) 'Allelic polymorphism of the Trypanosoma brucei polyubiquitin gene', *Mol Biochem Parasitol,* 55(1-2), pp. 187-95.
Woo, J. S., Imm, J. H., Min, C. K., Kim, K. J., Cha, S. S. and Oh, B. H. (2006) 'Structural and functional insights into the B30.2/SPRY domain', *EMBO J,* 25(6), pp. 1353-63.
World Health Organisation (2020) *Leishmaniasis* World Health Org Fact Sheet. www.who.int/en/news-room/fact-sheets/detail/leishmaniasis (Accessed: 27 Aug 2020).
Wu, L., Grigoryan, A. V., Li, Y., Hao, B., Pagano, M. and Cardozo, T. J. (2012) 'Specific small molecule inhibitors of Skp2-mediated p27 degradation', *Chem Biol,* 19(12), pp. 1515-24.
Wu, P. Y., Hanlon, M., Eddins, M., Tsui, C., Rogers, R. S., Jensen, J. P., Matunis, M. J., Weissman, A. M., Weisman, A. M., Wolberger, C., Wolberger, C. P. and Pickart, C. M. (2003) 'A conserved catalytic residue in the ubiquitin-conjugating enzyme family', *EMBO J,* 22(19), pp. 5241-50.
Wu, X. and Karin, M. (2015) 'Emerging roles of Lys63-linked polyubiquitylation in immune responses', *Immunol Rev,* 266(1), pp. 161-74.
Wu, X., Yamamoto, M., Akira, S. and Sun, S. C. (2009) 'Regulation of hematopoiesis by the K63-specific ubiquitin-conjugating enzyme Ubc13', *Proc Natl Acad Sci U S A,* 106(49), pp. 20836-41.
Wyllie, S., Brand, S., Thomas, M., De Rycker, M., Chung, C. W., Pena, I., Bingham, R. P., Bueren-Calabuig, J. A., Cantizani, J., Cebrian, D., Craggs, P. D., Ferguson, L., Goswami, P., Hobrath, J., Howe, J., Jeacock, L., Ko, E. J., Korczynska, J., MacLean, L., Manthri, S., Martinez, M. S., Mata-Cantero, L., Moniz, S., Nühs, A., Osuna-Cabello, M., Pinto, E., Riley, J., Robinson, S., Rowland, P., Simeons, F. R. C., Shishikura, Y., Spinks, D., Stojanovski, L., Thomas, J., Thompson, S., Viayna Gaza, E., Wall, R. J., Zuccotto, F., Horn, D., Ferguson, M. A. J., Fairlamb, A. H., Fiandor, J. M., Martin, J., Gray, D. W., Miles, T. J., Gilbert, I. H., Read, K. D., Marco, M. and Wyatt, P. G. (2019) 'Preclinical candidate for the treatment of visceral leishmaniasis that acts through proteasome inhibition', *Proc Natl Acad Sci U S A,* 116(19), pp. 9318-9323.
Wyllie, S., Thomas, M., Patterson, S., Crouch, S., De Rycker, M., Lowe, R., Gresham, S., Urbaniak, M. D., Otto, T. D., Stojanovski, L., Simeons, F. R. C., Manthri, S., MacLean, L. M., Zuccotto, F., Homeyer, N., Pflaumer, H., Boesche, M., Sastry, L., Connolly, P., Albrecht, S., Berriman, M., Drewes, G., Gray, D. W., Ghidelli-Disse, S., Dixon, S., Fiandor, J. M., Wyatt, P. G., Ferguson, M. A. J., Fairlamb, A. H., Miles, T. J., Read, K. D. and Gilbert, I. H. (2018) 'Cyclin-dependent kinase 12 is a drug target for visceral leishmaniasis', *Nature,* 560(7717), pp. 192-197.
Xia, Z. P., Sun, L., Chen, X., Pineda, G., Jiang, X., Adhikari, A., Zeng, W. and Chen, Z. J. (2009) 'Direct activation of protein kinases by unanchored polyubiquitin chains', *Nature,* 461(7260), pp. 114-9.
Xie, S. T. (2014) 'Expression, purification, and crystal structure of N-terminal domains of human ubiquitin-activating enzyme (E1)', *Biosci Biotechnol Biochem,* 78(9), pp. 1542-9.

Xu, G., Paige, J. S. and Jaffrey, S. R. (2010) 'Global analysis of lysine ubiquitination by ubiquitin remnant immunoaffinity profiling', *Nat Biotechnol,* 28(8), pp. 868-73.
Xu, G. W., Ali, M., Wood, T. E., Wong, D., Maclean, N., Wang, X., Gronda, M., Skrtic, M., Li, X., Hurren, R., Mao, X., Venkatesan, M., Beheshti Zavareh, R., Ketela, T., Reed, J. C., Rose, D., Moffat, J., Batey, R. A., Dhe-Paganon, S. and Schimmer, A. D. (2010) 'The ubiquitin-activating enzyme E1 as a therapeutic target for the treatment of leukemia and multiple myeloma', *Blood,* 115(11), pp. 2251-9.
Xu, L., Fan, J., Wang, Y., Zhang, Z., Fu, Y., Li, Y. M. and Shi, J. (2019) 'An activity-based probe developed by a sequential dehydroalanine formation strategy targets HECT E3 ubiquitin ligases', *Chem Commun (Camb),* 55(49), pp. 7109-7112.
Yagoubat, A., Crobu, L., Berry, L., Kuk, N., Lefebvre, M., Sarrazin, A., Bastien, P. and Sterkers, Y. (2020) 'Universal highly efficient conditional knockout system in Leishmania, with a focus on untranscribed region preservation', *Cell Microbiol,* 22(5), pp. e13159.
Yang, Y., Kitagaki, J., Dai, R. M., Tsai, Y. C., Lorick, K. L., Ludwig, R. L., Pierre, S. A., Jensen, J. P., Davydov, I. V., Oberoi, P., Li, C. C., Kenten, J. H., Beutler, J. A., Vousden, K. H. and Weissman, A. M. (2007) 'Inhibitors of ubiquitin-activating enzyme (E1), a new class of potential cancer therapeutics', *Cancer Res,* 67(19), pp. 9472-81.
Yang, Z., Hou, Y., Hao, T., Rho, H. S., Wan, J., Luan, Y., Gao, X., Yao, J., Pan, A., Xie, Z., Qian, J., Liao, W., Zhu, H. and Zhou, X. (2017) 'A Human Proteome Array Approach to Identifying Key Host Proteins Targeted by Toxoplasma Kinase ROP18', *Mol Cell Proteomics,* 16(3), pp. 469-484.
Yaseen, N. R. and Blobel, G. (1999) 'Two distinct classes of Ran-binding sites on the nucleoporin Nup-358', *Proc Natl Acad Sci U S A,* 96(10), pp. 5516-21.
Ye, K., Zhang, X., Ni, J., Liao, S. and Tu, X. (2015) 'Identification of enzymes involved in SUMOylation in Trypanosoma brucei', *Sci Rep,* 5, pp. 10097.
Ye, Y. and Rape, M. (2009) 'Building ubiquitin chains: E2 enzymes at work', *Nat Rev Mol Cell Biol,* 10(11), pp. 755-64.
Yoon, H. J., Feoktistova, A., Wolfe, B. A., Jennings, J. L., Link, A. J. and Gould, K. L. (2002) 'Proteomics analysis identifies new components of the fission and budding yeast anaphase-promoting complexes', *Curr Biol,* 12(23), pp. 2048-54.
Yu, Z., Chen, T., Li, X., Yang, M., Tang, S., Zhu, X., Gu, Y., Su, X., Xia, M., Li, W., Zhang, X., Wang, Q., Cao, X. and Wang, J. (2016) 'Lys29-linkage of ASK1 by Skp1-Cullin 1-Fbxo21 ubiquitin ligase complex is required for antiviral innate response', *Elife,* 5.
Yuan, T., Yan, F., Ying, M., Cao, J., He, Q., Zhu, H. and Yang, B. (2018) 'Inhibition of Ubiquitin-Specific Proteases as a Novel Anticancer Therapeutic Strategy', *Front Pharmacol,* 9, pp. 1080.
Yuan, W. C., Lee, Y. R., Lin, S. Y., Chang, L. Y., Tan, Y. P., Hung, C. C., Kuo, J. C., Liu, C. H., Lin, M. Y., Xu, M., Chen, Z. J. and Chen, R. H. (2014) 'K33-Linked Polyubiquitination of Coronin 7 by Cul3-KLHL20 Ubiquitin E3 Ligase Regulates Protein Trafficking', *Mol Cell,* 54(4), pp. 586-600.
Zachariae, W., Shevchenko, A., Andrews, P. D., Ciosk, R., Galova, M., Stark, M. J., Mann, M. and Nasmyth, K. (1998) 'Mass spectrometric analysis of the anaphase-promoting complex from yeast: identification of a subunit related to cullins', *Science,* 279(5354), pp. 1216-9.
Zhang, J., Liu, J., Norris, A., Grant, B. D. and Wang, X. (2018) 'A novel requirement for ubiquitin-conjugating enzyme UBC-13 in retrograde recycling of MIG-14/Wntless and Wnt signaling', *Mol Biol Cell,* 29(17), pp. 2098-2112.
Zhang, M., Windheim, M., Roe, S. M., Peggie, M., Cohen, P., Prodromou, C. and Pearl, L. H. (2005) 'Chaperoned ubiquitylation--crystal structures of the CHIP U box E3 ubiquitin ligase and a CHIP-Ubc13-Uev1a complex', *Mol Cell,* 20(4), pp. 525-38.
Zhang, W., Zhang, J., Xu, C., Wang, T., Zhang, X. and Tu, X. (2009) 'Solution structure of Urm1 from Trypanosoma brucei', *Proteins,* 75(3), pp. 781-5.
Zhang, W., Zhuang, Y., Zhang, Y., Yang, X., Zhang, H., Wang, G., Yin, W., Wang, R., Zhang, Z. and Xiao, W. (2017) 'Uev1A facilitates osteosarcoma differentiation by promoting Smurf1-mediated Smad1 ubiquitination and degradation', *Cell Death Dis,* 8(8), pp. e2974.

Zhang, W. W. and Matlashewski, G. (2015) 'CRISPR-Cas9-Mediated Genome Editing in Leishmania donovani', *mBio,* 6(4), pp. e00861.
Zhang, X., Linder, S. and Bazzaro, M. (2020) 'Drug Development Targeting the Ubiquitin-Proteasome System (UPS) for the Treatment of Human Cancers', *Cancers (Basel),* 12(4).
Zhao, G. Y., Sonoda, E., Barber, L. J., Oka, H., Murakawa, Y., Yamada, K., Ikura, T., Wang, X., Kobayashi, M., Yamamoto, K., Boulton, S. J. and Takeda, S. (2007) 'A critical role for the ubiquitin-conjugating enzyme Ubc13 in initiating homologous recombination', *Mol Cell,* 25(5), pp. 663-75.
Zheng, Z., Tweten, R. K. and Mensa-Wilmot, K. (2005) 'Intracellular glycosylphosphatidylinositols accumulate on endosomes: toxicity of alpha-toxin to Leishmania major', *Eukaryot Cell,* 4(3), pp. 556-66.
Zhou, X., Dong, R., Zhang, J. Y., Zheng, X. and Sun, L. P. (2020) 'PROTAC: A promising technology for cancer treatment', *Eur J Med Chem,* 203, pp. 112539.
Zhou, Z., He, M., Shah, A. A. and Wan, Y. (2016) 'Insights into APC/C: from cellular function to diseases and therapeutics', *Cell Div,* 11, pp. 9.
Zoltner, M., Leung, K. F., Alsford, S., Horn, D. and Field, M. C. (2015) 'Modulation of the Surface Proteome through Multiple Ubiquitylation Pathways in African Trypanosomes', *PLoS Pathog,* 11(10), pp. e1005236.